Yuji Ohashi

Crystalline State Photoreactions

Direct Observation of Reaction Processes and Metastable Intermediates

Springer

Crystalline State Photoreactions

Yuji Ohashi

Crystalline State Photoreactions

Direct Observation of Reaction Processes and Metastable Intermediates

Springer

Yuji Ohashi
Ibaraki Quantum Beam Research Center
Tokyo Institute of Technology
Tokai, Japan

ISBN 978-4-431-54372-5 ISBN 978-4-431-54373-2 (eBook)
DOI 10.1007/978-4-431-54373-2
Springer Tokyo Heidelberg New York Dordrecht London

Library of Congress Control Number: 2014930334

Preface

If the atomic movement or bond breaking and formation can be directly observed in the process of a chemical reaction, the following questions can be made clear very easily: why the reaction occurred although no reaction was detected for the related compounds, how the product molecule was made from the reactant molecule, and what the factor to control the reaction rate is, and so on. It is surely a dream for most chemists to be able to answer those questions.

In order to observe the atomic movement directly in a molecular or crystal structure, the diffraction method should be applied to the three-dimensional lattice structure, that is, a single crystal. However, it seemed impossible for all the molecules in a crystal to react uniformly but keep the periodic structure during the reaction. The three-dimensional intensity data should be collected within a micro or a nano second. Moreover, the observed structure is not a single molecule but an averaged structure forming the lattice structure. How to observe the structural change of molecules during chemical reactions has long been a landmark for most crystallographers.

I found about 35 years ago that the crystallinity was kept during the photoisomerization of a cobalt complex, although the unit–cell dimensions were gradually changed [1]. Such a solid state reaction was called "crystalline state reaction." The characteristics of the reaction were well explained by first-order kinetics until the final stage of the reaction, and the structures at the initial, several intermediate, and final stages were analyzed by the diffraction method. The structural change of the averaged molecule was clearly observed, although the dynamical structural change of one molecule was not seen. From the change, the process of the reaction can be easily assumed as if we can observe the movement of a molecule during the reaction [2].

The purpose of this book is to explain how to observe the process of a variety of reactions that occur in a single crystal. In lucky cases, the metastable intermediate structures can be seen directly during the reactions. The structures of metastable reaction intermediates, whose existence has been believed more than 80 years [3], can be observed in the crystal structures [4]. Moreover, the molecular structure at the photo-exited state can be seen together with that of the ground state [5].

This book is in two sections. The first section (Chaps. 2–6) provides a variety of photoisomerization of cobaloxime complexes and techniques for how to obtain the crystalline state reactions. The second section (Chaps. 7 and 8) deals with the structures of various metastable and unstable reaction intermediates, including the structures of excited states. From the direct observation of the above reaction processes and their intermediate structures, I will be delighted if readers understand that the diffraction method can provide the information not only of the static structures but also of the dynamical nature of molecules and crystals in the reaction processes.

I would like to express my appreciation to my staff members Akira Uchida, Hidehiro Uekusa, and Akiko Sekine; post-doctoral fellows Masaki Kawano and Jun Harada; and many post-graduate students who contributed to the work in this book. I also thank Yoshio Sasada for his strong support and valuable discussions when I started this work at the Tokyo Institute of Technology. I also express my appreciation to Yoshiaki Ohgo and Seiji Takeuchi for providing samples and valuable discussions in the work involving cobaloxime complexes in the first section. I am grateful to Nobuo Niimura and Ichiro Tanaka, who collaborated with me in neutron experiments, and I am also grateful to Hitoshi Iwasaki and Nobuo Kamiya, and to Tohru Tanimori and Atsuhiki Ochi, who made the IP diffractometer and the MSGC detector for rapid data collection to observe the reaction intermediates in collaboration with me. I express my appreciation to Jiro Abe, Hideo Tomioka, Tadashi Sugawara, and to Yoko Kaizu, Koshiro Toriumi, and Yoshiki Ozawa who, respectively, provided samples and valuable discussions in the work involving lophyl radicals, carbenes, nitrenes, and excited structures of platinum complexes in the second section.

The work in this book was partly supported by a Grant-in-Aid for Scientific Research on a Priority Area from the Ministry of Education, Science and Culture, Japan and by a CREST fund from the Japan Science and Technology Corporation.

Tokai, Japan Yuji Ohashi

References

1. Ohashi Y, Sasada Y (1977) Nature 267:142
2. Ohashi Y, Yanagi K, Kurihara T, Sasada Y, Ohgo Y (1981) J Am Chem Soc 103:5805
3. Bertho A (1924) Chem Ber 57:1138
4. Mitsumori T, Sekine A Uekusa H, Ohashi Y (2010) Acta Crystallogr B66:647
5. Yasuda N, Uekusa H, Ohashi Y (2004) Bull Chem Soc Jpn 79:1362

Contents

About the Author

Yuji Ohashi was born in 1941 in Fukui, Japan. He received his B.Sc., M.Sc., and D.Sc. degrees from the University of Tokyo and joined the Tokyo Institute of Technology as a research associate in 1968. He moved to Ochanomizu University in 1985 and then returned to the Tokyo Institute of Technology in 1988 as a professor in the Department of Chemistry. He retired from IQBRC in 2013. He was a professor until his retirement in 2005. After retirement, Dr. Ohashi moved to SPring-8 as a coordinator and moved to the Ibaraki Quantum Beam Research Center (IQBRC) as a coordinator of single-crystal neutron diffraction at J-PARC. His research focused on the reaction mechanisms of organic compounds in the crystalline state and the structure analysis of metastable reaction intermediates. He was the President of the Crystallographic Society of Japan (CrSJ) from 1998 to 2000, the President of the Asian Crystallographic Association (AsCA) from 1999 to 2002, and the President of the International Union of Crystallography (IUCr) from 2005 to 2008.

Chapter 1
Crystalline-State Photoreactions: Direct Observation of Reaction Processes and Metastable Intermediates

Abstract Since the topochemical postulate was proposed in the solid-state reactions by Schmidt et al. based on the X-ray crystal structure analyses of related compounds, a variety of organic solid-state reactions have been studied analyzing the crystal structures of the reactant molecules in these 50 years. The postulate has been a powerful tool to understand the reaction mechanism at a rough estimate.

Keywords Reaction mechanism • Solid-state reaction • Topochemical postulate

1.1 Introduction

Although a variety of solid-state reactions of molecular crystals have long been studied, the reaction mechanisms have been considered very difficult because the mechanisms similar to those applied to the reactions in gas or solutions have sometimes been inadequate. In 1964, Schmidt et al. analyzed a series of crystal structures of cinnamic acid derivatives and correlated the structures with the photo-reactivity in the solid state. They made clear the following factors in the solid-state reactions: (1) the chemically closely related compounds show significant differences in chemical behavior in the solid state; (2) a given compound reacts differently in the solid-state and dispersed phases; and (3) polymorphic modifications of a given compound show significant differences in chemical behavior. From these three factors, they proposed the "topochemical postulate," which means the reaction in the solid state occurs with a minimum of atomic or molecular movement [1]. Although the word "topochemical" was conceptually proposed by Hertel [2], their postulate was proposed on the bases of the crystal structures analyzed by X-rays. The postulate gave a surprise to most organic chemists and crystallographers, because it was very difficult to analyze the crystal structures of a series of organic compounds by X-rays in the 1960s. After the direct method and the convenient software systems were developed in the 1970s, most chemists were able to analyze the crystal structures by X-rays. A great number of topochemical reactions have been reported.

Y. Ohashi, *Crystalline State Photoreactions: Direct Observation of Reaction Processes and Metastable Intermediates*, DOI 10.1007/978-4-431-54373-2_1,

Reactions in molecular crystals are divided into four types: photo-induced, thermal, gas–solid, and solid–solid reactions. Most reactions in the solid state are regioselective and stereoselective because the reactions usually proceed topochemically. A variety of regio- and stereoselective reactions in the solid state have been reviewed [3–18].

Solid-state reactions have several distinct advantages compared with the reactions in solutions. The first one is that the regio- and stereoselective reactions sometimes occur very easily. This brings about the following favorable conditions: (1) the sub-products are fewer than those produced from the same starting compounds in solutions, (2) the products are sometimes different from those obtained from the same reactants in solutions, and (3) different reactivity may be obtained by different polymorphic forms of reactant molecules. For example, very complicated products are sometimes obtained in only one step in the solid state on exposure to light; otherwise many reaction steps are required in solutions [19]. If the achiral reactants are irradiated with light or exposed to halogen gas, the asymmetric products sometimes produced in a chiral crystal environment, which is known as absolute asymmetric reaction, since the asymmetry is deduced only by the chiral crystal packing without any chemical reagent. Such an absolute asymmetric reaction was found for the first time in the gas–solid reaction between bromine gas and chiral crystals of a chalcone compound in 1969 [20]. We reported that a chiral β-lactam was produced from an achiral oxoamide in a chiral crystal environment on exposure to a Hg lamp [21, 22]. Recently a variety of the absolute asymmetric reactions have been reviewed by several authors [23–25].

The second one is the reaction rate. Since the molecules are sometimes ideally aligned in a crystalline lattice to react with each other, the molecules in a crystal react much faster than those in solutions. Many reactions in the solid state proceed much faster than those in solutions as described by Toda [26]. We reported that the polymerization rate of *N*-carboxy-amino acid anhydride of L-leucine (L-leucine NCA) in the solid state is much faster than that in solution [27].

The third one is that the reactions in the solid state proceed under milder conditions than those in solutions. It was found that only by mixing and grinding the reactant crystals in a mortar, a variety of thermal and photochemical reactions occur without any solvent at room temperature [28]. This may indicate that the reactant molecules make a complex in a mortar only by mixing and grinding. We observed a variety of complex formation between the aromatic compounds and the surfactant molecules only by mixing and grinding the two components in a mortar. The structures of the complexes are the same as those of the crystals obtained in solutions if the powder patterns were compared with each other [29]. The solvent-free condition is very advantageous for the solid-state reactions.

It is a matter of course to consider that a new chemistry or materials science will be born if we can design and control the crystal structures. The term of crystal engineering was defined as the understanding of intermolecular interactions in the context of crystal packing and in the utilization of such understanding in the design of new solids with desired physical and chemical properties [30]. Many works on crystal engineering have been published [31–35]. Recently photochromism and

thermochromism have been extensively developed utilizing chemical and physical properties of organic solids. A variety of works are reviewed [36–39].

In spite of the fascinating factors described above, several problems have remained unsolved in the solid-state reactions: (1) it is essential that the crystal structures can be predicted and controlled, if desired compounds are to be prepared topochemically in the solid-state reactions, (2) the dynamic process of the reaction in a crystal must be clarified, and (3) the complex crystals containing at least two reactant molecules must be prepared easily. If the problems will be solved, the solid-state reaction will take the place of the reaction in solutions.

Many attempts have been performed to calculate the energy of crystals and to predict the crystal structures by Kitaigorodsky [40–42]. However, as Maddox pointed out in 1988 [43], "one of the continuing scandals in the physical sciences is that it remains impossible to predict the structure of even the simplest crystalline solids from a knowledge of their chemical composition," this serious problem has not been solved yet. In the 1990s, the development of computer made it possible to perform full-scale crystal energy calculation and several methods were developed [44] and the crystal structure of benzene was predicted [45]. Further development was reviewed [46–48].

References

1. Cohen MD, Schmidt GMJ (1964) J Chem Soc 1996
2. Hertel Z (1931) Elektrochem 37:536
3. Green B, Lahav M, Ravinovich D (1979) Acc Chem Res 12:191
4. Scheffer JR (1980) Acc Chem Res 13:283
5. Paul IC, Curtin Y (1981) Chem Rev 81:525
6. Gavezzoti A, Simonetta M (1982) Chem Rev 82:1
7. Hasegawa M (1983) Chem Rev 83:507
8. Ramamurthy V, Venkatesan K (1987) Chem Rev 87:433
9. Desiraju G (ed) (1987) Organic solid state chemistry. Elsevier, Amsterdam
10. Ohashi Y (1988) Acc Chem Res 21:268
11. Pierrot M (1990) Structure and properties of molecular crystals. Elsevier, Amsterdam
12. Ohashi Y (1993) Reactivity in molecular crystals. Tokyo, VCH-Kodansha
13. Ohashi Y (1996) Curr Opin Solid State Mater Sci 1:522
14. Schenk H (1998) Crystallography across the sciences. IUCr
15. Boldyreva E, Boldyrev V (1999) Reactivity of molecular solids. Wiley, New York
16. Coppens P, Hahn P (2001) X-rays in chemistry. Chem Rev 101:1567
17. Toda F (ed) (2002) Organic solid-state reactions. Kluwer, Dordecht
18. Boeyens JCA, Ogilvie JF (2008) Models, mysteries and magic of molecules. Springer, New York
19. Chen J, Scheffer J, Trotter J (1992) Tetrahedron 48:3251
20. Penzien K, Schmidt GM (1969) J Angew Chem 8:608
21. Sekine A, Hori K, Ohashi Y, Yagi M, Toda F (1989) J Am Chem Soc 111:697
22. Hashizume D, Kogo H, Sekine A, Ohashi Y, Miyamoto H, Toda Y (1995) Acta Crystallogr C51:929
23. Sakamoto M (2004) In: Inoue Y, Ramamurthy V (eds) Chiral photochemistry. Dekker, New York, p 415

24. Koshima H (2004) In: Inoue Y, Ramamurthy V (eds) Chiral photochemistry. Dekker, New York, p 485
25. Weissbuch I, Lahav M (2011) Chem Rev 111:3236
26. Toda F (1995) Acc Chem Res 28:480
27. Kanazawa H, Ohashi Y, Sasada Y (1982) J Polym Sci Polym Phys Ed 20:1847
28. Tanaka K, Toda F (2000) Chem Rev 100:1025
29. Ohashi Y, Sawada K, Iimura N (2010) In: Tiekink ERT, Vittal J, Zaworotko M (eds) Organic crystal engineering: frontier in crystal engineering. Wiley, New York, p 101
30. Seddon KR, Zaworotko M (1999) Crystal engineering: the design and application of functional solids. Kluwer Academic Publishers, Dordrecht
31. Braga D, Grepioni F, Desiraju GR (1998) Chem Rev 98:1375
32. Braga D, Grepioni F, Orpen AG (1999) Crystal engineering: from molecules and crystals to materials. Kluwer Academic Publishers, Dordrecht
33. Moulton B, Zaworotko M (2001) J Chem Rev 101:1629
34. Desiraju GR (ed) (2003) Crystal design structure and function. Wiley, New York
35. Tiekink RT, Vittal JJ, Zaworotko MJ (2010) Organic crystal engineering: frontier in crystal engineering. Wiley, New York
36. Crano JC, Guglielmetti RJ (1998) Organic photochromic and thermochromic compounds, vol 1, 2. Plenum, New York
37. Ramamurthy V, Schanze KS (1999) Organic molecular photochemistry. Dekker Inc, New York
38. Irie M (2000) Chem Rev 100:1685
39. Yokoyama Y (2000) Chem Rev 100:1717
40. Kitaigorodsky AI (1973) Molecular crystals and molecules. Academic, New York
41. Kitaogorodsky AI (1984) Mixed crystal. Springer, New York
42. Pertsin AJ, Kitaigorodsky AI (1987) The atom-atom potential method. Springer, New York
43. Maddox J (1988) Nature 335:201
44. Osawa E (1993) In: Ohashi Y (ed) Reactivity in molecular crystals. VCH Publisher, New York, p 1
45. Tajima N, Hirano T (1993) In: Ohashi Y (ed) Reactivity in molecular crystals. Kodansha, Tokyo, p 9
46. Gavezzotti A (ed) (1997) Theoretical aspects and computer modeling of the molecular solid state. Wiley, New York
47. Day GM (2010) In: Tiekink ED, Vittal J, Zaworotko M (eds) Organic crystal engineering. Wiley, New York, p 43
48. Oganov A, Lyakhov AO, Valle M (2011) Acc Chem Res 44:227

Chapter 2
Crystalline-State Reaction and Reaction Cavity

Abstract There are two types of solid-state reactions keeping the single crystal form: single crystal-to-single crystal (SCSC) transformations and crystalline-state reactions. In the former reactions, the crystal structures before and after the reaction are very similar to each other, but the crystallinity is not kept during the reaction. In the latter reactions, the crystallinity is kept in a whole process of the reaction. The reaction cavity was defined to estimate the void space around the reactive group. For the crystalline-state reaction, it was easy to understand the way how the void space is effectively utilized in the process of the reaction, comparing the void space before and after the reaction.

Keywords Crystalline-state reaction • Reaction cavity • Single crystal-to-single crystal transformation

2.1 Finding of Crystalline-State Reaction

It has long been believed that the crystallinity should be decomposed after a reaction occurs in a crystal since the molecular structure in the crystal is largely changed during the reaction. However, we found in 1977 that a crystal of [(*R*)-1-cyanoethyl][(*S*)-phenylethylamine]bis(dimethyl-glyoximato)cobalt(III), (*R*-1-ce)(*S*-pea)cobaloxime shown in Scheme 2.1, gradually changed its unit-cell dimensions by X-ray exposure without degradation of the crystallinity [1]. The crystal belongs to the monoclinic system and the space group is $P2_1$. Figure 2.1 shows the changes of the cell dimensions, a, b, c, β, and V, with exposure time by MoKα radiation on a four-circle diffractometer. The a and c values decreased slightly, whereas b and β increased to a considerable extent. The unit-cell volume, V, significantly increased. After 20 days exposure, the changes became within the experimental errors. The space group remained unaltered. The variation curves of the cell dimensions are well explained by first-order kinetics. The rate constants for the variations of a, b, c, β, and V were obtained by least-squares fitting, assuming first-order kinetics. The average value is 3.06×10^{-6} s^{-1}.

Y. Ohashi, *Crystalline State Photoreactions: Direct Observation of Reaction Processes and Metastable Intermediates*, DOI 10.1007/978-4-431-54373-2_2, © Springer Japan 2014

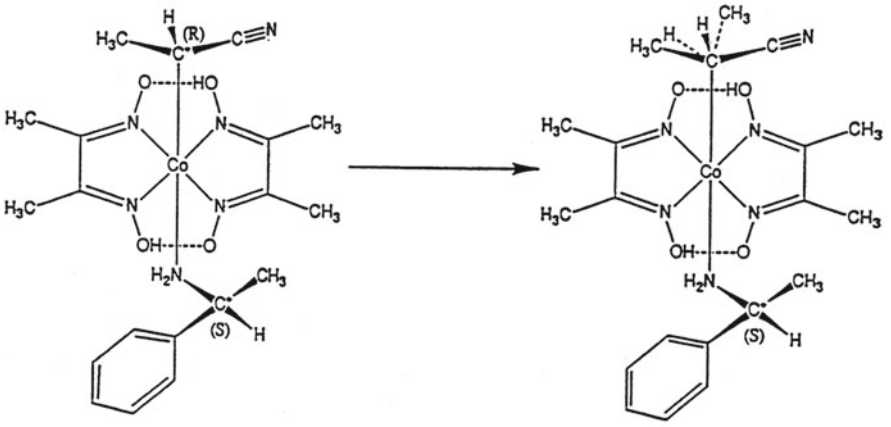

Scheme 2.1 The chiral *R*-1-cyanoethyl group in a crystal of (*R*-1-ce)(*S*-pea)-cobaloxime is racemized on exposure to X-rays or visible light without degradation of the crystallinity

In order to examine why such changes occurred, the three-dimensional intensity data were collected at seven stages, A, B, C, D, E, F, and G, indicated in Fig. 2.1, using the four-circle diffractometer [2]. Figure 2.2 shows the crystal structure viewed along the *c* axis at the stage A. There are two molecules correlated by a twofold screw axis in a unit cell. Significant change in electron density was observed only in the vicinity of *R*-1-ce group. Figure 2.3 shows the electron density map of *R*-1-ce group viewed normal to the cobaloxime plane at the initial A and final G stages. To examine the change of the electron density more precisely, the difference electron density maps at five stages from B to F were calculated, which is shown in Fig. 2.4. There appeared a trough at the position of the methyl of *R*-1-ce group and a peak in the neighborhood of the methyl group. The new peak grew higher and the trough became deeper. Finally at the stage G, a half of the methyl group was shifted to the new position as shown in Fig. 2.3b. The change of the electron density map during the reaction clearly indicated that the chiral alkyl group bonded to the cobalt atom, *R*-1-ce group, was racemized. When the crystal was irradiated with X-rays below 173 K, such a racemization was no longer observed [3]. To our knowledge, this is the first example of direct observation of the intermediate stages of a chemical reaction occurred in a crystal. Since such a solid-state reaction keeping the single crystal form from initial to final stages is very important in examining the reaction mechanism, we call the reaction "crystalline-state reaction," to distinguish it from the conventional solid-state reactions, in which the crystal is gradually decomposed during the reaction [2].

Hasegawa et al. proved in 1977 after long structural studies on polymerization of 2,5-distyrylpyradine (DSP) that the monomer crystal occurs [2+2] photocycloaddition to form the polymeric crystal with retention of the single crystal form as shown in Scheme 2.2 [4]. They found that systematically substituted diolefin crystals were polymerized into crystalline polymers as shown in Fig. 2.5 [5].

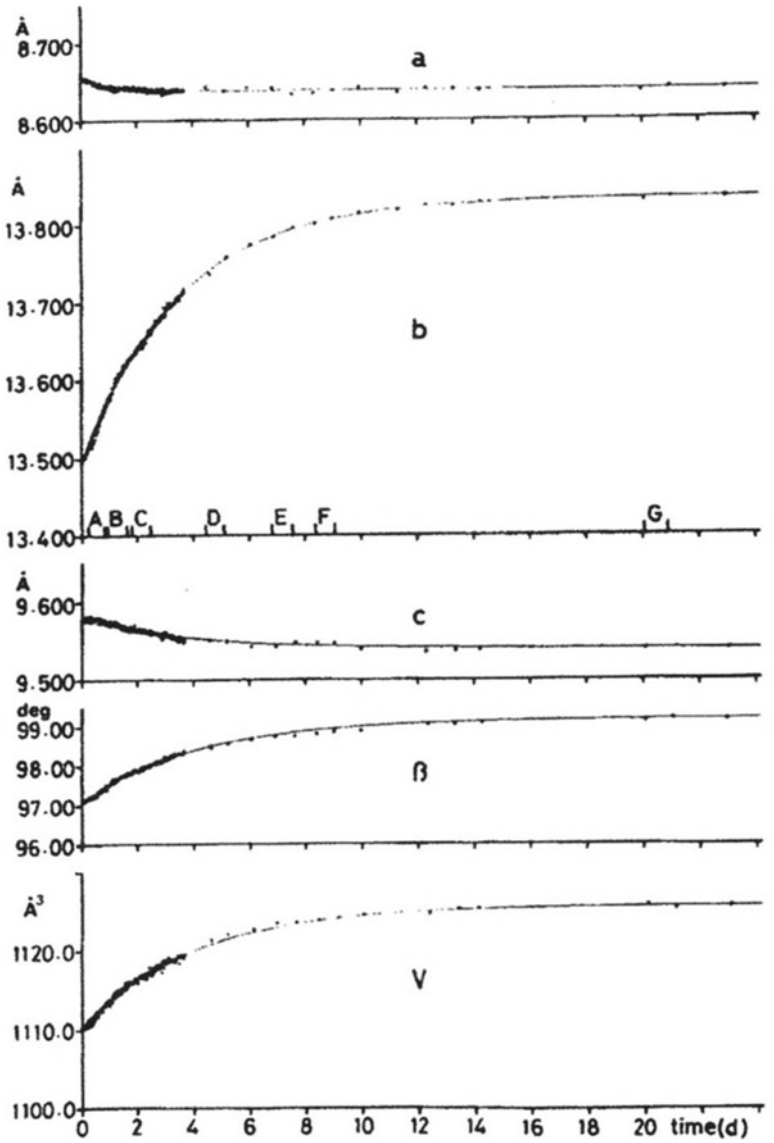

Fig. 2.1 Change of cell dimensions, a, b, c, β, and V with exposure time (d). The three-dimensional intensity data were collected at A–G stages

Since the stacking separation of the monomer in the monomer crystals is largely different from the repeating unit length of the produced polymers and the separate diffraction spots due to the monomer and polymer crystals appeared during the reaction, the change was explained as the transformation from a single crystal of the monomer to a single crystal of the polymer. Although the structures at the

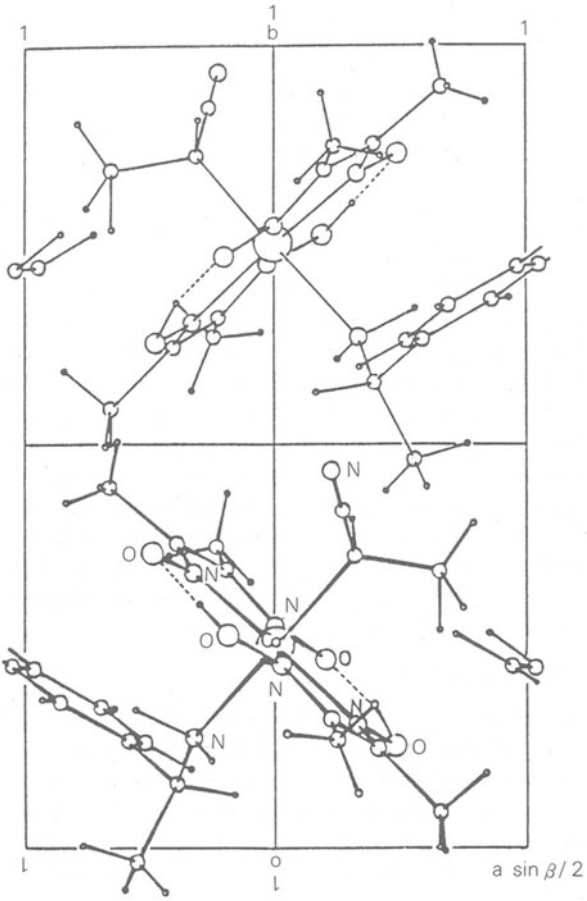

Fig. 2.2 Crystal structure viewed along the c axis at the initial stage A. Two molecules are in the $P2_1$ cell

intermediate stage cannot be observed in such a single crystal-to-single crystal (SCSC) transformation, it is easy to assume the reaction process from the two structures before and after the reaction.

Enkelmann et al. reported the monomer structure of a diacetylene derivative and made clear the mechanism of the polymerization in 1980 as shown in Scheme 2.3 [6, 7]. Since the radiation polymerization usually occurs very quickly, it was difficult to analyze both structures of the monomer and the polymer. However, the 1,6-di (*N*-carbazolyl)-2,4-hexadiyne (DCH) is stable and both the monomer and polymer crystal structures were successfully analyzed as shown in Fig. 2.6. Since the stacking distance of the monomer is 4.55 Å and the produced polymer unit is 4.91 Å, the very complicated SCSC transformation should occur in a monomer crystal.

Although it appears no clear limitation exists between the crystalline-state reaction and the SCSC transformation if there are only two states, initial and final states, during the reaction, the former reaction is completely different from the latter one. As shown in Fig. 2.1, the changes of the unit-cell dimensions in the crystalline-state photoracemization are expressed exponentially and are well explained by first-order kinetics.

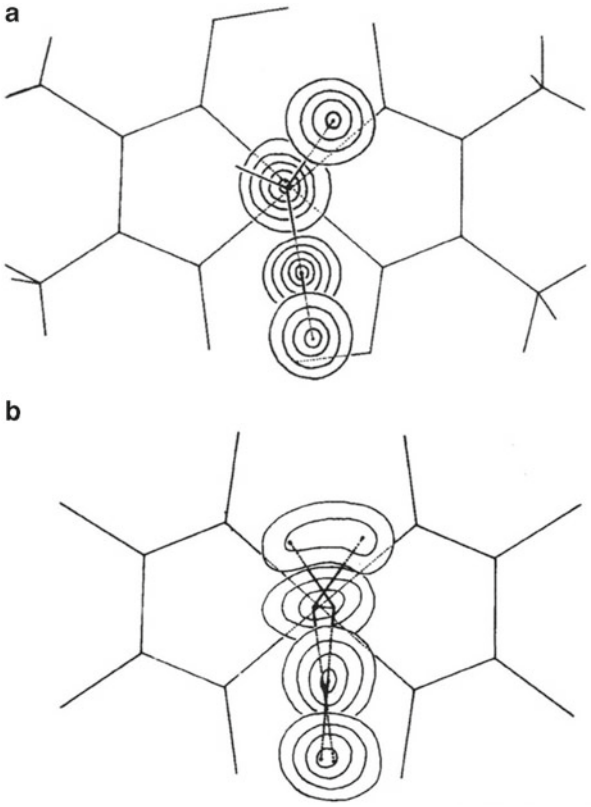

Fig. 2.3 Electron density map of *R*-1-ce group viewed normal to the cobaloxime plane, (**a**) at the initial stage A, and (**b**) at the final stage G

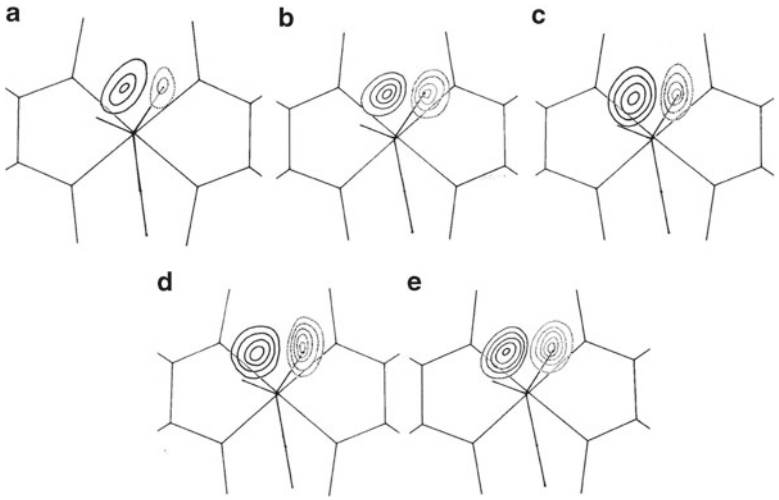

Fig. 2.4 Difference electron density maps at five stages, (**a**) B, (**b**) C, (**c**) D, (**d**) E, and (**e**) F stages. The *solid* and *dotted* curves correspond to positive and negative difference electron densities, respectively

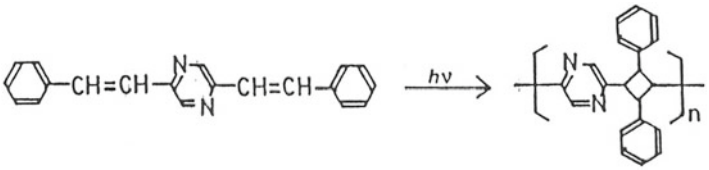

Scheme 2.2 The photo-polymerization of 2,5-distyrylpyradine

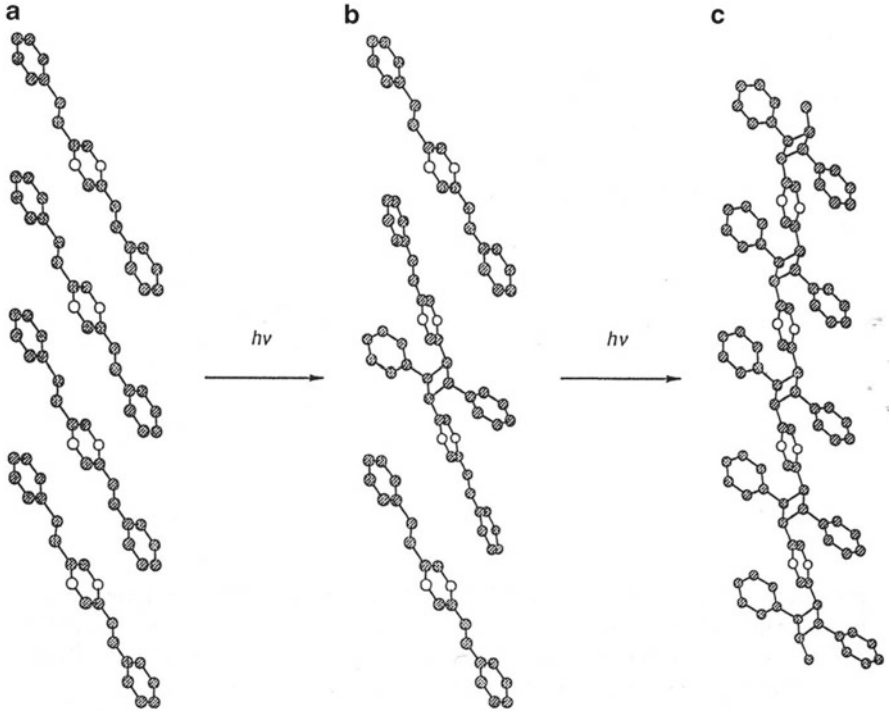

Fig. 2.5 Single crystal-to-single crystal photo-polymerization of DSP, showing (**a**) monomer, (**b**) intermediate assumed and (**c**) polymer structures

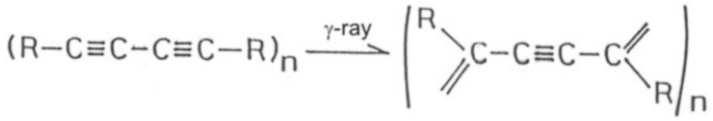

Scheme 2.3 The radiation polymerization of 1,6-di(*N*-carbazolyl)-2,4-hexadiyne

On the other hand, the change of unit-cell length of *b* during the reaction observed in the SCSC polymerization of DCH is shown in Fig. 2.7. The conversion of the monomer crystal suddenly increased after the induction period and is expressed sigmoidally as shown in Fig. 2.7a. The diffraction spots during the conversion rates between 30

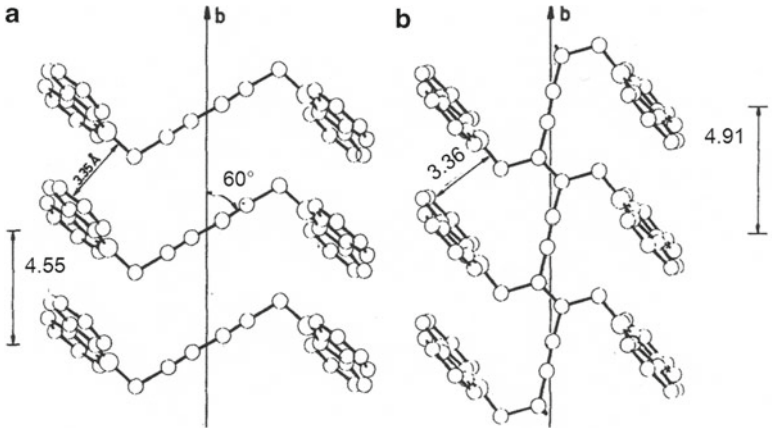

Fig. 2.6 Single crystal-to-single crystal radiation polymerization of DCH, showing (**a**) monomer and (**b**) polymer crystal structures

and 50 % disappeared as shown in Fig. 2.7b. This indicates that the lattice structure of DCH crystal was largely decomposed and the change included very complicated processes in which vapor or liquid state or dislocation may appear in the transformation from an old single crystal to a new single crystal. This may be a reason why the mechanism of the SCSC transformation is very difficult to be explained, although the result of the polymerization is clear.

If there is an intermediate state during the reaction as shown in Fig. 2.8, the intermediate structure can be observed only in the crystalline-state reaction. Several examples are shown in the following chapters. It may be adequate to classify the SCSC transformation into a reaction between the solid-state reaction and crystalline-state reaction.

Nakanishi et al. reported the [2+2] photo-dimerization of 5-benzylidenecyclopentanones in 1981 as shown in Scheme 2.4a [8]. Although the change of the unit-cell dimensions was shown in a complicated manner in their original paper, it showed first-order kinetics in the later experiment [9]. Probably the process of the dimerization should be classified into the crystalline-state reaction.

Miller et al. reported the thermal dimerization of o-benzyldithiol cobalt complex as shown in Scheme 2.4b [10]. Since the change of unit-cell dimensions and molecular transformation is too large during the reaction, the reaction should be an example of the SCSC transformation.

After these findings, a variety of crystalline-state reactions and SCSC transformation have been reported, although they are not so clearly classified into two types. We found that the crystal of an overcrowded distibene derivative, 2,4,6-tris[bis(trimethylsilyl)methyl]phenyldistibene, reacted with atmospheric oxygen gas to form a molecule with a four-membered ring composed of Sb_2O_2, as shown in Scheme 2.5. Since the unit-cell expansion is considerably large by 46.3(4) Å [3] and the cell dimensions sigmoidally increased after 30 h as shown in Fig. 2.9, the

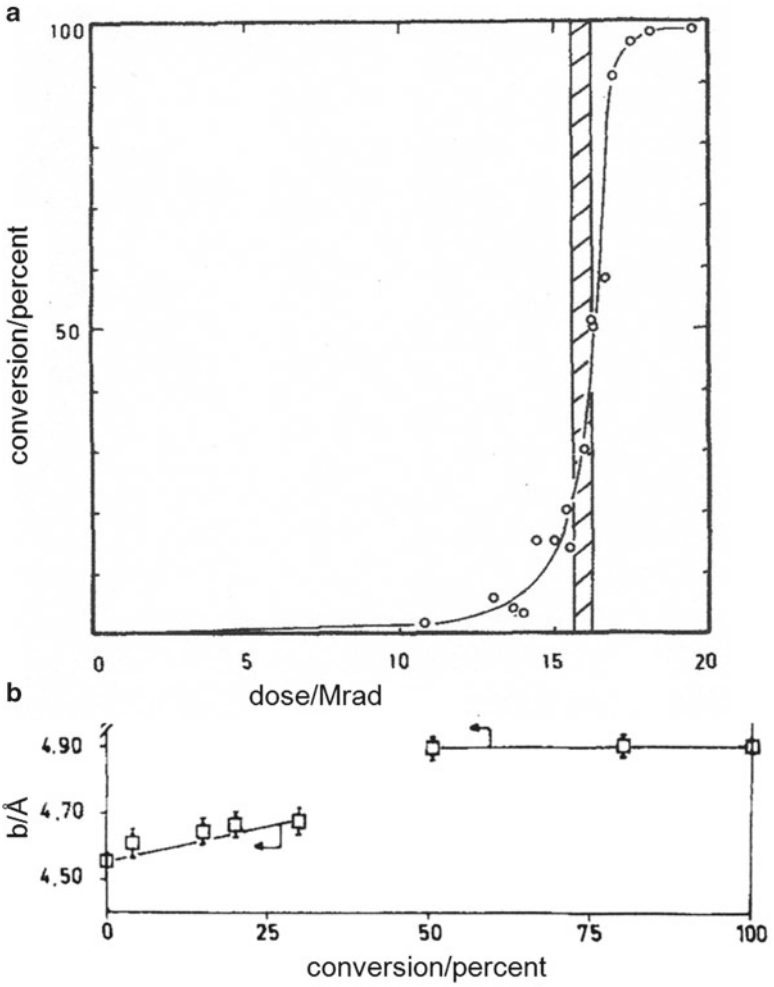

Fig. 2.7 (**a**) Change of the conversion rate with the dose quantity and (**b**) the change of the unit-cell length of *b* with the conversion rate observed in the SCSC polymerization of DCH

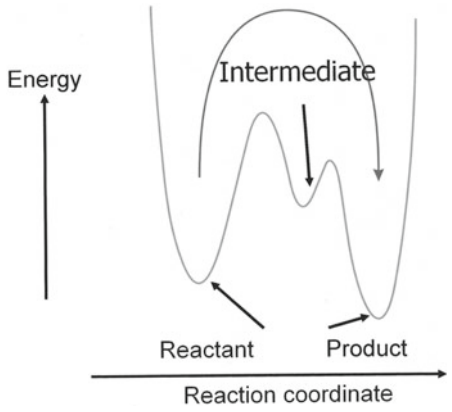

Fig. 2.8 Reaction intermediate observed in the crystalline-state reaction

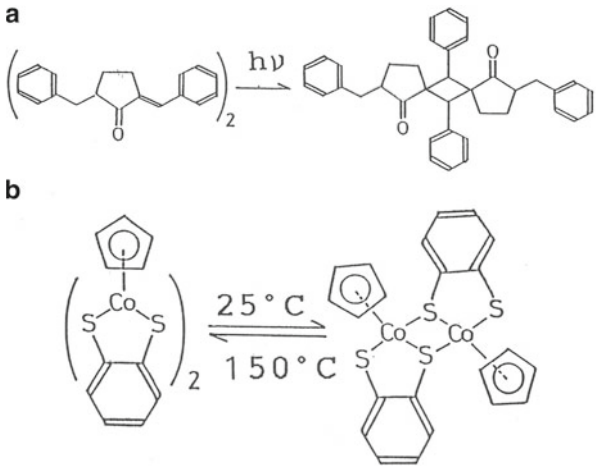

Scheme 2.4 (**a**) The [2+2] photo-dimerization of 5-benzylidenecyclo-pentanone and (**b**) the thermal dimerization of o-benzyldithiol cobalt complex

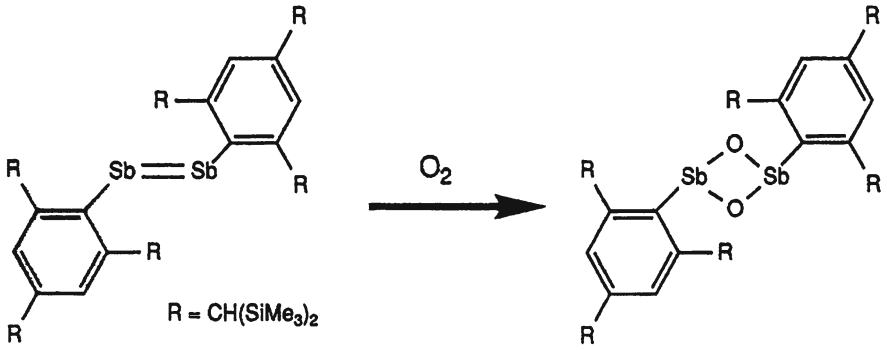

Scheme 2.5 The insertion reaction of the atmospheric oxygen gas to 2,4,6-tris[bis(trimethylsilyl) methyl]phenyldistibene

reaction should be classified into the SCSC transformation [11]. The crystal structures before and after the reaction are shown in Fig. 2.10. Recently a review on SCSC polymerization was published [12].

Recently Nakai et al. reported that the rhodium dinuclear complex crystal $[(RhCp^*)_2(\mu\text{-}CH_2)_2(\mu\text{-}O_2SSO_2)]$ (**1**) with a photo-responsive dithionite group (μ-O_2SSO_2) and two pentamethylcyclopentadienyl ligands ($Cp^* = \eta^5\text{-}C_5Me_5$) undergoes a 100 % reversible unimolecular photochromism upon interconversion to $[RhCp^*]_2(\mu\text{-}CH_2)_2(\mu\text{-}O_2SOSO)]$ (**2**), as shown in Scheme 2.6. They claimed that the reversible reaction should be assigned to a crystalline-state reaction. Although the irradiation time-resolved UV-vis spectra of the powdered sample of **1** indicated a gradual change to **2**, the reaction cannot be assigned to the crystalline-state reaction because the gradual change of the cell dimensions was not shown [13, 14].

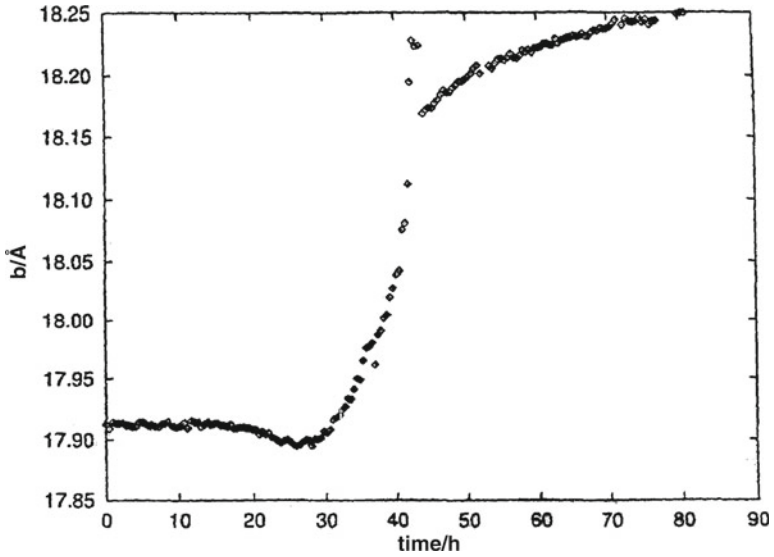

Fig. 2.9 Sigmoidal change of the cell dimension of b in the SCSC oxygen insertion reaction of a distibene derivative crystal

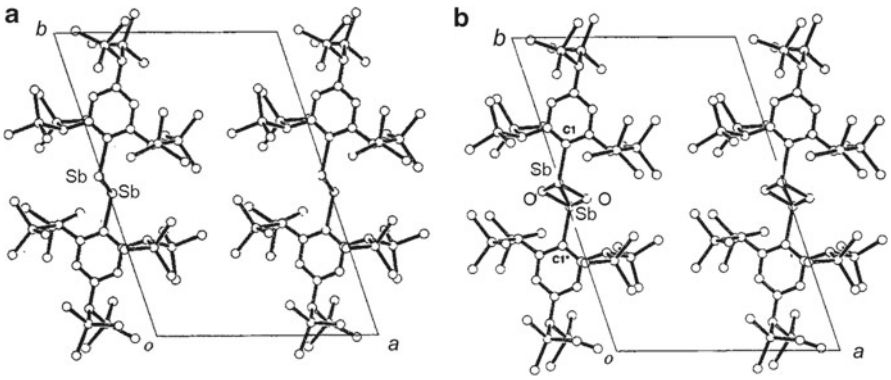

Fig. 2.10 Crystal structures (**a**) before and (**b**) after the oxygen insertion reaction of the distibene crystal

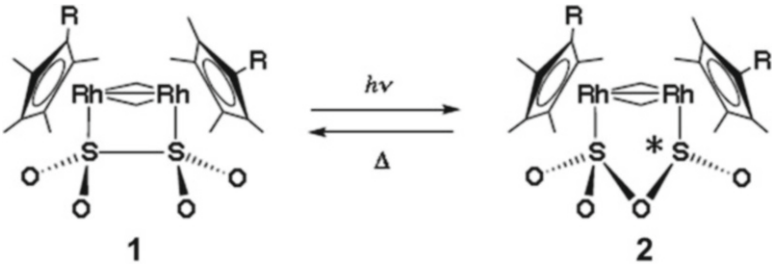

Scheme 2.6 Reversible photoreaction between (1) and (2)

2.2 Concept of Reaction Cavity

Although the prediction of the crystal structure from the theoretical calculation has not been solved yet, it seems possible to predict the reaction process from the crystal structure of reactant molecule, since the product molecule should be made suffering from steric repulsion in the crystalline lattice of the reactant crystal. The term of reaction cavity was first proposed by Lee and Richards to interpret the reaction region within the enzyme molecule [15]. Cohen proposed a qualitative concept of the reaction cavity, as shown in Fig. 2.11 [16]. He proposed that since the reacting molecules occupy a space of a certain size and shape in the starting crystal, the reaction cavity is surrounded by the contact surface of the surrounding molecules. The topochemical principle can be interpreted to mean that those reactions which proceed under lattice control do so with minimum distortion of the surface of the reaction cavity. Therefore, the reaction of the route (a) is more favorable than that of (b).

We proposed the reaction cavity more precisely and quantitatively [2].

Since the crystalline-state reaction proceeds in a crystal with retention of the single crystal form, it should be an essential factor for the reactive group to have a void space around the group. The reaction cavity proposed by us is to estimate the void space around the reactive group in the starting crystal. The volume of the void space, not the minimum distortion at the transition state, should control the reactivity of the crystal. As shown in Fig. 2.12, the cavity is defined as the concave space limited by the envelop surface of the spheres, whose centers are positions of intra- and intermolecular atoms in the neighborhood of the reactive group and the radius of each sphere is greater by 1.2 Å than the van der Waals radius of the corresponding atom. Since the surface of the reactive group is usually covered with the hydrogen atom with the van der Waals radius of 1.2 Å, any point in the cavity is then considered to be accessed by the centers of atoms of the reactive group. The volume of the cavity can easily be calculated. Figure 2.13a–c shows the reaction cavities for the *R*-1-ce group viewed normal to the cobaloxime plane in the initial structure before photo-irradiation at 293 and 173 K and the corresponding one in the final structure after photo-irradiation at 293 K, respectively. When the crystal was cooled down to 173 K, the cavity size clearly decreased and the reaction was not observed.

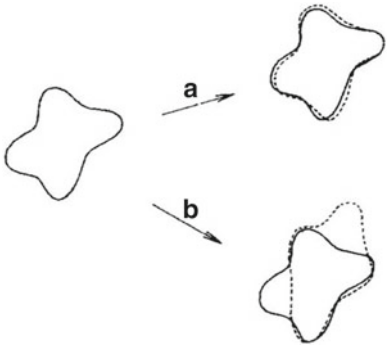

Fig. 2.11 Reaction cavity before reaction (*full line*) and at the transition state (*broken line*) (**a**) for energetically favorable and (**b**) for energetically unfavorable reactions

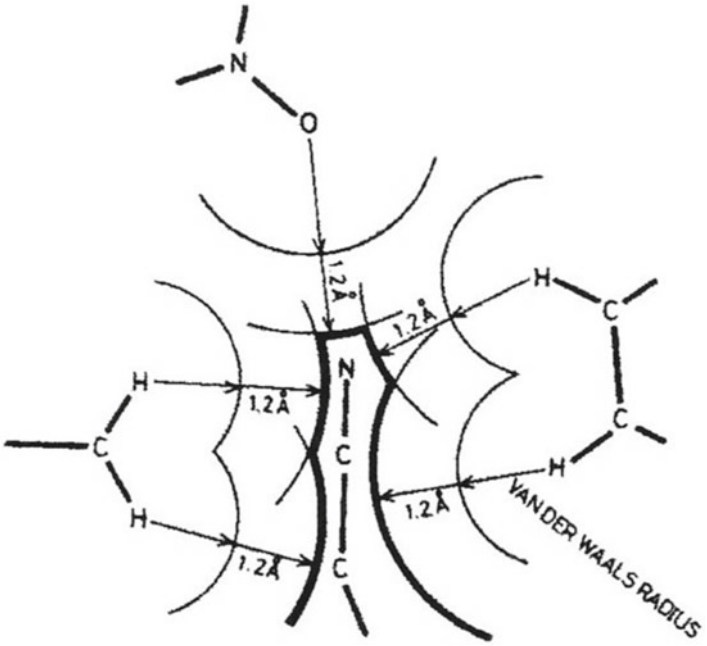

Fig. 2.12 One section of the reaction cavity. The spheres are drawn from the center of the atoms in the neighborhood of the reactive group. The radius of each sphere is greater by 1.2 Å than the van der Waals radius of the corresponding atom

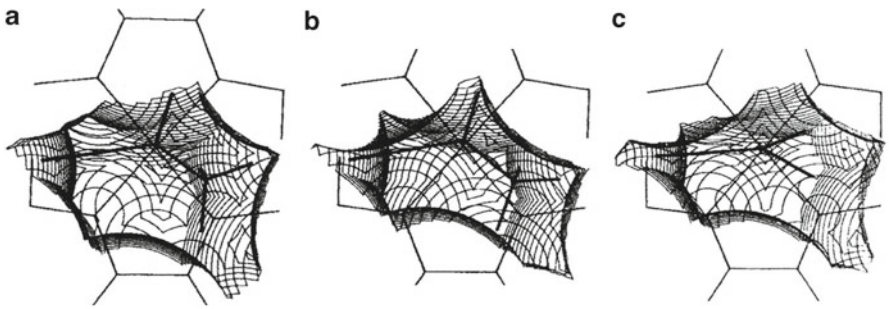

Fig. 2.13 Composite reaction cavities for *R*-1-ce group viewed normal to the cobaloxime plane, (**a**) before irradiation at 293 K, (**b**) before irradiation at 173 K, and (**c**) after irradiation at 293 K

The reaction cavities of Fig. 2.13a–c are compared in Fig. 2.14 in which the cobaloxime plane is fixed in the same position and only peripheral curves of the cavities are drawn. The solid, dotted, and dot and dashed curves indicate the peripheral ones before photoreaction at 293 and 173 K and after photoreaction at 293 K, respectively. There are two void spaces, (A) and (B), in the cavity before photoreaction at 293 K, compared with the cavity at 173 K. The void space of (B) disappears and is

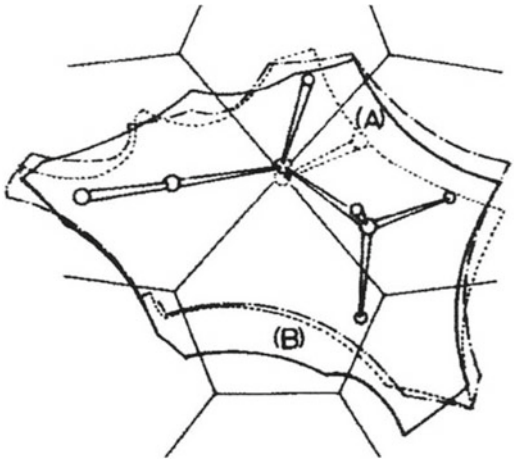

Fig. 2.14 Comparison of the three reaction cavities. The *solid*, *dotted*, and *dot* and *dashed curves* indicate the peripheral ones before photoreaction at 293 and 173 K and after photoreaction at 293 K, respectively. There are two void spaces, (A) and (B), in the cavity before photoreaction at 293 K, compared with the cavity at 173 K

transferred and added to the void space (A) in the cavity after photoreaction, in which the methyl group of the photo-produced *S*-1-ce group is accommodated. The composite reaction cavity shown in Fig. 2.14 corresponds to that proposed by Cohen as shown in Fig. 2.11. But the composite reaction cavity is not an ideal space but a real space calculated from the crystal structures before and after the reaction.

Although the composite reaction cavity in Fig. 2.14 is very important in explaining the reaction mechanism, it cannot be obtained for the conventional solid-state reactions. However, the reaction cavity before reaction as shown in Fig. 2.13a can clearly indicate where the void space is and how the reactive group can move in the void space.

The similar quantitative concepts of reaction cavities were proposed independently by Arad-Yellin et al. [17] and by Gavezzotti [18]. Ariel et al. proposed another approach [19]. McBride proposed the steric compression [20]. Luty and Eckhardt developed the theory of chemical pressure by introducing crystal elasticity into it [21]. They asserted that elastic multipoles are ideal for description both the geometry and energies of the reaction cavity. A concept of a mini-crystal lattice was introduced by Zimmerman and Zhu [22]. A mini-crystal, although simple, contains essential information concerning the real crystal structure. A computer program was developed to generate a mini-crystal lattice having a central molecule surrounding by reactant molecules with the appropriate space group symmetry and X-ray coordinates. Replacement of the central molecule with a transition state molecule provided a new mini-lattice. A test utilizing the MM3 program for geometry optimization of the reacting species imbedded in the rigid mini-lattice provided a measure of the increase in intra- and intermolecular energy of this molecule.

In the above empirical and semi-empirical consideration in the solid-state reactions the intermolecular interaction is represented by the atom–atom potential energy. Since the reactive group is, in general, very closely packed in the crystalline lattice, the reaction cavity proposed by us may be enough to estimate the reaction process in the solid state.

References

1. Ohashi Y, Sasada Y (1977) Nature 267:142
2. Ohashi Y, Yanagi K, Kurihara T, Sasada Y, Ohgo Y (1981) J Am Chem Soc 103:5805
3. Ohashi Y, Sasada Y, Ohgo Y (1978) Chem Lett 457
4. Nakanishi H, Hasegawa M, Sasada Y (1977) J Polym Sci Polymer Phys Ed 15:173
5. Hasegawa M (1995) Adv Phys Org Chem 30:117
6. Enkelmann V, Schleier G, Wegner G, Eichele H, Schwoerer M (1977) Chem Phys Lett 52:314
7. Enkelmann V, Leyrer RJ, Schleier G, Wegner G (1980) J Mater Sci 15:168
8. Nakanishi H, Jones W, Thomas JM, Hursthouse MB, Motevalli M (1981) J Phys Chem 85:3636
9. Honda K, Nakanishi F, Feeder N (1999) J Am Chem Soc 121:8246
10. Miller E, Brill TB, Rheingold AL, Fultz WC (1983) J Am Chem Soc 105:7580
11. Tokitoh N, Arai Y, Sasamori T, Okazaki R, Nagase S, Uekusa H, Ohashi Y (1998) J Am Chem Soc 120:433
12. Lauher JW, Fowler FW, Goroff NS (2008) Acc Chem Res 41:1215
13. Nakai H, Mizuno M, Nishioka T, Koga N, Shiomi K, Miyano Y, Irie M, Breedlove BK, Kinoshita I, Hayashi Y, Ozawa Y, Yonezawa T, Toriumi K, Isobe K (2006) Angew Chem Int Ed 45:6473
14. Nakai H, Nonaka T, Miyano Y, Mizuno M, Ozawa Y, Toriumi K, Koga N, Nishioka T, Irie M, Isobe K (2008) J Am Chem Soc 130:17836
15. Lee B, Richards FM (1971) J Mol Biol 55:379
16. Cohen MD (1975) Angew Chem Int Ed 14:386
17. Arad-Yellin R, Brunie S, Green BS, Knossow M, Tsoucalis G (1979) J Am Chem Soc 101:7529
18. Gavezzotti A (1983) J Am Chem Soc 105:5220
19. Ariel A, Askari S, Evans SV, Hwang C, Jay J, Scheffer JR, Trotter J, Walsh L, Wong YF (1987) Tetrahedron 43:1253
20. McBride JM (1983) Acc Chem Res 16:304
21. Luty T, Eckhardt CJ (1995) J Am Chem Soc 117:2441
22. Zimmerman HE, Zhu Z (1995) J Am Chem Soc 117:5245

Chapter 3
Racemizations of Alkyl Groups in Cobaloxime Complex Crystals

Abstract The mechanism of racemization was examined with theoretical calculation and neutron diffraction. Various racemization processes were observed changing the axial base ligand and chiral alkyl group in the crystals of cobaloxime complex crystals. For racemization of the cyanoethyl group bonded to the cobalt atom, three different types of racemization were observed owing to the different structures before the reaction. The reaction process and the reaction rate are well explained by the size and shape of the reaction cavity. Moreover, the unusual racemic-to-chiral transformation was made clear using the size and shape of the reaction cavity. For the bulkier (methoxycarbonyl)ethyl groups, not only the inversion of the chiral carbon atom bonded to the cobalt atom but also the *anti-to-syn* transformation of the methoxyl group occurs cooperatively. Moreover, solvent molecules in a crystal play an important role in racemization.

Keywords Photo-racemization • Reaction rate • Racemic-to-chiral transformation • *Anti-to-syn* transformation • Neutron diffraction

3.1 Racemization of 1-Cyanoethyl (1-ce) Group

3.1.1 Co–C Bond Cleavage

It was assumed that the Co–C bond should be cloven by X-rays in racemization of the 1-ce group. This is because an ESR signal due to the cyanoethyl radical formation [1–3] was observed on exposure to X-rays and the rate of racemization was too late when the crystal was not exposed to X-rays. However, it was found that the cell dimensions changed significantly faster than before when a small lamp used for centering of the crystal was kept on. This result clearly indicated that the visible light is more effective than X-rays to cleave the Co–C bond with retention of the single crystal form. When the crystal was irradiated with a xenon lamp, the similar ESR signal was observed.

Y. Ohashi, *Crystalline State Photoreactions: Direct Observation of Reaction Processes and Metastable Intermediates*, DOI 10.1007/978-4-431-54373-2_3, © Springer Japan 2014

In the experiments at early days, the crystal on the diffractometer was irradiated by a weak room light in addition to X-rays and the change of cell dimensions were measured on the diffractometer [4]. The reaction rate was so slow (more than 20 days) that it was possible to check the change of cell dimensions and to take the three-dimensional intensity data using a four-circle diffractometer. Such a slow reaction rate, however, was very important to discover the crystalline-state reaction.

After the finding that racemization is more effectively performed on exposure to visible light, a crystal mounted on the diffractometer was exposed to a xenon lamp through a glass fiber and the diffractometer was covered with black sheets to shut out the room light, because the reaction rate by the xenon lamp is significantly faster (2 or 3 days) than before (room light + X-rays, 2 or 3 weeks). Usually a pair of filters to cut off the light with short wavelengths and infrared rays were inserted between the crystal and the top of the glass fiber, since the longer wavelengths are more effective for the photoreaction in the solid state [5, 6], but the infrared rays heat up the crystal.

When it was necessary, however, to compare the reaction rate with those observed by a room light and X-rays at early days, the photoreaction was performed under the same conditions as before.

The Co–C bond dissociation energy of the cobaloxime complexes has systematically been studied spectroscopically [7].

3.1.2 Motion of the Cyanoethyl Radical by Theoretical Calculation

The motion of the cyanoethyl radical in the crystalline lattice was theoretically calculated [8]. The program OPEC (organic packing energy calculation) was used [9], in which the packing potential energy (PPE) was estimated as a sum of Buckingham-type atom–atom potential energy. The cutoff value of the interatomic distances was taken to 7 Å. No electrostatic contributions and energy changes associated with the cleavage and formation of the Co–C bond were included in the calculation. Three parameters, Δl, θ_1, and θ_2, were systematically changed, which are shown in Fig. 3.1. Although another parameter, a pyramidal form of the radical, was introduced to find out the minimum energy, it may be adequate to consider only the planar conformation even if the radical was created in the crystalline lattice.

The energies were calculated at all the grid points of the adequate intervals for the three parameters. The minimum energy valley was obtained when the planar cyanoethyl radical rotated clockwise around the C–C–N bond, changing θ_2. The rotation angle around the Co–C bond, θ_1, was zero and the elongation of the Co–C bond was about 0.8 Å. Figure 3.2 shows the minimum energy path in the rotation around the C–C–N bond. At $\theta_2 = 100°$, the radical turns its methine H atom toward the cobalt atom, where the PPE energy becomes a maximum, where it is higher by ca. 4.8 kJ mol^{-1} than the energy at the initial $\theta_2 = 0°$ and final 180° positions. Since the bond dissociation energy is ca. 6.9 kJ mol^{-1}, the radical can go over the energy pass.

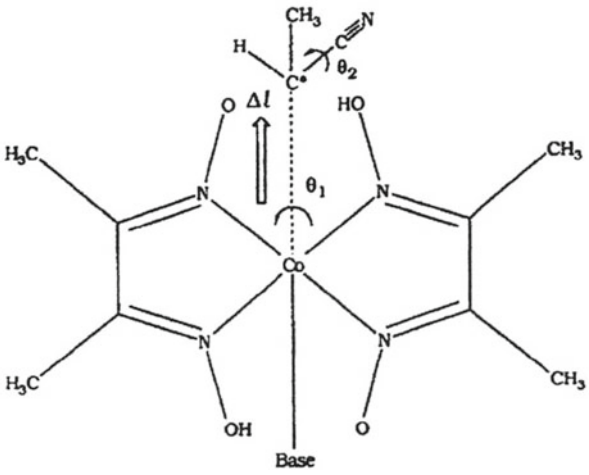

Fig. 3.1 Parameters of Δl, θ_1, and θ_2 for the theoretical calculation using OPEC program

Although this calculation seems to be oversimplification, the movement of the cyanoethyl radical is clearly shown in a crystal environment composed of the initial crystalline lattice. The packing energy calculation may be a very convenient method if we want to know more detailed information than that estimated from the reaction cavity in the solid-state reactions.

3.1.3 Mechanism by Neutron Diffraction

The above calculation made clear the inversion mechanism of the cyanoethyl group in the following three steps: the hemolytic cleavage of Co–C bond by photo-irradiation, the rotation of the resulting cyanoethyl radical to invert the radical face upside down, and the recombination of the radical with the cobalt atom. However, the mechanism of the reaction remains unsolved because there is little knowledge on the migration of H atoms in the reaction process. To answer the question, it is necessary to observe the crystalline-state reactions using the neutron diffraction technique. The neutron diffraction distinguishes between H and D atoms, because H atom has negative scattering length while D has positive one. If the methine H atom of the cyanoethyl group is replaced with the D atom and the crystal is irradiated with visible light, the structure after photo-irradiation clearly indicates the movement of the methine D atom. If the D atom is observed in the same position of the inverted group as that of the original one after photo-irradiation, the above mechanism should be confirmed.

However, the neutron diffraction analysis of the crystal after photo-irradiation has two difficulties: (1) a very large crystal (>5 mm^3) is required due to the weak intensity of the neutron beam and (2) the visible light must penetrate into the crystal and the photoreaction must occur uniformly inside the crystal without deteriorating the crystallinity.

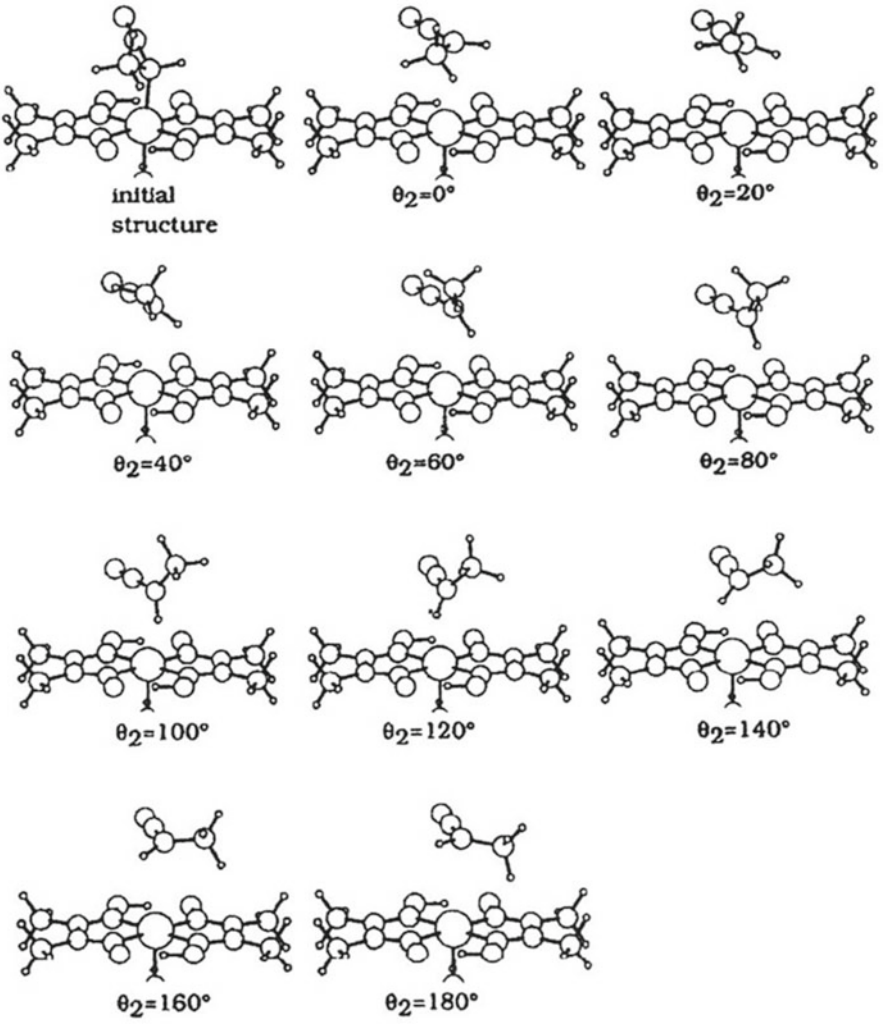

Fig. 3.2 Minimum energy path in the rotation around the C–C–N bond

The crystals of the deuterated pyridine and piperidine complexes [*R*-1-cyanoethyl-d$^{\alpha}$](pyridine)cobaloxime and [*racemic*-1-cyanoethyl-d$^{\alpha}$]-(piperidine) cobaloxime were prepared. Each complex has two crystallographically independent molecules, A and B, in an asymmetric unit and only the 1-ce group of B is inverted to the opposite configuration, while the 1-ce group of A remains unaltered. It was already observed by X-ray analysis that the 1-ce group of B in the pyridine complex was completely inverted to the opposite configuration, whereas a half of the 1-ce group of B in the piperidine complex was inverted.

A crystal of $3.0 \times 3.0 \times 0.6$ (~5.4) mm^3 was prepared for the pyridine complex and the crystal was irradiated with a fluorescent lamp for 36 h, while a crystal of

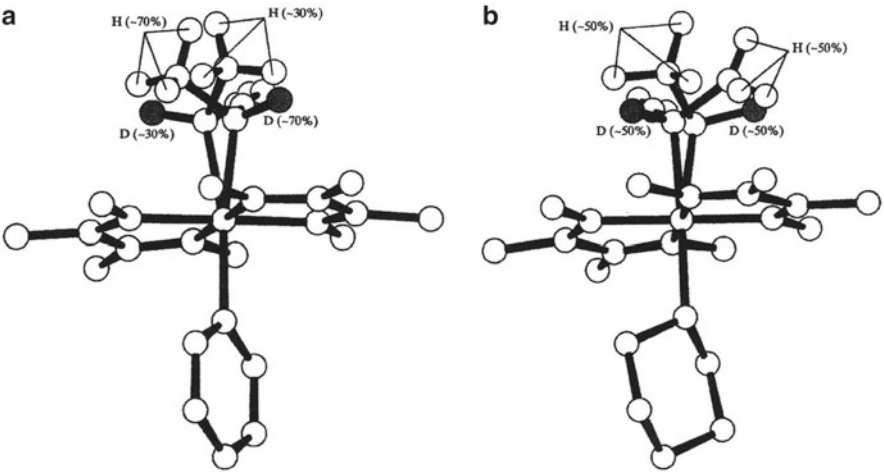

Fig. 3.3 Molecular structures of B after irradiation in the crystals of (**a**) pyridine and (**b**) piperidine complexes

$3.0 \times 3.0 \times 1.0$ (~9.0) mm^3 was exposed to a xenon lamp for 28 days for the piperidine complex [10]. The intensity data were collected on the BIX-1 diffractometer at the JRR-3M reactor of the Japan Atomic Energy Research Institute (JAERI). The crystal structures of the pyridine and piperidine complexes after photo-irradiation determined by neutron diffraction are essentially the same as those by X-ray diffraction.

The A molecules of the two crystals remained unaltered and have the R configuration. The D atom attached to the chiral carbon atom remained unaltered. No H/D exchange with the methyl hydrogen atoms was observed in the 1-ce group of A. The molecular structures of B in the pyridine and piperidine complex crystals are shown in Fig. 3.3a, b, respectively. For the pyridine complex, about 30 % of the 1-ce group of B is inverted to the opposite S configuration. Probably the exposure time was too short to invert the 1-ce group of B completely to the opposite configuration as observed in the X-ray experiment. The original 1-ce group with 70 % composition has D atoms completely at the original position and the inverted 1-ce group with 30 % composition has D atoms at the inverted position. No H/D exchange with the methyl hydrogen atoms was observed in the 1-ce group of B.

For the piperidine complex, almost 50 % of the 1-ce group of B was inverted to the opposite R configuration. The D9 atom is completely bonded to the chiral carbon atom, C9. No H/D exchange with the methyl hydrogen atoms was observed in the 1-ce group of B.

Four 1-ce groups in the two crystals, two A and two B, showed no hydrogen migration with the methyl hydrogen atoms during the photo-irradiation. It is clear that the inversion of the 1-ce group proceeds through the three steps: the Co–C bond cleavage, the rotation of the cyanoethyl radical, and the recombination of the radical with the Co atom.

3.1.4 Three Modes of Racemization

It must be emphasized why such crystalline-state reactions of cobaloxime complexes are interesting from a chemical point of view. As shown in Fig. 2.2, the *R*-1-ce group and the axial amine are surrounded by the rigid equatorial ligands. Since the movement of the photo-produced alkyl radical is limited or controlled by the neighboring amine and the surrounding equatorial ligands in the original crystal, it may be possible to observe the different reaction pathways changing the alkyl group, axial amine, and equatorial ligands with the related ones. The photo-irradiation to break the Co–C bond is an initiator of the radical motion. The radical may change to more stable form and remake a bond with the cobalt atom. After many times of bond breaking and formation, the alkyl group will reach the most stable form in the crystal lattice. This is very similar to the processes in the catalytic and enzymatic reactions. We can "observe" the process by X-ray analysis even if it is strange or complicated. It may be possible to slow down the reaction rate at low temperatures if the rate is too fast.

In order to analyze the crystalline-state racemization of the 1-cyanoethyl group more systematically, a variety of cobaloxime complex crystals with different axial base ligands were prepared. Sixteen amines and phosphines were used, as shown in Scheme 3.1, for the axial base ligands: **1**, *S*-1-phenylethylamine [11], *S*-pea; **2**, *R*-pea [12, 13]; **3**, pyrrolidine [14, 15], pyrr; **4**, dimethylphenylphosphine [16, 17], dmpp; 5, triphenylphosphine [18], tpp; 6, tributylphosphine [18], tbp; **7**, diphenylethylphosphine [19], dpep; **8**, diethylphenylphosphine [19], depp; **9,** pyridine [20], py; **10**, 4-cyanopyridine [21], 4cnpy; **11**, 4-methylpyridine [22], 4mpy; **12**, diphenylmethylphosphine [23], dpmp; **13**, 3-methylpyridine [24], 3mpy; **14**, tri(p-chlorophenyl)phosphine [25], tclpp; **15**, piperidine [26], pip; and **16**, 3-hydroxypyridine, [27] 3hpy. The crystal structure analyses of the complex crystals with the amines and phosphines revealed that the crystals with the axial base ligands of **1– 8** have only one molecule per asymmetric unit ($Z' = 1$). The space groups of the crystals are $P2_1$ and $P2_12_12_1$. The 1-ce group in each crystal, therefore, is surrounded by the moieties other than the 1-ce groups of the neighboring molecules. This means that each photoactive 1-ce group is isolated from the other 1-ce groups of the neighboring molecules in the crystal. The crystals with **1**, **2, 3,** and **4** among the eight crystals showed crystalline-state racemization. The ordered 1-ce groups were gradually changed to the disordered racemates. The other crystals with **5**–**8** showed no change at room temperature. This mode of racemization is classified as the first mode.

The crystals with the axial base ligands of **9–16** have two crystallographically independent molecules, A and B, in the asymmetric unit ($Z' = 2$). Among of them, the crystals with **9–11** showed a similar type of racemization. For the crystal with pyridine as an axial base ligand, **9**, the initial structure is shown in Fig. 3.4a. The space group is $P2_1$ and there are two molecules in an asymmetric unit. Two molecules are related by a pseudo inversion center between the two molecules. When the crystal was exposed to X-rays, the volume of the unit cell gradually contracted.

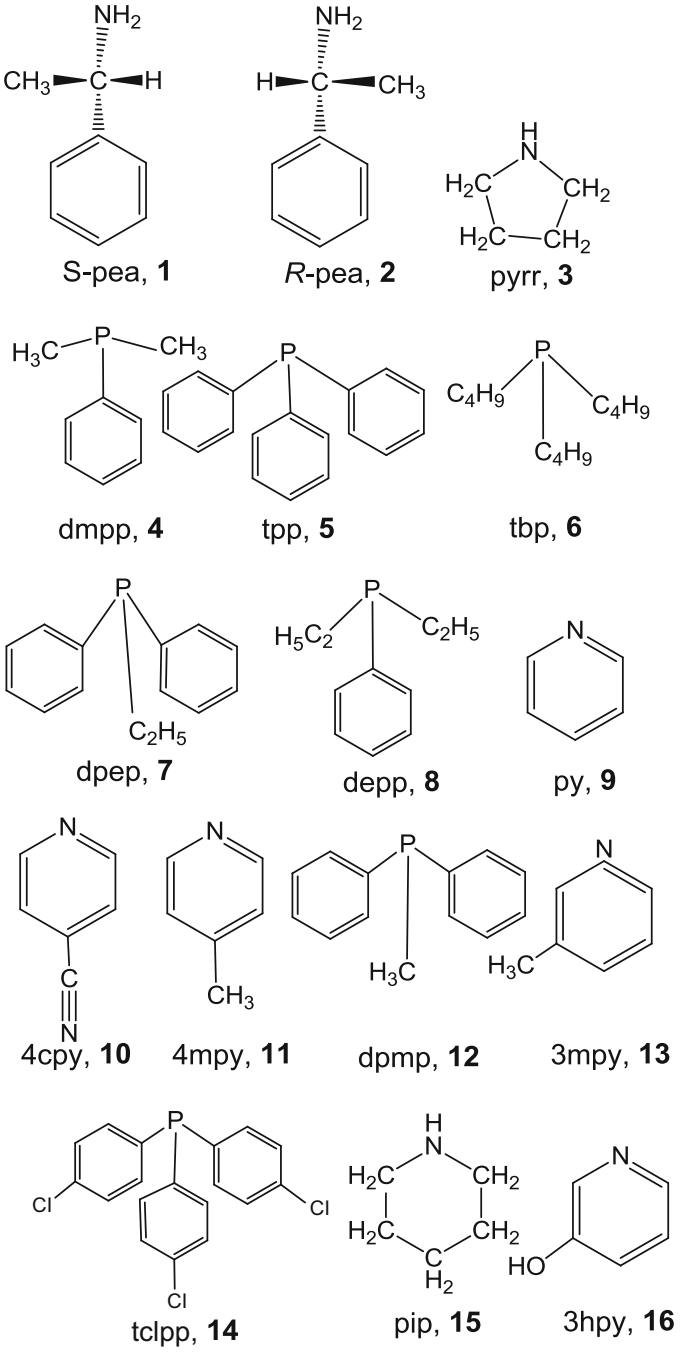

Scheme 3.1 Sixteen axial base ligands for the cobaloxime complexes

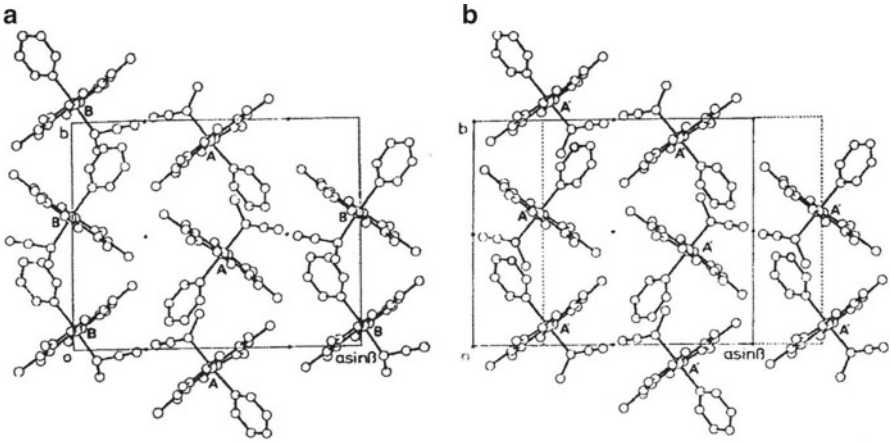

Fig. 3.4 Crystal structure viewed along the *c* axis, (**a**) before and (**b**) after the irradiation. The *dotted lines* in (**b**) indicate the unit cell of the initial one

Moreover, the intensities of h0l reflections with h+l=odd gradually decreased and became zero at the final stage. This means that the space group changed from $P2_1$ to $P2_1/n$. The structure at the final stage is shown in Fig. 3.4b. The 1-ce group of the B molecule is completely inverted to the opposite configuration, whereas the 1-ce group of A remains unaltered and the pseudo inversion center became a crystallographic one. The racemization proceeded with the order-to-order transformation of the 1-ce group. However, the 1-ce group of B showed a disordered structure at the intermediate stages. The photo-produced racemic crystal is the same as that obtained from an aqueous methanol solution including the racemic complex. For the crystals with **10** and **11**, the same order-to-order racemization as that with **9** was observed, although the space group was changed from $P2_1$ to $P2_1/a$ for **10** and from $P1$ to $P1$- for **11**. This mode of racemization is classified as the second mode.

The crystal of **12** and **16** also underwent racemization. At the initial stage, two crystallographically independent molecules, A and B, are related by a pseudo inversion symmetry, which became a crystallographic one at the final stage. The space groups of **12** and **16** changed from the non-centrosymmetric $A2$ and $P1$ to centrosymmetric $A2/a$ and $P1$-, respectively. Although this change is similar to the second mode observed in the pyridine complex, both of the 1-ce groups of A and B were transformed to the disordered racemates in these crystals. Such a transformation is a combined one of the first and second modes and is classified as the third mode. The three modes of racemization are schematically drawn in Fig. 3.5.

3.1.5 Reaction Rate and Reaction Cavity

Before we examine the racemization processes of the crystals of **13**, **14**, and **15**, it is necessary to explain the reason why the crystalline-state racemization shows the

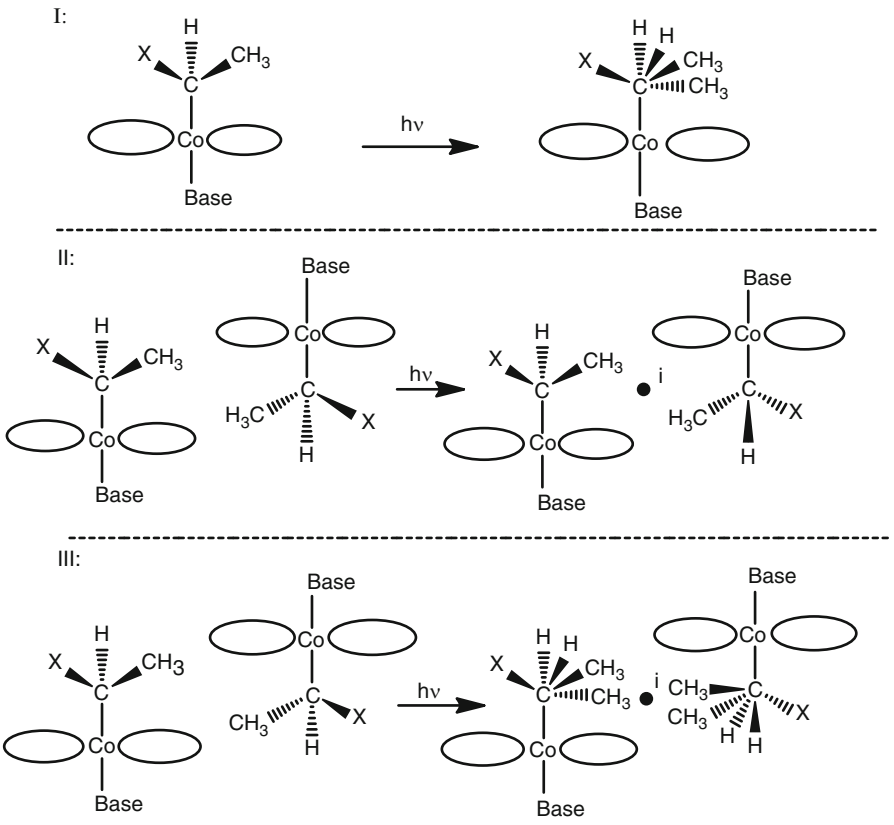

Fig. 3.5 Three modes of racemization observed in the cobaloxime complex crystals

different three modes and the reaction rates of racemization are so different among the related crystals.

In the racemization process, the Co–C bond was cloven homolytically to produce the cyanoethyl radical and the Co(II) complex. The Co–C bond dissociation energy for these cobaloxime complexes was estimated to be 117–122 kJ mol^{-1} [28]. The racemization rate of the complex crystal by X-rays is far lower than that by visible light not only in the solid state but also in an aqueous methanol solution [20]. It seemed adequate to consider that the secondary radiation produced by the interaction with the Co atom may be responsible for the cleavage of the bond.

The crystals of **1**–**8** have only one molecule per asymmetric unit. The space groups of the crystals are $P2_1$ and $P2_12_12_1$. This means that each 1-ce group in the crystal is mostly surrounded by the moieties other than the 1-ce groups of the neighboring molecules and each is isolated from the other 1-ce groups. Table 3.1 lists the reaction rates of the eight crystals classified into the first mode, which were obtained from the changes of the cell dimensions, assuming first-order kinetics.

Table 3.1 Rate constant of racemization, cavity volume, and density at room temperature for the first mode crystals

Crystal	Rate constant ($\times 10^{-6}$ s^{-1})	Volume (Å^3)	Density (g cm^{-3})
dmpp, **4**	4.80	17.4	1.403
S-pea, **1**	3.06	14.5	1.388
R-pea, **2**	2.10	12.2	1.391
pyrr, **3**	1.69	11.6	1.422
tpp, **5**	–[a]	11.3	1.431
tbp, **6**	–[a]	10.6	1.255
dpep, **7**	–[a]	10.2	1.405
depp, **8**	–[a]	8.4	1.381

[a]The racemization was not observed at room temperature

Crystalline-state racemization was observed for the crystals of **1**, **2, 3**, and **4**, although the reaction rates were different from each other. The rate constants of **1–3** crystals were obtained by the change of the cell dimensions, whereas the rate constant of **4** was deduced from the change of occupancy factor of the original 1-ce group since the crystal **4** showed small and slow changes of the cell dimensions. The other four, **5**, **6**, **7**, and **8**, were inactive at room temperature. Such differences in reactivity should be due to differences in the packing of molecules in the crystals. However, there appears to be no correlation between the reactivity and the density of the crystal. In spite of having the lowest density, the crystal of **6** was not racemized. These facts suggest that the packing around the reactive 1-ce group, not the packing of the whole molecule, plays an important role in determining the reactivity.

In order to represent the degree of packing around the reactive group, the reaction cavity described in Chap. 2 was applied. The cavity volumes are listed in Table 3.1. The larger is the volume of the cavity, the greater is the reaction rate. The volume necessary for racemization appears to be greater than 11.5 Å^3 at room temperature. These facts suggest that the cavity size for the reactive group should be a good criterion for racemization.

3.1.6 Second and Third Modes of Racemization

Each of the cobaloxime complex crystals, **9–12**, contains two crystallographically independent molecules, A and B, in an asymmetric unit. The reaction cavities for the 1-ce groups of A and B and the racemization rates are listed in Table 3.2. For the crystals of **9–11**, which are classified in the second mode, the 1-ce group of A retained unaltered whereas the 1-ce group of B was inverted completely to the opposite configuration and the crystallographic inversion center appeared between the two molecules. The reaction cavities of the 1-ce groups of B in three crystals have significantly greater volume than those of the 1-ce groups of A. This fact well

Table 3.2 Relation between the rate constant of racemization and the cavity size at room temperature for the second and third mode crystals

Crystal	Mode	Volume (Å^3)		Rate constant ($\times 10^{-6}$ s^{-1})
		A	B	
py, **9**	II	8.9	11.3	2.86
4epy, **10**	II	8.0	10.4	1.56
4mpy, **11**	II	11.1	12.6	0.57
dpmp, **12**	III	17.1	18.0	4.81
3hpy, **16**	III	8.0	10.4	2.30

explains why only 1-ce group of B can be inverted to the opposite configuration and the 1-ce group of A remains unaltered. Although the 1-ce group of B in **11** has the largest volume, the rate constant is the smallest. This is probably due to the fact that the 1-ce groups A and B in **9** and **10** face each other around a pseudo inversion center whereas those of **11** do not face each other. The 1-ce group of B in the former crystals may be able to utilize the cavity for the 1-ce group of A during the inversion.

Both of the 1-ce cavities of A and B in the crystal **12**, which is classified in the third mode, have large volume. Since the change of the cell dimensions was small, the rate constant was obtained from the intensity variation of reflections which should be zero after racemization due to the extinction rule (F(h0l), h = odd). The 1-ce groups of A and B have enough volume for racemization and have nearly the equal size to each other. This may be a reason why both of the groups became the disordered racemates.

Although the A and B cavities of **16** have small cavities, there are favorite conditions for **16** as follows: two 1-ce groups of A and B contact with each other around a pseudo inversion center and the cyano and methyl groups were exchanged in racemization, whereas the methyl group and hydrogen were exchanged in racemization of **12**. Moreover, the two benzene solvate molecules per one complex may relax the crystal lattice.

3.1.7 Temperature Dependence of Reaction Cavity and Reaction Rate

In order to examine the temperature dependence of the relation between the reaction cavity and the reaction rate, the changes of cell dimensions with exposure time and the three-dimensional intensity data were collected at four temperatures, 223, 253, 298, and 333 K for the crystals of **1**, **2**, and **4** [17]. The changes of cell dimensions were well explained with first-order kinetics. The rate constants were estimated by least-squares fitting using the values of *a*, *b*, and *c*, whose changes were significantly greater than their estimated standard deviations. The cavities for the three crystals at four temperatures were calculated. Although the shapes of the cavities at different temperatures for each crystal are very similar to each other, the volumes are significantly different.

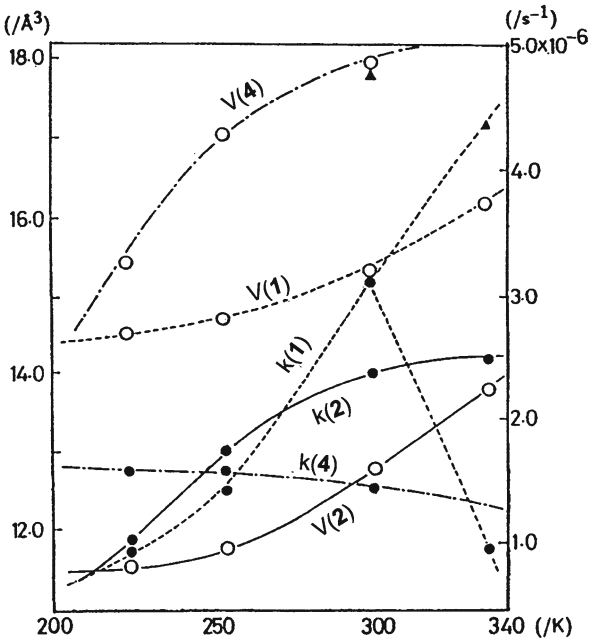

Fig. 3.6 Variation of cavity volume (*V*) and rate constant (k) with temperature for the crystals of **1** (R-S, *dotted lines*), **2** (S-S, *solid lines*), and **4** (dmpp, *dot and dash lines*)

Figure 3.6 shows the cavity volumes and the rate constants at four temperatures for the three crystals. For the crystal of **2**, the cavity volume and the rate constant gradually increase with temperature and the latter depends roughly on the former. On the other hand, the rate constant of **1** abruptly decreases at 333 K and that of **4** does not vary significantly with temperature.

The change in occupancy factor of the inverted 1-ce group with exposure time was obtained at 333 K for **1** using the structures with different exposure time. The rate constant was estimated to be 4.35×10^{-6} s^{-1}. This is approximately the same as the value if the rate constant obtained by the cell dimensions is extrapolated to 333 K. The change in occupancy factor with different exposure time at 298 K for the crystal of **4** gave 4.85×10^{-6} s^{-1}, which is much greater than the corresponding one obtained from the change of the cell dimensions with exposure time, 1.42×10^{-6} s^{-1}.

These results indicate that the rate constant deduced from the cell change is correlated with the size of cavity only when the cavity is not too large. When the cavity size for the 1-ce group exceeds 16 $Å^3$, the rate constant should not be estimated by the cell change but the change of the occupancy factor of the reactive group. This is due to the fact that it is unnecessary to expand the unit cell in order to accommodate the inverted 1-ce group when the cavity is large enough. This may be a reason why the reactivity estimated by the powder pattern is often very complicated.

The Arrhenius plots were drawn for the crystals of **1** and **2,** as shown in Fig. 3.7a, b, respectively. The activation energies were estimated to be 8.9 and 4.8 kJ mol^{-1} for **1** and **2**, respectively. Since the activation energy of the crystal **1** is greater than that of **2**, one might expect that the temperature dependence of the cavity size for the former crystal is greater than that of the latter one. This well explains the results in Fig. 3.6.

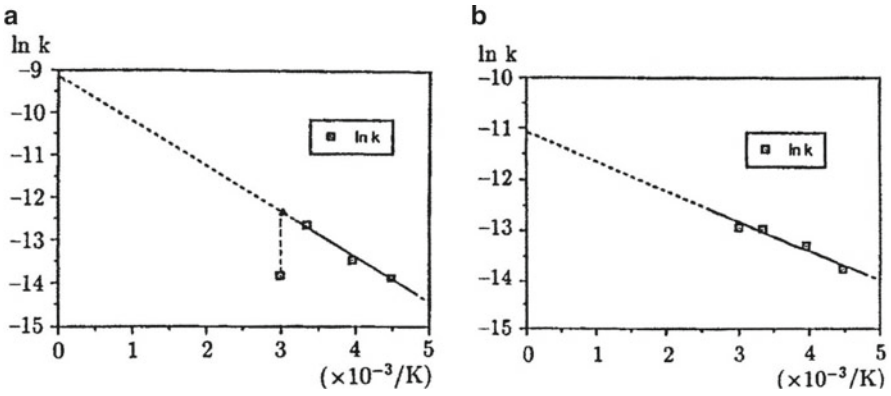

Fig. 3.7 Arrhenius plots for the crystals of (**a**) **1** and (**b**) **2**

3.1.8 Concerted Process of Racemization

The crystal with 3-methylpyridine, **13**, as an axial base ligand was also racemized by X-ray exposure, but the process does not belong to any mode of racemization [26]. Figure 3.8 shows the changes of cell dimensions with exposure time at 293 and 343 K. The space group is $P2_12_12_1$. The changes of a and c are well explained by first-order kinetics. However, the variations of b and unit-cell volume V have maxima at the intermediate stage. A similar trend was observed at 343 K. In order to clarify the reason why such a complicated cell change was observed, the stepwise structure analyses were performed at six stages (I–VI) at 293 K and at three stages (I′ to III′) at 343 K.

Figure 3.9a is the crystal structure at the initial stage. There are two crystallographically independent molecules, A and B, in an asymmetric unit. When the crystal was exposed to X-rays, both of the 1-ce groups of A and B gradually inverted to the opposite configuration, as shown in Fig. 3.9b. Figure 3.10 shows the A and B molecules at the stage VI, viewed along the normal to the cobaloxime plane. The molecular structures of A and B at the stage III′ are essentially the same as the corresponding ones at the stage VI.

Since the changes of b and V are significantly deviated from first-order kinetics, the inversion rates of the 1-ce groups of A and B were obtained from the changes of the occupancy factors at the six stages at 293 K and at three stages at 343 K. Figure 3.11 shows the change of the occupancy factors of the 1-ce groups of A and B with exposure time. The change of the 1-ce group of B follows first-order kinetics at the two temperatures of 293 and 343 K. The ratio of the inverted group reaches 90 % after 900 h. The rate constants, k_B, were calculated to be 0.66×10^{-6} and 0.56×10^{-6} s^{-1} at 293 and 343 K, respectively. On the other hand, the conversion of the 1-ce group of A has a maximum (0.35) at 400 h exposure and then gradually decreases to 0.25 at 900 h at the two temperatures. The inversion rate of the 1-ce

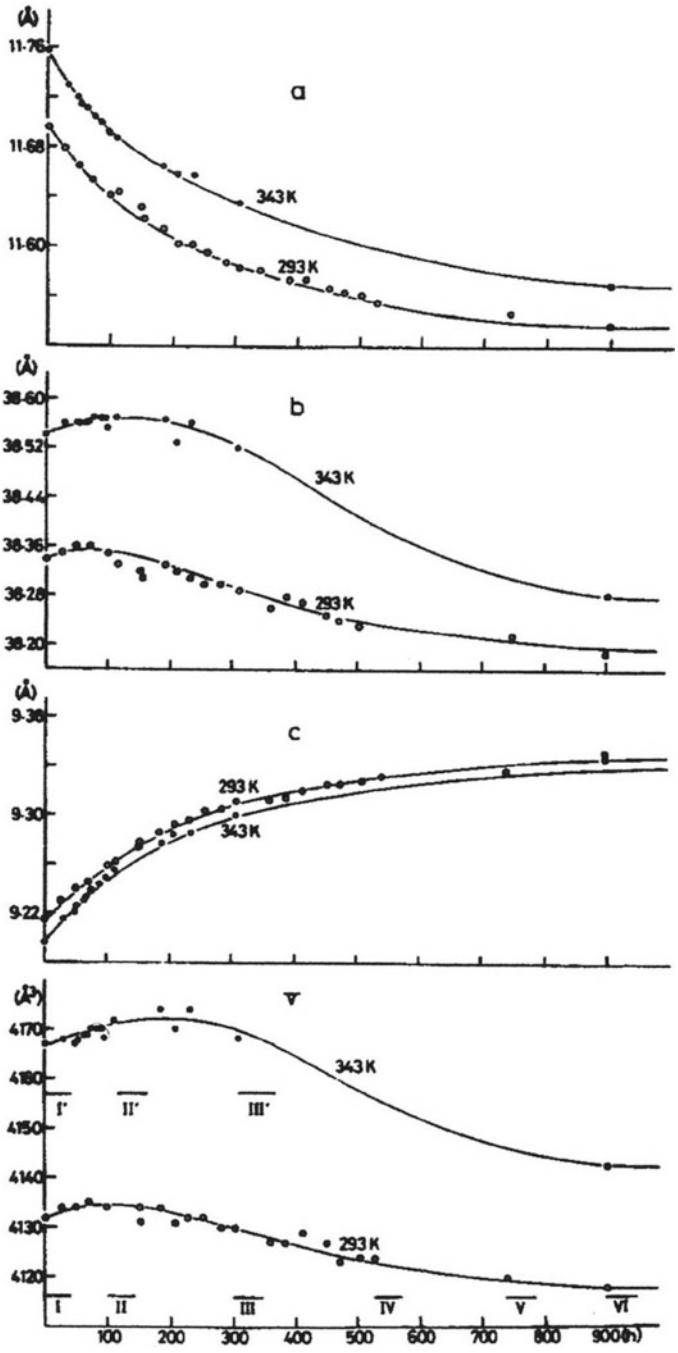

Fig. 3.8 Change of cell dimensions with exposure time for crystal of **13** at 293 and 343 K. The intensity data were collected at I–VI stages at 293 K and at I′ to III′ stages at 343 K

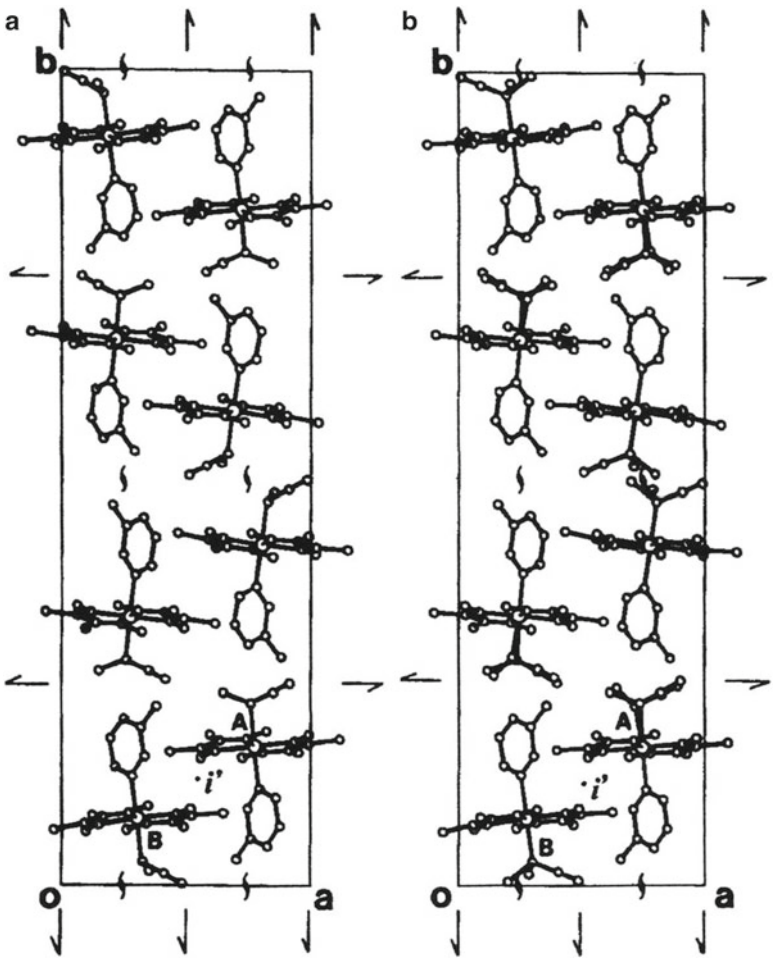

Fig. 3.9 Crystal structures viewed along the *c* axis (**a**) before and (**b**) after the irradiation

group of B is twice that of A at early stages. It must be emphasized that the crystal is fully racemized after 400 h exposure since 35 % of A and 65 % of B have opposite configuration. Nevertheless, the conversion of both groups still continues after 400 h. The 1-ce group of B seems to be completely inverted to the opposite configuration while the 1-ce group of A is probably restored to the original configuration after infinite exposure.

In order to explain the different rates of A and B, the reaction cavities were calculated for 1-ce groups of A and B at two temperatures. The volumes of the A and B cavities are 10.2 and 14.3 $Å^3$ at 293 K and 10.8 and 12.8 $Å^3$ at 343 K, respectively. Surprisingly, the volume of the B cavity decreases with the increase in temperature, although the unit cell expands by 35 $Å^3$ at 343 K. The A cavity, on the other hand, has approximately the same volume at the two temperatures. The inversion rate

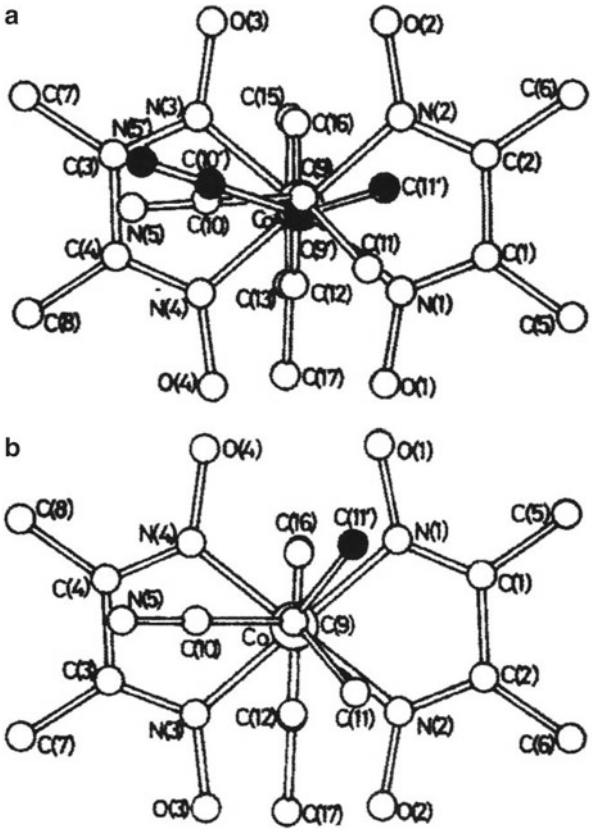

Fig. 3.10 Structures of *R*-1-ce groups at the stage VI, viewed normal to the cobaloxime plane for (**a**) A and (**b**) B molecules

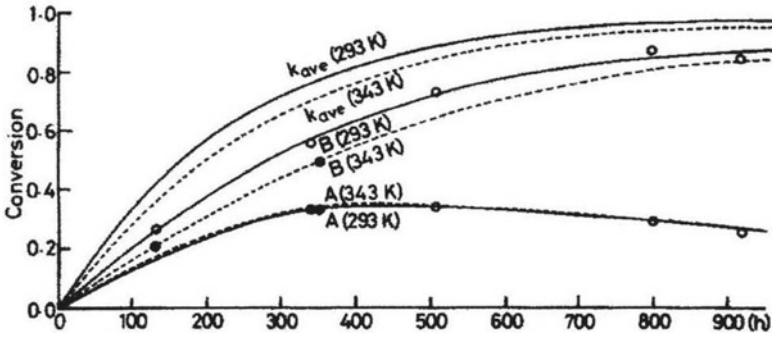

Fig. 3.11 Change of the occupancy factors for the 1-ce groups of A and B and the rate constants with exposure time at 293 and 343 K

constant of the 1-ce group of B at 343 K is significantly smaller than that at 293 K, whereas the 1-ce group of A has nearly the same inversion rate at both temperatures. The positive correlation between the reaction rate and the volume of the reaction cavity holds well even if temperature is changed.

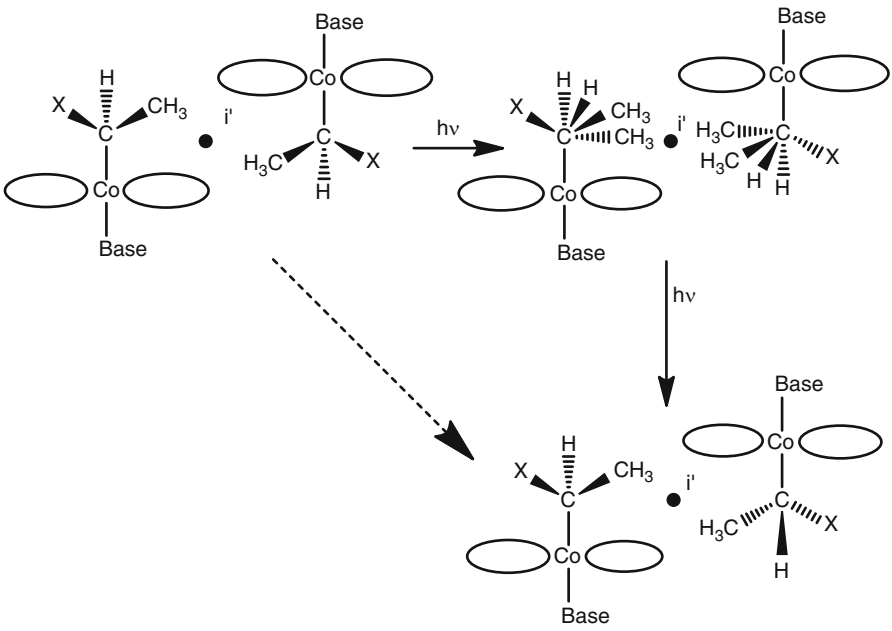

Fig. 3.12 New mode of racemization observed in the crystal of **13**

The modes of the crystalline-state racemization were divided into three classes. If the crystal has two crystallographically independent molecules, there are two modes, the second and third modes as shown in Fig. 3.5. In both classes, the pseudo inversion center becomes a crystallographic one after photo-irradiation. The process of the inversion in the present crystal is schematically shown in Fig. 3.12. The 1-ce groups of A and B molecules gradually inverted into the opposite configuration. The rate of the inversion of B is about twice as large as that of A. After 400 h exposure, the 1-ce group of B is further inverted while that of A is gradually restored to the original configuration. If the pseudo inversion center can be a crystallographic one, the change is the same as that in the second mode. However, the pseudo inversion center cannot become a crystallographic one since it does not meet the crystal symmetry, $P2_12_12_1$. The cavity volumes of A and B molecules are greater than those in the second mode crystals but are smaller than those in the third mode crystal. These facts well explain why the present crystal shows an intermediate mode of racemization between the second and third modes.

3.1.9 Uneven Racemization at the Independent Reaction Sites

The complex crystal with tri(p-chlorophenyl)phosphine, **14**, as an axial base ligand also revealed crystalline-state racemization [24]. The crystal has two crystallographically

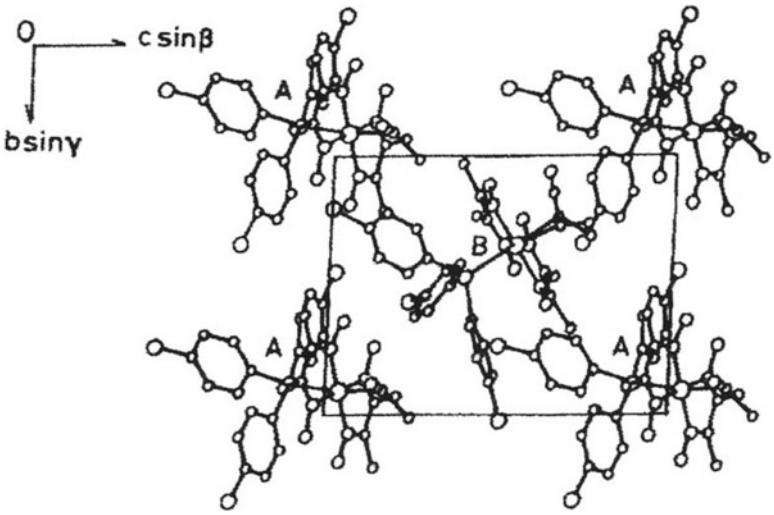

Fig. 3.13 Crystal structure of **14** at the initial stage

independent molecules, A and B, in the unit cell with the space group of *P*1, which is shown in Fig. 3.13. The two molecules are related by a pseudo glide plane. Since the reaction rate was too small at room temperature, the crystal was warmed at 343 K. After 700 h exposure, the pseudo glide plane becomes a crystallographic one and the space group varies to Cc, which is non-centrosymmetric but has the mirror image in the unit cell. The structure viewed along the *c* axis is shown in Fig. 3.14. The *c* axis is common, while the *a* and *b* axes become the diagonal ones during the photoreaction. Since the change of the cell dimensions was very small, the three-dimensional intensity data were collected at five intermediate stages. During the data collection the crystal was kept at room temperature. The analyzed crystal structures indicated both of 1-ce groups of A and B partly inverted to the opposite configuration but the inversion rates of the two groups are significantly different to each other. The change of A is much smaller than that of B. After 700 h exposure, 74 % of B had the opposite configuration whereas 26 % of A had the opposite configuration. This means that the chiral crystal is changed to the racemic one, in which two disordered molecules are related by a mirror (glide) plane.

In order to explain why such a racemization process was observed, the reaction cavities for 1-ce groups of A and B molecules were drawn and the volumes were calculated. The volumes of the cavities for A and B molecules in the initial stage are 9.5 and 10.0 $Å^3$, respectively. Since the photoreaction was performed at 343 K, the cavity volumes should be significantly expanded. Although the difference between the A and B cavities is small at the initial stage, the inversion rate of B is triple as large as that of A. This is because the shape of the cavity of B at the initial stage is in accord with the structure of the 1-ce group with the opposite configuration. Another question is why the inversion rates of A and B were converged to 26:74 and 74:26, respectively. This is because both of the cavity volumes of A and B at 343 K

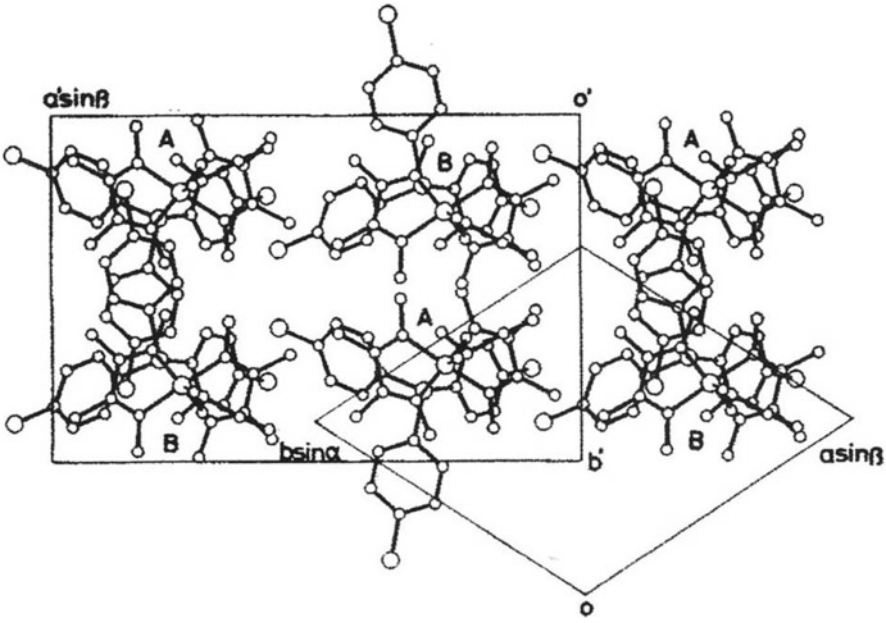

Fig. 3.14 Crystal structure of **14** after 700 h exposure. The relation between the triclinic and monoclinic cells is indicated

are greater than those of the corresponding ones in the second mode but are smaller than those in the third mode. The void space may offer an entropy gain by mixing 1-ce groups with different configuration. When the mixing ratio became 24:76 and 76:24 for A and B, respectively, a crystallographic glide plane appeared between A and B molecules and the crystal became stable energetically.

3.1.10 Racemic-to-Chiral Transformation

The above examples clearly suggest that the reaction cavity is very effective to classify the reaction modes and to explain the rate of racemization. The next example indicates that the reaction cavity is an indispensable tool to explain the mechanism.

The (*R*-1-ce)cobaloxime complex crystal with piperidine as an axial base ligand, **15**, has two crystallographically independent molecules, A and B, in an asymmetric unit of the $P2_12_12_1$ cell, as shown in Fig. 3.15. When the crystal was exposed to X-rays at 333 K, only the 1-ce group of B was gradually inverted to the opposite configuration with retention of the single crystal form, although no change was observed at 293 K [25]. The 1-ce group of A was unchanged at either temperature. The reaction cavities for the 1-ce groups of A and B were calculated at 293 and

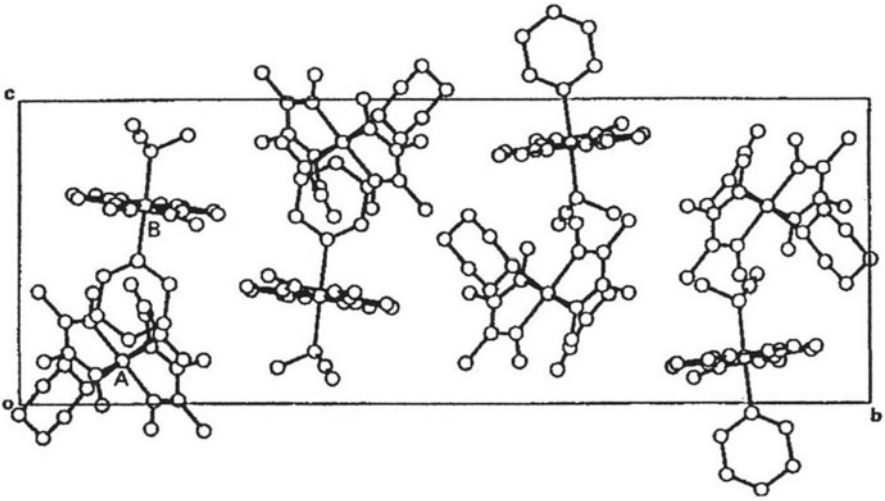

Fig. 3.15 Crystal structure of (*R*-1-ce)(piperidine)cobaloxime viewed along the *a* axis before the photo-irradiation

333 K. They are 7.49 and 11.57 Å^3 at 293 K and 7.88 and 14.04 Å^3 at 333 K for the 1-ce groups of A and B, respectively. Since only the 1-ce group of B at 333 K has enough size for racemization, the 1-ce group of B was changed to the disordered racemates. At the final stage, the *R:S* ratio of the crystal became 75:25 within experimental error.

The crystals were prepared from a solution containing the complexes with the *R*-1-ce and *S*-1-ce groups in the ratio of 1:1. Surprisingly, the crystal is isomorphous to the above chiral one with only *R* configuration. The structure analysis revealed that the A molecule has the 1-ce group with *R* configuration while B has *S*-1-ce group as shown in Fig. 3.16a. The crystal is, therefore, racemic but has a chiral space group, $P2_12_12_1$. This crystal has the chirality of D. It is possible to obtain the crystal with the opposite chirality of L, in which the 1-ce groups of A and B have *S* and *R* configurations, respectively.

When the crystal was exposed to a xenon lamp at 293 K, the unit-cell dimensions gradually changed with retention of the single crystal form. After a week, the change became within the experimental error. The structure analysis showed no change in A, whereas significant peaks appeared around the 1-ce group in B. These peaks were assigned to the 1-ce group with the opposite configuration. The occupancy factors of the newly appeared *R*-1-ce and the original *S*-1-ce groups in B seemed to be converged to 50:50. The crystal structure is shown in Fig. 3.16b. The *R:S* ratio in a crystal changed from 50:50 to 75:25. This result indicated that a partial racemic-to-chiral transformation or optical enrichment occurred in a crystal only by X-ray exposure [29–31]. This is the first observation that a racemic crystal showed optical enrichment only by photo-irradiation.

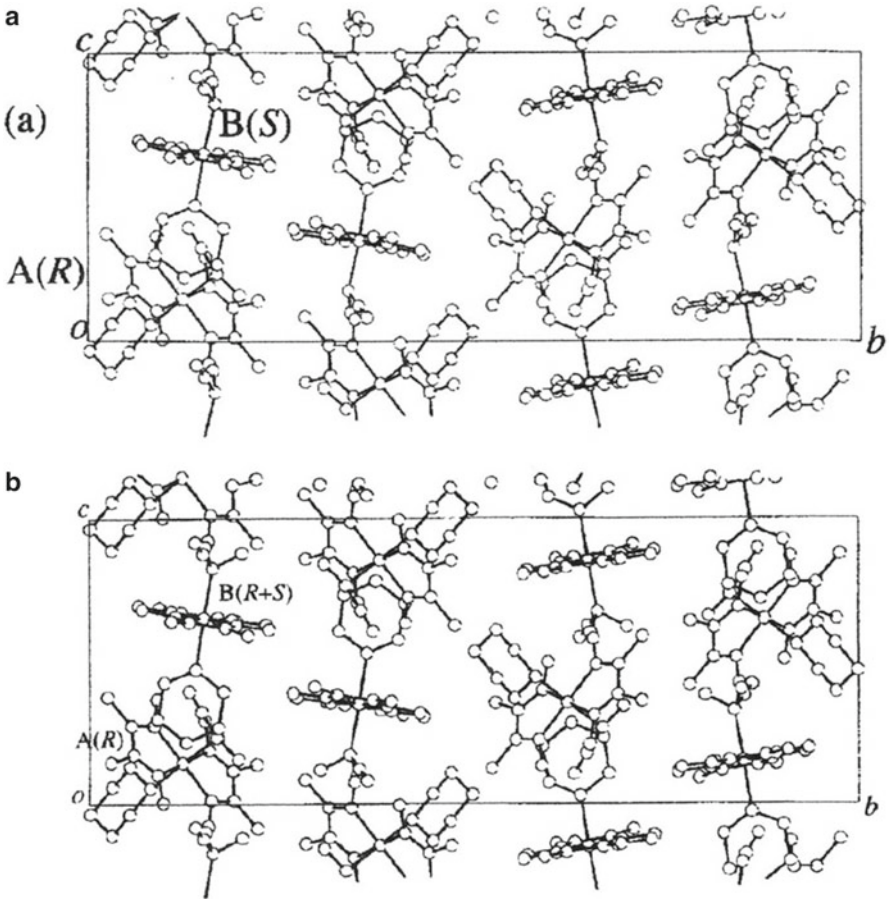

Fig. 3.16 Crystal structure of (*R,S*-1-ce)(piperidine)cobaloxime viewed along the *a* axis (**a**) before photo-irradiation and (**b**) after the irradiation

In order to make clear the mechanism of the above unusual result, the mixed crystals with different *R:S* ratios were grown from an aqueous methanol solution. The five kinds of crystals with the *R:S* ratios of 50:50, 62:38, 75:25, 87:13, and 100:0 were prepared, which is called pip-1, pip-2, pip-3, pip-4, and pip-5, respectively [32]. All the five crystals are isomorphous but the *R:S* ratio of the B molecule has 0:50, 12:88, 25:25, 37:13, and 50:0, respectively, whereas the A molecule always has *R* configuration. The cell volume has a minimum around 62:38, not at 50:50 or 75:25.

Each crystal was mounted on a four-circle diffractometer which was covered with black sheets to avoid the room light and was irradiated with a xenon lamp using an optical fiber at room temperature. Figure 3.17 shows the changes of the *c* axis length in the three crystals, pip-1, pip-3, and pip-5, with exposure time. Each *c* length gradually converged to the same value. The other cell dimensions showed the

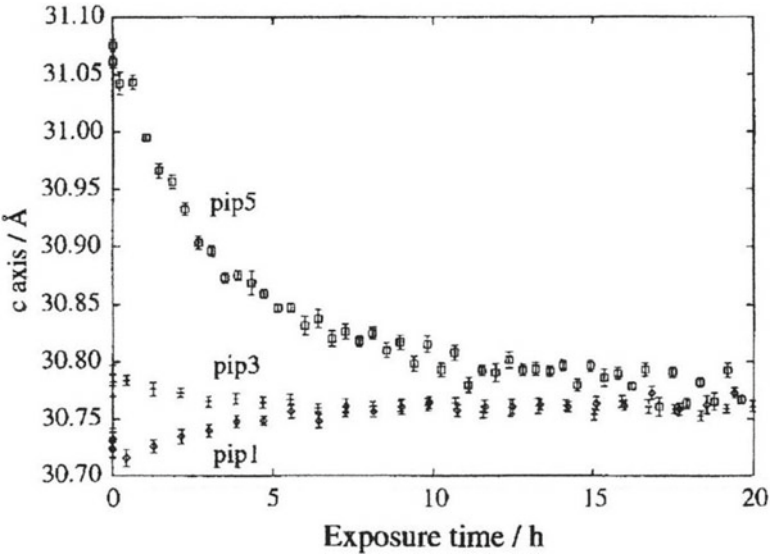

Fig. 3.17 Changes of the *c* axis lengths of pip-1, pip-3, and pip-5 with exposure time

similar variation, although they are not so clear. From the figure, it is clear that the crystal structure at the final stage is different from that of pip-3, whose *R:S* ratio of the 1-ce group of B is 50:50.

The crystal structures of pip-1, pip-3, and pip-5 after 40 h photo-irradiation were analyzed by X-rays. The three structures are identical to each other within experimental error. The *R:S* ratios of the 1-ce group of B in the three crystals became 19:31, 19:31, and 21:29 for pip-1, pip-3, and pip-5 crystals, respectively, which are 20:30 within experimental error. It must be emphasized that the converged *R:S* ratio of the 1-ce group of B is not 25:25 but 20:30.

The *R:S* ratio in the racemic crystal of pip-1 before photo-irradiation was 50:50. After photo-irradiation, the *R:S* ratio became 70:30. Such a change brought about a partial racemic-to-chiral transformation or optical enrichment in a crystal. When the crystal after photo-irradiation was dissolved in chloroform solution, the specific rotatory power, $[\alpha]_D$, showed 30°.

When the crystal of pip-1 was photo-irradiated at 343 K, the change of the cell dimensions was slightly but significantly different from that at 296 K. The crystal structure after 15 h exposure at 343 K was also approximately the same as that at 296 K; however, the *R:S* ratio of the disordered 1-ce group of B was different, that is, the *R:S* ratio was not 20:30 but 25:25.

It must be explained why only the 1-ce group of B is partly inverted to make disordered racemates. The volumes of the reaction cavities for the 1-ce groups of A and B before irradiation are drawn in Fig. 3.18. Since the 1-ce group of A has a too small cavity whereas the 1-ce group of B has enough (more than 11.5 $Å^3$) volume at any composition, such different cavity volumes of the two 1-ce groups explain the

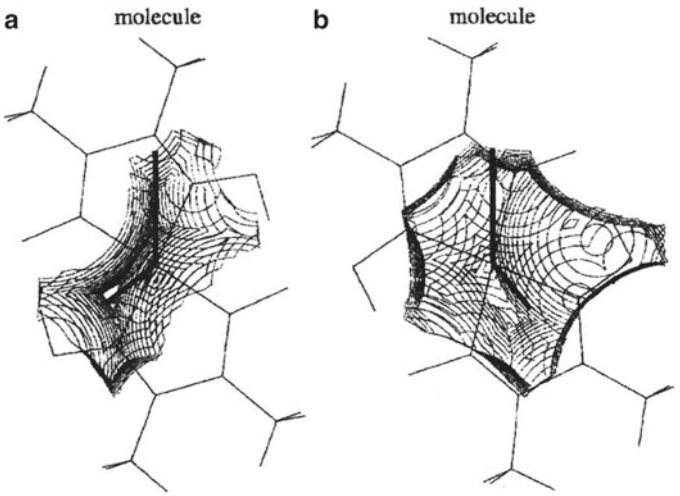

Fig. 3.18 Reaction cavities for A and B 1-ce groups before the irradiation viewed along the normal to the cobaloxime plane

different behavior, that is, the 1-ce group of A retained unaltered while the 1-ce group of B was partly inverted.

A next question why the converged *R:S* ratio is not 75:25 but 70:30 should be answered. The reaction cavities for the 1-ce groups of B in pip-1, pip-3, and pip-5 before and after the photo-irradiation are shown in Fig. 3.19. Each cavity is divided into two parts by the plane including the Co–C–C–N bonds and the volumes of the two parts were calculated. The ratios of the left and right parts of the cavities before photo-irradiation are 45:55 and 56:44 and 63:37 for the 1-ce groups of B in pip-1, pip-3, and pip-5, respectively. The ratios became 48:52, 49:51, and 52.48, respectively, after the irradiation. The final ratios were 50:50 within experimental error. This suggests that the inversion ratio of the 1-ce group of B depends on the symmetry of the cavity. In other words, the inversion ratio is determined by the steric repulsion from the neighboring molecules around the 1-ce group of B after photo-irradiation. Since the minimum unit-cell volume was obtained around the ratio of 62:38, which is close to 70:30, the enthalpy term may be responsible to the ratio of 70:30. When the crystal was irradiated with the visible light at 343 K, the *R:S* ratio of the 1-ce group of B became 25:25. Although the reaction cavity at 343 K was not calculated because the precise positions of the hydrogen atoms were not obtained, it must have enough size to accommodate the 1-ce groups with both of *R* and *S* configurations. The ratio of the left and right parts of the cavity would be 50:50. This means that the entropy term is dominant at high temperatures, since the reaction cavity may be enlarged and the enthalpy term has no effect on the *R:S* ratio.

For the complex crystal with pyrrolidine as an axial base ligand, the similar results were obtained [14, 15, 30, 32]. The racemic crystal obtained from an aqueous methanol solution has four crystallographically independent molecules, A, B,

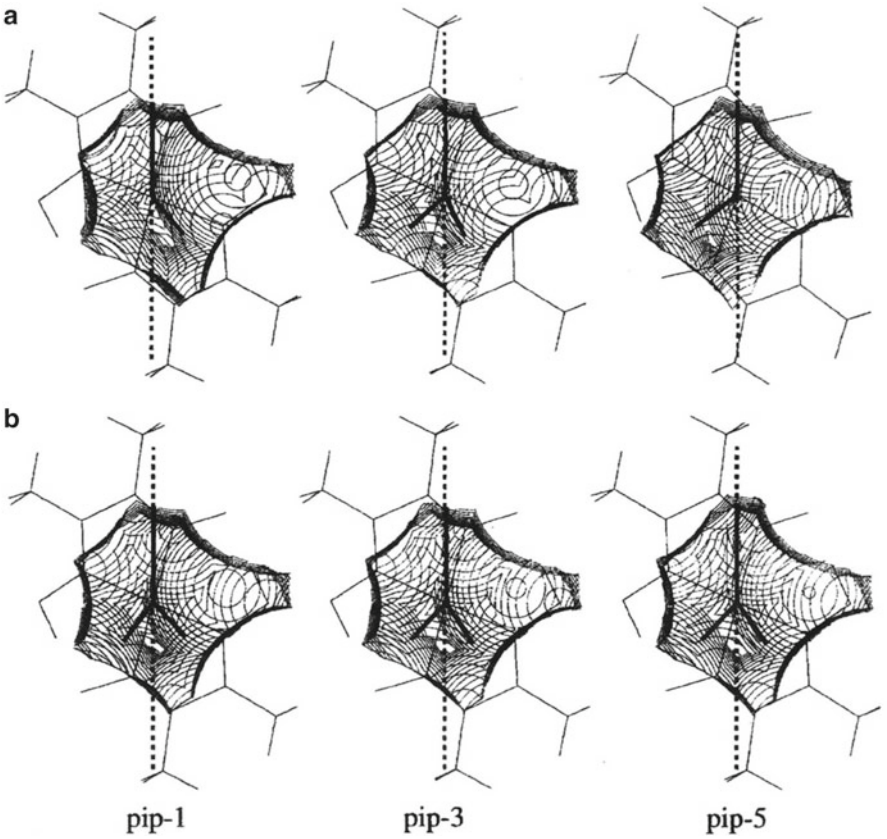

Fig. 3.19 Reaction cavities for the B 1-ce groups in the pip-1, pip-3, and pip-5 viewed along the normal to the cobaloxime plane, (**a**) before and (**b**) after the irradiation. The *dotted line* indicates the plane including the Co–C–C–N bonds

C, and D, in the chiral *P1* cell as shown in Fig. 3.20. The A and B molecules have the *R*-1-ce groups while C and D have the *S*-1-ce groups. When the racemic crystal was exposed to the xenon lamp, the *R:S* ratios of the C and D molecules were gradually changed while A and B remained unaltered. The optical enrichment was also observed. In order to examine the process of the racemic-to-chiral transformation, four kinds of crystals with the different *R:S* ratios of 50:50 (racemic), 75:25, 80:20, and 90:10, which are called pyrr-1, pyrr-2, pyrr-3, and pyrr-4, respectively, were prepared from solutions containing the *R*-1-ce and *S*-1-ce complexes with the desired compositions. Although the complex crystal with the *R:S* ratio of 100:0 was also obtained, it was not isomorphous to the above four crystals but was the hydrated one with the space group $P2_12_12_1$. The trials to obtain the isomorphous crystal have been unsuccessful.

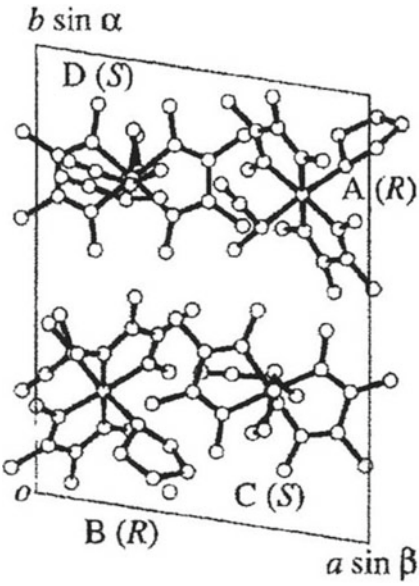

Fig. 3.20 Crystal structure of (*R,S*-1-ce)(pyrrolidine) cobaloxime viewed along the *c* axis before irradiation

When the racemic crystal of pyrr-1 was exposed to the xenon lamp for 40 h, the cell dimensions were gradually changed with retention of the single crystal form and the *R:S* ratios became from 0:25 to 8:17 and 14:11 for the 1-ce groups of C and D, respectively. This means that the crystal, as a whole, changed from racemic to chiral (*R:S* = 72:28). The *R:S* ratios of pyrr-2, pyrr-3, and pyrr-4 after photo-irradiation became 72:28, 72:28, and 71:29, respectively. The pyrrolidine complex crystals also converged to about 70:30 after infinite irradiation.

The volumes of the reaction cavities for the 1-ce groups of A, B, C, and D before photo-irradiation were calculated to be 10.1, 8.4, 16.9, and 15.0 $Å^3$, respectively. These values well explain the reason why only the 1-ce groups of C and D were partially inverted to the opposite configuration. It is impossible to divide the cavities for the 1-ce groups of C and D into two parts by the plane composed of the Co–C–C–N bonds after irradiation, because the groups take very complicated disordered structures. Probably the ratios of the left and right parts of each cavity should be 50:50 after photo-irradiation as observed in the piperidine complex.

It was found that the cobaloxime crystal with the racemic-1-ce group and methyl-S-alaninate as axial ligands crystallizes in the chiral *P1* cell [33]. The crystal structure has two molecules, A and B, in the unit cell and A has the *S*-1-ce group, while B has the *R*-1-ce group, as shown in Fig. 3.21. The crystal has a pair of diastereomers. This result well explains why the fractional resolution of the diastereomeric pair was impossible in the usual way. The crystal structure indicates that the CN group of the 1-ce group of B is N–H···N hydrogen bonded to the NH_2 group of the methyl-*S*-alaninate of the neighboring molecule.

When the crystal was exposed to the xenon lamp, the cell dimensions gradually changed with retention of the single crystal form. The crystal after photo-irradiation

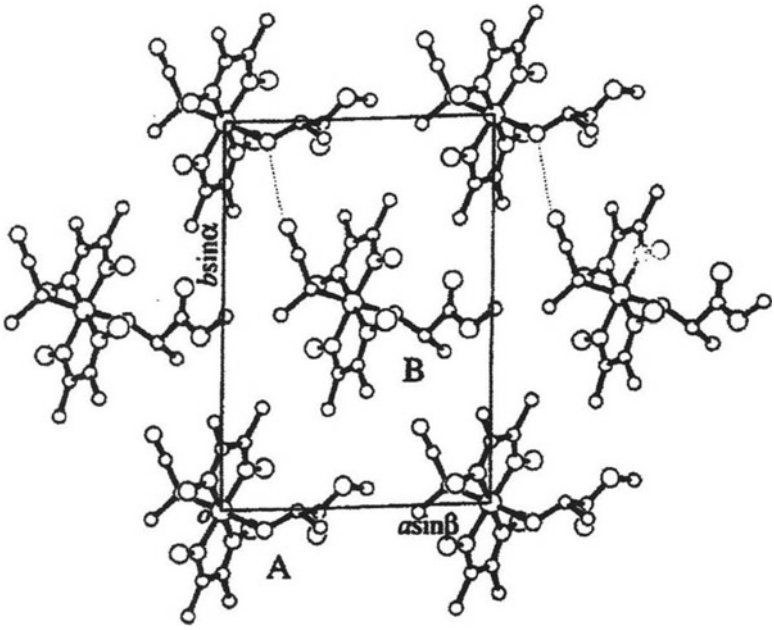

Fig. 3.21 Crystal structure of (*R,S*-1-ce)(methyl-*S*-alaninate)cobaloxime viewed along the *c* axis before irradiation

indicated that only the *R*-1-ce group of B was changed to disordered racemates. Optical enrichment was also observed in the crystal. The reaction cavities for the 1-ce groups of A and B were drawn and the cavity volumes were calculated to be 11.5 and 13.6 $Å^3$ for A and B, respectively. This well explains why only B is changed to the disordered structure. For the methyl-*S*-alaninate complex, the 1-ce group is isolated in the crystal structure. Moreover, the inversion of the 1-ce group of B in the methyl-*S*-alaninate crystal should cleave the hydrogen bond of the CN group with the neighboring molecule. The cavity shape divided into two by the Co–C–H bond does not approach the symmetric one after the partly inversion of the 1-ce group. The motive force to optical enrichment has been unsolved for this crystal.

These results suggest that the racemic-to-chiral transformation will be commonly observed if the crystallization of the racemic compounds or the compounds with the diastereomeric pair(s) would be extensively studied. Since the racemic crystals with the opposite chirality for these crystals are, in general, equally grown in a solution, the racemic-to-chiral transformation does not change the *R:S* ratio, that is, 50:50 as a whole. If the *D:L* ratio of the chiral crystals obtained from a racemic solution would not be 50:50 due to some environmental conditions, the present racemic-to-chiral transformation by photo-irradiation should be an origin of asymmetric induction in nature.

3.2 Racemization of Bulky Groups in Cobaloxime Complexes

3.2.1 Cooperative Motion of the Chiral 1-Methoxy-carbonylethyl Groups

When the chiral 1-ce group was replaced with the chiral 1-methoxy-carbonylethyl (1-mce) group as shown in Scheme 3.2, a new type of racemization was observed for the complex crystals with 4-chloropyridine (4clpy, **1**) and pyridine (py,**2**) as axial base ligands. Figure 3.22 shows the crystal structure of the 4clpy complex before photo-irradiation [34]. The crystal belongs to $P2_1$ and has two crystallographically independent molecules, A and B, in the asymmetric unit. Except for the chiral 1-mce group, the two molecules are closely related by a pseudo inversion center between them. At room temperature, the crystal showed no change on exposure to a fluorescent lamp. When the crystal was warmed up to 353 K, the cell dimensions gradually changed with retention of the single crystal form on exposure to a fluorescent lamp. The pseudo inversion center changed to a crystallographic one and the space group became $P2_1/n$. The rate constant was calculated to be 6.9×10^{-6} s^{-1}, assuming first-order kinetics. At the final stage, both of the 1-mce groups of A and B were transformed to the disordered racemates. This is the same as that in the third mode as observed in racemization of the 1-ce group.

In order to examine the conformational and configurational changes of the 1-mce groups of A and B in racemization, the structures of the A and B molecules without the axial 4clpy ligand viewed along the normal to the cobaloxime plane before and after irradiation are compared in Fig. 3.23. Both of the 1-mce groups with *R* configuration before irradiation changed to the disordered racemates. Moreover, the

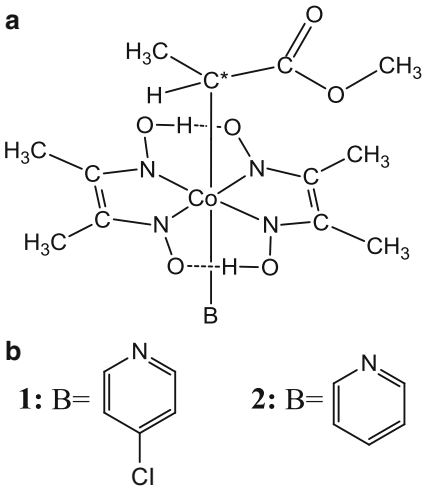

Scheme 3.2 The (*R*-1-mce) cobaloxime complexes with (**a**) 4-chloropyridine and (**b**) pyridine as axial base ligands

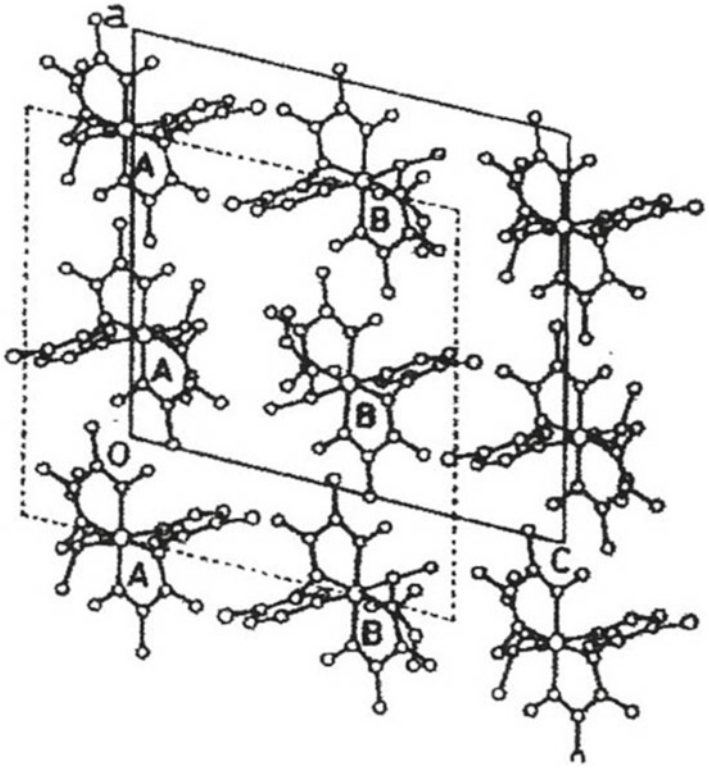

Fig. 3.22 Crystal structure of (*R*-1-mce)(4clpy)cobaloxime before the irradiation viewed along the *b* axis

methyl of 1-mce group of B was changed from *anti*-periplanar to *syn*-periplanar conformation to the carbonyl oxygen, while that of A remained unaltered. The *syn* conformation is stabler energetically than the *anti*, because the van der Waals radius of the carbonyl oxygen is slightly smaller than the oxygen of the methoxyl group. In racemization, the 1-mce group of B with unstable *anti* conformation changed to the stable *syn* conformation. This result brought about another question: Which occurs more easily, *anti*-to-*syn* conformational or *R* to *S* configurational change in racemization? The difference in energy of steric repulsion between the conformational and configurational changes seems to be similar to each other.

The question may be answered in the structural change in complex of **2**, which has two pyridine complexes and solvate methanol molecules in its asymmetric unit of the $P2_1$ cell [35, 36]. The crystal structure viewed along the *c* axis before photoirradiation at 223 K is shown in Fig. 3.24. Two crystallographically independent complexes, A and B, without axial ligands and surrounding methanol molecules are shown in Fig. 3.25a. The 1-mce group of A has *syn*, while that of B has *anti* conformation.

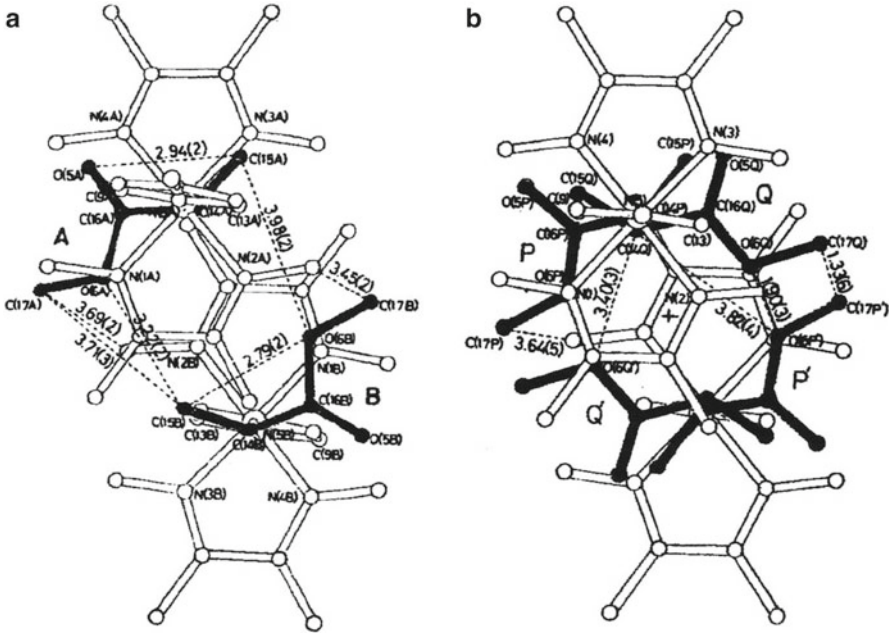

Fig. 3.23 Conformational and configurational change of *R*-1-mce group viewed along the normal to the cobaloxime plane, (**a**) before and (**b**) after the irradiation

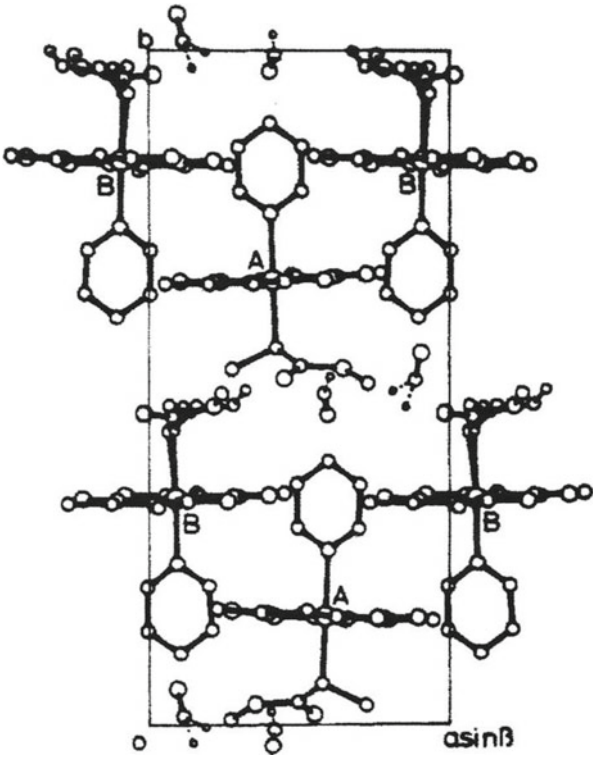

Fig. 3.24 Crystal structure of (*R*-1-mce)(py)cobaloxime with methanol solvent viewed along the *c* axis at 223 K before the irradiation. Small atoms of methanol molecules with *dotted bonds* are disordered atoms

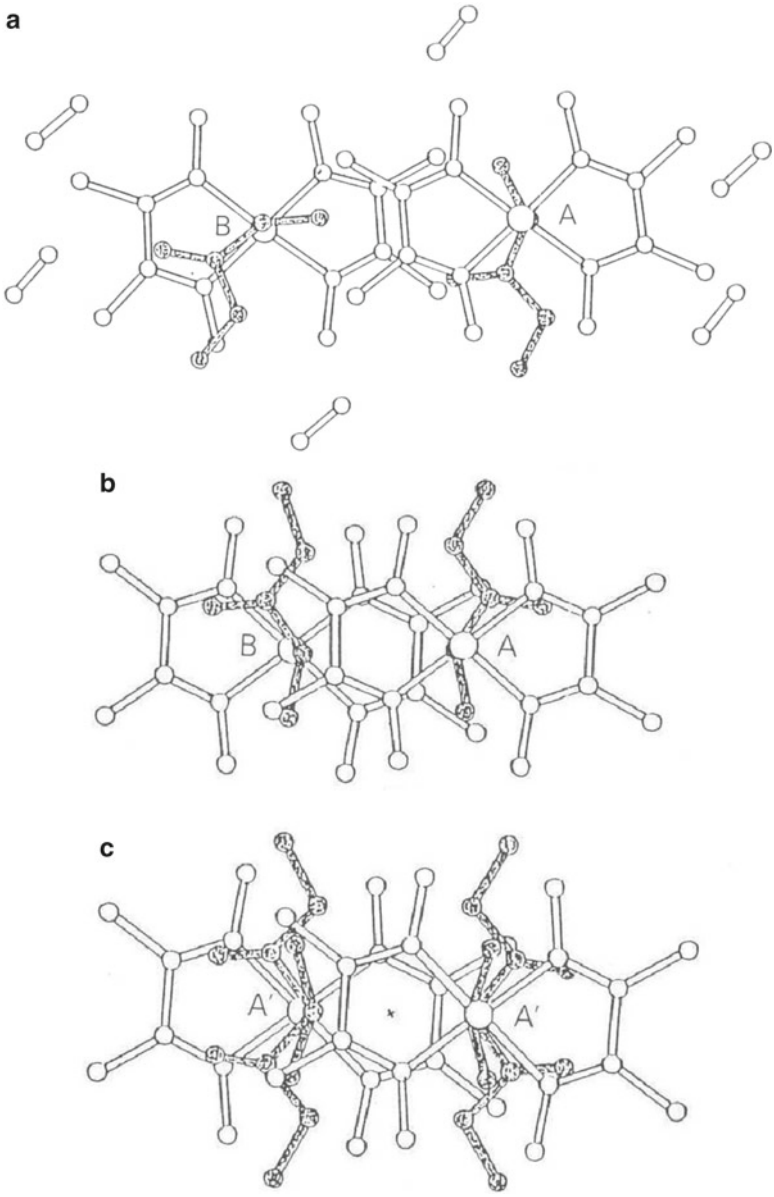

Fig. 3.25 Molecular structures of A and B (**a**) around a pseudo inversion center before irradiation at 223 K, (**b**) after desolvation at room temperature, and (**c**) after irradiation at 333 K around an inversion center

When the crystal was kept in open air at room temperature, the solvent molecules gradually went out from the crystals without degradation of the crystal. Since the change of the *b* length is too large, the 0k0 reflections are split at the intermediate stages. This indicates that the desolvation step is not a crystalline-state reaction but

a single crystal-to-single crystal transition. As shown in Fig. 3.25b after desolvation, the 1-mce groups of A rotated by 180° around the Co–C bond, the *syn* conformation being conserved, whereas that of B rotated by 100° around the Co–C bond, the *anti* conformation being changed to *syn*.

When the crystal warmed up to 333 K, the crystal was gradually changed on exposure to the fluorescent lamp. The pseudo inversion center became a crystallographic one and both of the 1-mce groups of A and B were changed to disordered racemates as shown in Fig. 3.25c. This racemization belongs to the third mode. These results clearly indicate that the conformational change from *anti* to *syn* is easier than the configurational change in the crystalline-state reaction.

In the above experiment, the solvent methanol molecules were lost from the crystal without deteriorating the crystallinity. And then the crystal was warmed to 333 K and was irradiated with visible light. In order to analyze the desolvation mechanism, the intensity data in several intermediate stages were collected using a new diffractometer with imaging plate designed by us [37] and the structures were analyzed in the three steps [38]. The crystal was kept at 296 K for 3 h and then was cooled to 253 K. The change of the cell dimensions became negligibly small. The intensity data were collected and the structure was analyzed (step I). The crystal warmed to 296 K and was kept 3 h and then the intensity data were collected at 253 K. The structure of step II was obtained, which means 6 h desolvation. The step III structure was obtained in the same way after 9 h desolvation.

The three structures indicate that the molecule A and the methanol A neighboring to A are approximately the same as those before desolvation while the molecule B and the methanol B neighboring to B are changed. The 1-mce group of B takes a disordered structure around the Co–C bond. Moreover, the occupancy factor of methanol B gradually decreased; it became 0.67 at step I, 0.60 at step II, and 0.55 at step III. These results clearly indicated that the methanol B went out from the crystal and then the 1-mce group of B neighboring to the methanol B rotated around the Co–C bond and took the disorder structure. This may initiate racemization of the 1-mce groups on exposure to the fluorescent lamp.

It seemed more interesting to examine whether or not racemization might occur without desolvation. The crystal was sealed in a glass capillary, whose diameter was 0.7 mm, and was irradiated with a fluorescent lamp put apart 30 cm from the crystal [38]. After 5 days' irradiation, the intensity data were collected and the structure was analyzed. Although the cell change was not converged, the reflections of h0l with h+1=odd became zero within experimental errors. This meant that the space group was changed from $P2_1$ to $P2_1/n$. The inversion center appeared between A and B molecules. The crystal had two methanol molecules. The two mce groups and two methanol molecules around an inversion center are shown in Fig. 3.26, which are similar to the racemized structure after the desolvation shown in Fig. 3.25c. However, the conformation of the disordered 1-mce group was different between the two structures; both of the disordered 1-mce groups took the stable *syn* conformation in crystal after desolvation, whereas one of the 1-mce groups has syn and the other has anti in the solvated crystal. It is clear that the solvent methanol prevents the two molecules to come close and does the 1-mce group of B to change the

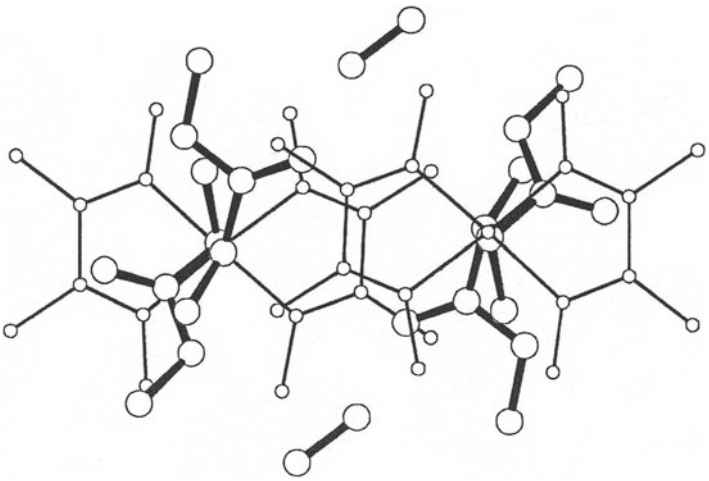

Fig. 3.26 Molecular structures of 1-mce groups around an inversion center after the irradiation without desolvation

conformation from *anti* to *syn*. It must be emphasized that even if the reactant is the same, the product is different whether the solvent exists or not.

In order to make sure the quantitative relation between the reaction rate and the reaction cavity for the 1-mce group, four cobaloxime complexes with the *R*-1-mce group were prepared, changing the axial base ligand, which is *R*-1-phenylethylamine [39] (*R*-pea, **3**), *S*-1-phenylethylamine [40] (*S*-pea, **4**), 4-cyanopyridine [41] (4cpy, **5**), and 4-ethylpyridine [42] (4etpy, **6**). For the *S*-pea complex, two crystal forms were obtained under the same conditions: triclinic (**4**-T) and monoclinic (**4**-M) forms. None of the five crystals revealed crystalline-state racemization at room temperature on exposure to visible light. Each crystal has one molecule in the asymmetric unit. The reaction cavity was drawn and the volume was calculated. Each 1-mce group is neatly accommodated in the cavity and it seems impossible for the 1-mce group to be racemized without destroying the crystalline lattice. Probably the concerted motion of the two 1-mce groups may be necessary for the crystalline-state racemization.

When the crystal was irradiated with visible light at 353 K, it was gradually decomposed. In order to ascertain whether or not the decomposition was caused by racemization of the 1-mce group, the powdered crystals of 4cpy were exposed at 353 K in the fluorescent lamp and the optical rotation of the chloroform solution was measured. Although the measurement points were limited, racemization seemed to follow first-order kinetics and the rate constant was calculated to be 2.3×10^{-6} s^{-1}.

3.2.2 Cooperative Motion with Solvent Molecules

Next example of the cobaloxime complex has a cyclohexylamine (cha, **7**) as an axial base ligand [43]. The crystal structure belongs to the monoclinic system and the

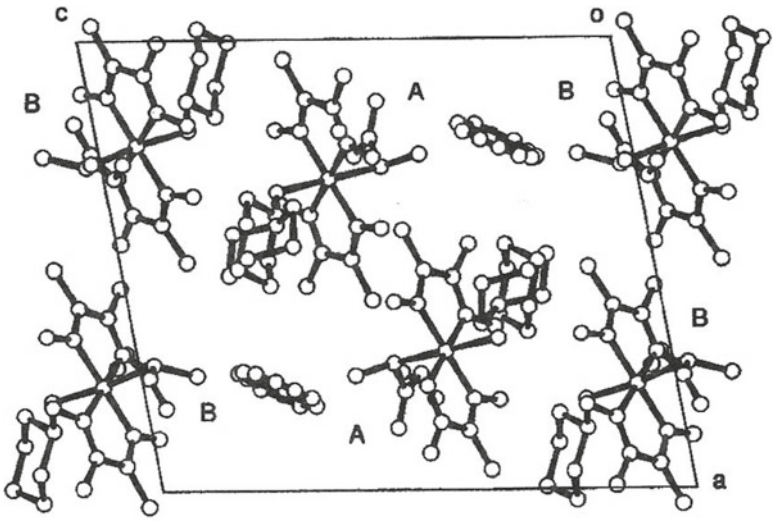

Fig. 3.27 Crystal structure of (*R*-1-mce)(cha)cobaloxime with benzene solvate viewed along the *b* axis

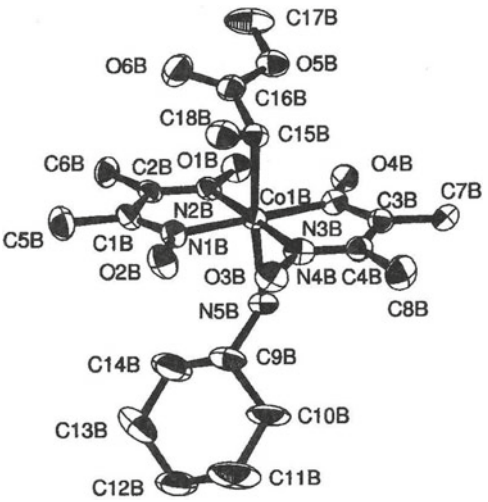

Fig. 3.28 Molecular structure of B in the (*R*-1-mce)(cha)cobaloxime crystal

space group $P2_1$. There are two crystallographically independent molecules, A and B, in an asymmetric unit cell as shown in Fig. 3.27. The two molecules are closely related by a pseudo inversion center. There is a benzene molecule between the 1-mce groups of A and B as solvent, which are situated on another pseudo inversion center and are disordered. The molecular structure of B is shown in Fig. 3.28. The A molecule has almost the same structure except that the axial ligand of cha is disordered. Both of the conformations of A and B 1-mce group are *syn*.

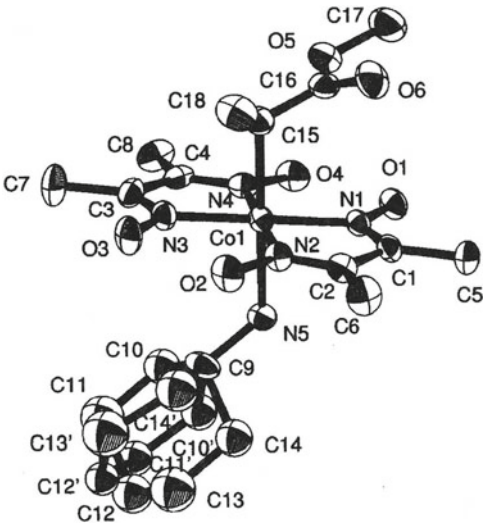

Fig. 3.29 Molecular structure of B after the irradiation. The configuration is changed from *R* to *S*

When the crystal was irradiated with a fluorescent lamp, the cell volume gradually increased. After 600 h exposure, the change of cell dimensions was converged. The pseudo inversion center became a crystallographic one and the space group became $P2_1/n$. This indicates that A and B are related by a crystallographic inversion center. The 1-mce group of B is completely inverted to the opposite configuration and takes an ordered structure and the cha ligand has a disordered structure, as shown in Fig. 3.29. On the other hand, the A molecule has nearly the same structure as before. A slight motion of the benzene molecule between the two 1-mce groups may accelerate the inversion of B. Such a racemization is completely different from those of the complexes of **1** and **2** described in the previous section. The racemization is classified into the second mode, compared with racemization modes of the cobaloxime complexes with the 1-ce group.

The racemic crystal was prepared from a benzene solution containing racemic compounds. The crystal has a benzene molecule in an asymmetric unit and the structure is very similar to that produced by photo-irradiation. However, the 1-mce group of the complex takes a complicated disordered form.

The racemization process of the two molecules is shown in Fig. 3.30. The A and B 1-mce groups around a pseudo inversion center have no direct contacts between them, but a solvent benzene molecule occupies the pseudo inversion center between the two 1-mce groups. Before the photo-irradiation, the shortest contacts between the 1-mce groups of A and B and benzene are 3.89 and 3.60 Å, respectively. The short contacts changed to 4.01 Å, which is slightly loose contact. The short contact between 1-mce group of B and benzene may be a motive force to invert the configuration of 1-mce group of B. Such a cooperative racemization is similar to the racemization processes of the complex crystals of **1** and **2**.

The reaction cavities for the 1-mce groups of A and B before photo-irradiation are drawn as shown in Fig. 3.31. The *R* configuration of the A mce group is well

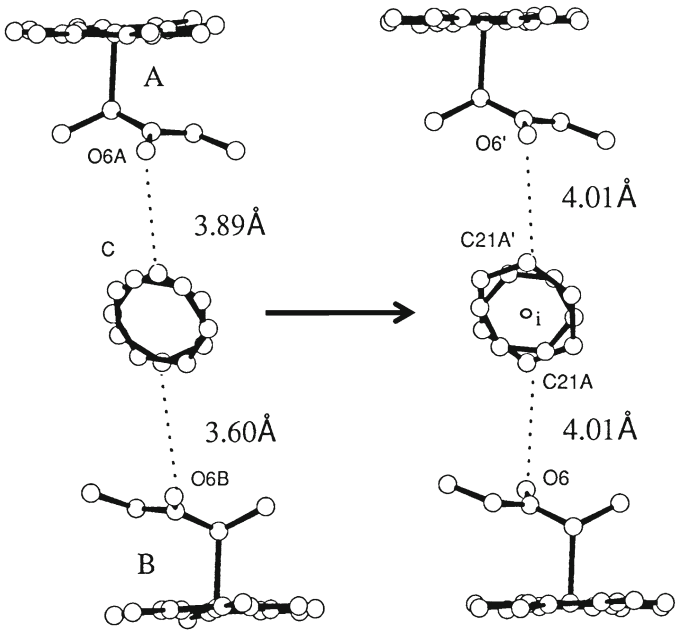

Fig. 3.30 Racemization process of the B molecule accompanying slight movement of the benzene molecule

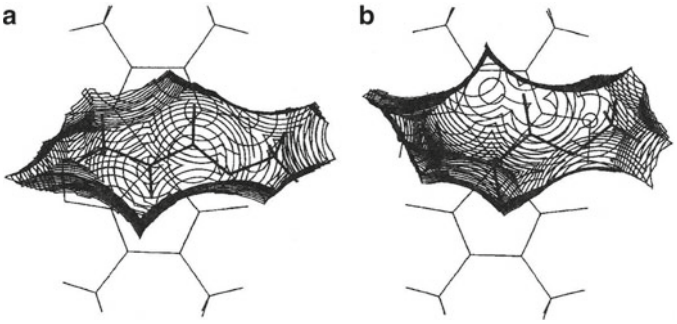

Fig. 3.31 Reaction cavities of the 1-mce groups of (**a**) A and (**b**) B molecules

suited to the *R* configuration. It seems impossible to accommodate the inverted group. On the other hand, the B cavity may accommodate the opposite configuration. This may be a reason why only B 1-mce group is inverted to the opposite configuration on exposure to visible light although the cavity volumes of A and B are nearly the same: 23.1 and 23.8 $Å^3$ for A and B, respectively.

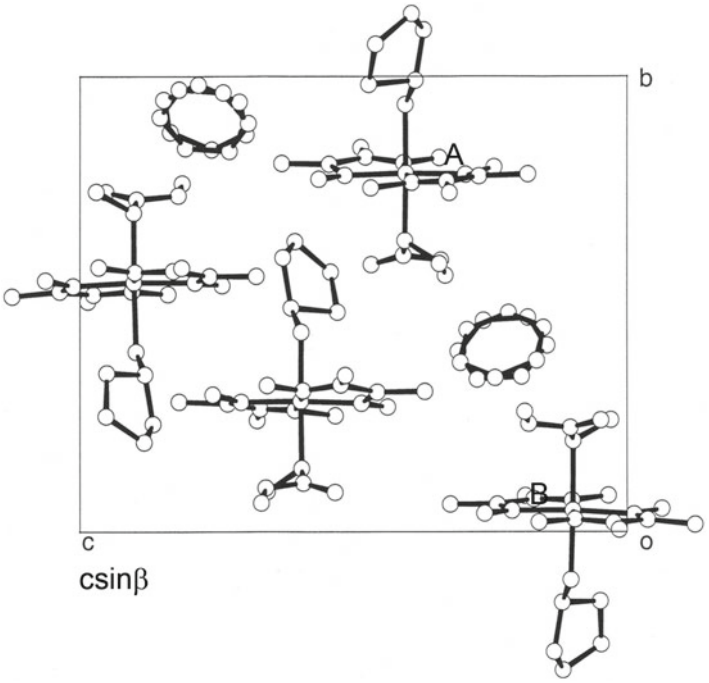

Fig. 3.32 Crystal structure of (*R*-1-mce)(cpa)cobaloxime with benzene solvate viewed along the *a* axis

3.2.3 Another Mode of Cooperative Racemization with Solvent Benzene

When the crystal of [*R*-1-(methoxycarbonyl)ethyl](cyclopentylamine)-cobaloxime, (*R*-1-mce)(cpa)cobaloxime, **8**, was exposed to visible light, another mode of racemization was observed [42]. The crystal belongs to the monoclinic system and the space group is $P2_1$. There are two crystallographically independent molecules, A and B, and one solvent benzene molecule in the asymmetric unit as shown in Fig. 3.32. There is a pseudo inversion center between A and B. A disordered benzene molecule is situated on the pseudo inversion center between the chiral 1-mce groups of A and B. The molecular structures of A and B are shown in Fig. 3.33. The 1-mce groups of A and B take *syn* and *anti* conformations, respectively. This structure is very similar to that of the previous cha complex except that the two 1-mce groups have different conformations.

On exposure to a xenon lamp, the space group changed from non-centrosymmetric $P2_1$ to centrosymmetric $P2_1/n$. The pseudo inversion center became a crystallographic one. Both of the 1-mce groups of A and B changed to disordered racemates, exchanging the positions of the methyl group with that of the hydrogen atom as

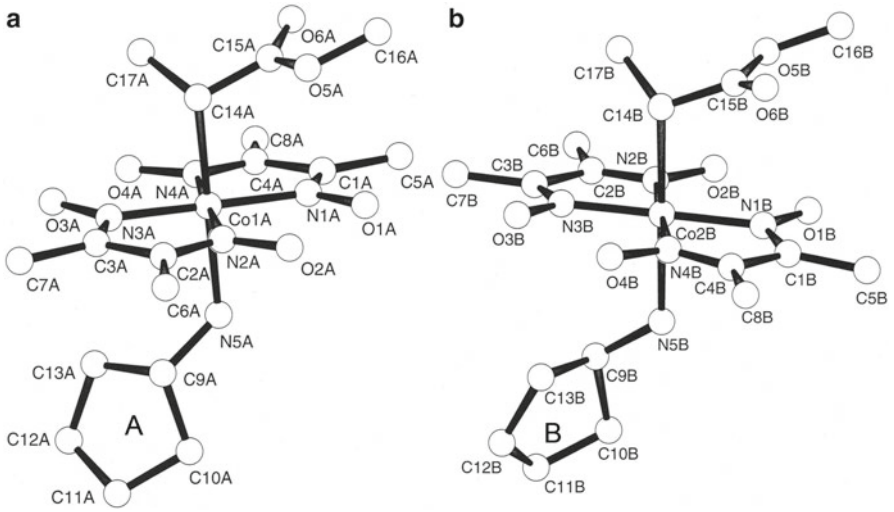

Fig. 3.33 Molecular structures of (**a**) A and (**b**) B of (*R*-1-mce)(cpa) cobaloxime

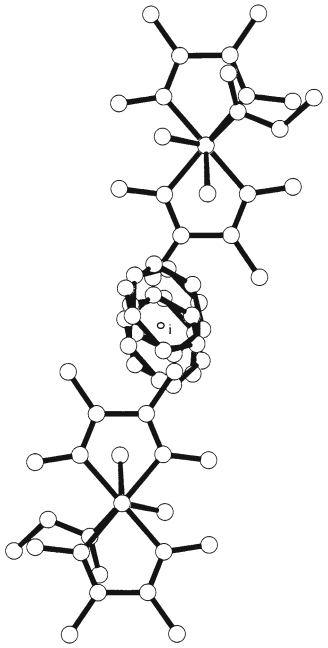

Fig. 3.34 Structural change after the irradiation

shown in Fig. 3.34. There appeared an inversion center between A and B and the disordered benzene molecule is situated on the inversion center. Although the racemization process is very similar to that of the cha crystal, racemization is classified to the third mode.

When the axial base was replaced with benzylamine (ba, **9**), some interesting results were obtained. The crystals were grown from methanol [38, 42, 44], ethanol [44], acetonitril [44], and methyl acetate [45]. Four kinds of crystals with different solvent molecules were obtained. Each crystal revealed the photo-racemization. However the processes were different with each other. The details of the racemization processes with the solvent molecules were recently reviewed [46].

The above results clearly indicate that the existence of the solvent and the relative position between the reactive group and the solvent molecule should control the reaction pathway and may produce the different products.

References

1. Giannotti C, Bolton JR (1975) J Organomet Chem 91:357
2. Giannotti C, Merle G, Bolton JR (1975) J Organomet Chem 99:145
3. Giannotti C, Bolton JR (1976) J Organomet Chem 110:383
4. Ohashi Y, Sasada Y (1977) Nature 267:142
5. Enkelmann V, Wegner G, Novak K, Wegener KB (1993) J Am Chem Soc 115:10390
6. Novak K, Enkelmann V, Wegner G, Wagener KB (1993) Angew Chem Int Ed Engl 32:1614
7. Ikeda K, Liu W, Shen YR, Uekusa H, Ohashi Y, Koshihara S (2005) J Chem Phys 122:141103
8. Uchida A, Dunitz JD (1990) Acta Crystallogr B46:45
9. Gavezzotti A (1983) J Am Chem Soc 105:5220
10. Ohhara T, Uekusa H, Ohashi Y, Tanaka I, Kumazawa S, Niimura N (2001) Acta Crystallogr B57:351
11. Ohashi Y, Yanagi K, Kurihara T, Sasada Y, Ohgo Y (1981) J Am Chem Soc 103:5805
12. Ohashi Y, Sasada Y, Ohgo Y (1978) Chem Lett 743–746
13. Takenaka Y, Kojima Y, Ohashi Y (1993) Acta Crystallogr B49:852–859
14. Takenaka Y, Ohashi Y, Tamura T, Uchida A, Sasada Y (1993) Acta Crystallogr B49:272–277
15. Takenaka Y, Ohashi Y, Tamura T, Uchida A, Sasada Y (1993) Acta Crystallogr B49: 1015–1020
16. Kojima Y, Iwasaki S, Ohashi Y, Baba S, Ohgo Y (1991) Acta Crystallogr C47:300
17. Takenaka Y, Kojima Y, Ohashi Y, Ohgo Y (1992) Mol Cryst Liq Cryst 219:153
18. Kurihara T, Uchida A, Ohashi Y, Sasada Y, Ohgo Y, Baba Y (1983) Acta Crystallogr B39:431
19. Tomotake Y, Uchida A, Ohashi Y, Sasada Y, Ohgo Y, Baba S (1984) Acta Crystallogr B40:1684
20. Ohashi Y, Yanagi K, Kurihara T, Sasada Y, Ohgo Y (1982) J Am Chem Soc 104:6353
21. Ohashi Y, Uchida A, Sasada Y, Ohgo Y (1983) Acta Crystallogr B39:54
22. Uchida A, Ohashi Y, Sasada Y, Ohgo Y (1984) Acta Crystallogr B40:473
23. Tomotake Y, Uchida A, Ohashi Y, Sasada Y, Ohgo Y, Baba S (1985) Isr J Chem 25:327
24. Ohashi Y, Tomotake Y, Uchida A, Sasada Y (1986) J Am Chem Soc 108:1196
25. Danno M, Uchida A, Ohgo Y, Sasada Y, Ohgo Y, Baba S (1987) Acta Crystallogr B43:266
26. Osano YT, Danno M, Uchida A, Ohashi Y (1991) Acta Crystallogr B47:702
27. Ohgo Y, Ohashi Y (1996) Bull Chem Soc Jpn 69:2425
28. Ohgo Y, Orisaku K, Hasegawa E, Takeuchi S (1986) Chem Lett 27
29. Osano YT, Uchida A, Ohashi Y (1991) Nature 352:510
30. Ohashi Y, Nemoto T, Takenaka Y (1994) Mol Cryst Liq Cryst 242:103
31. Ohashi Y, Nemoto T, Sekine A (1996) Mol Cryst Liq Cryst 277:1
32. Nemoto T, Ohashi Y (1999) Bull Chem Soc Jpn 72:1971
33. Hashizume D, Ohashi Y (2000) J Phys Org Chem 13:415
34. Kurihara T, Ohashi Y, Sasada Y (1983) Acta Crystallogr B39:243
35. Kurihara T, Ohashi Y, Sasada Y (1982) Acta Crystallogr B38:2484

36. Kurihara T, Uchida A, Ohashi Y, Sasada Y, Ohgo Y (1984) J Am Chem Soc 106:5718
37. Ohashi Y, Uekusa H (1996) J Mol Struc 374:37
38. Tanaka T (1998) Master Thesis, Tokyo Institute of Technology
39. Ohashi Y, Sasada Y (1977) Bull Chem Soc Jpn 50:2863
40. Kurihara T, Uchida A, Ohashi Y, Sasada Y (1984) Acta Crystallogr B40:478
41. Kurihara T, Uchida A, Ohashi Y, Sasada Y (1984) Acta Crystallogr C40:1557
42. Saitoh M (1996) Master Thesis, Tokyo Institute of Technology
43. Sekine A, Saitoh M, Hashizume D, Uekusa H, Ohashi Y, Ohgo Y (1998) Enantiomer 3:159
44. Saito T (2003) Master Thesis, Tokyo Institute of Technology
45. Takabayashi H (2000) Master Thesis, Tokyo Institute of Technology
46. Ohashi Y (2013) Cryst Rev 19(suppl):2–146

Chapter 4
Characteristic Processes of Various Racemizations

Abstract Further bulkier groups revealed very complicated racemization. For the (ethoxycarbonyl)ethyl group bonded to the cobalt atom, the chirality was inverted to the opposite configuration. The shape of the reaction cavity for the chiral group explained the reason why such an unusual reaction occurred. For the 1,2-bis(methoxycarbonyl)ethyl group, one of the two chiral groups was completely inverted to the opposite configuration. In the process of the inversion, the chiral group revealed two-step inversion, that is, the conformational change of a part of the chiral group and then inversion of the group. For the 1,2-bis(ethoxycarbonyl)ethyl group, only the two bonds connecting the chiral carbon of the produced radical rotated and opposite side of the radical made a bond to the cobalt atom. Such a two-bond rotation, which is called "hula-twist" as observed in rhodopsin, may be caused by long substituents bonded to the carbon radical.

Keywords Chirality inversion • Hula-twist • Intermediate structure • Two-bond rotation • Two-step racemization

4.1 Chirality Inversion Process

The nest example shows a very unusual phenomenon in the crystalline state. When the crystal of [*S*-1-cyclohexylamine][*S*-1-(ethoxycarbonyl)-ethyl]bis(dimethylglyoximato) cobalt(III), (*S*-cha)(*S*-1-ece)cobaloxime, as shown in Scheme 4.1, was irradiated with a halogen lamp, the configuration of the *S*-1-ece group gradually changed from *S* to *R* with retention of the single crystal form and most of the *S*-1-ce group was inverted to the *R* configuration only by photo-irradiation [1]. This is the first finding that the chirality of the molecule can be inverted to the opposite one only by photo-irradiation.

Figure 4.1 shows the crystal structure before photo-irradiation. The space group is $P2_12_12_1$. There is one molecule in an asymmetric unit. The chiral *S*-1-ece groups have contacts with each other as a ribbon along the 2_1 axis parallel to the *a* axis.

Y. Ohashi, *Crystalline State Photoreactions: Direct Observation of Reaction Processes and Metastable Intermediates*, DOI 10.1007/978-4-431-54373-2_4, © Springer Japan 2014

Scheme 4.1 The complex of (*S*-cha)(*S*-1-ece)cobaloxime

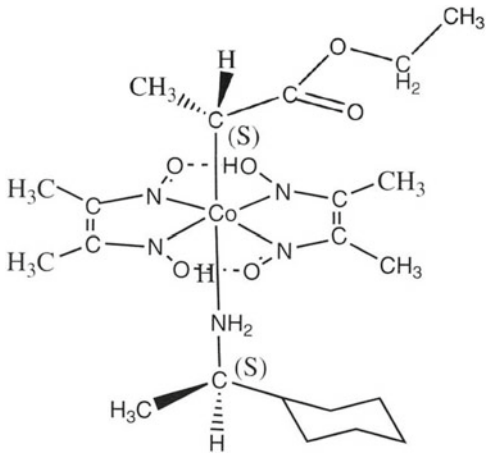

Fig. 4.1 Crystal structure of (*S*-1-ece)(*S*-cha)cobaloxime viewed along the *a* axis

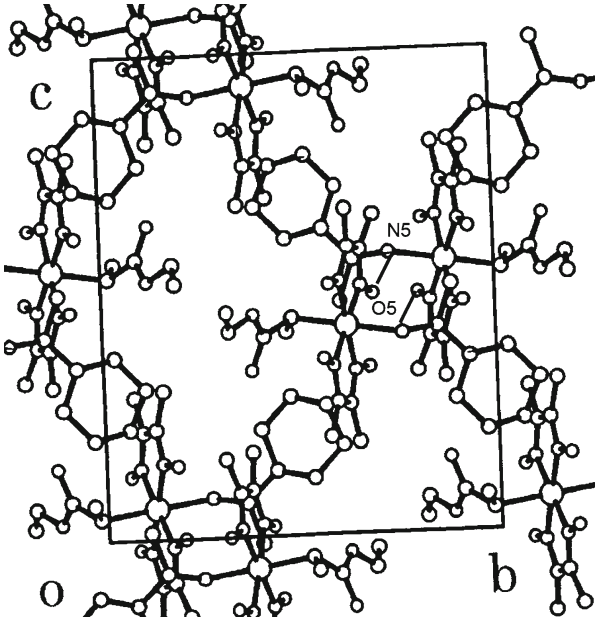

Figure 4.2 shows the molecular structure. The methyl group of the 1-ece group takes a *syn* conformation to the carbonyl group, O2–C3–C4–C5, and the ethyl of ece group has a *trans* conformation around the O1–C2 bond.

When the crystal was exposed to a halogen lamp with a long-path filter (R64), the unit-cell dimensions were gradually changed; the *a* and *b* axes slightly contracted, whereas the *c* axis and the unit-cell volume *V* significantly expanded. The crystal structure, however, is nearly the same as before, except that the 1-ece group has a disordered structure due to the partial inversion. Figure 4.3 shows the structural change of the 1-ece group viewed along the normal to the cobaloxime plane. Most of the 1-ece group was inverted from *S* to *R* configuration. The *S:R* ratio became

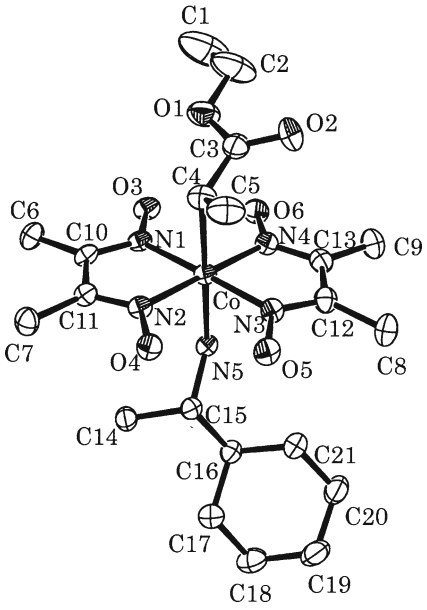

Fig. 4.2 Molecular structure of (*S*-1-ece)(*S*-cha) cobaloxime

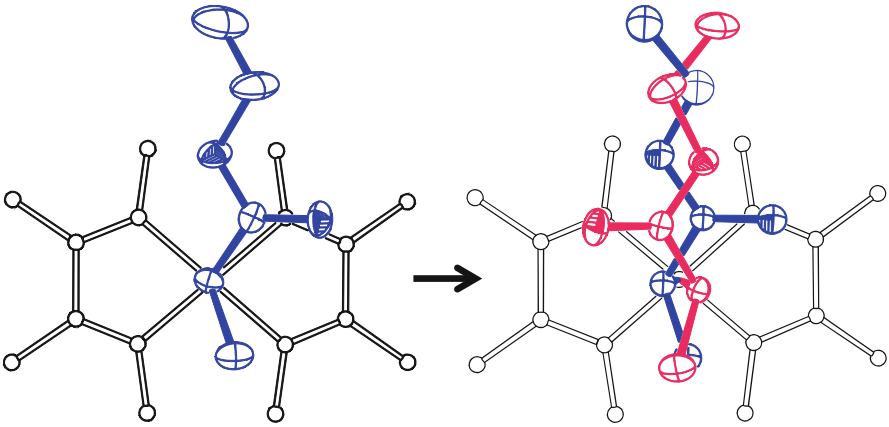

Fig. 4.3 Structural change of the 1-ece group after the irradiation. *Blue colored* 1-mce group has *S* configuration whereas *red colored* has *R*

from 100:0 to 18:82 after 24 h exposure. The ratio of 18:82 was not changed after prolonged irradiation. It is clear that the chirality of the 1-ece group was inverted only by photo-irradiation. The optical rotation of the solution containing the photo-product was inverted since the optical rotation of the molecule is determined by the chirality of the 1-ece group, although this molecule has another chiral molecule, *S*-cha, as an axial ligand.

It seemed very interesting to examine whether or not the chirality of the 1-ece group might be inverted when the crystal of the diastereomer, (*S*-cha)(*R*-1-ece)

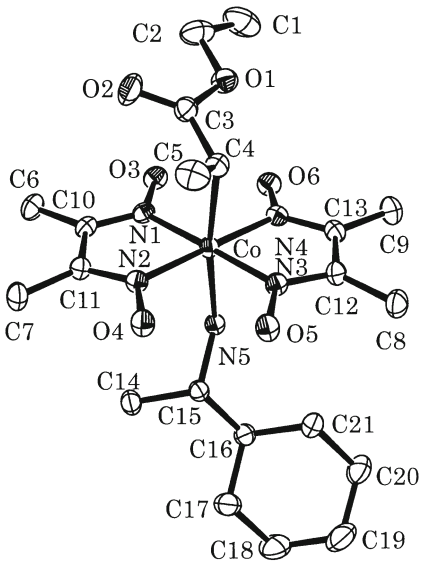

Fig. 4.4 Molecular structure of (*R*-1-ece)(*S*-cha) cobaloxime

cobaloxime, would be exposed to visible light. The crystal was prepared and the structure before irradiation was analyzed by X-rays. To our surprise, the structure is isomorphous to the previous one with the *S*-1-ece group, as shown in Fig. 4.1. The molecular structure is shown in Fig. 4.4. The structure of the *R*-1-ece group is the mirror image of that of the *S*-1-ece group as shown in Fig. 4.2 and the same as the corresponding one of the photo-produced disordered ece group as shown in Fig. 4.3.

When the crystal was irradiated with the halogen lamp, the cell dimensions gradually changed. They converged to the values observed in the photo-irradiated crystal with the *S*-1-ece group. The structure analyzed by X-rays after 24 h exposure revealed that it is essentially the same as the photo-produced one shown in Fig. 4.3. The *S:R* ratio converged to 18:82, which is the same as that observed in the photo-irradiated crystal with the *S*-1-ece group.

In order to check the ratio of 18:82, the mixed crystal with the equal amounts of *S*- and *R*-1-ece groups, that is, the *racemic*-1-ece group, was prepared. The crystal structure analyzed by X-rays showed that it is isomorphous to the crystals with *S*- and *R*-1-ece groups and that has a disordered structure of the ece group with the *S:R* ratio of 50:50. When the mixed crystal was irradiated with the halogen lamp, the cell dimensions gradually changed and were converged to the values observed in the photo-irradiated crystals of *S* and *R* isomers. The *S:R* ratio in the photo-irradiated crystal is 18:82. It is clear that the *S:R* ratio of 18:82 is the most stable when the crystal with any composition of the *S* and *R* isomers is exposed to the halogen lamp.

The question why the ratio of 18:82 is the most stable should be answered. Figure 4.5a–c shows the reaction cavities for the *S*-1-ece, *racemic*-1-ece, and *R-1-ece* group, respectively, before photo-irradiation. Each cavity is divided into two by the plane, which passes through the Co atom and is perpendicular the cobaloxime plane and parallel to the C–C bond of cobaloxime. The volume ratios of the left to right sides in the cavities are 38:61, 46:54, and 47:53 for *S*-1-ece, *racemic*-1-ece, and *R*-1-ece complex crystals, respectively. It must be emphasized that the volume

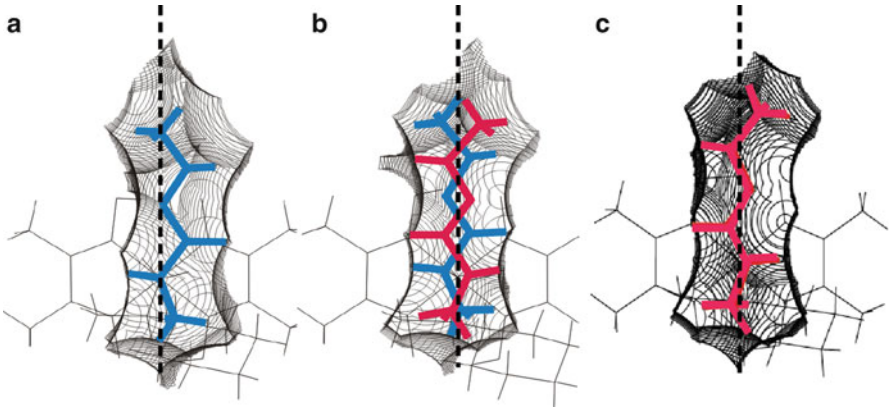

Fig. 4.5 Reaction cavities for the 1-ece groups in the crystals of (**a**) (*S*-1-ece)(*S*-cha)cobaloxime, (**b**) (*R*,*S*-1-ece)(*S*-cha)cobaloxime, and (**c**) (*R*-1-ece)(*S*-cha)cobaloxime. The *blue* and *red colored* 1-ece groups have *S* and *R* configurations, respectively. The *dashed lines* indicate the mirror planes dividing the cavities into two parts

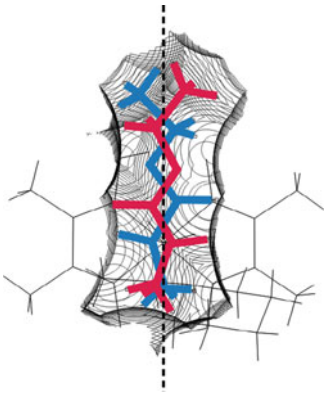

Fig. 4.6 Reaction cavity after irradiation. The ratio of the *left* and *right sides* of the cavity becomes ca. 50:50

ratio of *racemic*-1-ece crystal is not 50:50 but 46:54. This is probably due to the asymmetric environment around the *racemic*-1-ece group in the chiral $P2_12_12_1$ cell. After the photo-irradiation, the 1-ece groups of the three crystals became essentially the same disordered structure with the *S*:*R* ratio of 18:82. The reaction cavity for the disordered 1-ece group is shown in Fig. 4.6. The ratio of the left to right sides in the cavity for the photo-produced 1-ece groups of *S*-1-ece, *racemic*-1-ece, and *R*-1-ece crystals became 51:49, which is almost the same as 50:50.

It is clear that the steric repulsion from the surrounding atoms would have equal effect on either of the *R*- and *S*-1-ece groups after the irradiation. The enthalpy term of the ece group plays an important role in the chirality inversion process.

In the crystallization of (*S*-cha)(*S*-1-ece)cobaloxime, a pseudo polymorphic crystal was obtained, which has one water molecule as a solvent. On exposure to the halogen lamp, the cell dimensions gradually changed with retention of the single crystal form. The structural change of the *S*-1-ece group before and after

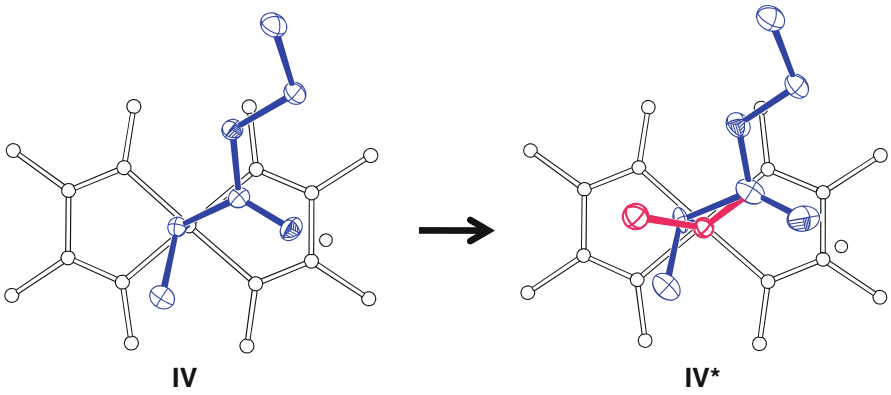

Fig. 4.7 Structural change of the *S*-1-ece group before and after the irradiation

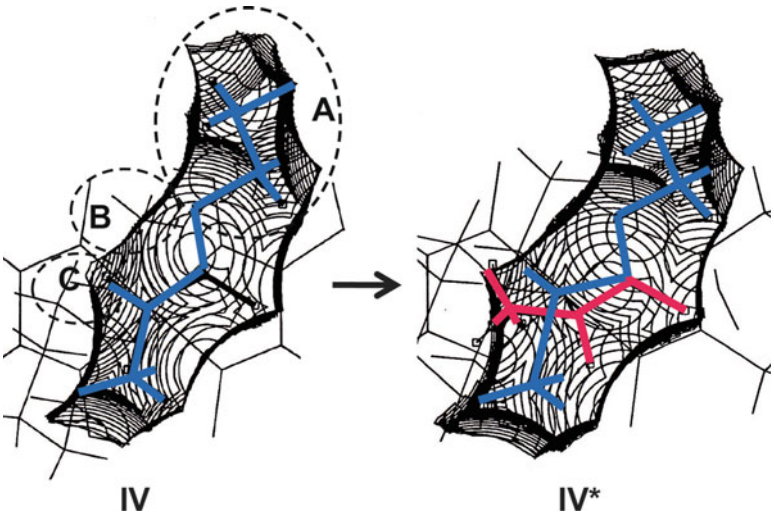

Fig. 4.8 Change of the reaction cavity before and after the irradiation in the monohydrate crystal. *A*, *B*, and *C* indicate the regions, in which the inverted group should be accommodated in the same way as that of the non-hydrate crystal

photo-irradiation is shown in Fig. 4.7. Only the methyl group is inverted to the opposite configuration. As shown in Fig. 4.8, the reaction cavity in the monohydrate crystal is smaller and narrower than that in the non-hydrate crystal. The cavity volumes in the neighboring of A and B regions, which should accommodate the inverted 1-ece group, are too small. Only the volume of the C region is available for the racemization. After 24 h exposure the *S*:*R* ratio of the 1-ece group became 50:50. This type of photo-racemization has been observed in many cobaloxime crystals. The reason why two crystal forms showed different reaction pathways is easily explained if the size and shape of the reaction cavities for *S*-1-ece groups of the two crystals are taken into account.

Further bulkier groups such as 1-(*sec*-propoxycarbonyl)ethyl and 1-(*tert*-*butoxycarbonyl*)ethyl groups were replaced with the 1-ece group and the

Scheme 4.2 Three (*R*-1-bce) cobaloxime complexes with *R*-cha: **1**, pyridine; **2,** water; **3,** as axial ligands

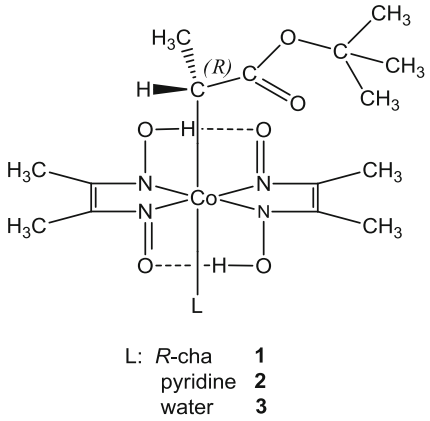

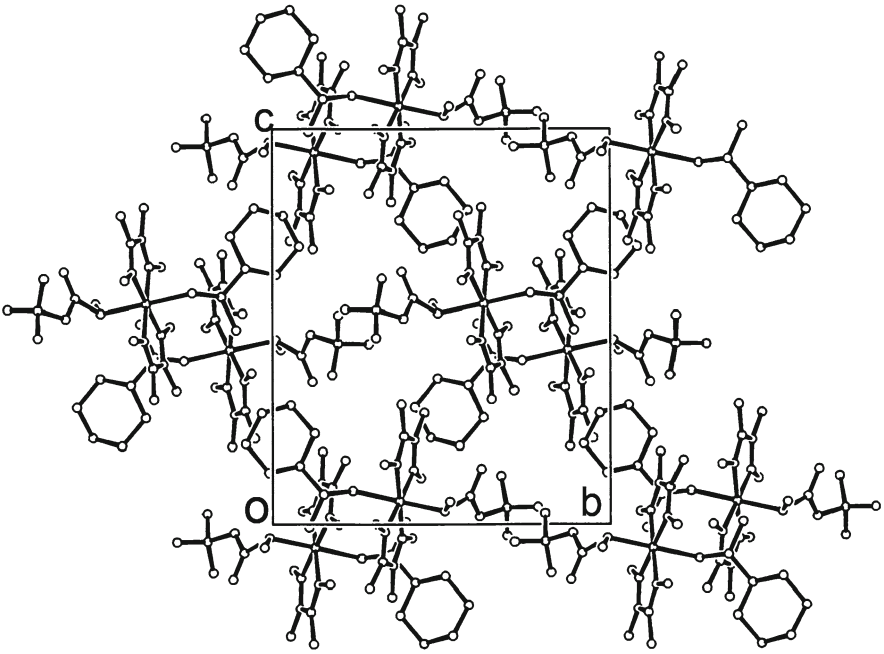

Fig. 4.9 Crystal structure of (*R*-1-bce)(*R*-cha)cobaloxime viewed along the *a* axis before photo-irradiation

photoreactions were examined. After many trials, it was successful to prepare the crystal with the *R*-1-*tert*-butoxycarbonylethyl, *R*-1-bce, group as shown in Scheme 4.2 [2]. The crystals were obtained for the three complexes with *R*-cha, pyridine (py), and water (aqua) as axial base ligands.

The crystal structure of *R*-cha viewed along the *a* axis before photo-irradiation is shown in Fig. 4.9. There is one molecule in an asymmetric unit of the $P2_12_12_1$ cell. There is no intermolecular hydrogen bond and no unusually short contacts

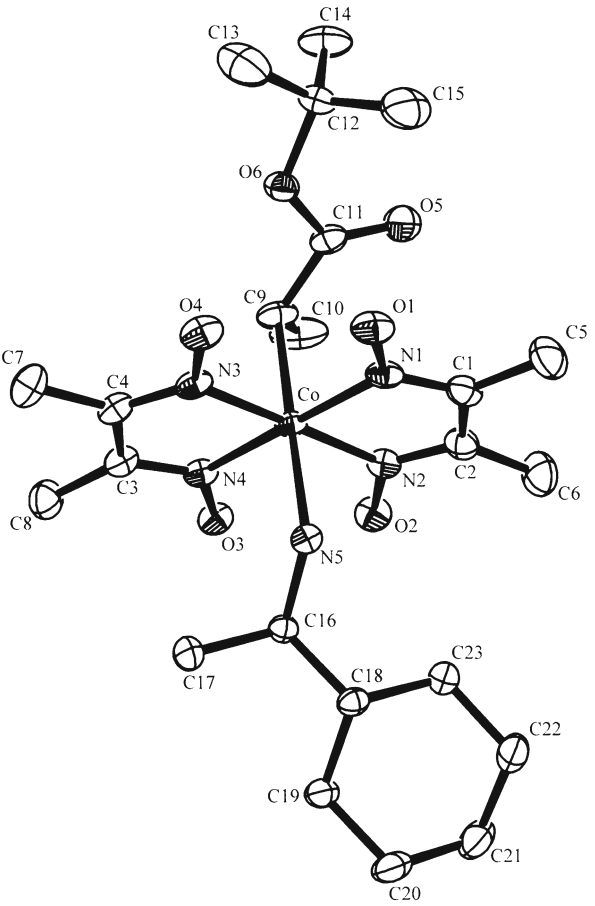

Fig. 4.10 Molecular structure of (*R*-1-bce)(*R*-cha) cobaloxime

between the molecules. The molecular structure is shown in Fig. 4.10. The absolute configuration of the 1-bce group is *R* and the methyl of 1-bce group is a *syn-periplanar* conformation to the carbonyl oxygen atom.

When the crystal was exposed to the xenon lamp, the cell dimensions gradually changed with retention of the single crystal form and the change became within experimental error after 72 h. The crystal structure after photo-irradiation is essentially the same as that before photo-irradiation except the several peaks around the *R*-1-bce group. The peaks were assigned to the *S*-1-bce group. The disordered molecular structure is shown in Fig. 4.11. A part of the *R*-1-bce group with black bonds was inverted to the *S*-1-bce group with white bonds by photo-irradiation. The *R:S* ratio became 0.753(4):247(4). The conformation of the 1-bce group retained *syn*-periplanar after photo-irradiation. It is noticeable that the *tert*-butyl and methyl groups in the peripheral parts of the 1-bce group occupy nearly the same positions during the inversion process although the central –C–C(=O)–C– atoms of the 1-bce group shifted to a fairly large extent.

Figure 4.12 shows the change of the reaction cavities for the *R*-1-bce group before and after the photo-irradiation. In order to examine the reason why the *R:S*

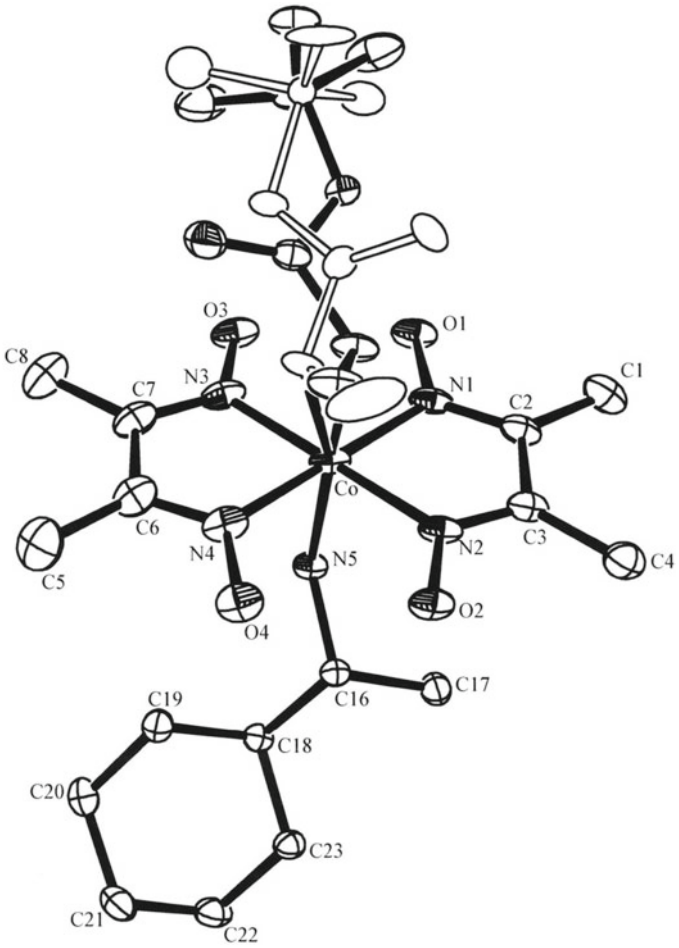

Fig. 4.11 Molecular structure of (*R*-1-bce)(*R*-cha)cobaloxime after the irradiation. The *R*-1-bce group with *black bonds* and the inverted *S*-1-bce group with *white bonds* are disordered

ratio converged ca. 75:25, the reaction cavity after the photo-irradiation was divided into two as shown in Fig. 4.13. The dotted line indicates the least-squares plane using the middle points of the corresponding atoms of the disordered bce groups and the plane is also adjusted to pass through the cobalt atom and to be perpendicular to the cobaloxime plane. The ratio of the volumes of the right and left halves is 45:55 before photo-irradiation, whereas it becomes ca. 50:50 after photo-irradiation.

It is clear that the strange ratio of 75:25 is caused by the equal intermolecular interaction between the original *R*-1-bce group and the newly produced *S*-1-bce group with the neighboring molecules. In order to make clear the chirality generation only by photo-irradiation, the photoreactions using the complex crystals with *S*-1-bce and *racemic*-1-bce groups should be necessary. The crystals, however, have not been obtained yet.

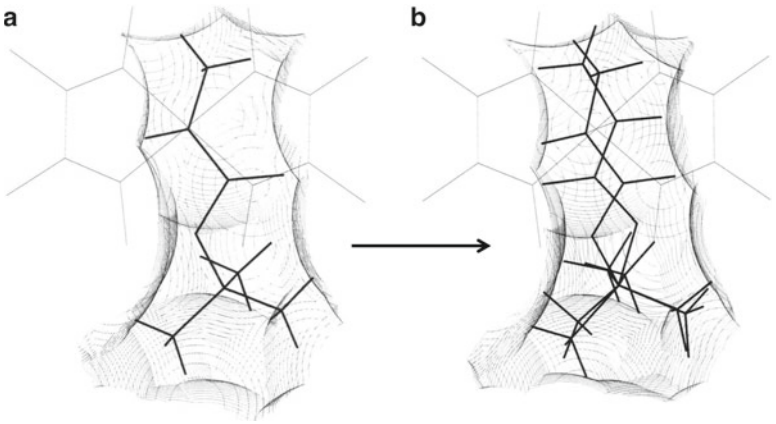

Fig. 4.12 Changes of the structure and reaction cavity for the *R*-1-bce group (**a**) before and (**b**) after the irradiation

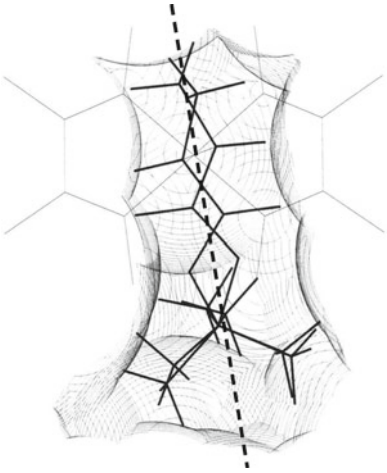

Fig. 4.13 Reaction cavity divided into two by the plane with *dotted line* after the irradiation

4.2 Various Racemization Paths of Bulkier Alkyl Groups

4.2.1 Two-Step Racemization of the 1,2-Bis(methoxycarbonyl) ethyl Group

The cobaloxime complexes with a bulky *R*-1,2-bis(methoxycarbonyl)ethyl group, (*R*-bmce) group, were prepared to examine whether the crystalline-state racemization would occur or not, because the powdered samples of the complexes were found to

Scheme 4.3 Five (*R*-1-bce) cobaloxime complexes with *S*-pea: **1**, *R*-pea; **2**, propylamine; **3**, dpmp; **4**, py; **5**, as axial ligands

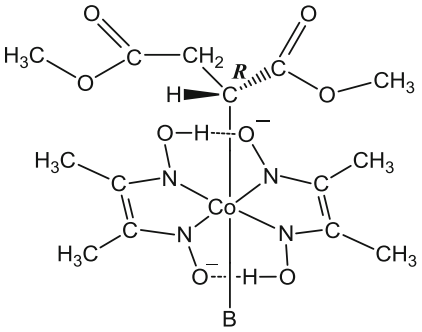

Fig. 4.14 Change of the *a* axis length observed in the crystal of (*R*-bmce)(dmpp) cobaloxime during the photo-irradiation

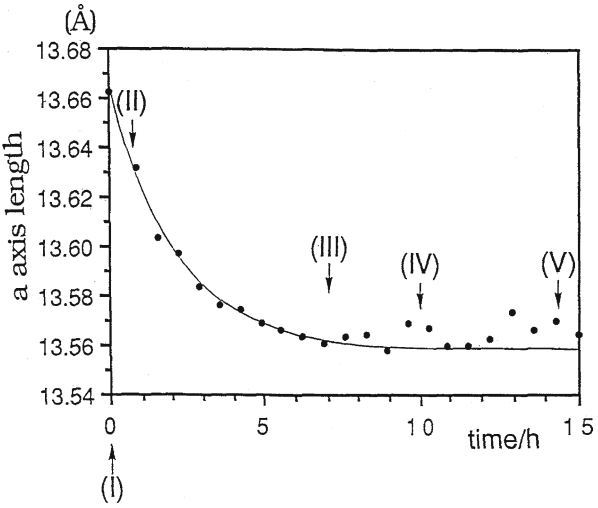

be racemized very fast on exposure to visible light [3]. Five kinds of complexes with different axial base ligands were crystallized as shown in Scheme 4.3. The crystals with *S*-1-phenylethylamine (*S*-pea, **1**), *R*-1-phenylethylamine (*R*-pea, **2**), and 1-propylamine (pa, **3**) as axial base ligands, which have the space groups of $P3_2$, $P2_1$, and $P2_1$, respectively, and only one molecule in the asymmetric unit, showed no racemization with retention of the single crystal form [4–6]. The crystal with diphenylmethylphosphine (dpmp, **4**) was racemized at 298 K [6], and the crystal with pyridine (py, **5**) was racemized only at 358 K [4]. Those crystals have two crystallographically independent molecules, A and B, in the asymmetric unit of the $P2_1$ cell.

When the dpmp crystal was irradiated with the xenon lamp at room temperature, the complex crystal was racemized without degradation of the crystallinity. After about 10 h exposure, the change of the cell dimensions became within experimental error. The change of the *a* axis length is shown in Fig. 4.14. Although the change of

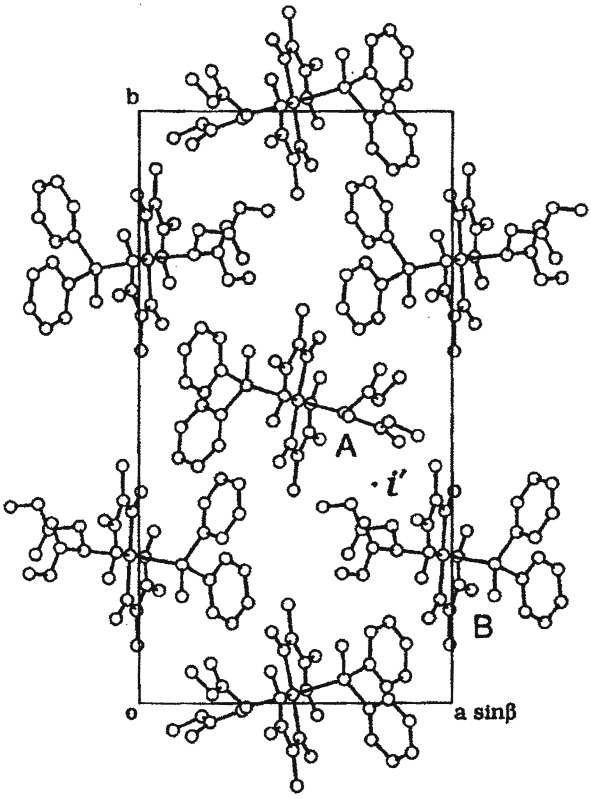

Fig. 4.15 Crystal structure of (*R*-bmce)(dmpp) cobaloxime at stage I

cell dimensions was small, it follows approximately first-order kinetics. The rate constant was calculated to be 1.3×10^{-4} s^{-1}. Because the intensities of reflections with h + l = odd gradually decreased and became zero, the space group changed from non-centrosymmetric $P2_1$ to centrosymmetric $P2_1/n$ [7]. Since the reaction rate was too fast, the three-dimensional intensity only at the final stage was collected with a four-circle diffractometer. In order to determine the structure at the initial and intermediate stages, a new type of diffractometer with two imaging plates for data recording was designed and made by Iwasaki and Kamiya [8]. The new diffractometer made it possible to collect a whole intensity data within 45 min.

The intensity data were collected at the initial stage and the three stages after 45 min and 7 and 10 h exposures. From the intensity data the structures at the first, second, third, and fourth stages, respectively, were obtained. The crystal structure at stage I is shown in Fig. 4.15. There are two crystallographically independent molecules, A and B, in an asymmetric unit. Except for the chiral bmce group, two molecules are related by a pseudo inversion center, *i'*. At stage IV, the bmce group of B is almost inverted to the opposite configuration and a crystallographic inversion center appeared between the two molecules. The space group is changed to $P2_1/n$. This transformation belongs to the second mode racemization as observed

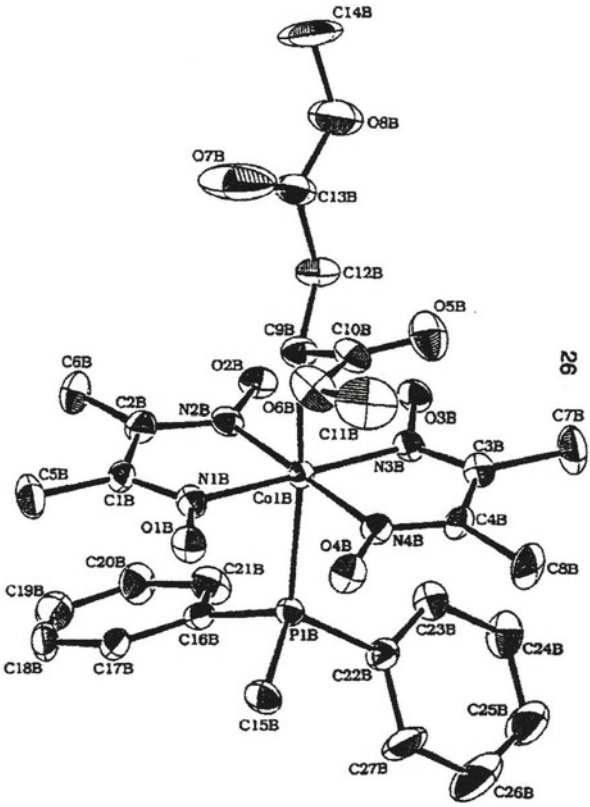

Fig. 4.16 Molecular structure of B in the crystal of (*R*-bmce)(dmpp) cobaloxime at stage I

for the chiral 1-ce and 1-mce groups. The molecular structure of B at stage I is shown in Fig. 4.16. The A molecule at stage I has a similar structure to B [7].

The reaction cavities for the A and B bmce groups were drawn and the cavity volumes were calculated to be 42.1 and 56.8 Å^3, respectively. It is clear that the B bmce group with larger cavity is inverted to the opposite configuration. This is also the same as that observed in the cobaloxime complexes with the chiral 1-ce and 1-mce groups.

The conformational and configurational changes of the B bmce group are shown in Fig. 4.17. The configuration of the chiral carbon atom is completely inverted to the opposite configuration. Moreover, the conformation around the perpendicular methoxyl group rotates by about 100° anticlockwise around the C–C bond [7].

Figure 4.18 shows the structural change of the B bmce group in the process of the inversion. At stage II, the disordered structure was observed around the perpendicular methoxyl group, which indicated the rotation around the C–C bond. At stage III, the disordered structure also appeared around the parallel methoxyl group, which indicated the inversion of the chiral carbon atom. Most of the perpendicular methoxyl group already rotated by 100°. The structures at the II and III stages clearly indicate that the B bmce group undergoes a conformational change

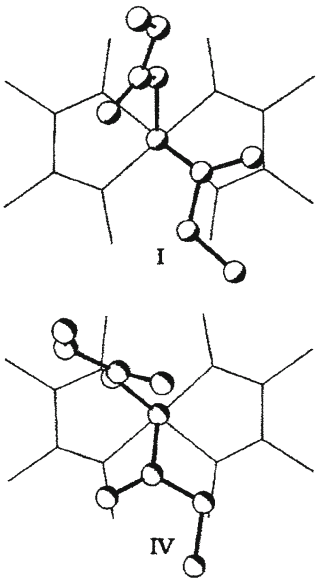

Fig. 4.17 Conformational and configurational changes of the B bmce group from stages I to IV

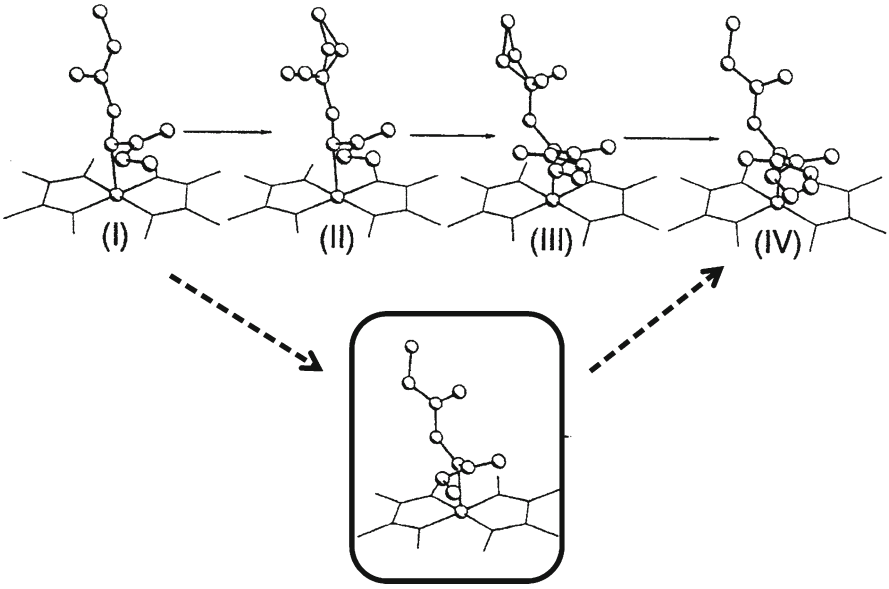

Fig. 4.18 Perspective view of the structural change of the B bmce group from stages I to IV. The lower structure means the intermediate structure during the reaction

at the first step and then is followed by the inversion to the opposite configuration. It is clear that the B bmce group should take an unstable intermediate structure different from the initial and final ones, as shown in the bottom of Fig. 4.18 [7].

For the complexes with 1-ce and 1-mce groups in the second mode, the structures of the B molecules were obtained only at the initial and final stages, that is, the structures before and after the inversion. Since the bmce group has a rotational freedom around the single bond, the metastable intermediate structure was able to be observed. Of course, the rapid data collection is an indispensable tool for the observation of unstable intermediate structures.

4.2.2 Hula-Twist Racemization of the 1,2-Bis(ethoxycarbonyl) ethyl Group

Further bulkier chiral groups than bmce group, 1,2-bis(ethoxycarbonyl)ethyl (bece) and 1,2-bis(allyoxycarbonyl)ethyl (bace) groups, bonded to the cobalt atom with various axial base ligands were prepared. The crystal structures of the bece complexes with *S*-pea [9], py [9], propylamine(pa) [9], and dpmp [10] were analyzed by X-rays. Each of four crystals has only one molecule in the asymmetric unit. The crystals with *S*-pea and dpmp have the space group of $P2_1$, while those with py and pa have the space group of $P2_12_12_1$. The *S*-pea crystal has a solvent 2-propanol molecule. For the bace complexes, the crystal structures with *R*-pea [11] and *S*-pea [12] were analyzed by X-rays. Each crystal has only one molecule in the asymmetric unit of the $P2_1$ cell.

It was thought that the crystalline-state racemization would not be observed for the above complex crystals, because the cooperative motion of the two reactive groups may be impossible to occur as observed in the bmce complex crystal. However, the powdered sample of the bece complex with py as an axial base ligand showed photo-racemization very rapidly whereas those of the other five powdered samples with the bece and bace groups were racemized very slowly. A single crystal of the py complex was carefully irradiated with a xenon lamp. Figure 4.19 shows the crystal structure viewed along the *c* axis before photo-irradiation. There is one molecule in an asymmetric unit of the $P2_12_12_1$ cell. The bece groups of the molecules, however, are connected with the neighboring bece groups. There is no unusually short contact between the molecules. The molecular structure is shown in Fig. 4.20.

The bece group before photo-irradiation has only *R* configuration. After irradiation with a xenon lamp for 15 h, the volume of the unit cell increased by 32 $Å^3$ and the disordered bece group appeared around the original bece group. In order to make clear the disordered structure of the bece group, it was projected on the cobaloxime plane as shown in Fig. 4.21. The new bece group has *S* configuration. The original *R* and photo-produced *S*-bece groups have the same occupancy factors, 50:50. This means that such a large group is completely racemized by photo-irradiation with retention of the single crystal form and the racemization mode is the same as the first mode observed in the 1-ce complex crystals.

The size of the reaction cavity plays an important role in the first mode of racemization as observed in the 1-ce complex crystals. The cavities for the bece groups

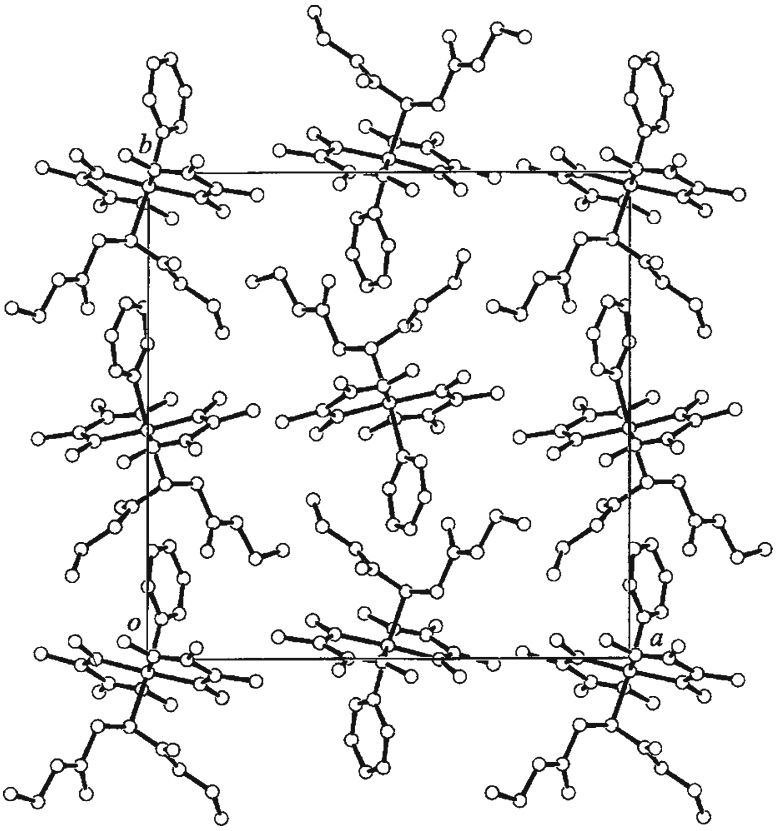

Fig. 4.19 Crystal structure of (*R*-bece)(py)cobaloxime before the irradiation, viewed along the *c* axis

in the four crystals were drawn and the volumes were calculated. They are 68.8, 76.5, 58.9, and 75.8 Å^3 for the *S*-pea, py, pa, and dpmp complexes, respectively. Since the cavity size of py is the largest, the crystalline-state racemization can be observed. Although the dpmp crystal has approximately the same cavity size as that of the py crystal, the racemization was observed only in the powdered sample. This is because the reactive groups in the py crystal are related to each other with a two-fold screw axis along the *a* axis as shown in Fig. 4.19. The partial cooperative motion between the bece groups may play an important role in the crystalline-state racemization. In the $P2_1$ cell of the dpmp crystal, such a cooperative motion cannot occur since the bece group is completely isolated from each other.

It may be possible for the bece group to be inverted to the opposite configuration through some unstable intermediate stages as observed for the bmce group in the dpmp complex crystal. However, it was very difficult to observe the peaks other than those of the inverted group in the intermediate stages. Although the definite information other than X-ray data such as spectroscopic data were necessary, it is

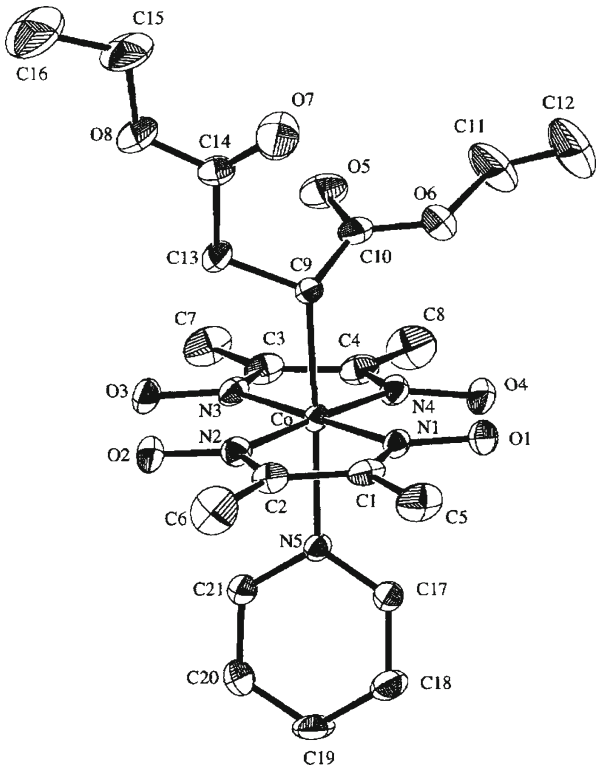

Fig. 4.20 Molecular structure of (*R*-bece)(py) cobaloxime before the irradiation

impossible to assign the minor structure with different conformation from the spectroscopic data.

For the bace complex crystals, the volumes of the reaction cavities were calculated to be 68.3 and 68.0 $Å^3$, respectively. The volumes of cavities are too small for the bace group to be racemized without destroying the crystalline lattice.

It was made clear by neutron diffraction that the chiral 1-ce group was inverted in the three steps: the Co–C bond cleavage, rotation of the produced cyanoethyl radical around the C–C–N bond, and the recombination of the Co–C bond. However, the bece group seemed too bulky to be inverted in the similar process. Although the Co–C bond cleavage by the photo-irradiation and the recombination may be the same as those of the 1-ce group, the second step, rotation of the produced radical, may be impossible. The photo-inversion process of such a bulky group in the crystalline lattice is very interesting as it would be a model of enzymatic activities or catalytic reactions in a restricted environment.

Arai and Ohgo proposed a mechanism of 1,2-hydrogen migration from the ^{1}H NMR measurements [13]. They prepared a deuterated cobaloxime complex [*R*-1,2-bis(ethoxycarbonyl)ethyl-$d_2^{\beta,\beta}$](pyridine)cobaloxime as shown in Scheme 4.4. On exposure to visible light, the NMR signals of the powdered sample indicated that another deuterated complex was produced due to the migration of a

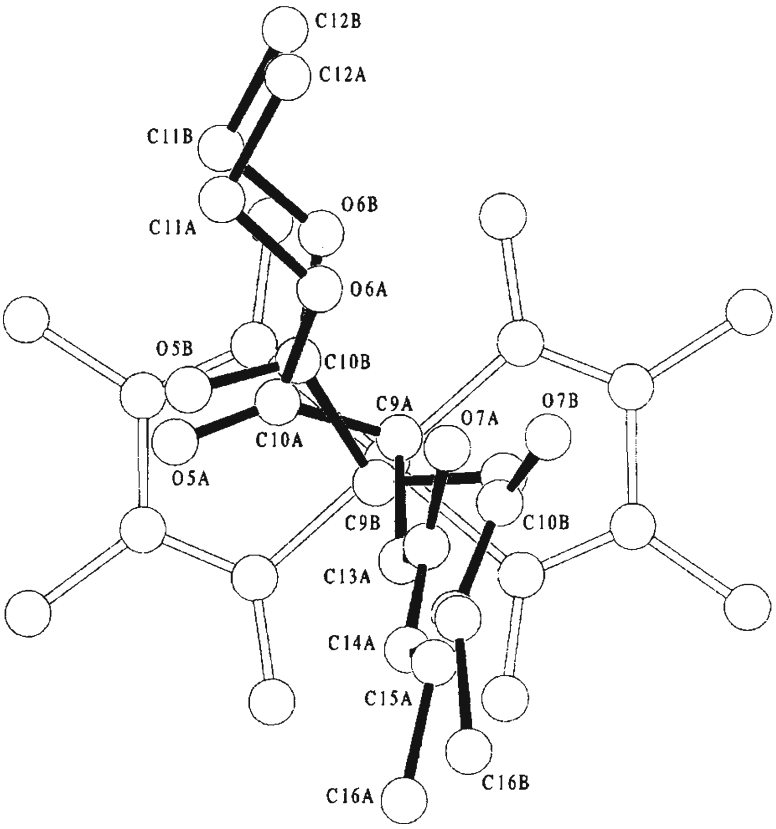

Fig. 4.21 Conformation and configurations of the disordered bece group after the irradiation

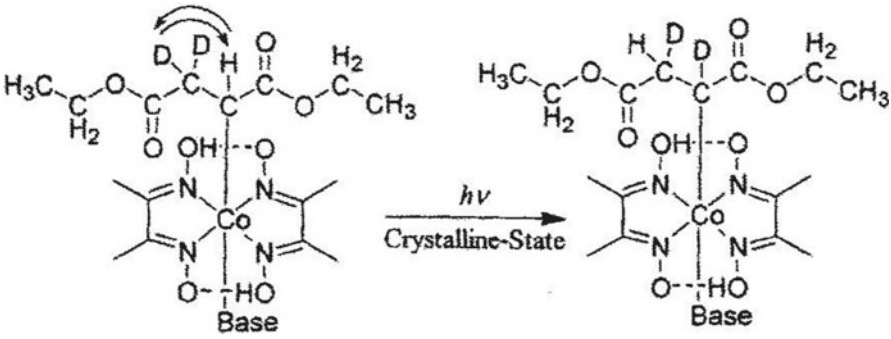

Scheme 4.4 A proposed mechanism of 1,2-hydrogen migration from the ^{1}H NMR measurements in a deuterated cobaloxime complex

Scheme 4.5 The complex of [*R*-1,2-bis(ethoxycarbonyl) ethyl-d_1^{α}]-(pyridine-d_5) cobaloxime

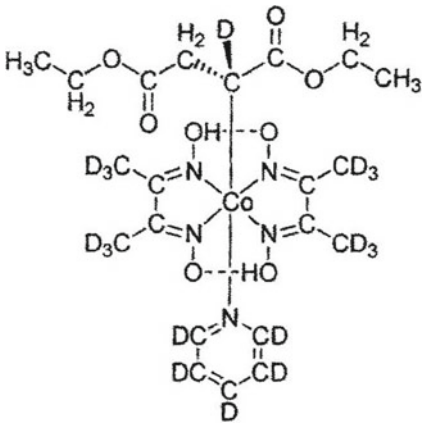

hydrogen atom from the α-carbon to the neighboring β-carbon. This mechanism is more probable than that estimated from the same model as that of the 1-ce group from the topochemical point of view. In fact, the methine H atom of the cyanoethyl group was replaced with the D atom and the cobaloxime crystal with *S*-pea was irradiated with visible light. The structure after photo-irradiation indicated the exchange of the methine D atom with the H atoms of the methyl group occurred, although the exchange rate was small in spite of very long exposure to visible light [14]. In addition, the X-ray structure of the pyridine complex with the bece group after photo-irradiation well explained the migration mechanism since the two ethoxycarbonyl groups of bece occupy nearly the same positions as those before photo-irradiation as shown in Fig. 4.21.

To make clear the mechanism, the complex of [*R*-1,2-bis(ethoxycarbonyl)ethyl-d_1^{α}] (pyridine-d_5)cobaloxime, as shown in Scheme 4.5, was prepared [15]. A big crystal suitable for the neutron work was obtained after many trials and was irradiated with visible light. A small portion of the crystal was cut from the photo-irradiated crystal and the structure was analyzed by X-rays. The disordered molecular structure is the same as that shown in Fig. 4.21. About 48 % of *R*-bece groups were inverted to the opposite configuration.

The neutron data were obtained using the main portion of the photo-irradiated crystal with the BIX-3 diffractometer at JAERI. Although the analyzed structure is essentially the same as that analyzed by X-rays, only 33 % of *R*-bece groups were inverted to the opposite configuration. This indicated that it was very difficult for the light to penetrate into the large crystal. The disordered molecular structures after the irradiation are shown in Fig. 4.22. The deuterium atom bonded to the chiral carbon atom is not changed to the other carbon atom not only in the original *R*-bece group but also in the inverted *S*-bece group. The two hydrogen atoms bonded to the neighboring methylene moiety in the bece group do not change their positions after the inversion.

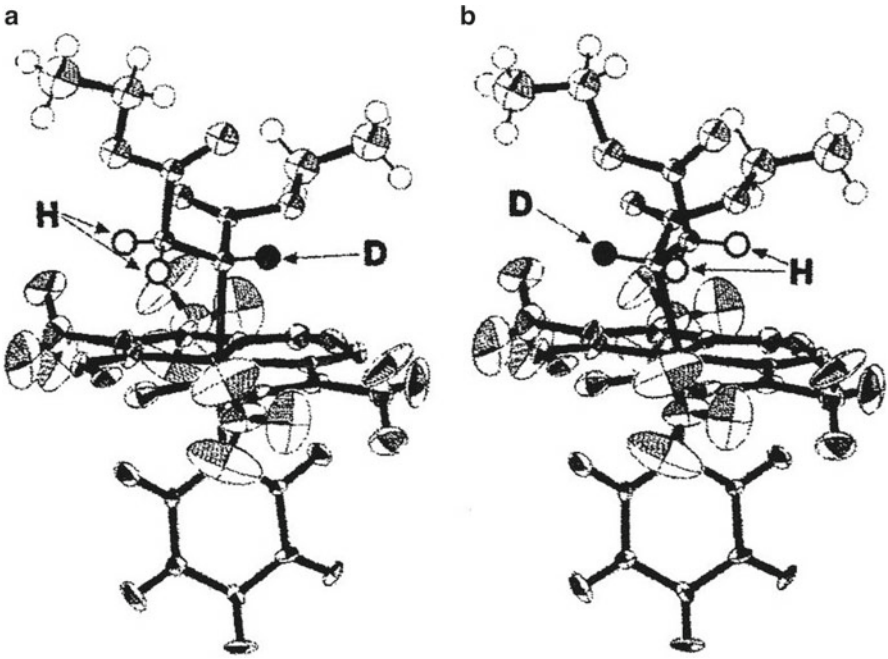

Fig. 4.22 Molecular structure of the deuterated (R-bece)(py)cobaloxime, (**a**) before irradiation and (**b**) after irradiation

These results suggest that the photo-inversion of the bulky alkyl groups does not follow the proposed mechanism from ^{1}H NMR measurement as shown in Scheme 4.4. The C*–D bond is kept in the inversion process even if the alkyl group is very bulky. This indicates a new mechanism of photo-inversion of the bulky group in the crystalline lattice as shown in Fig. 4.23. On exposure to visible light, the Co–C* bond is cloven and the bece radical and Co(II) are produced. The two bonds of C*–CH_2 and C*–CO_2 of the radical rotate in the sense indicated by arrows. The deuterium atom passes over the cobalt atom following the rotation of the C*–D bond and then the D atom moves to the opposite side. Finally the radical carbon and the cobalt atom are recombined to form the opposite configuration of the alkyl group. In this mechanism, the 1,2-hydrogen migration is not required and the amount of the atomic movement of the whole bece group is very small.

This motion is very similar to the "hula-twist motion," a model of the *cis–trans* isomerization of retinylidene chromophore in rhodopsin as shown in Fig. 4.24 [16–19]. Such a motion is believed to be very suitable for isomerization in a highly restricted environment, for example, in enzymatic reactions in a living cell or

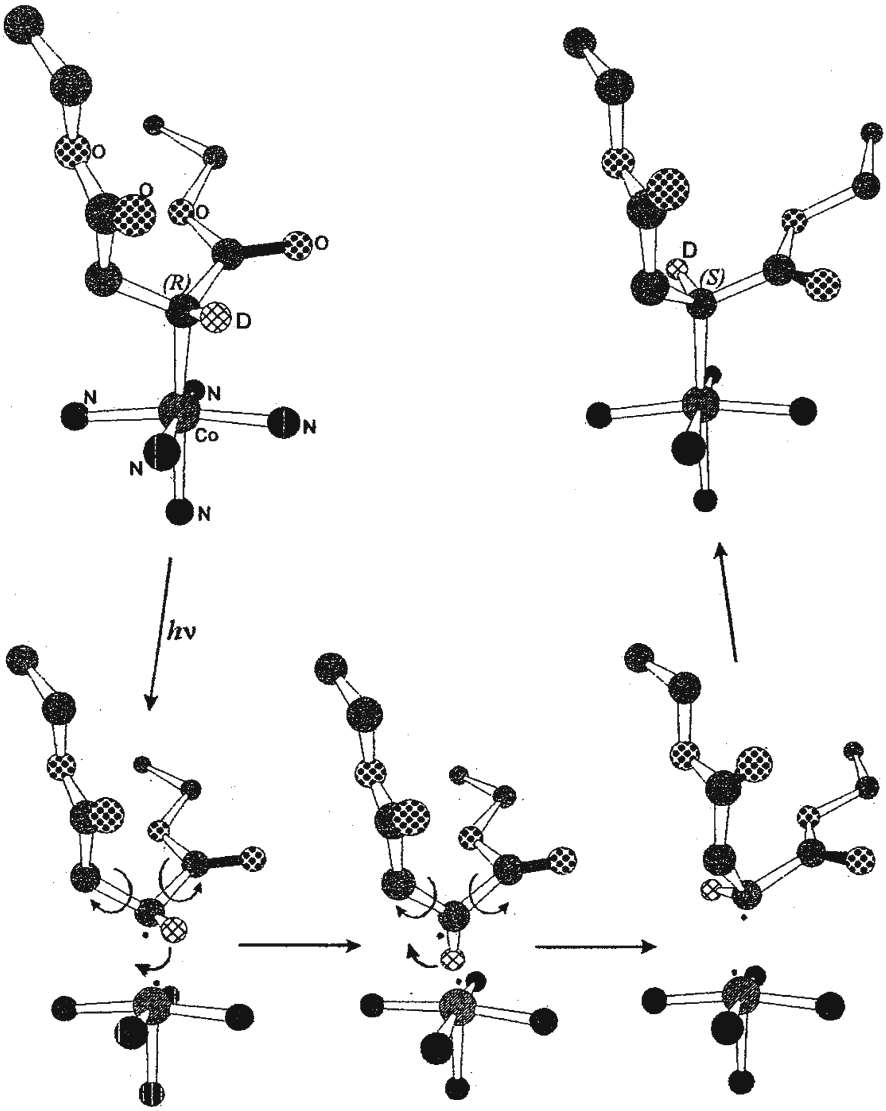

Fig. 4.23 Inversion process of the bece group deduced from the neutron diffraction

catalytic reactions. The present inversion process seems to be the first direct observation of hula-twist motion in a restricted environment, crystalline lattice, although the sp^2 carbon of the double bond is replaced with the sp^2 radical carbon.

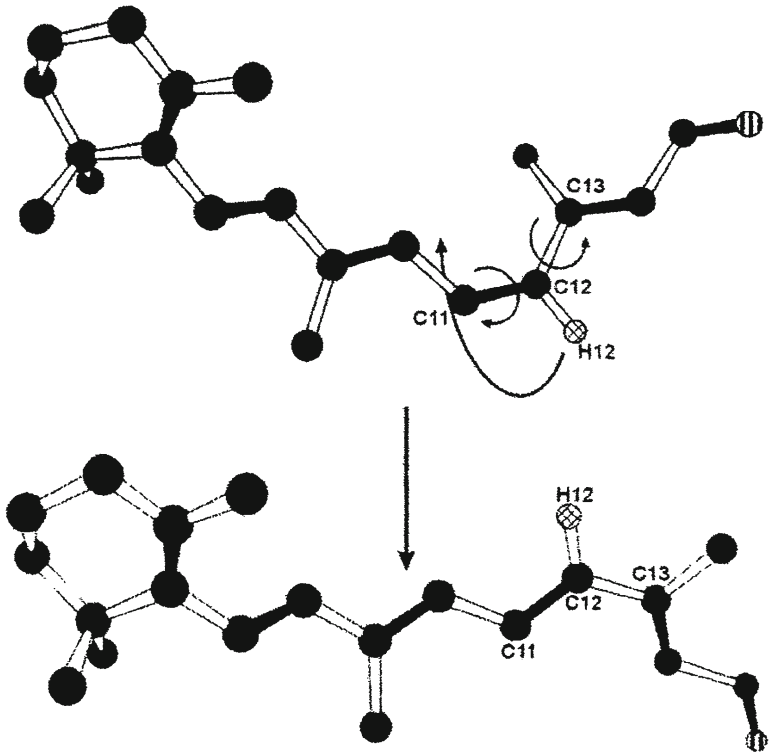

Fig. 4.24 "Hula-twist motion" in the *cis–trans* isomerization of retinylidene in rhodopsin

References

1. Nitami T, Sekine A, Uekusa H, Ohashi Y (2011) Bull Chem Soc Jpn 84:1066
2. Takeoka H, Sekine A, Uekusa H, Ohashi Y (2013) J Chin Chem Soc 60:898–906
3. Ohgo Y, Arai Y, Takeuchi S (1991) Chem Lett 455
4. Sakai Y, Ohashi Y, Arai Y, Ohgo Y (1992) Mol Cryst Liquid Cryst 219:149
5. Sakai Y, Tamura T, Uchida A, Ohashi Y, Hasegawa E, Arai Y, Ohgo Y (1991) Acta Crystallogr C47:1196
6. Sakai Y, Ohashi Y, Yamanaka M, Kobayashi Y, Arai Y, Ogho Y (1993) Acta Crystallogr B49:1010
7. Ohashi Y, Sakai Y, Sekine A, Arai Y, Ohgo Y, Kamiya N, Iwasaki H (1995) Bull Chem Soc Jpn 68:2517
8. Kamiya N, Iwasaki H (1995) J Appl Cryst 28:745
9. Sato H, Ohashi Y (1999) Bull Chem Soc Jpn 72:367
10. Yamada T, Sekine A, Uekusa H, Ohashi Y (1995) Acta Crystallogr C51:828
11. Sakai Y, Sato H, Ohashi Y, Arai Y, Ohgo Y (1995) Anal Sci 11:873
12. Sato H, Sakai Y, Ohashi Y, Arai Y, Ohgo Y (1996) Acta Crystallogr C52:1086
13. Arai Y, Ohgo Y (1998) Bull Chem Soc Jpn 71:1871

14. Ohgo Y, Ohashi Y, Klooster WT, Koetzle TF (1997) Enantiomer 2:241
15. Ohhara T, Ikeda S, Imura H, Uekusa H, Ohashi Y, Tanaka I, Niimura N (2002) J Am Chem Soc 124:14736
16. Liu RSH, Asato AE (1985) Proc Natl Acad Sci USA 82:259
17. Lie RSH, Browne DT (1986) Acc Chem Res 19:42
18. Liu RSH, Hammond GS (2000) Proc Natl Acad Sci USA 97:11153
19. Ishiguro M (2000) J Am Chem Soc 122:444

Chapter 5
Photoisomerization of Alkyl Groups in Cobaloxime Complexes

Abstract The 2-cyanoethyl group bonded to the cobalt atom is isomerized to the 1-cyanoethyl group. The reaction rate was accelerated if the reactant molecule was mixed with the product molecule. The enlarged reaction cavity in the mixed crystal accelerated the reaction. If the cavity shape is asymmetric, the produced 1-cyanoethyl group is chiral, that is, one of the *R* and *S* configurations is preferentially produced. Chirality generation was estimated from the shape of the cavity before the reaction. The 3-cyanopentyl and 4-cyanobutyl groups are also isomerized to 1-cyanopentyl and 3-cyanobutyl groups, respectively. The 3-cyanobutyl group was not isomerized to the 2-cyanobutyl and 1-cyanobutyl groups, keeping the single crystal form. For the 2-butenyl group, the *trans–cis* isomerization occurs with retention of the single crystal form. For the 3-butenyl group, the *trans–cis* isomerization does not occur, keeping the single crystal form, although the isomerization occurred in the solid state.

Keywords Chirality generation • Mixed crystal • Photoisomerization • *Trans–cis* isomerization

5.1 Photoisomerization of 2-Cyanoethyl Group

It was found that the 2-cyanoethyl (2-ce) group bonded to the cobalt atom is isomerized to the 1-ce group on exposure to visible light only in the solid state as shown in Scheme 5.1 [1]. The reaction is not observed in solutions probably because the complicated coupling reactions between the produced alkyl radicals would occur. Since the crystals are usually decomposed as the reaction proceeded, the reaction rate is estimated from the change of the IR spectra due to the C–N triple bond. Several KBr discs of a cobaloxime complex were irradiated with a xenon lamp under the same conditions and the IR spectra were measured one by one at a constant interval. The spectra due to the stretching vibration mode of the cyano

Y. Ohashi, *Crystalline State Photoreactions: Direct Observation of Reaction Processes and Metastable Intermediates*, DOI 10.1007/978-4-431-54373-2_5,

Scheme 5.1 The 2-cyanoethyl group in the (2-ce)cobaloxime complex is photoisomerized to the 1-ce group only in the solid state

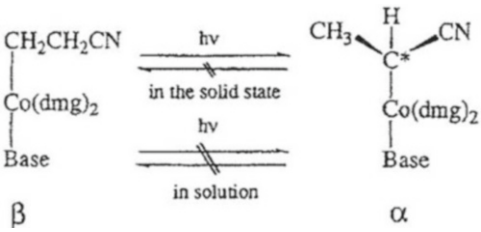

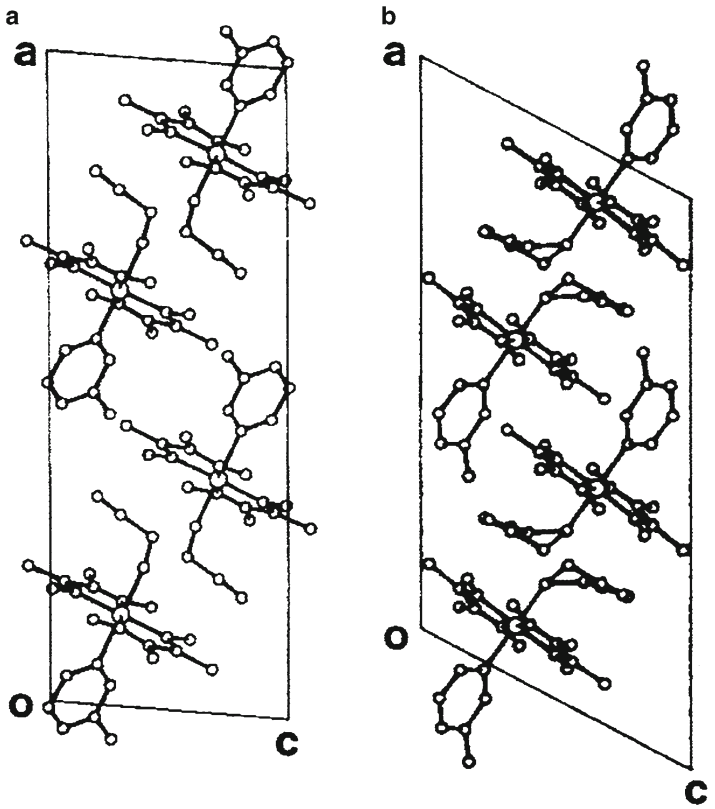

Fig. 5.1 Two crystal forms of (**a**) I and (**b**) II forms obtained from (2-ce)(3mpy)cobaloxime

group gradually changed from ca. 2,250 cm^{-1} of the 2-ce group to ca. 2,200 cm^{-1} of the 1-ce group. The reaction rate was estimated from the decrease of the spectrum of the 2-ce group and the increase of that of the 1-ce group.

Two crystal forms were obtained under the same conditions when 3-methylpyridine (3mpy) was used as an axial base ligand [2]. The crystal structures of the two forms, **I** and **II**, are shown in Fig. 5.1. There is one molecule in an asymmetric unit in the $P2_1/a$ cell in each crystal. The molecular structures of **I** and **II** are shown in

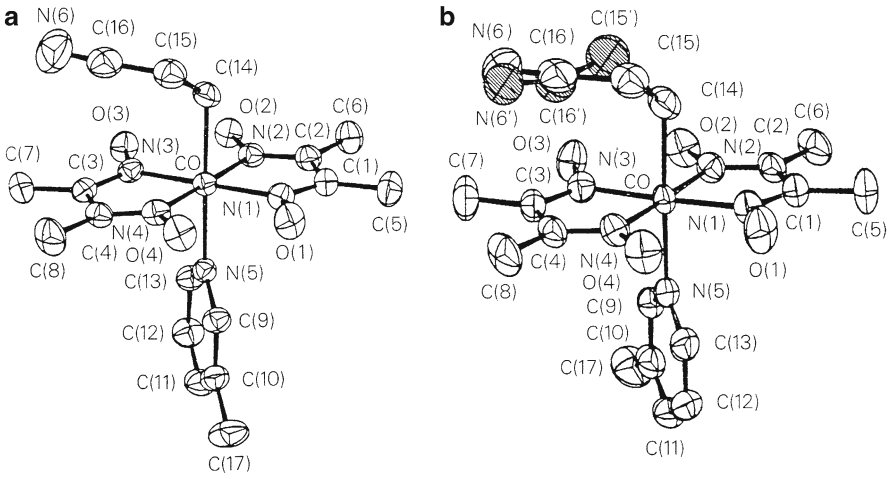

Fig. 5.2 Molecular structures of (**a**) I and (**b**) II forms. Disordered atoms are shaded

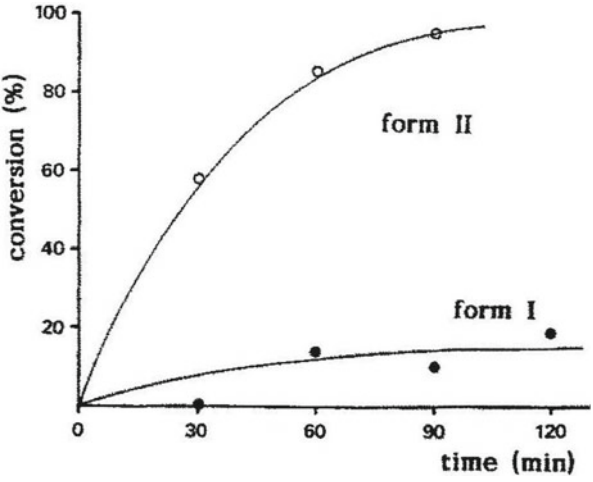

Fig. 5.3 Isomerization rates with exposure time for the I and II forms

Fig. 5.2. The 2-ce group of **I** has an ordered structure while that of **II** takes a disordered one. The isomerization rates of the two forms are quite different, as shown in Fig. 5.3. The reaction rate of **II** is remarkably greater than that of **I**. The reaction cavity for the 2-ce group was drawn and the volume was calculated for each crystal. The volumes are 10.4 and 11.9 $Å^3$ for **I** and **II**, respectively. It is clear that the 2-ce group with greater reaction cavity has greater reaction rate than that with smaller cavity. The relation between the reaction rate and the cavity size holds well for the photoisomerization in the solid state. It is clear that the cavity size is the first factor controlling the reaction rate.

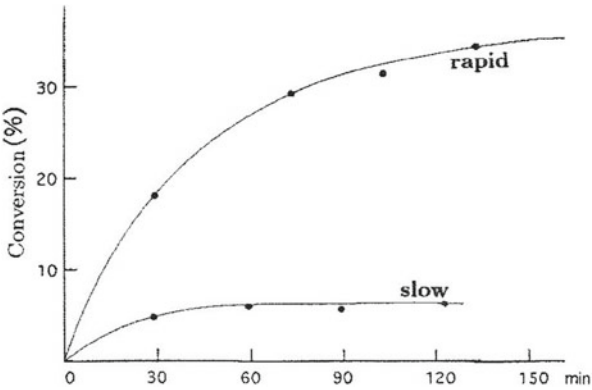

Fig. 5.4 Isomerization rates with exposure time for the powdered samples of (2-ce)(tpp) cobaloxime obtained in the rapid and slow crystallizations

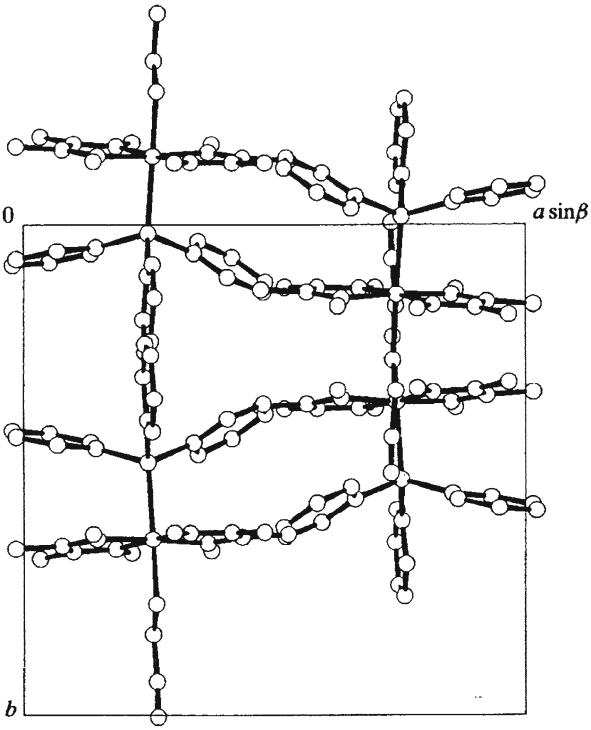

Fig. 5.5 Crystal structure of the form I of (2-ce)(tpp) cobaloxime viewed along the *c* axis

The powdered sample of the complex with triphenylphosphine as an axial base ligand gave a strange result; the sample obtained by rapid crystallization showed a significantly larger reaction rate than that of the sample obtained by slow crystallization, as shown in Fig. 5.4 [3]. Both samples, of course, contain no impurity. The 14 and 10 crystals suitable for X-ray analysis were picked up from the rapid- and slow-crystallization samples, respectively. To our surprise, there were four crystal

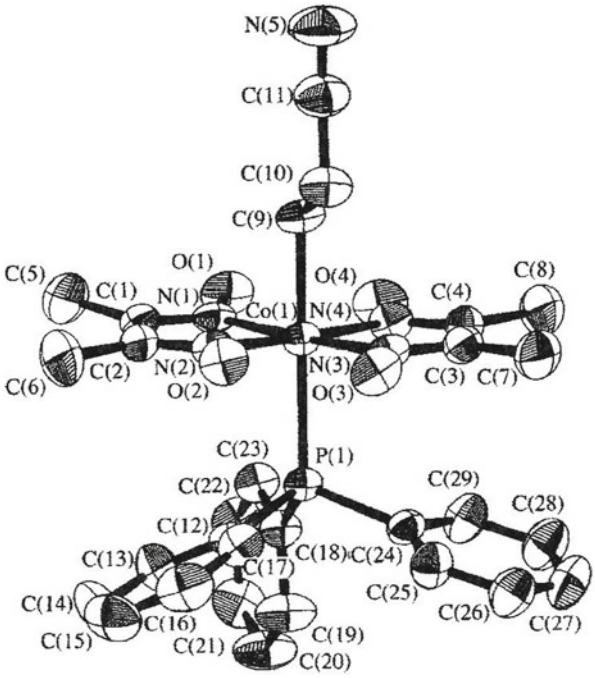

Fig. 5.6 Molecular structure of the form I of (2-ce)(tpp) cobaloxime

forms, **I**, **II**, **III**, and **IV**, in the former sample, while there were only two forms, **I** and **II**, in the latter sample.

The crystal structures of four forms were analyzed by X-rays. Although the four crystals have different space groups and unit-cell dimensions, the discrimination from their appearance on a microscope is very difficult, since the four crystal forms have similar colors and shapes. The crystal and molecular structures of form **I** are shown in Figs. 5.5 and 5.6, respectively. There is one molecule in an asymmetric unit of the $P2_1/c$ cell. The 2-ce group has a perpendicular conformation to the cobaloxime plane. The crystal **II** has two crystallographically independent molecules, A and B, in the asymmetric unit of the *Pbca* cell. Both of the 2-ce groups have the perpendicular conformations, but have different torsion angles around the Co–C bond. The crystals **III** and **IV** have one molecule in the asymmetric unit of the $P2_1/c$ and $P2_12_12_1$ cell, respectively. The molecular structure of **III** is shown in Fig. 5.7. The 2-ce group takes a disordered structure, both of which are perpendicular conformations. The molecular structure of **IV** has a disordered structure similar to that of **III**. The volumes of the reaction cavities for the 2-ce groups of five molecules, **I**, **II**A, **II**B, **III**, and **IV**, are calculated to be 13.7, 10.9, 14.0, 15.7, and 19.0 Å^3, respectively. If it may be possible to assume that the compositions of the four crystal forms in the sample obtained by rapid crystallization are the same as those of the crystals suitable for X-rays, the composition ratio of I:II:III:IV is 1:8:1:4. This indicates that approximately one third of the powdered samples (5/14) have larger reaction cavities than those obtained by slow crystallization, in which the ratio of I:II is 1:9. This

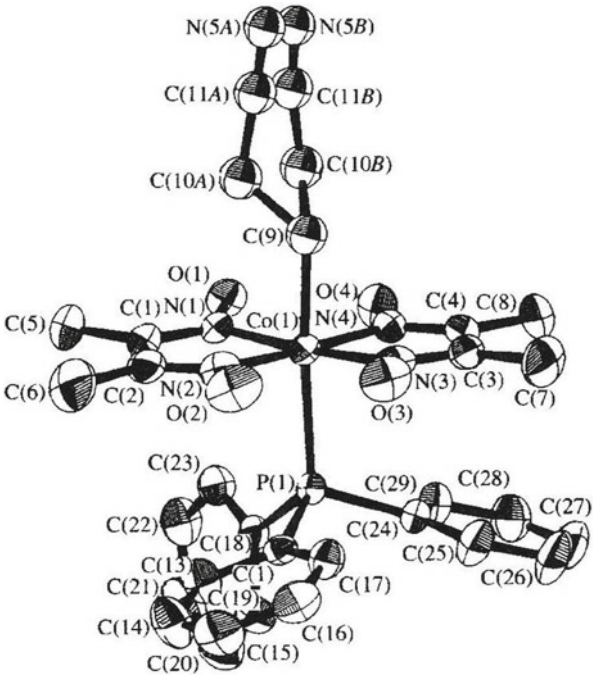

Fig. 5.7 Molecular structure of the form III of (2-ce)(tpp)cobaloxime

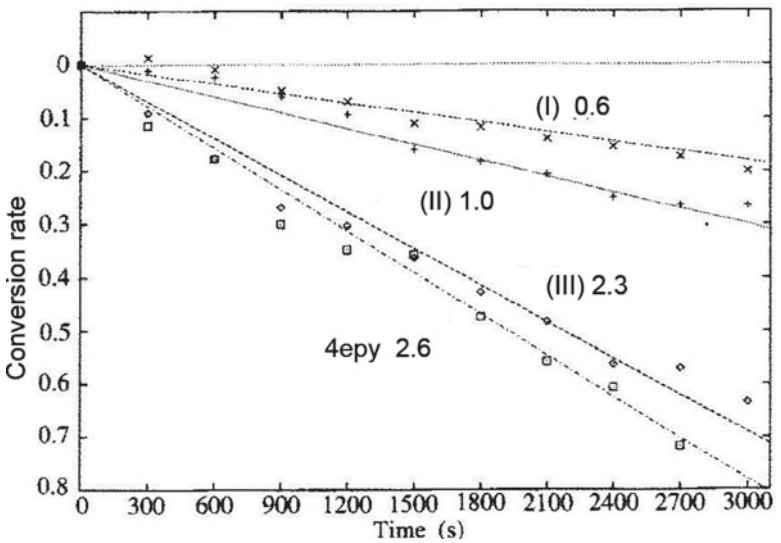

Fig. 5.8 Reaction rates of the I, II, and III forms and the corresponding one of the (2-ce)(4epy) cobaloxime for comparison. Each rate constant (s^{-1}) is multiplied by 10^4

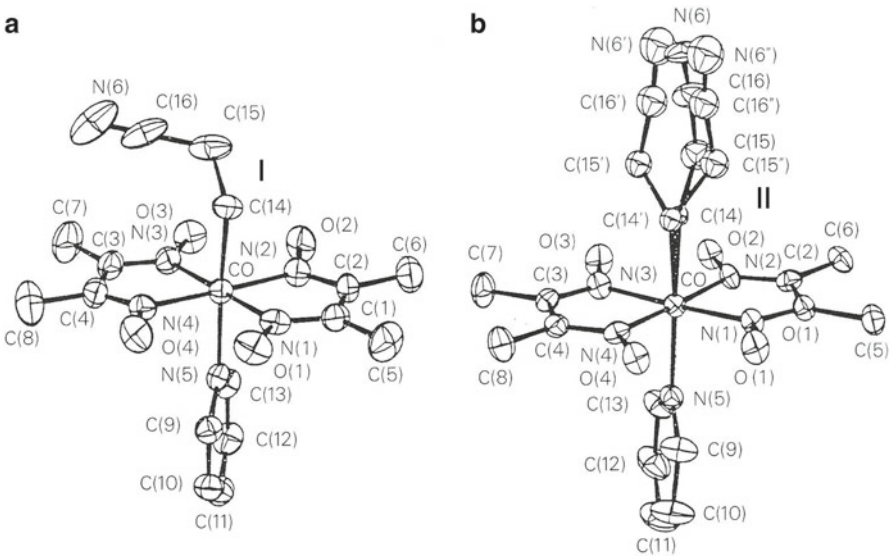

Fig. 5.9 Molecular structures of (2-ce)(py)cobaloxime in the crystals of (**a**) form I and (**b**) form II

is a reason why the powdered sample by rapid crystallization showed a significantly larger reaction rate than the sample by slow crystallization as shown in Fig. 5.4.

In order to elucidate the relation between the reaction cavity for the 2-ce group and the reaction rate more directly, many trials to obtain each crystal form separately were performed. Finally, the crystal forms **I**, **II**, and **III** were obtained successfully, but all the attempts to get the form **IV** were in vain [4]. The KBr discs of each crystal were exposed to a xenon lamp and the IR spectra were measured at intervals of 5 min. The log plots of the reaction rates at early stages are shown in Fig. 5.8. The change of each crystal is well explained by first-order kinetics. The rate constants were calculated to be 0.6, 1.0, and 2.3×10^{-4} s^{-1} for **I**, **II**, and **III**. Crystal **II** has two independent molecules. It seems plausible to assume that the 2-ce group with a larger reaction cavity may change more rapidly than that with a smaller cavity in the early stages. It is clear that the reaction rate has a good correlation with the size of the reaction cavity. It is noteworthy that the "pure" sample in the solid-state reaction should be composed of "only one crystal form" and that it is distinct from the "pure" sample in solution, in which different molecules are not included as impurities.

When the axial base ligand was replaced with pyridine (py), two crystal forms, **I** and **II**, were obtained under the same conditions [5]. Figure 5.9 shows the molecular structures of the two forms. The 2-ce group of **I** has an approximately parallel conformation to the cobaloxime plane, whereas that of **II** has a perpendicular conformation to the plane. Moreover, the 2-ce group of **II** has a disordered structure. The isomerization rates of the two crystal forms were measured in the same way as those of the two forms of the 3mpy crystals. Form **I** with parallel conformation has significantly a faster rate than form **II** with perpendicular conformation, as shown in Fig. 5.10.

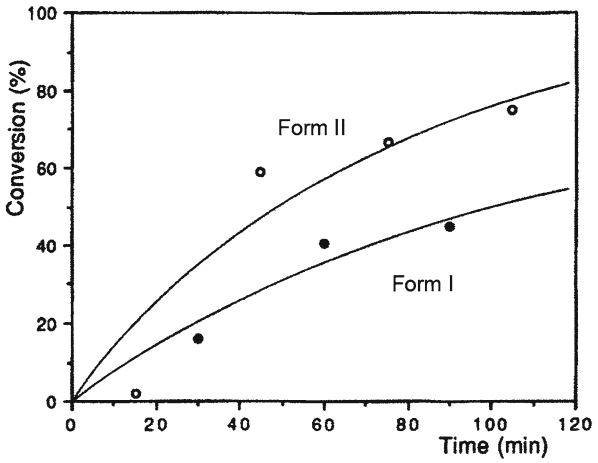

Fig. 5.10 Reaction rates for the I and II forms of (2-ce)(py)cobaloxime

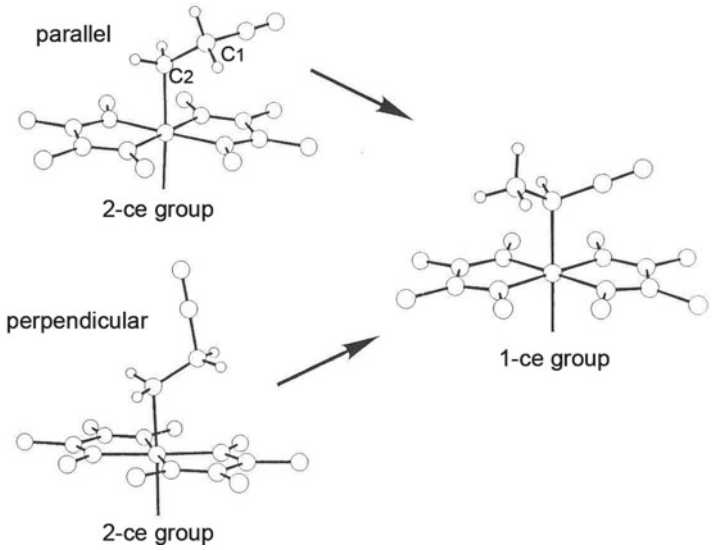

Fig. 5.11 Isomerization process of the 2-ce to 1-ce group with the parallel and perpendicular conformations

The cavities for the 2-ce groups of **I** and **II** were drawn and the volumes are 10.5 and 12.3 $Å^3$, for **I** and **II**, respectively. Although the cavity of **I** is smaller than that of **II**, the reaction rate of **I** is faster than that of **II**. As shown in Fig. 5.11, the cobalt atom makes a bond with the C_1 atom of the 2-ce group, following the extraction of one of the two hydrogen atoms bonded to the C_1 atom and transferring it to the C_2

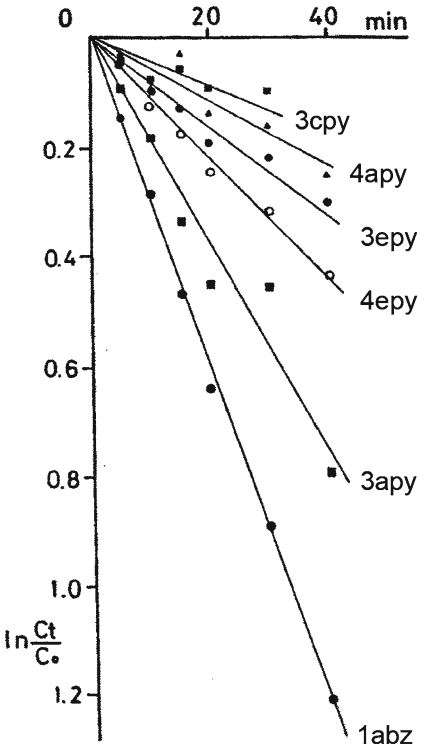

Fig. 5.12 Isomerization rates of six cobaloxime crystals with different axial base ligands

atom to be a methyl group. If the 2-ce group has the parallel conformation, one of the H atoms bonded to C_1 comes close to the cobalt atom and the 2-ce group would be more easily transformed to the 1-ce group than that with the perpendicular conformation. The displacement of the 2-ce group with the parallel conformation is clearly smaller than that of the perpendicular conformation. The topochemical process is the second factor controlling the reaction rate.

In order to examine the relation between the reaction rate and the crystal structure more systematically, ten cobaloxime complexes with different axial base ligands were prepared. They have piperidine (pip) [6], 3-cyanopyridine (3cpy) [7], 4-aminopyridine (4apy) [7], 3-ethylpyridine (3epy) [8], 4-ethylpyridine (4epy) [8], 3-aminopyridine (3apy) [9, 10], 1-aminobenzene (1abz) [9, 10], *S*-phenylalaninol (*S*-pala) [11], *S*-phenylalanine methyl ester (*S*-pame) [11], and diphenylmethylphosphine (dpmp) [11] as the axial base ligands. The molecular structures of the ten crystals are similar to those observed in the two forms of the py complex as shown in Fig. 5.9. The 2-ce groups of pip, *S*-pala, *S*-pame, dpmp, 3cpy, and 4apy have the perpendicular conformations while those of 3epy, 4epy, 3apy, and 1abz have the parallel conformations.

Table 5.1 Cavity size (V/Å3), reaction rate (k/s^{-1} × 104), conformation, and intermolecular hydrogen bond of the 2-ce group in the ten

Complexes axial base	*V*	*k*	Conformation	Hydrogen bond
pip	10.3	–	Perpendicular	Absence
S-pala	11.2	–	Perpendicular	Presence
S-pame	10.0, 13.2	0.1	Perpendicular	Absence
3cpy	12.2	0.8	Perpendicular	Absence
dpmp	13.9	1.9	Perpendicular	Absence
4apy	15.0	1.1	Perpendicular	Absence
3epy	13.1	1.4	Parallel	Absence
4epy	14.0	1.6	Parallel	Absence
3apy	10.1	3.2	Parallel	Presence
1abz	15.0	4.2	Parallel	Presence

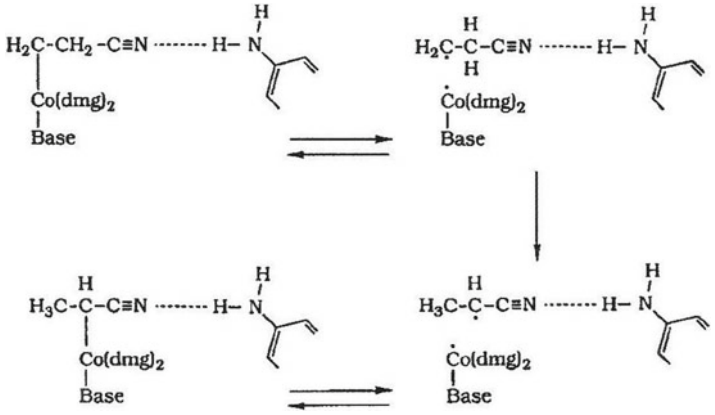

Fig. 5.13 Role of hydrogen bond in the isomerization of the parallel 2-ce group

The rate of the isomerization with the exposure time did not obey first-order kinetics during the entire reaction process, but it appeared to follow first-order kinetics in the early stages. Figure 5.12 shows the isomerization rates for the six complex crystals except for pip, *S*-pala, *S*-pame, and dpmp, the former two of which showed no change at room temperature and the latter two were obtained under the different conditions. They were well explained by first-order kinetics within 40 min. The rate constants were calculated by least-squares fitting and the reaction cavities for the 2-ce groups are drawn. Table 5.1 lists the cavity volumes and rate constants of the ten crystals.

For the crystals with the parallel conformation, there appears no relation between the rate constant and the cavity size. Although the cavity of 3apy is the smallest, the rate constant is greater than those of 3epy and 4epy. This may suggest that another factor should be taken into account. In the crystals of 3apy and 1abz, the nitrogen atoms of the 2-ce groups make hydrogen bonds with the amino groups of the neighboring molecules, whereas no hydrogen bonds are formed in the other crystals. The

hydrogen bond is schematically shown in Fig. 5.13. When the Co–C bond is cleaved on exposure to visible light, the 2-ce radical will be produced. The radical is transformed to the 1-ce radical and then the Co–C bond will be recombined. The transformation from 2-ce to 1-ce radical occurs energetically. Since the isomerization occurs only in the solid state, the radical transformation should be rate-determining step. If the CN group makes a hydrogen bond with the neighboring amino group, the 2-ce radical would be stabilized and the extent of the radical transformation would increase. This may cause the higher reaction rates in the crystals with the intermolecular hydrogen bonds. The hydrogen bond formation is the third factor controlling the reaction rate. The 2-ce groups of 3epy and 4epy have parallel conformation but no intermolecular hydrogen bonds and the 2-ce groups of 3apy and 1abz have parallel conformation and intermolecular hydrogen bonds. In each class the crystal with greater reaction cavity has the greater reaction rate.

For the crystals with perpendicular conformation, pip, *S*-pala, *S*-pame, dpmp, 3cpy, and 4apy crystals, it should be divided into two classes whether the 2-ce group makes a hydrogen bond with the neighboring molecule or not. It was found that such a hydrogen bond was found in the crystal with *S*-pala as an axial base ligand. In the crystal of the (2-ce)(*S*-pala)cobaloxime, the amino group of *S*-pala is hydrogen bonded to the cyano group of the neighboring molecule with N–H···N. The OH group of *S*-pala is hydrogen bonded to the oxygen of cobaloxime moiety of the neighboring molecule, with O–H···O. The *S*-pame crystal has two molecules, A and B, in an asymmetric unit, and the 2-ce group of A takes an ordered structure while that of B does a disordered one. The cavity volume, 11.6 $Å^3$, was obtained by averaging the A and B cavities (10.0 and 13.2 $Å^3$). The dpmp crystal has one molecule in an asymmetric unit and the 2-ce group takes a disordered structure.

For six crystals with perpendicular conformation, the rate constants of pip and *S*-pala are significantly small or almost zero, although the cavity volume of *S*-pala is significantly greater than that of pip crystal and is nearly the same as the averaged value of *S*-pame. This indicates that the intermolecular hydrogen bond of the 2-ce group with the neighboring molecule does not accelerate the reaction rate when the 2-ce group takes the perpendicular conformation.

The 2-ce radical produced by photo-irradiation may be easily transformed to the 1-ce radical and be stabilized if the nitrogen atom of the cyano group is hydrogen bonded to the neighboring molecule. However, the 1-ce radical must move to a greater distance than that produced from the 2-ce group with parallel conformation, which is schematically shown in Fig. 5.14. This suggests that the hydrogen bond in the perpendicular conformation should prevent the isomerization. The nonreactivity of *S*-pala is brought about by the intermolecular hydrogen bond. The correlation between the cavity size and the rate constant holds well in the crystals without intermolecular hydrogen bond of the 2-ce group, except the dpmp crystal, in which the two 2-ce groups face each other around an inversion center. The cooperative motion of the two groups will accelerate the reaction rate as observed in the crystalline-state racemization of the 1-mce group.

It is clear that the reaction rate is well explained by three factors in the solid-state photoisomerization from 2-ce group to 1-ce group of cobaloxime complexes, that is,

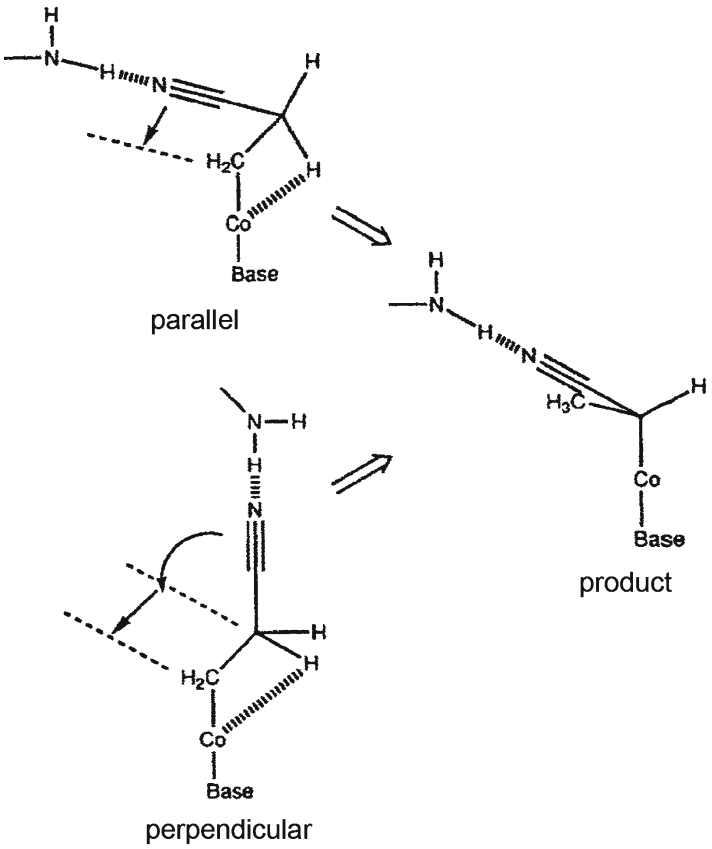

Fig. 5.14 Different role of hydrogen bond in the isomerization of the parallel and perpendicular 2-ce groups

the size of the cavity, the conformation of the 2-ce group, and the hydrogen bond of the 2-ce group with the neighboring molecule. If the second and third factors are the same, the reaction rate is clearly determined by the cavity size.

5.2 Mixed Crystal Formation and Accelerated Reactivity

When 3-methylpyridine (3mpy) was used as an axial base ligand, the mixed crystal between the complex with the 2-ce group and its photoproduct with the 1-ce group was formed from an aqueous methanol solution [12]. Figure 5.15a, b shows the structures of the complex crystal with the 2-ce group only (pure crystal) and the mixed crystal, respectively. The two crystals are isostructural. The composition of

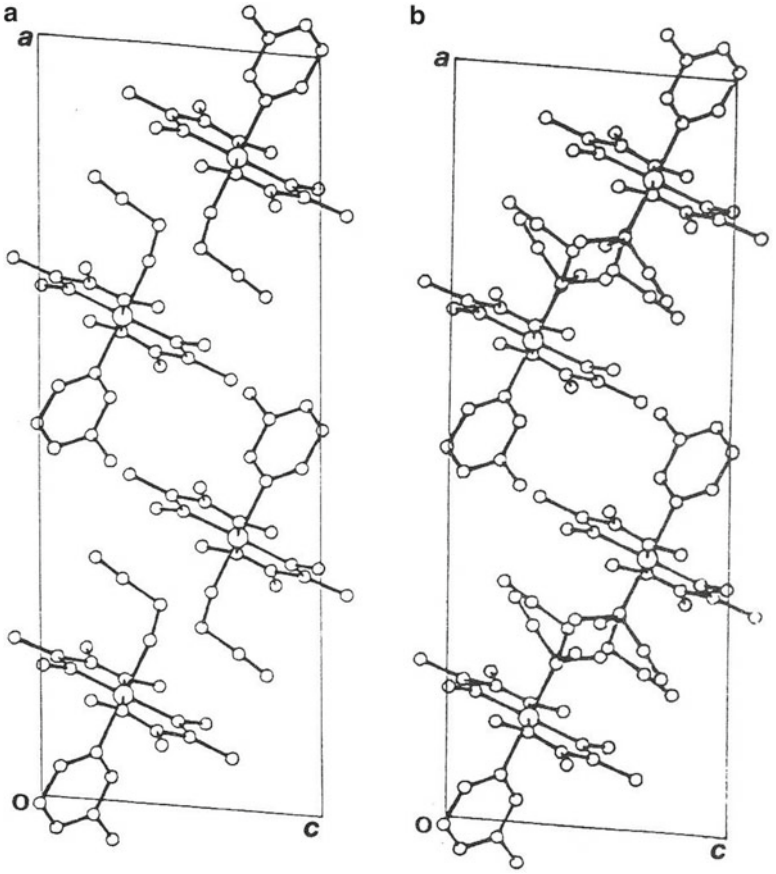

Fig. 5.15 Crystal structures of (**a**) pure (2-ce)(3mpy)cobaloxime and (**b**) mixed one of (2-ce)(3mpy)cobaloxime and (1-ce)(3mpy)cobaloxime

the two complexes with the 2-ce and 1-ce groups in the mixed crystal is nearly the same as that in the solution from which the mixed crystal was grown. Figure 5.16 shows the molecular structure of the mixed crystal, in which the ratio of the complexes with the 2-ce and 1-ce groups is 0.66:0.34. The isomerization rates between the pure crystal and the mixed crystal were measured using the Hg lamp, which is shown in Fig. 5.17. The mixed crystal has a significantly greater reaction rate than the pure crystal. Mixed crystal formation greatly accelerates the photoisomerization. The acceleration can be explained by the enlarged reaction cavity for the mixed crystal, since the size of the reaction cavity for the mixed crystals is significantly greater than that for the pure crystal. This result demonstrates the possibility of controlling the reaction rate by artificial modification of the crystalline field.

Fortunately, it was found that the 2-ce complexes with 3-chloropyridine (3clpy) and 3-bromopyridine (3brpy) as axial base ligands form isomorphous structures to

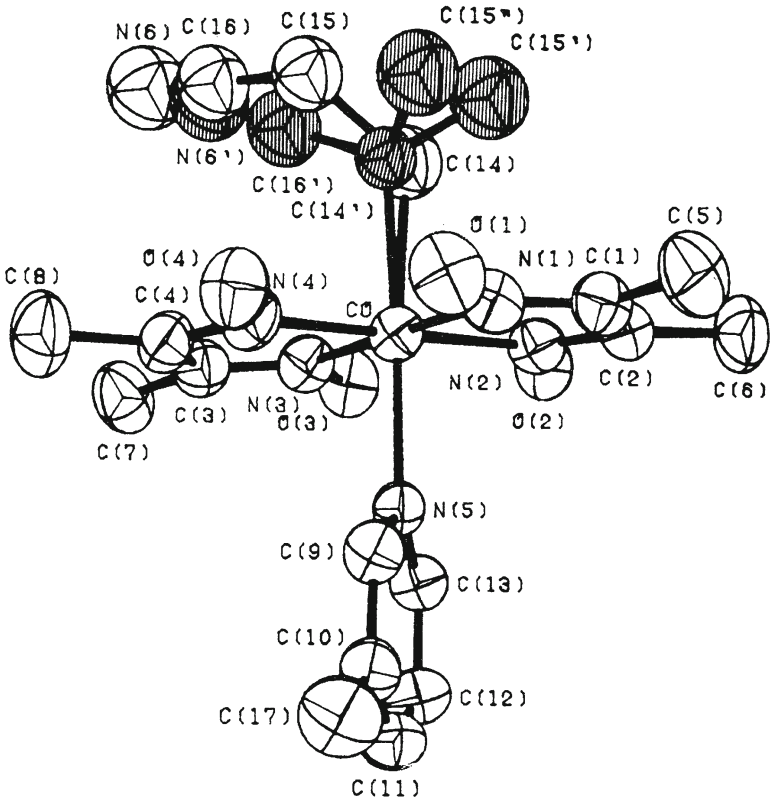

Fig. 5.16 Molecular structure of the mixed crystal. The shaded atoms belong to the 1-ce group with *R* and *S* configurations

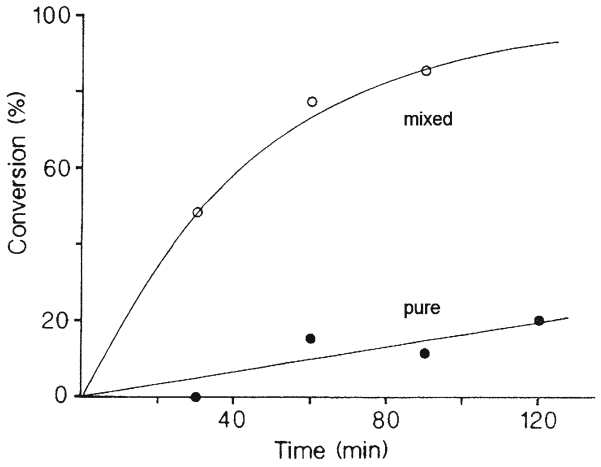

Fig. 5.17 Isomerization rates of pure and mixed crystals of (2-ce)(3mpy)cobaloxime

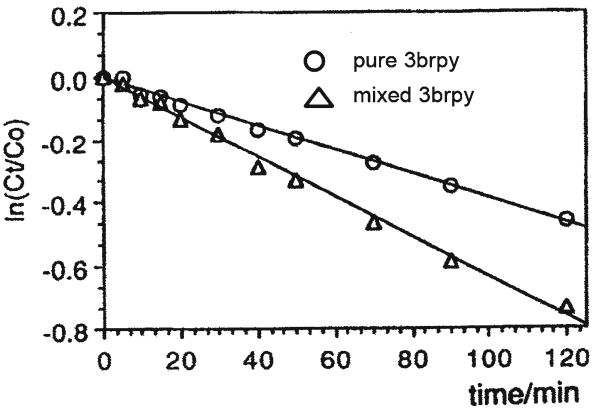

Fig. 5.18 Isomerization rates of pure and mixed crystals of (2-ce)(3bypy)cobaloxime

the 2-ce complex with 3mpy as an axial base ligand. Moreover, the 3clpy and 3brpy complexes made mixed crystals with their photo-produced 1-ce complexes [13]. The crystal structures of the pure 2-ce complexes and mixed ones with 3clpy and 3brpy as axial base ligands are almost the same as the corresponding ones with 3mpy as shown in Fig. 5.15. The molecular structures in mixed crystals of 3clpy and 3brpy are approximately the same as the structure shown in Fig. 5.16.

The reaction rates of pure and mixed crystals for 3mpy, 3clpy, and 3brpy were obtained under the same conditions. The log plots for the reaction rate with the exposure time for 3brpy are shown in Fig. 5.18. Similar log plots were obtained for the pure and mixed crystals with 3mpy and 3clpy. The rate constants and the volumes of reaction cavities of pure and mixed crystals for 3mepy, 3clpy, and 3brpy complexes are obtained. Since the volumes of reaction cavities for three complexes are approximately equal to each other not only in the pure crystals, 11.7–12.3 eÅ^3, but also in the mixed ones, 12.8–13.5 eÅ^3, the same rate constants are observed in the three complexes, 0.9×10^{-4} s^{-1} for the pure crystals and 1.5×10^{-4} s^{-1} for the mixed crystals. Mixed crystal formation greatly accelerated the isomerization and the rate constant became 1.7 times larger than that of the pure 2-ce crystal.

Although the solid-state reaction is very convenient to measure the reaction rate from the change of the IR spectra, it depends on the assumption that the spectral change is closely related with the structural change in the crystal. Although the assumption may be adequate qualitatively, it is better to examine the structural change directly to discuss the quantitative relationship. After many trials we succeeded the isomerization to occur with retention of the single crystal form not only for the pure 2-ce crystal but also for the mixed crystal [13]. The most important point to obtain the crystalline-state reaction is the application of the high flux xenon lamp as a light source. The changes of cell dimensions were measured at a constant interval and the photo-irradiation was stopped when the cell change converged. For the pure crystal of the 2-ce complex with 3mpy as an axial base ligand, the ratio of the 2-ce and 1-ce complexes became 0.45. Further change was

impossible even if the irradiation time was elongated. For the mixed crystal the ratio became 0.55 under the same conditions.

A crystal of the pure 2-ce crystal was mounted on a four-circle diffractometer and was irradiated with a xenon lamp using a glass-fiber tube. The unit-cell dimensions were measured at constant intervals. The normalized unit-cell volume change, $(V_e - V_t)/(V_e - V_i)$, was converted to the isomerization rate, assuming that the change depends linearly on the extent of newly produced 1-ce complex. The V_i, V_e, and V_t are the unit-cell volume at the initial, final, and any time t stages, respectively. Since V_e were unavailable due to decomposition of the crystal, it was deduced from the structure at an intermediate state. The log plot of the isomerization ratio with exposure time seems to indicate that the isomerization process should be divided into three stages, early stage within 3 h, intermediate stage between 3 and 10 h, and the converging stage from 10 to 75 h. The rate constants are calculated to be 13.0, 5.3, and 1.8×10^{-6} s^{-1} for early, intermediate, and converging stages, respectively.

For a mixed crystal, the rate constants were obtained under the same conditions. Although it was difficult to separate the stages, the rate constant at early stages within 3 h is significantly greater than that of the pure 2-ce crystal. The rate constant was calculated to be 18.0×10^{-6} s^{-1}, which is greater by 1.4 times than that of the pure 2-ce crystal and is nearly the same value observed for the powder samples, 1.7 times, as shown in Fig. 5.18. Although the initial rate of the mixed crystal is greater than that of the pure 2-ce crystal, the mixed crystal was decomposed in a shorter time than that of the pure crystal. This may be due to the crystallinity of the mixed crystal, which may be worse than that of the pure crystal.

The essentially the same results were obtained for the crystals of 3clpy and 3brpy as that of the 3mpy crystal. The final important question must be answered: why the reaction rate does not increase more and more in the process of isomerization. When the crystal is irradiated with visible light, the reaction may proceed from the surface to inner part of the crystal. The surface lattice of the crystal may be partly decomposed even if the lattice may be retained as a whole in the crystalline-state reactions. The light gradually becomes difficult to penetrate into the crystal due to the partial decomposition of the surface lattice. This causes the decrease in reaction rate. This indicates that the cavity expansion due to the product formation increases the reaction rate at early stages but that the degree of light penetration decreases due to the decomposition of the surface lattice. If the crystalline lattice may be remade at the intermediate stage, as shown in the mixed crystal, the reaction rate is greater than that in the initial stage. The reason why the reaction rate of the powdered sample is greater by ten times than that of the single crystal is also explained by the fact that the powder is composed of tiny crystals and the light can penetrate into the inner part if the tiny crystals are distributed in the transparent KBr disc.

The above discussion should be applied to the crystalline-state reactions. For the single crystal-to-single crystal reactions, however, the initiators of the reaction, which means tiny nuclei composed of the product, were already distributed in a crystal, but the crystal structure was similar to that of the reactant crystal, as observed in the reactions of the oxygen insertion to the distibene derivative and the

photopolymerization of the distyrylpyradine and 2,4-hexadiyne derivatives, as described in Chap. 2. After some induction period the reaction rate would increase more and more until the most reactant molecules would be exhausted and the crystalline lattice would suddenly grow, which is similar to the phase transition. Such reaction processes are well explained by a sigmoidal curve, as shown in Figs. 2.7 and 2.9. This may be an ideal image of the single crystal-to-single crystal (SCSC) reactions.

5.3 Chirality Generation

The chiral 1-ce group was produced from the achiral 2-ce group in the photoisomerization as shown in Scheme 5.1. This gave an idea that the asymmetric induction would be observed if the isomerization occurs in the chiral crystal environment. A very high optical yield (~82 % *ee*) was observed using *R*-2-amino-2-phenylethanol as an axial base ligand [14]. This section describes the chirality generation in the two types of 2-ce complex crystals with perpendicular and parallel conformations.

5.3.1 Perpendicular Conformation of 2-Cyanoethyl Group

In order to examine the asymmetric induction, a cobaloxime complex with *S-2-butylamine* (*S*-2ba) as an axial base ligand was prepared since the amine is the simplest [15]. The crystal structure is shown in Fig. 5.19. There is one molecule in an asymmetric unit of the *C*2 cell. The molecules are aligned along the *a* axis. The molecular structure is shown in Fig. 5.20. The 2-ce group takes a perpendicular conformation to the cobaloxime plane and has disordered conformations (A, B, and C) around the Co–C bond.

The reaction yield and diastereomeric excess of the 1-ce group were obtained from HPLC analysis of the crystal after the powdered crystals were irradiated with a xenon lamp at adequate intervals. The diastereomeric excess of the molecule or enantiomeric excess of the produced 1-ce group converged to 27 % after 256 min. The conversions of the 2-ce group to the *R*-1-ce and *S*-1-ce groups are shown in Fig. 5.21. The rate constants at early stages (256 min) are calculated to be 1.17×10^{-5} and 0.59×10^{-5} s^{-1} for the *R*- and *S*-1-ce groups, respectively, assuming first-order kinetics. It is clear that the *R*-1-ce group is preferentially produced when the *S*-2ba is used as an axial base ligand.

In order to explain why the *R*-1-ce group is preferentially produced, the reaction cavity for the 2-ce group was drawn in the initial crystal structure. The three cavities for the A, B, and C 2-ce groups viewed normal to the cobaloxime plane are shown in Fig. 5.22. Each cavity is divided into two by the plane comprising the C–C–C–N atoms of the 2-ce group. The volumes of the two parts were also calculated and are given in the figure. Since the CN group has a greater volume than the CH_3 group, it

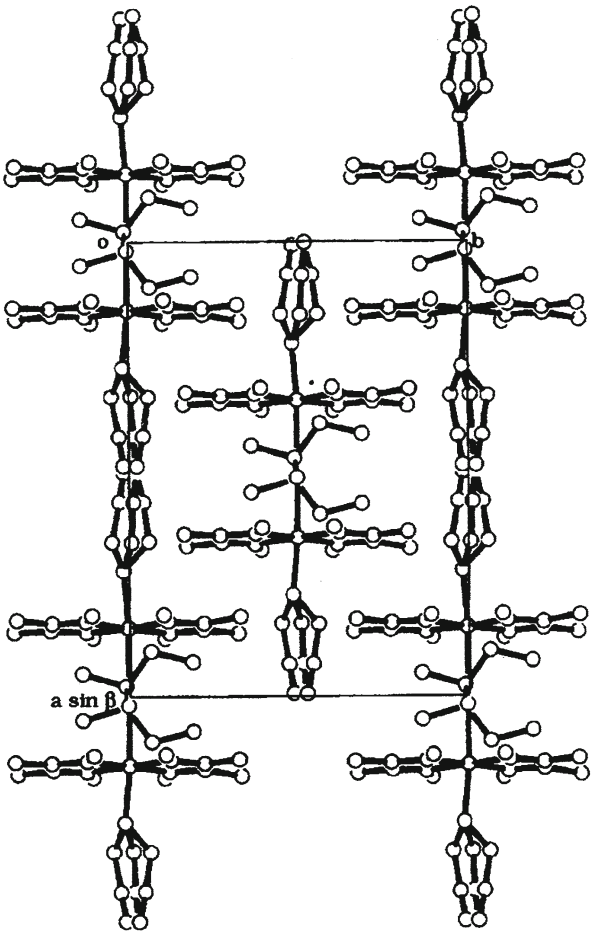

Fig. 5.19 Crystal structure of (2-ce)(*S*-2ba)cobaloxime viewed along the *c* axis

is favorable that the CN and CH_3 groups occupy the greater and smaller parts of the reaction cavity, respectively, after the conformers A and B are converted to the 1-ce group. This explains that the *R*-1-ce group is preferentially produced from the A and B conformers of the *S*-2ba complex. For conformer C, on the other hand, the right part is significantly greater than the left part. From the conformer C, therefore, *S*-1-ce group would be preferentially produced. This may be a reason why this complex showed a low optical yield with *R* configuration.

In order to examine the above discussion more quantitatively, the conformation and configuration of the produced 1-ce group after irradiation were calculated by the molecular mechanics method using the program Cerius [2, 16]. Energy minimization was carried out, changing the conformation of the *R*-1-ce group around the Co–C bond in the original crystal structure before irradiation. The structure of

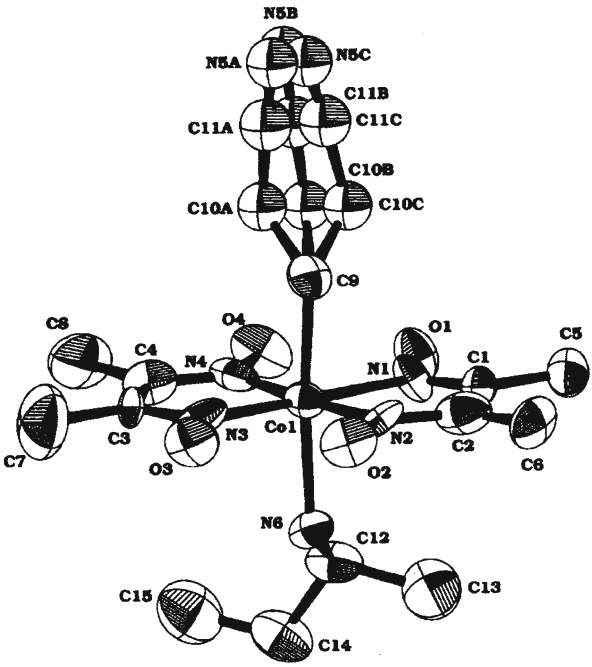

Fig. 5.20 Molecular structure of (2-ce)(*S*-2ba) cobaloxime. The 2-ce groups have disordered conformations (*A*, *B*, and *C*) around the Co–C bond

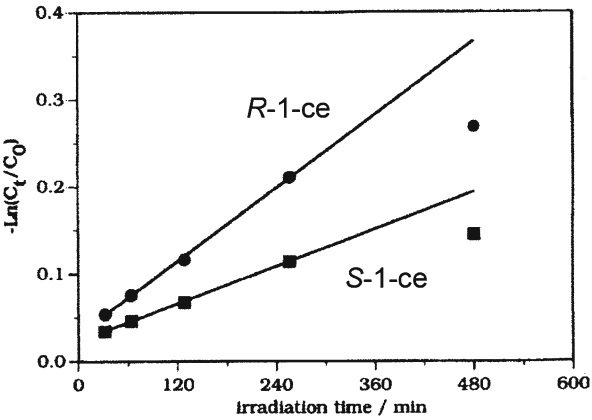

Fig. 5.21 Reaction rates of *R*-1-ce and *S*-1-ce groups from the 2-ce group obtained from HPLC measurement during the irradiation

the *R*-1-ce group with the lowest energy in the reaction cavity of the 2-ce group is shown in Fig. 5.23. The same calculation was performed for the *S*-1-ce group. The lowest energy is higher by 10.33 kJ mol^{-1} than that for the *R*-1-ce group. Although the energy difference is too high considering from the optical yield, this result well explains the observed configuration of the major part and the reaction model based on the shape of reaction cavity.

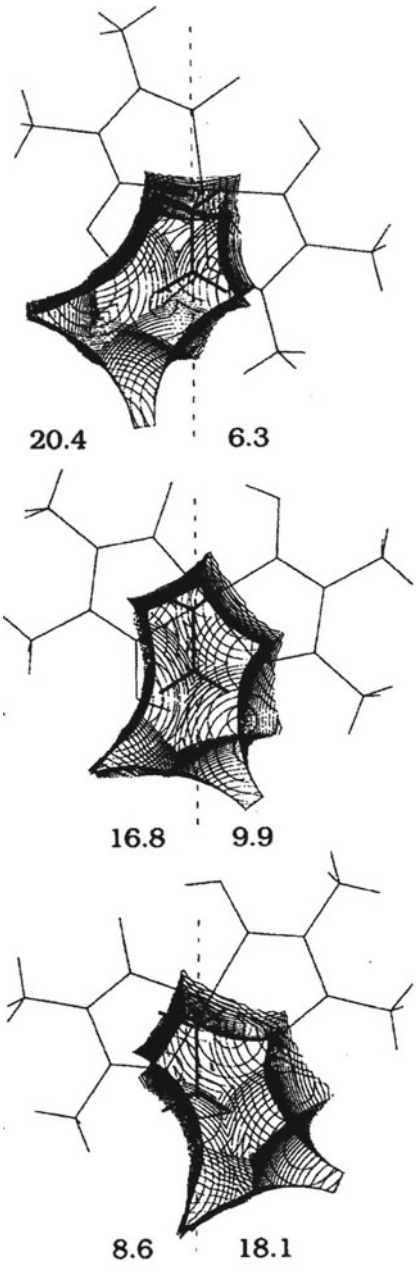

Fig. 5.22 Reaction cavities for the three conformations of the 2-ce group. The dotted line indicates the plane dividing the cavity into two parts

After many trials, it was successful to observe the photoisomerization of the *S-2ba* complex crystal without degradation of the single crystal form, although the occupancy factor of the produced 1-ce group was only 13 % [15]. Since the *R*-2ba, not the *S* isomer, was used as an axial base ligand, the configuration of the produced

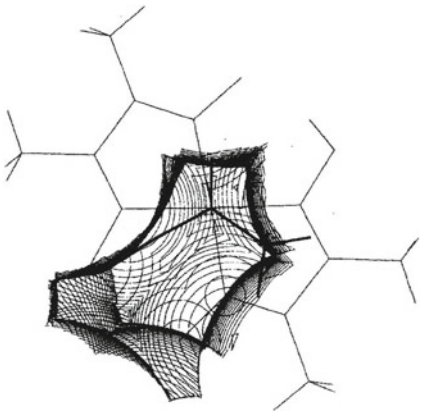

Fig. 5.23 Estimated structure of the produced *R*-1-ce group with the lowest energy in the reaction cavity of the original 2-ce group

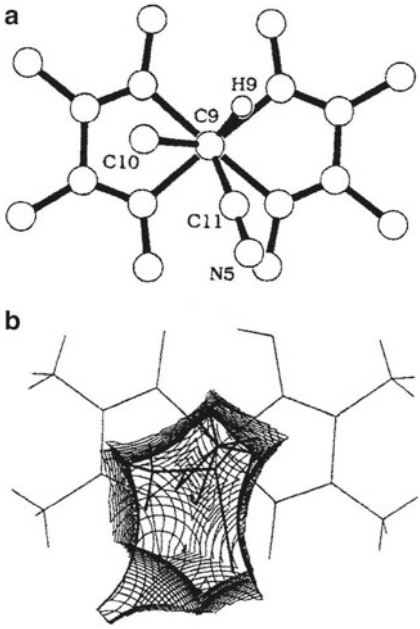

Fig. 5.24 (**a**) Structure of the photo-produced 1-ce group and (**b**) the reaction cavity

1-ce group is *S*. The structure of the photo-produced 1-ce group and the reaction cavity are shown in Fig. 5.24, which is in good agreement with the mirror image shown in Fig. 5.23. The crystalline-state reaction clearly confirmed that the structure estimated by molecular mechanics or simply by reaction cavity is quite reliable. The similar results were obtained for the crystals with the other six axial base ligands, *R*-1,2-diaminopropane (*R*-dap), *S*-2-amino-1-propanol (*S*-apl), *S*-2-amino-1-butanol (*S*-abl), *S*-1-cyclohexylamine (*S*-cha), *cis*-myrtanylamine (myr), and pyrrolidine (pyrr) [17].

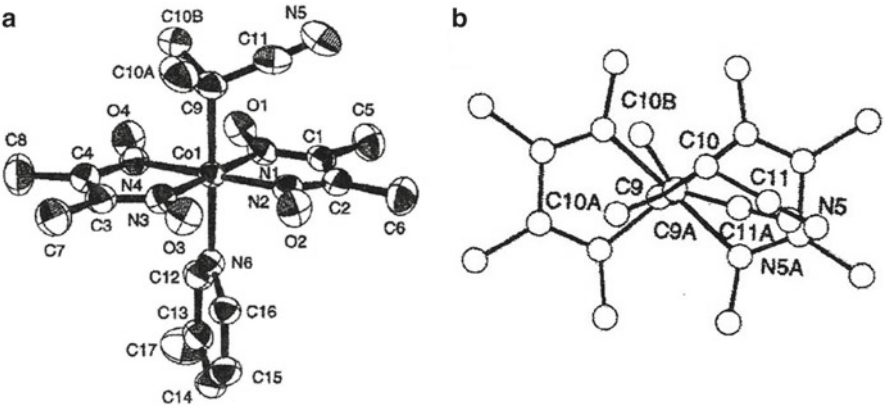

Fig. 5.25 (**a**) Molecular structure of the photo-produced (1-ce)(3mpy)cobaloxime and (**b**) the conformation of the original (2-ce) and photo-produced (1-ce) groups viewed along the normal to the cobaloxime plane

5.3.2 Parallel Conformation of 2-Cyanoethyl Group

In the experiment of crystalline-state photoisomerization, it was found that the ratio of the *R* and *S* configurations of the produced 1-ce group in the 3mpy complex crystal was not 1:1 but 4:7 (or 7:4) in one site of the crystal structure [18]. The molecular structure is shown in Fig. 5.25a. The original 2-ce group and produced 1-ce group viewed along the normal to the cobaloxime plane before and after photo-irradiation are shown in Fig. 5.25b. The occupancy factors of C10A and C10B are 0.19(4) and 0.36(4), respectively, whereas the occupancy factor of the original 2-ce group becomes 0.45. It must be emphasized that the crystal was not changed to chiral one, since the crystal has the inversion center before and after the photo-irradiation.

In order to make clear a reason why the uneven *R:S* ratio of the 1-ce group is produced in one site around an inversion center, the axial base ligand was replaced with 4-methylpyridine (4mpy) instead of 3mpy. The crystal showed a single crystal-to-single crystal phase transition at ca. 343 K [19]. The unit-cell dimensions gradually changed with retention of the single crystal form on exposure to a xenon lamp above the phase transition (346 K), although the crystal was easily decomposed below the transition temperature. After 18 h the change became within experimental error. The molecular structure after photo-irradiation revealed that only one configuration of the 1-ce group was produced, which is shown in Fig. 5.26. The ratio of the 2-ce and 1-ce groups is 0.7 and 0.3, respectively [20].

In the process of the photoisomerization, the produced 1-ce group would be more easily restored if the group has smaller repulsion from the surrounding atoms. The ratio of the *R* and *S* configurations should depend on the shape of the reaction cavity. The reaction cavities for the 2-ce groups of the 3mpy and 4mpy before photo-irradiation are compared in Fig. 5.27a, b, respectively. The space at the

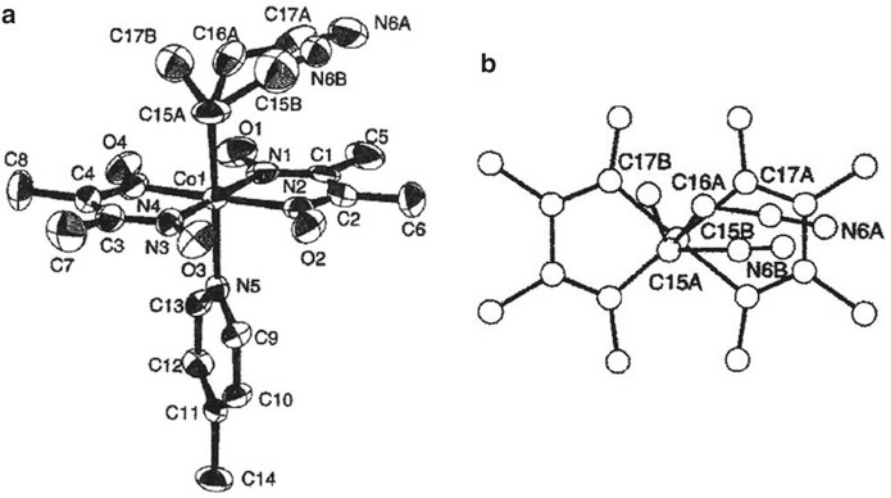

Fig. 5.26 (**a**) Molecular structure of the 4mpy complex after the irradiation. The original 2-ce and photo-produced 1-ce groups are shown and (**b**) the conformations of the 2-ce and 1-ce groups viewed along the normal to the cobaloxime plane

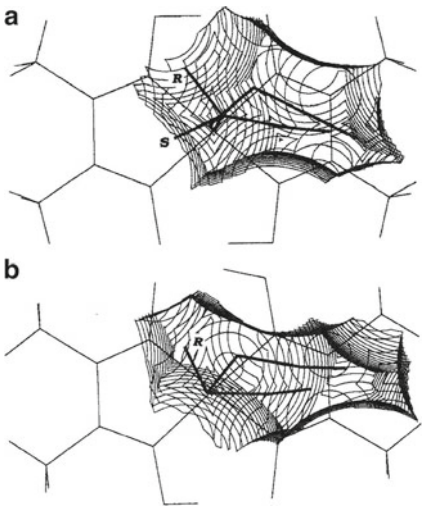

Fig. 5.27 Reaction cavities for the 2-ce groups and the photo-produced 1-ce groups in (**a**) the 3mpy and (**b**) 4mpy crystals

position of the *R* methyl group after photo-irradiation in 3mpy is very thin and the methyl group protrudes from the cavity. On the other hand, a large part of the *S* methyl group is included in the cavity, since the cavity around the *S* methyl group is thicker than that around the *R* methyl group. The *R*-1-ce group should have higher repulsion with the surrounding atoms than the *S*-1-ce group. This causes the uneven

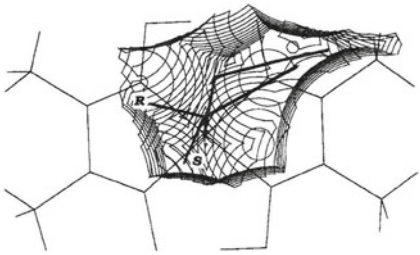

Fig. 5.28 Reaction cavity for the 2-ce group in the crystal of (2-ce)(*R*-phenylglycinol) cobaloxime and the photo-produced *R*- and *S*-1-ce groups

ratio of the *R* and *S* configurations of the produced 1-ce group in the 3mpy crystal. In the reaction cavity for the 2-ce group of the 4mpy crystal before photo-irradiation, the *R* methyl group occupies a wide space in the cavity, whereas the *S* methyl group has no space. This well explains the reason why only the *R*-1-ce group is produced in the 4mpy crystal.

The above results suggest that the asymmetric synthesis may be possible if the crystal has a chiral space group. Many attempts to obtain a chiral crystal containing an achiral molecule changing the axial base ligand were in vain. Therefore, several 2-ce complexes were prepared with chiral amines as axial base ligands. Among the complexes, the powdered sample of the complex with *R*-phenylglycinol as an axial base ligand was found to give a high optical yield (ca. 80 %), when it was irradiated with visible light [21]. The cavity for the 2-ce group before photo-irradiation is shown in Fig. 5.28, in which the estimated structures of the produced 1-ce groups with *R* and *S* configurations are drawn. Since the *R* methyl group appears to occupy the wider space than the *S* methyl group, the *R*-1-ce group would be made predominantly. This explains the high optical yield. However, it is necessary to undergo the isomerization with retention of the single crystal form if the mechanism should be considered quantitatively.

In order to observe the isomerization as a crystalline-state reaction, two factors seem to be necessary: (1) parallel conformation of the 2-ce group to the cobaloxime plane and (2) hydrogen bonds to retain the single crystal during the photoreaction. More than eight kinds of crystals with different base ligands were prepared. Among them, the complex crystal with *N*-(2-hydroxyethyl)isonicotineamide (heia) as an axial base ligand showed high reactivity with keeping the single crystal form [22]. The base ligand is achiral. The crystal structure is shown in Fig. 5.29. The molecules are linked by a fairly strong hydrogen bond of O–H···O along the *a* axis, the O···O distance being 2.82 Å. There is one molecule in an asymmetric unit of the $Pca2_1$ cell, which is not centrosymmetric but not chiral. The molecular structure is shown in Fig. 5.30a. The crystal satisfies the above two factors: parallel conformation and intermolecular hydrogen bond.

The crystal was irradiated with a xenon lamp at room temperature and the intensity data were collected before the crystal was decomposed. The molecular structure is shown in Fig. 5.30b. The produced 1-ce group has only *R* configuration at one site. The ratio of the photo-produced 1-ce group and the original 2-ce group became 73:27. Further irradiation was impossible to keep the single crystal form.

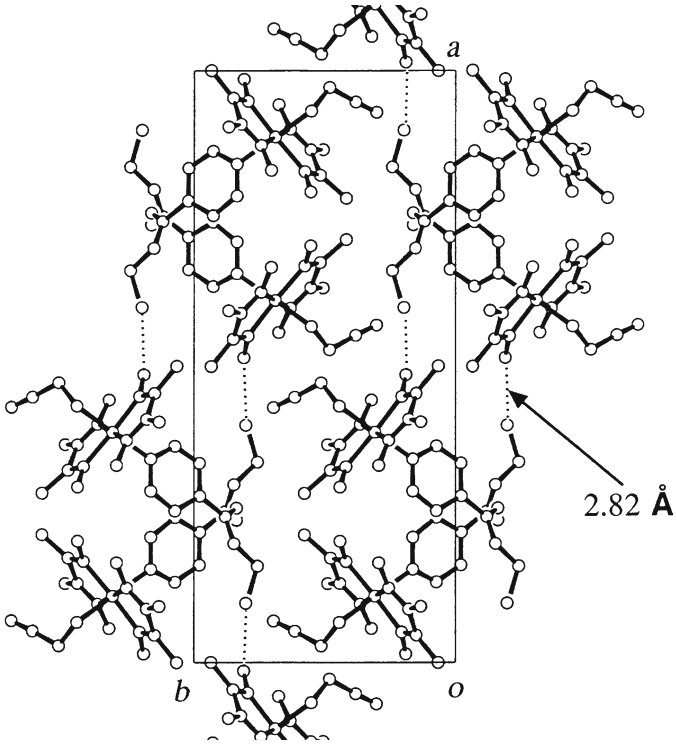

Fig. 5.29 Crystal structure of (2-ce)(heia)cobaloxime viewed along the *c* axis

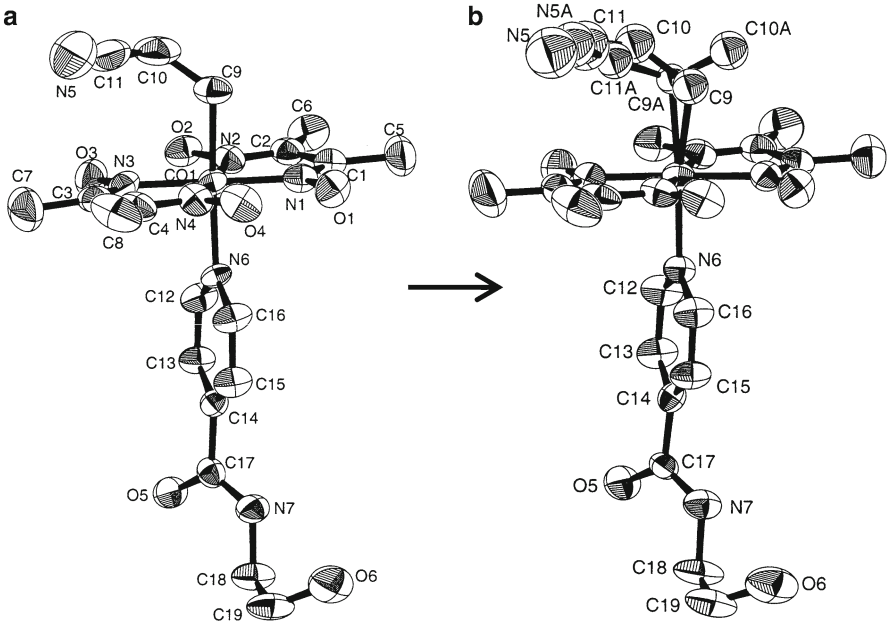

Fig. 5.30 Structural change of a molecule of (2-ce)(heia)cobaloxime during photo-irradiation. (**a**) Before and (**b**) after the photo-irradiation

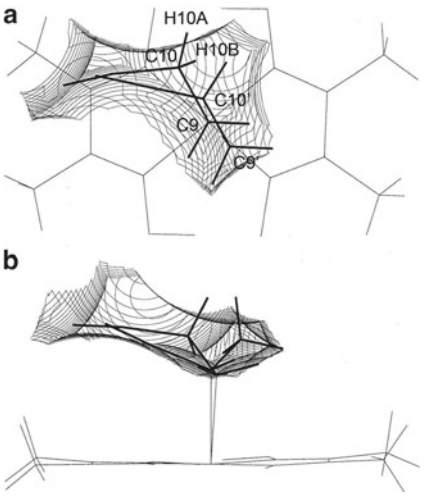

Fig. 5.31 Reaction cavity for the 2-ce group, (**a**) viewed along the normal to the cobaloxime plane and (**b**) the side view

The reaction cavity before photo-irradiation is shown in Fig. 5.31. The cavity size is considerably large, 17.2 $Å^3$, although the height of cavity is very low. It is clear that the produced 1-ce group with *R* configuration is well accommodated in the cavity. It seems impossible to include the 1-ce group with *S* configuration in the cavity.

When the Co–C bond is cloven by photo-irradiation, the closer hydrogen atom bonded to the C^1 atom, H10B, should be extracted by the cobalt atom at the first stage and then the cobalt atom makes a bond with C10 giving H10B to C9. Since the 2-ce group takes a parallel conformation, one of the hydrogen atoms bonded to the C^1 atom comes close to the Co atom, the distances of Co···H10A and Co···H10B being 3.83 and 3.04 Å, respectively. This may be a reason why the parallel conformation is effective to the photoisomerization.

About 73 % of the 2-ce group of the complex with heia as an axial base ligand was changed to the 1-ce group with retention of the single crystal form. Moreover, the reaction rate was considerably fast. This brought about an idea that the isomerization mechanism would be made clear if the structures before and after the reaction were analyzed by neutron diffraction.

Two deuterium atoms bonded to the C^1 atom were replaced with the hydrogen atoms to examine the movement of the deuterium atoms. Further replacement was performed for the hydrogen atoms of the methyl groups of the cobaloxime to reduce the background of the neutron diffraction, as shown in Scheme 5.2 [23, 24].

The molecular structure after photo-irradiation is a disordered structure composed of the original complex with the 2-ce group (70 %) and the produced complex with the 1-ce group (30 %), which is shown in Fig. 5.32. The positions of the two deuterium atoms are shown in Fig. 5.33. Two deuterium atoms are attached to the C^1 atom in the original molecule. In the produced molecule after the photo-irradiation, one of the deuterium atoms retains unaltered, whereas another one is transferred to the C^2 atom as one of the three hydrogen atoms bonded to the methyl carbon. Since the H and D atoms are disordered in the methyl group, any of the hydrogen atoms

Scheme 5.2 Two deuterium atoms were introduced to the C^1 atom of the 2-ce group in addition to the deuterium replacement of the methyl groups of the equatorial ligands

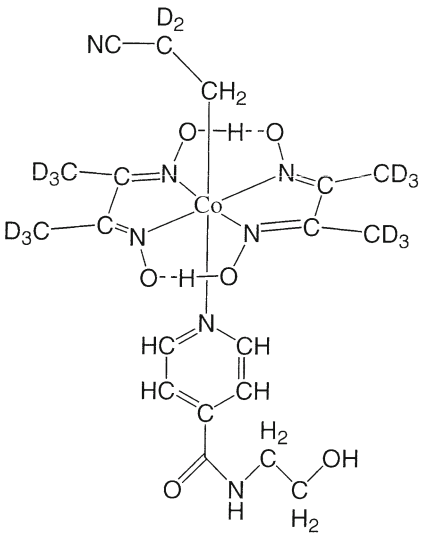

Fig. 5.32 Molecular structure of the deuterated (2-ce)(heia)cobaloxime complex after irradiation

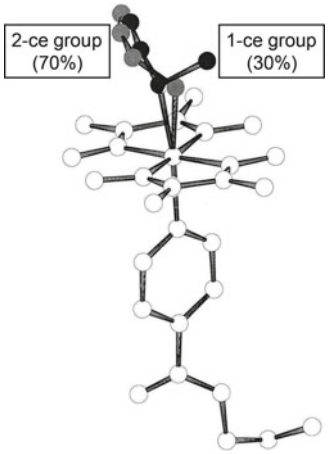

bonded to the methyl carbon is disordered with the H/D ratio of 2:1. As shown in Scheme 5.3a, the deuterium atoms in the 1-ce group clearly indicate that on exposure to visible light the Co atom makes a bond with C^1 and abstracts one of the deuterium atoms bonded to C^1 and transfers it to make a bond with the C^2 atom.

If the back reaction can occur, the hydrogen atoms would migrate from the methyl group to one of the hydrogen atoms bonded to C^1, as shown in Scheme 5.3b. It was also proved that the back reaction does not occur, because the 2-ce group in the disordered structure after photo-irradiation has two deuterium atoms bonded to the C^1 atom.

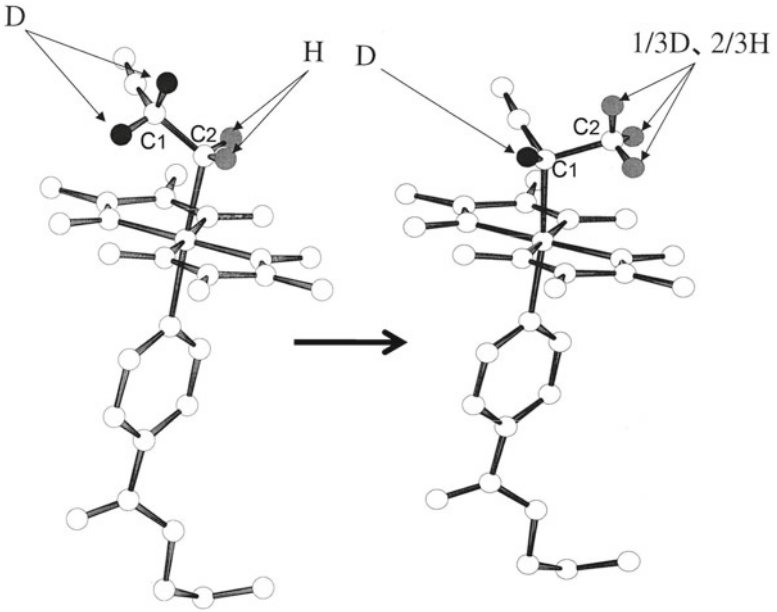

Fig. 5.33 The movement of the deuterium atoms during the photoisomerization

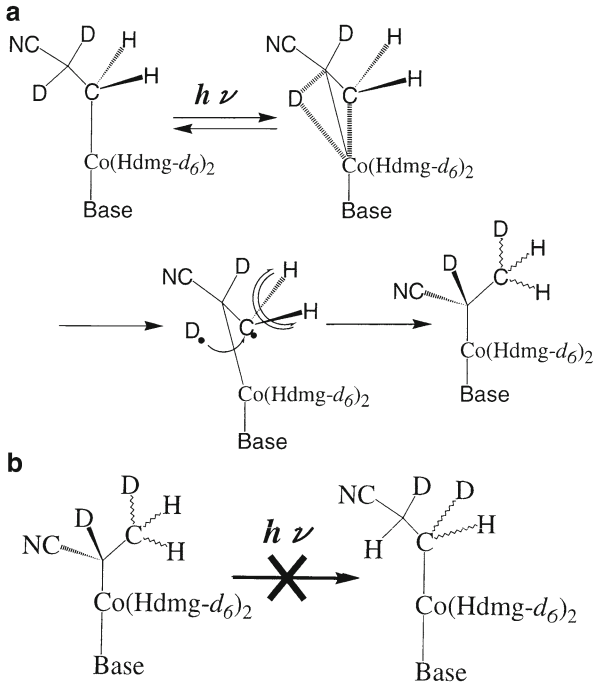

Scheme 5.3 (**a**) The mechanism of the deuterium transfer during the photoisomerization and (**b**) no indication of the back reaction

5.4 Isomerization of 3-Cyanopropyl and 4-Cyanobutyl Groups

A novel solid-state photoisomerization was found by Ohgo and coworkers as shown in Scheme 5.4 [25]. The 3-cyanopropyl (3-cp) group bonded to the cobalt atom was isomerized to the 1-cyanopropyl (1-cp) group on exposure to visible light. In order to make clear the reaction mechanism, the crystalline-state reactions were searched changing the axial base ligand. Since the final 1-cp group has a chiral carbon atom, the asymmetric induction may be possible when the isomerization proceeds in a chiral crystal environment. Three chiral amines were introduced as axial base ligands: *R*-1-phenylethylamine (*R*-pea), *S*-phenylalaninol (*S*-pal), and *R-2-aminobutanol* (*R*-abl) [26]. The powdered sample of each complex was irradiated with a xenon lamp and the isomerization rate from 3- to 1-cp group was measured by HPLC. Among them, the complex with *R*-pea has the greatest reaction cavity and showed the fastest reaction rate. The reaction rate, reaction yield, and enantiomer excess were 1.0×10^{-3} s^{-1}, 81.3 %, and 67.2 %, respectively. The crystal structure before irradiation is shown in Fig. 5.34. There is one molecule in the asymmetric unit of the $P2_1$ cell. On exposure to a xenon lamp, the cell dimensions were gradually changed. Since the cell change was converged after two weeks exposure, the structure was analyzed. The molecular structures before and after the photo-irradiation are shown in Fig. 5.35a, b, respectively. Surprisingly, the 3-cp group was completely transformed to the disordered 1-cp group with *R* and *S* configuration. The occupancy factors of *R*- and *S*-enantiomers are 0.07 and 0.93, respectively. The asymmetric induction was successfully performed in a chiral crystal environment.

Although the asymmetric synthesis was successful using the technique of crystalline-state reaction, there remained a question on which is the correct reaction mechanism (a) and (b) in Scheme 5.5. In (a) the 3-cp group is isomerized to the 1-cp group through the 2-cp group as proposed by Ohgo et al., whereas the direct translation of the cyano group in (b) was proposed by Bury et al. [27]. It is impossible to distinguish the two mechanisms only by X-ray crystal structure analyses before and after the reaction.

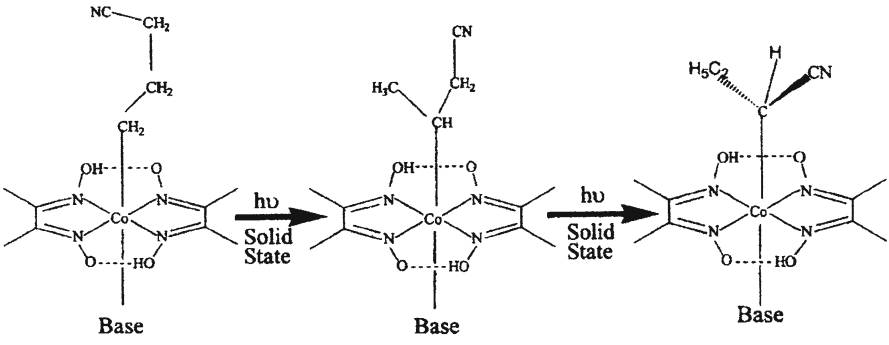

Scheme 5.4 Solid-state photoisomerization from the 3-cyanopropyl (3-cp) to 1-cp group through the 2-cp group in cobaloxime complexes

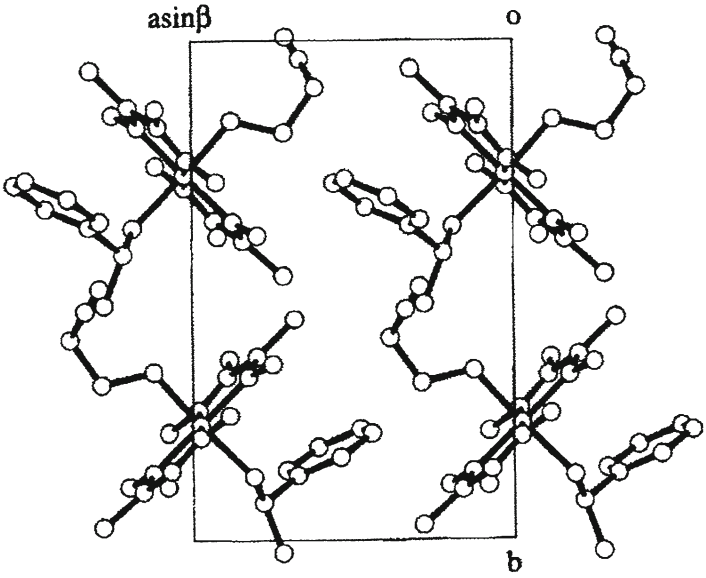

Fig. 5.34 Crystal structure of (3-cp)(*R*-pea)cobaloxime viewed along the *c* axis before the irradiation

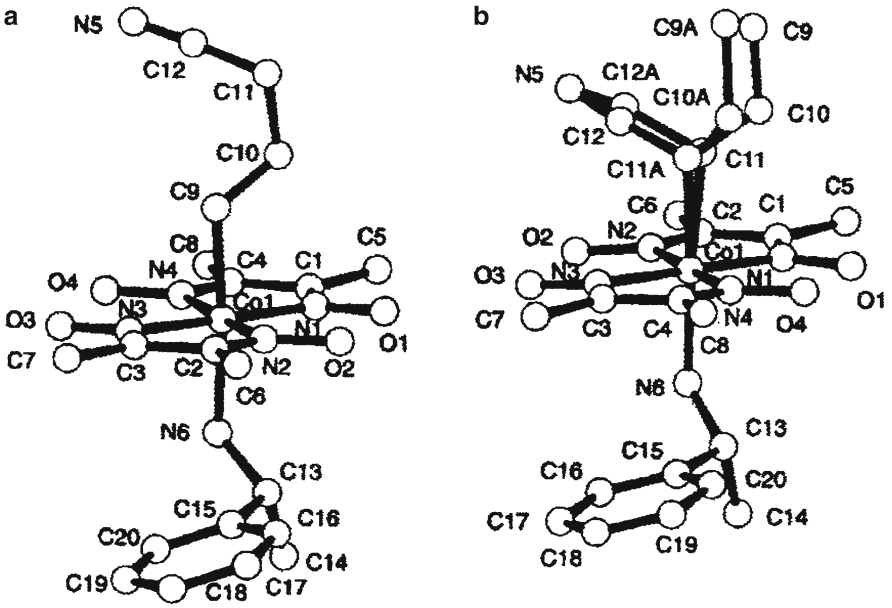

Fig. 5.35 Molecular structure of (3-cp)(*R*-pea)cobaloxime (**a**) before and (**b**) after the irradiation. The 3-cp group is completely transformed to 1-cp group after the irradiation

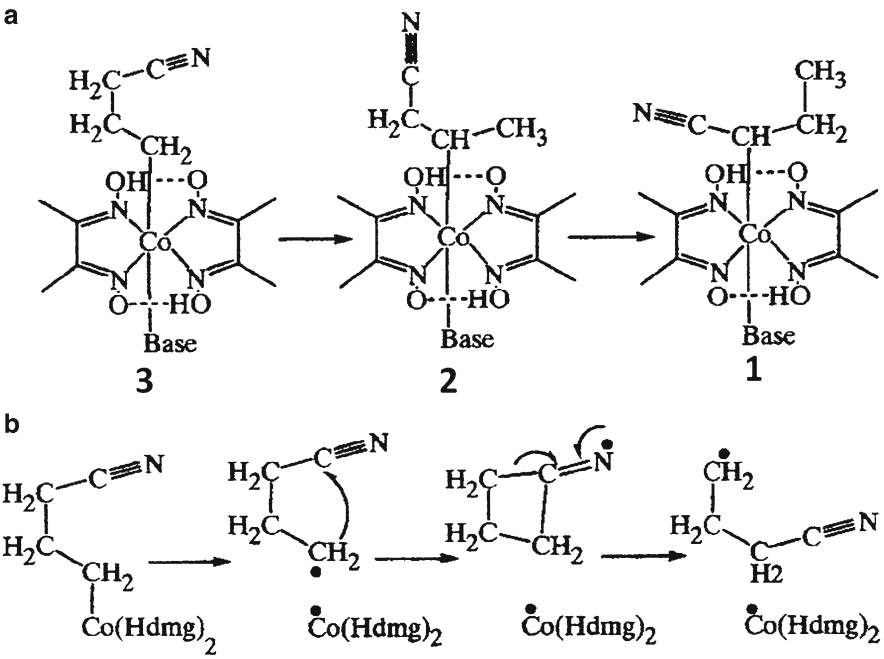

Scheme 5.5 Two reaction processes proposed for the photoisomerization from the 3-cp to 1-cp group

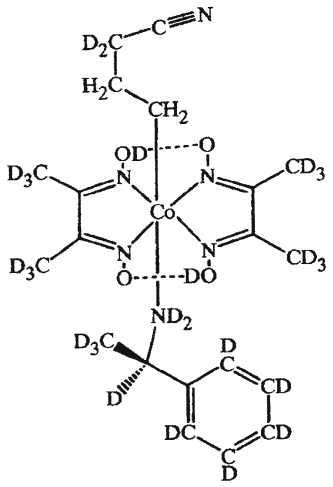

Scheme 5.6 The deuterated cobaloxime complex. All hydrogen atoms were replaced with deuterium atoms except for the four hydrogen atoms of the 3-cp group

In order to make clear the mechanism, the crystal structures of the deuterated complex shown in Scheme 5.6 before and after photo-irradiation were analyzed by neutron diffraction [28]. To reduce the background due to the incoherent scattering from H atoms in the neutron diffraction, all the H atoms of the equatorial ligands

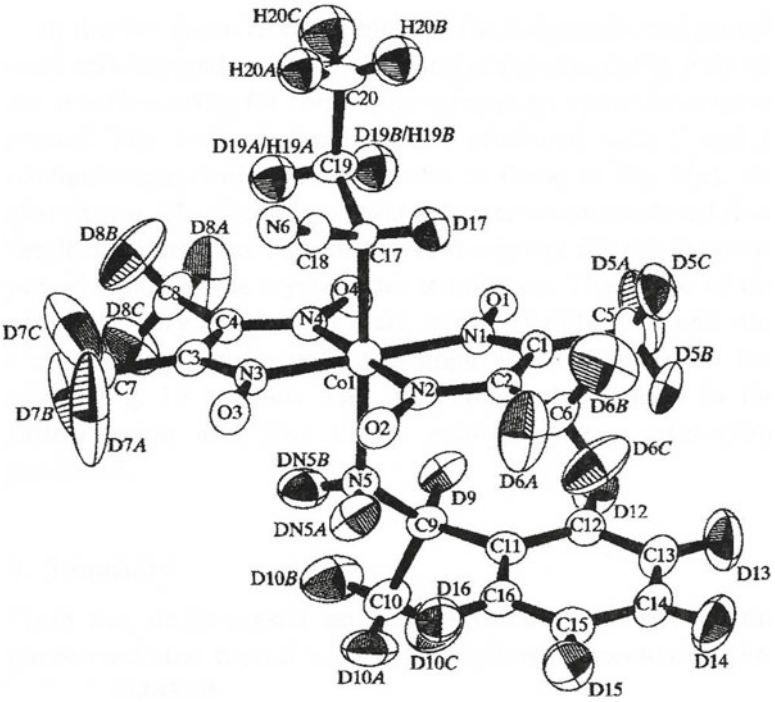

Fig. 5.36 Molecular structure of the *S*-1-cp with deuterium atoms after photo-irradiation

and axial base ligand were replaced with D atoms. For the 3-cp group, two H atoms bonded to the C_1 atom were replaced with D atoms. At least one of the D atoms should be transferred to the other position in any of the reaction processes.

After photo-irradiation, most of the 3-cp groups were transformed to the *S*-1-cp group. The other residual peaks were assigned to the *R*-1-cp group and the original 3-cp group. The occupancy factors of *S*- and *R*-1-cp groups and 3-cp group are 0.83, 0.06, and 0.11, respectively. The major part of the molecular structure with the *S*-1-cp group by neutron diffraction is shown in Fig. 5.36. The photo-produced *S*-1-cp group has a D atom bonded to the C_1 atom, D17, and another D atom bonded to the C_2 atom, D19A and D19B, disordered. The ratio of D/H at D17 is 100:0, whereas the ratio of D/H at D19A and D19B is 50:50. The structure clearly indicates that the reaction proceeds in two steps, 3-2 and 2-1 as shown in Scheme 5.5a. Moreover, the second 2-1 step should be irreversible, because the D17 atom would be partly exchanged with the H atom, H19A or H19B, if the second step were reversible. In the original 3-cp group observed as a minor part, no exchange between H and D atoms was observed.

The reason why the D19A and D19B bonded to the C^2 atom are disordered may be explained by the mechanism of olefin formation. The Co–C bond would be cloven by continuous exposure to the xenon lamp after the 1-cp group was produced.

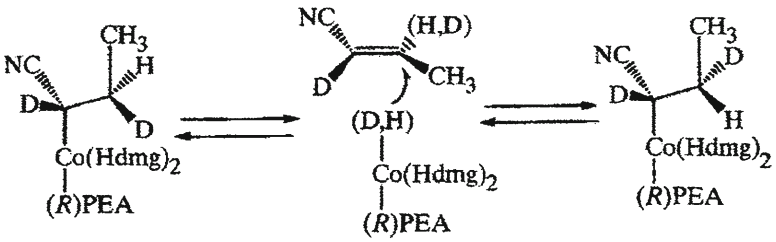

Scheme 5.7 Possibility of reversible-reaction of the 1-cp group

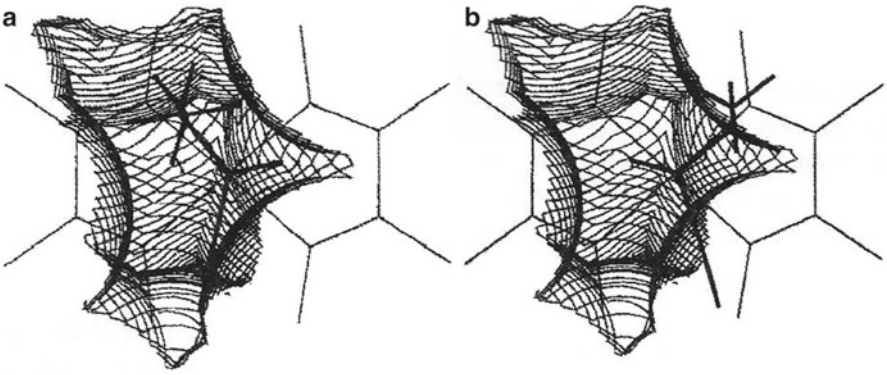

Fig. 5.37 Reaction cavity for the 3-cp group in the initial structure. (**a**) *S*-1-Cp group and (**b**) *R*-1-cp groups are drawn in the cavity

When the back reaction occurs, the olefin cobalt hydride would be produced in the intermediate stage as shown in Scheme 5.7. The H and D atoms are easily exchanged with each other. Another question should be explained: why is the *S*-1-cp group produced more than 93 %? The 1-cp group with *R* or *S* configuration is drawn in the reaction cavity for the 3-cp group in the crystal before irradiation. The *S* configuration is better accommodated in the cavity than the *R* configuration as shown in Fig. 5.37.

Since the 2-ce and 3-cp groups were isomerized to the 1-ce and 1-cp groups, respectively, the 4-cyanobutyl (4-cb) group was examined whether or not it would be isomerized to 1-cyanobutyl (1cb) group on exposure to visible light. After many trials, the cobaloxime complex with pyridine as an axial base ligand showed the cell change with retention of the single crystal form [29]. The molecular structure before photo-irradiation is shown in Fig. 5.38. The 4-cb group takes all-*trans* conformation.

After 66 h exposure to the xenon lamp, the cell volume increased by 27.2(8) $Å^3$. The molecular structure is shown in Fig. 5.39. There appeared the 3-cyanobutyl (3-cb) group around the 4-cb group. The 3-cb group has a chiral carbon atom, C10B, bonded to the cobalt atom, which is not disordered. To examine the reason why only one enantiomer was produced at one site of the crystal, the reaction cavity for the

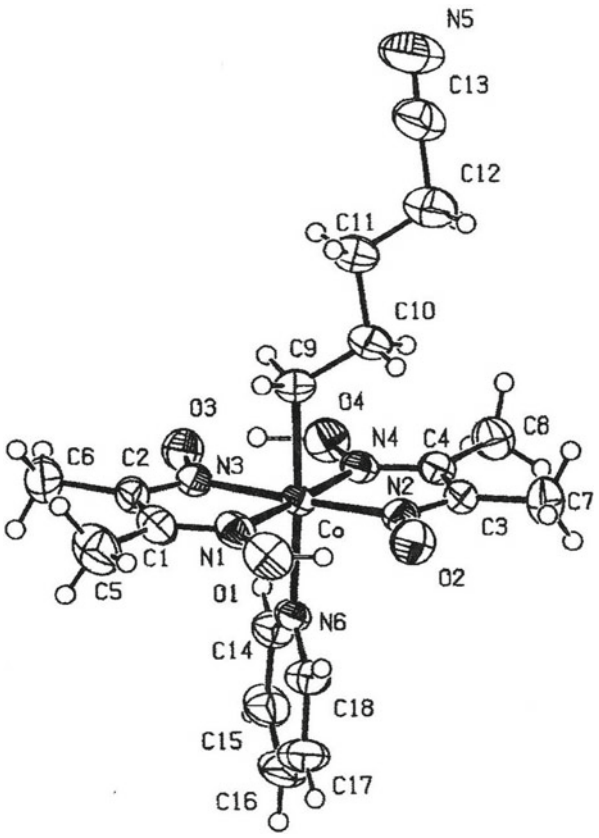

Fig. 5.38 Molecular structure of (4-cb)(py) cobaloxime before the irradiation

4-cb group is shown in Fig. 5.40, in which the 4-cb and 3-cb groups are shown. The produced 3-cb group is accommodated well in the cavity. The 3-cb group with the opposite configuration would suffer from heavy steric repulsion in the cavity. Since the crystal has a center of symmetry, another enantiomeric 3-cb group should be produced at the inverted site. Therefore, the product in a whole crystal is racemic.

The irradiated crystal was dissolved in a $CDCl_3$ solution and the NMR measurement was performed to examine whether the other photoproducts were made or not. The signals of methyl protons due to the 3-cb and 2-cb groups were observed. The amounts of the produced groups were estimated to be 27 % and 6 % for the 3-cb and 2-cb groups, respectively. The occupancy factor of the photo-produced 3-cb group was 0.214(7). This value is smaller than that obtained from NMR, 0.27. Probably some parts of the photoproducts may not have lattice structure. There is no clear indication for the isomerization to the 1-cyanobutyl (1-cb) group. The crystalline-state photoisomerization from 4-cb to 1-cb group is successfully observed, which is described in the next chapter.

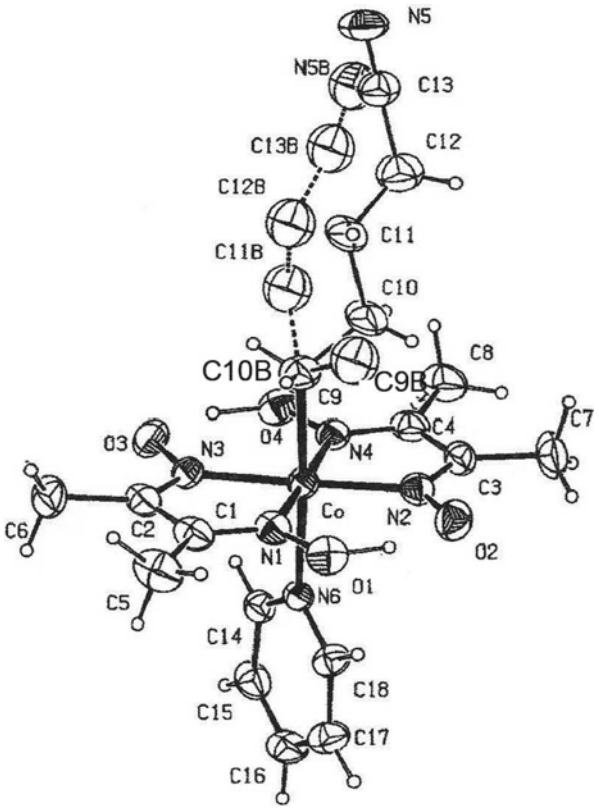

Fig. 5.39 Molecular structure of (4-cb)(py) cobaloxime after the irradiation. The 3-cb group with dotted bonds is clearly made

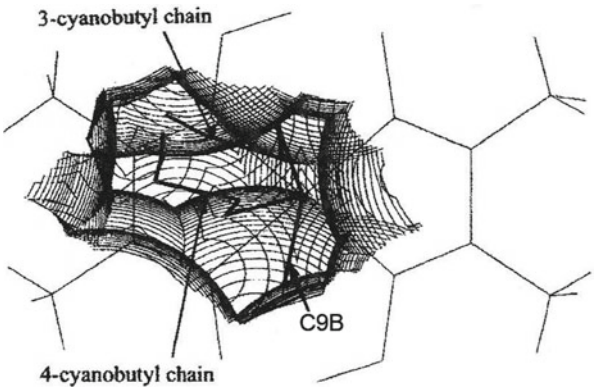

Fig. 5.40 Reaction cavity for the 4-cb group before the irradiation. The 3-cb group with *R* configuration well fits the cavity

5.5 *Trans–Cis* Photoisomerization

It was found that the *trans*-2-butenyl (*trans*-2-but) group bonded to the cobalt atom in a cobaloxime complex with pyridine (py) as an axial base ligand was isomerized to the *cis* conformation in the crystalline state on exposure to a xenon lamp as shown in Scheme 5.8 [30]. The crystal structure of the py complex has the space group *C*mca. Since there are eight molecules in the unit cell, the molecules lie on the mirror plane perpendicular to the *a* axis. The molecular structure is shown in Fig. 5.41. The Co1, C8, N3, and C7 atoms lie on the mirror plane, which is parallel to the long axis of the cobaloxime. When the crystal was exposed to a xenon lamp, the cell lengths were gradually changed. After 110 min exposure, the changes were insignificantly small. The structure was analyzed. The space group was not changed. The molecular structure after the irradiation is shown in Fig. 5.42, in which only a half of the disordered structures of the 2-but groups are drawn and their mirror images are omitted for clarity. The disordered structure viewed normal to the cobaloxime plane is shown in Fig. 5.43. There appeared two conformers of *cis*-2-but groups, B and C. The original *trans*-2-but group, A, has approximately the same conformation as that before irradiation. The occupancy factors are 0.17(1), 0.24(2), and 0.09(2) for A, B, and C 2-but groups, respectively. The 66 % of *trans*-2-but group is transformed to its *cis* isomer.

In order to examine the *trans–cis* isomerization in detail, other three complexes with 4-bromopyridine (4brpy), 3-chloropyridine (3clpy), and methylsulfide (mesul) were prepared as axial base ligands [31]. The crystal of 4brpy is isostructural to the

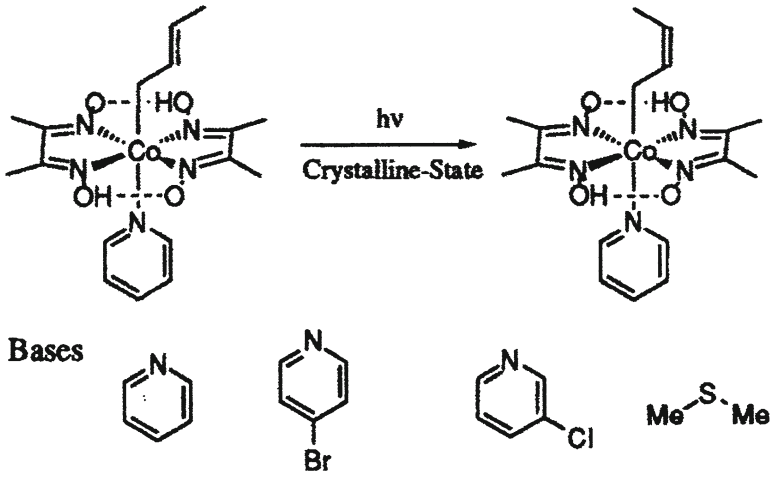

Scheme 5.8 Crystalline-state photoisomerization of the *trans*-2-butenyl (*trans*-2-but) group to the *cis*-2-but group in cobaloxime complexes. Four different axial bases were used: pyridine, 4-bromopyridine, 3-chloropyridine, and methylsulfide

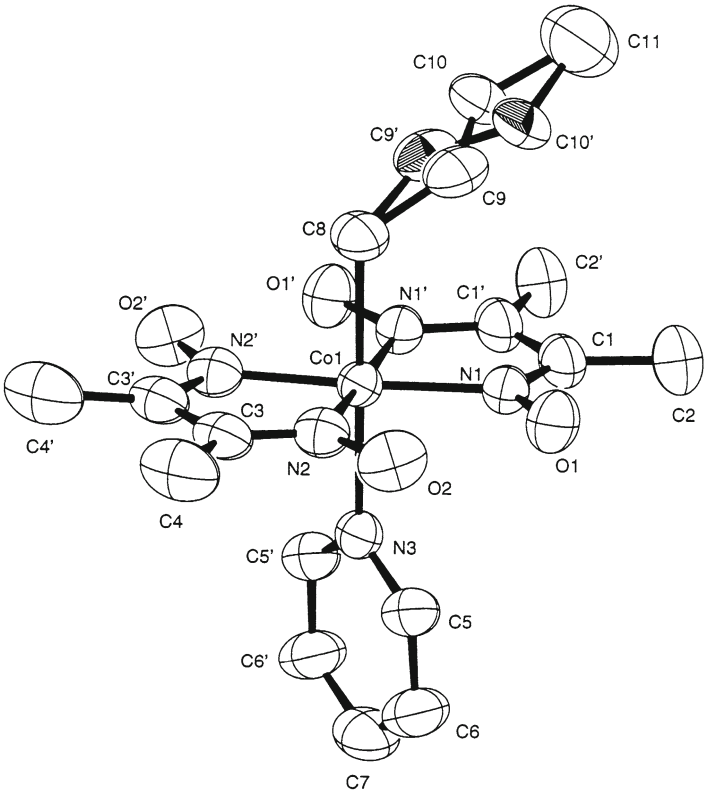

Fig. 5.41 Molecular structure of (*trans*-2-but)(py)cobaloxime. Two conformers of the *trans*-2-but group are disordered

py crystal. After 110 min irradiation, 42 % of *trans*-2-but group were isomerized to the *cis*-2-but group with retention of the single crystal form. The original *trans* and the produced *cis* conformers take disordered structure. There is only one *cis* isomer.

The 3clpy and mesul complex crystals showed no change on exposure to the xenon lamp for 15 h. The reaction cavities for the 2-but group of the four complex crystals were drawn and the volumes were calculated to be 17.9, 17.1, 17.0, and 14.1 $Å^3$, for the py, 4brpy, 3clpy, and mesul crystals, respectively. Since the mesul crystal has too small reaction cavity, it showed nonreactive on exposure to the xenon lamp. However, nonreactive 3clpy crystal has nearly the same size of the reaction cavity as that of the reactive 4brpy. The reaction cavities for the 2-but groups of 4brpy and 3clpy crystals are shown in Fig. 5.44a, b, respectively. The former cavity is wide enough to accommodate the resulting *cis* isomer in the void space, whereas the latter cavity is narrow not to include the *cis* isomer. The shape of the cavity is an important factor for the crystalline-state isomerization.

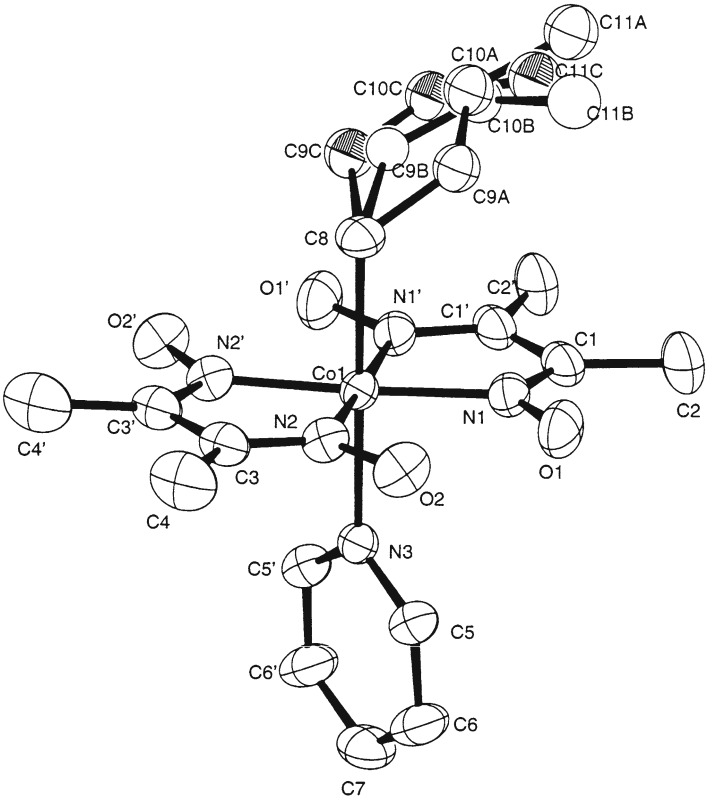

Fig. 5.42 Molecular structure of the 2-but group after the irradiation. There are two photo-produced *cis*-2-but (*B* and *C*) and one original *trans*-2-but (*A*) groups. The mirror images of the three groups are omitted

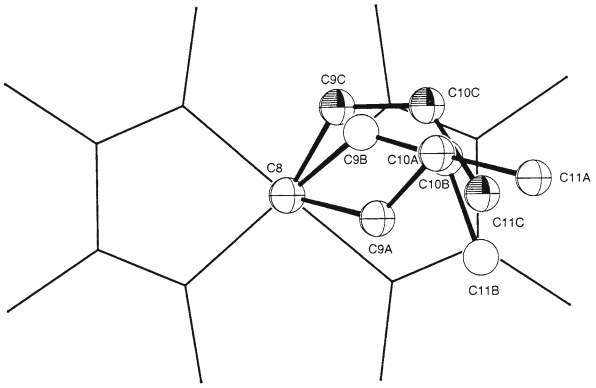

Fig. 5.43 Two *cis*-2-but (*B* and *C*) and one *trans*-2-but (*A*) groups viewed along the normal to the cobaloxime plane

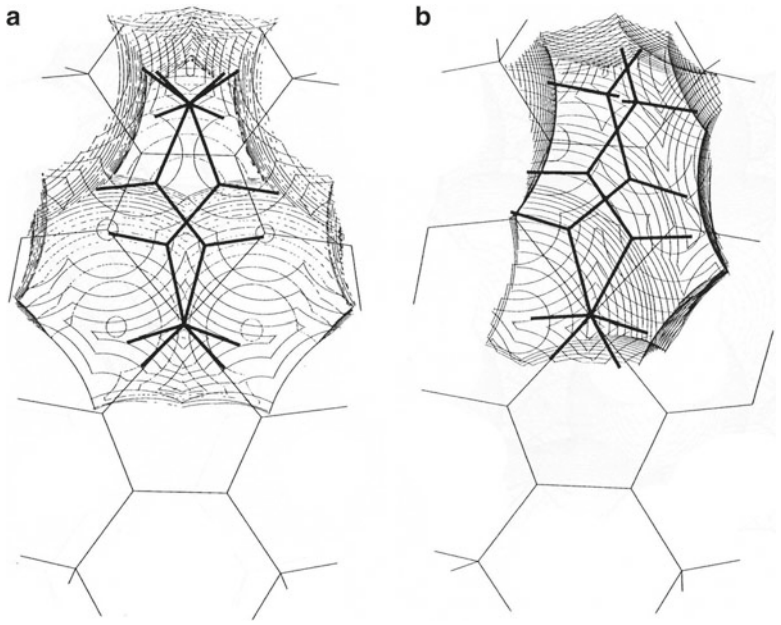

Fig. 5.44 Reaction cavities for the *trans*-2-but groups in the crystals of (**a**) 4brpy and (**b**) 3clpy before the irradiation

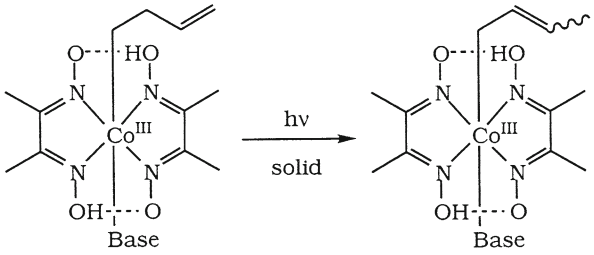

Scheme 5.9 Photoisomerization of the 3-butenyl to 2-butenyl group. *Trans* and *cis* conformers were observed for the product, which are indicated as waved line

For the 3-butenyl group, the photoisomerization was observed as shown in Scheme 5.9 [32]. However, the change occurs only in the solid state and not in the crystalline state.

The isomerization rates of the 2-ce to 1-ce groups in the cobaloxime complex crystals were found to be controlled by three factors: (1) the size of the reaction

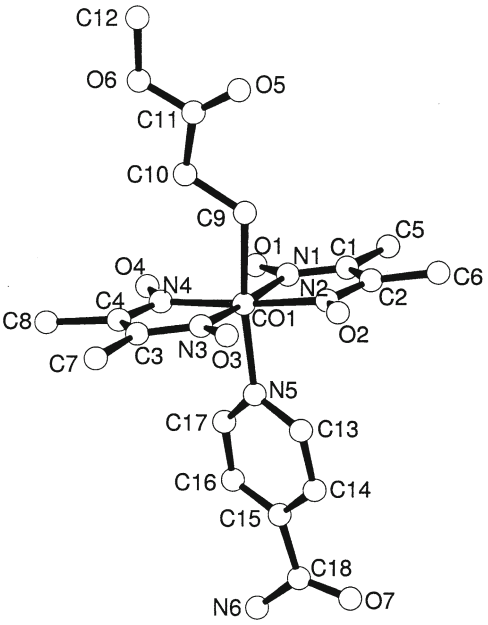

Fig. 5.45 Molecular structure of (2-mce) (isonicotinamide)cobaloxime

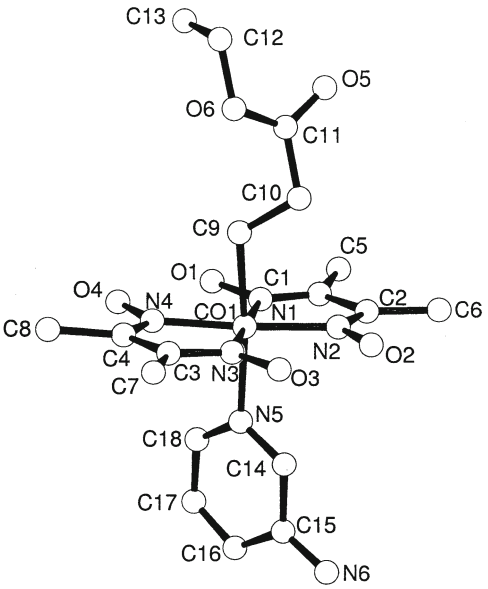

Fig. 5.46 Molecular structure of (2-ece) (3-aminopyridine)cobaloxime

cavity, (2) the conformation of the reactive group, and (3) the intermolecular hydrogen bond of the reactive group, as described in the previous section. In order to examine the other factors, the 2-ce group was replaced with the bulkier 2-(methoxycarbonyl)ethyl (2-mce) group, in which the CN group is replaced with CO_2CH_3 group [33]. Although more than 10 cobaloxime complex crystals with the different axial base ligands were prepared, the isomerizations from the 2-mce to 1-mce groups were found only in the solid state. The reaction rates were obtained from the change of the ^{1}H-NMR spectra of the powdered sample solved in $CDCl_3$ solution. In all the crystals, the conformations of the 2-mce groups are perpendicular to the cobaloxime plane, as shown in Fig. 5.45. The reaction cavity for the 2-mce group in each crystal structure was drawn and the volume was calculated. The rate constant for each crystal was obtained assuming first-order kinetics. The reaction rate is essentially dependent on the volume of the reaction cavity.

Then the reactive group was replaced with further bulkier group, 2-(ethoxycarbonyl)ethyl (2-ece) group [33]. The six complex crystals with different axial base ligands were prepared. The reaction rate for each crystal was obtained in the same way as those of the crystals with the 2-mce group. In all the crystals, the conformations of the 2-ece groups are perpendicular to the cobaloxime plane, as shown in Fig. 5.46. The relation between the reaction rate and the reaction cavity was not so clear.

References

1. Ohgo Y, Takeuchi S (1985) J Chem Soc Chem Commun 21
2. Uchida A, Danno M, Sasada Y, Ohashi Y (1987) Acta Crystallogr B43:528
3. Kato K (1984) Master Thesis, Tokyo Institute of Technology
4. Sawada K, Hashizume D, Sekine A, Uekusa H, Kato K, Ohashi Y, Kakinuma K, Ohgo Y (1996) Acta Crystallogr B52:303
5. Uchida A, Ohashi Y, Ohgo Y (1991) Acta Crystallogr C47:1177
6. Sekine A (1989) Master Thesis, Ochanomizu University
7. Sekine A, Ohashi Y, Hori K (1991) Acta Crystallogr C47:525
8. Sekine A, Ohashi Y, Shimizu E, Hori K (1991) Acta Crystallogr C47:53
9. Ohashi Y, Sekine A, Shimizu E, Hori K, Uchida A (1990) Mol Cryst Liq Cryst 186:37
10. Sekine A, Ohashi Y (1991) Bull Chem Soc Jpn 64:2183
11. Amano H, Sekine A, Ohashi Y, Hagiwara M, Sato J, Arai Y, Ohgo Y (1996) Bull Chem Soc Jpn 69:3107
12. Uchida A, Ohashi Y, Sasada Y (1986) Nature 320:51
13. Sekine A, Ohashi Y (1996) J Mol Struc 374:269
14. Ohgo Y, Arai Y, Hasegawa M, Takeuchi S, Kogo H, Sekine A, Uekusa H, Ohashi Y (1994) Chem Lett 715
15. Koura T, Ohashi Y (1997) Bull Chem Soc Jpn 70:2417
16. Cerius^2 (1994) release 1.0. Molecular Simulation Inc., Burlington
17. Koura T, Ohashi Y (2000) Tetrahedron 56:6769
18. Sekine A, Tatsuki H, Ohashi Y (1997) J Organomet Chem 536–537:389
19. Uchida A, Sasada Y, Ohashi Y (1988) Acta Crystallogr B44:249

20. Sekine A, Tatsuki H, Ohashi Y (1994) Mol Cryst Liq Cryst 242:109
21. Ohgo Y, Arai Y, Hasegawa M, Takeuchi S, Kogo H, Sekine A, Uekusa H, Ohashi Y (1994) Chem Lett 715
22. Yoshimiya T (1997) Master Thesis, Tokyo Institute of Technology
23. Imura H (2000) Master Thesis, Tokyo Institute of Technology
24. Ohashi Y, Hosoya T, Ohhara T (2006) Crystallogr Rev 12:83
25. Kurashima F, Takatsu N, Ishida I, Arai Y, Takeuchi S, Ohgo Y (1995) Annual Meeting of the Chemical Society of Japan, Kyoto, Abstract II, p 290
26. Sekine A, Yoshiike M, Ohashi Y, Ishida K, Arai Y, Ohgo Y (1998) Mol Cryst Liq Cryst 313:321
27. Bury A, Bougeard P, Corker SJ, Johnson MD, Perlmann M (1982) J Chem Soc Perkin Trans 2:1367
28. Ohhara T, Harada J, Ohashi Y, Tanaka I, Kumazawa S, Niimura N (2000) Acta Crystallogr B56:245
29. Vithana C, Uekusa H, Sekine A, Ohashi Y (2001) Bull Chem Soc Jpn 74:287
30. Yamada T, Uekusa H, Ohashi Y (1995) Chem Lett 187
31. Yamada T, Uekusa H, Ohashi Y (1996) Mol Cryst Liq Cryst 277:227
32. Yamada T, Ohashi Y (1998) Bull Chem Soc Jpn 71:2527
33. Amano H (1997) Doctor Thesis, Tokyo Institute of Technology

Chapter 6
Control of Reactivity

Abstract Although it is impossible to control the crystal structure, it is possible to modify the packing around the reactive group, making host–guest complexes or acid–base complexes between the cobaloxime complexes with carboxyl group and the amines. Usually the acid–base complexes were easily crystallized. The alkyl group with the modified reaction cavity in the acid–base complex revealed the different reactivity. When the bulky substituents are inserted to the cobaloxime moiety, the size and shape of the reaction cavity are largely changed. The completely different reaction process and reaction rate can be observed.

Keywords Acid–base complex formation • Insertion of bulky substituents

6.1 Acid–Base Complex Formation to Control the Reactivity

6.1.1 Different Reaction Rates

It is clear that the reaction rate and reactivity in the solid and crystalline states are greatly influenced by the intermolecular interaction of the reactive group with the surrounding atoms in the crystal structure. It has been proposed in the previous chapters that the size and shape of the reaction cavity for the reactive group before the reaction are very informative factors in considering the reactivity and reaction rate. However, the control of the solid- and crystalline-state reactions is very difficult because the design of the crystal structure of the reactant molecule is quite hard. In order to overcome the difficulty, the formation of the host–guest complex, which includes a reactant molecule as a guest, is one of the most promising methods. Investigations of solid-state photoreactions in the host–guest complexes have been carried out from the viewpoint of stereo- and enantioselective control [1–9]. The excellent review article was published by Toda [10]. Although the process of the selectivity induction has been explained based on the crystal and molecular

Y. Ohashi, *Crystalline State Photoreactions: Direct Observation of Reaction Processes and Metastable Intermediates*, DOI 10.1007/978-4-431-54373-2_6, © Springer Japan 2014

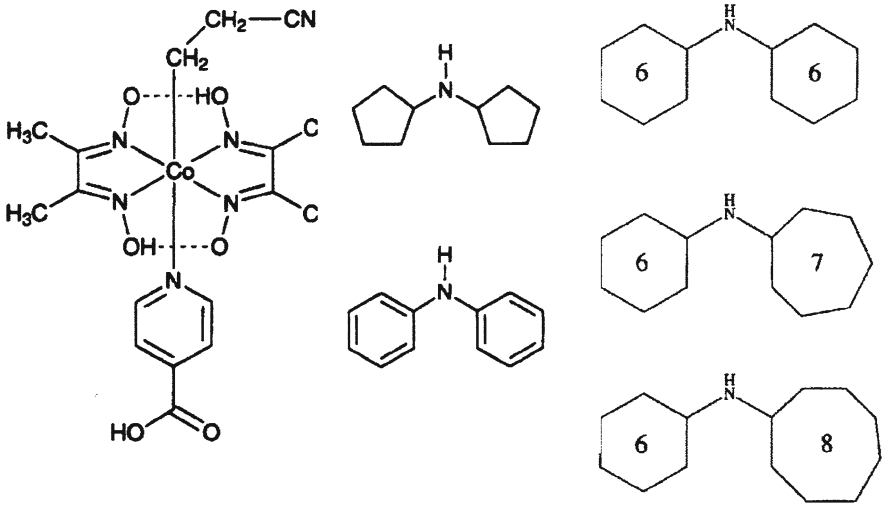

Scheme 6.1 Cobaloxime complexes with isonicotinic acid as the axial ligand, **I**, and secondary amines with aromatic rings in the various acid–base complex crystals

structures of the host–guest complexes, designing of the reaction paths is quite difficult and the factors determining the selectivity have not been elucidated.

The host molecules, of course, must be included in the crystalline lattice. This indicates that fairly strong interactions are necessary to form host–guest complexes. A most probable attractive force forming host–guest complexes is the hydrogen bond. Especially, acid–base interaction is very effective in forming the host–guest complexes and is a good pair of hydrogen bond donor and acceptor since the stoichiometry of the host–guest molecules can be predicted from the valences of the acid and base. The similar idea was applied to the asymmetric synthesis in the solid state [11].

On the basis of the idea, a variety of the host–guest complex crystals were prepared using the cobaloxime complexes with an acid group as guests and a variety of organic amines as hosts to control and design the reaction cavities for the reactive groups of the cobaloxime complexes. Cobaloxime complexes are soluble in polar organic solvents, such as methanol, ethanol, acetone, and chloroform, since the oxime moiety has the hydrophilic property. Nonpolar solvents can barely dissolve cobaloxime complexes although the latter have hydrophobic moieties, too. This suggests that the hosts appropriate to the cobaloxime complexes should be soluble in polar solvents and should not form any complexes with solvent molecules. In the crystals of cobaloxime complexes, the 2-ce and 1-ce groups are usually surrounded by the hydrophobic moieties of the neighboring molecules. This indicates that if the host has hydrophobic groups, they may pack the 2-ce and 1-ce groups.

Considering the above conditions, the cobaloxime complex with isonicotinic acid as a base ligand and secondary amines with aromatic rings as hosts were examined as acid–base complexes, as shown in Scheme 6.1 [12–14]. Hereafter, the crystals of the cobaloxime complex only and two acid–base complexes of the cobaloxime

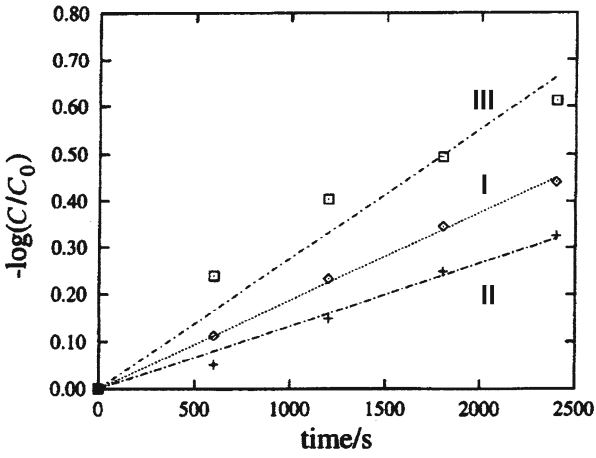

Fig. 6.1 Reaction rates of **I**, **II**, and **III** crystals at early stages within 40 min

complexes with dicyclopentylamine and diphenylamine are referred to as **I**, **II**, and **III**, respectively.

A KBr disc which contained 1 % of the powdered sample of **I**, **II**, or **III** was exposed to a xenon lamp. The change of the infrared spectra was measured at a constant interval of 10 min. The decrease of the absorption band at 2,250 cm^{-1} due to the 2-ce group within 40 min was explained by first-order kinetics for each sample as shown in Fig. 6.1. The rate constants were obtained by least-squares fitting. They are 1.88, 1.33, and 2.76×10^{-4} s^{-1} for **I**, **II,** and **III**, respectively.

The crystal structures before photo-irradiation were analyzed by X-rays. Although the hydroxyl group of the isonicotinic acid ligand makes a hydrogen bond with the oxime group of the neighboring molecule in the crystal structure of **I**, the hydroxyl groups in **II** and **III** make hydrogen bonds with the NH groups of the host amines. The crystal and molecular structures of **II** are shown in Figs. 6.2 and 6.3, respectively. The hydrogen atom of the carboxyl group is transferred to imino nitrogen N7 of dicyclopentylamine. The hydrogen bonds are formed between the carboxylate anion of isonicotinic acid and the ammonium cation of dicyclopentylamine, through O5···H72–N7 and O6···H71–N7. The cyclopentyl groups come close to the 2-ce group. This indicates that the environment around the reactive group is controlled by the host amines. No hydrogen bonds are formed with the 2-ce group. The 2-ce group takes a perpendicular conformation to the cobaloxime plane. The molecular structures of **I** and **III** are very similar to that of **II** and the 2-ce groups also take the perpendicular conformations. The 2-ce group in **III** is also packed with the neighboring dibenzylamine hosts.

In order to explain the differences in reactivity among the three crystals, the reaction cavities for the 2-ce groups were drawn and the volumes were calculated. The cavity volumes are 10.6, 8.6, and 15.3 $Å^3$, for I, II, and III, respectively. The most reactive crystal **III** has the largest cavity, whereas the least reactive crystal of **II** has the smallest cavity. Since the 2-ce groups in **II** and **III** are surrounded by the host amines, the difference in reactivity is caused by the packing of the host amine. This suggests that the reactivity in the solid-state reactions can be controlled by designing the host amine, even if the control of the crystal structure may be impossible.

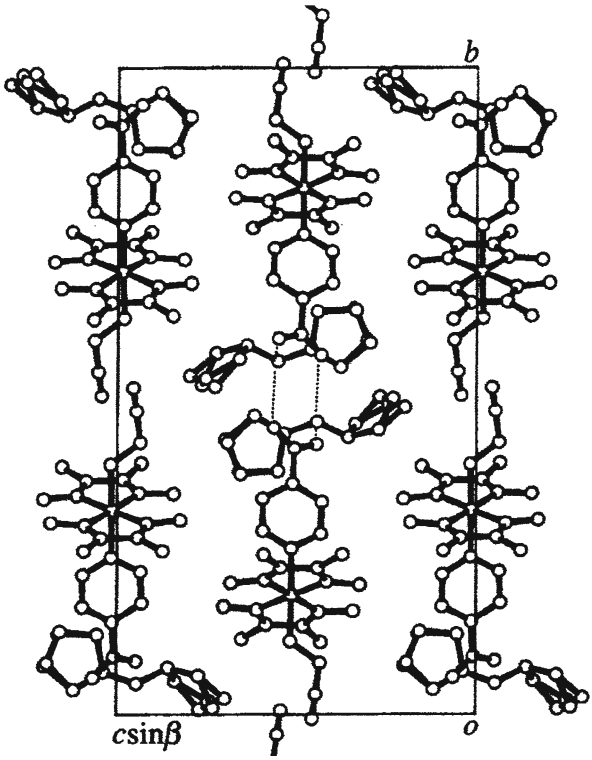

Fig. 6.2 Crystal structure of **II** viewed along the *a* axis. The hydrogen bonds are indicated with *dotted lines*

6.1.2 Control the Reaction Rate

In the above work, the acid–base complex crystals were formed between the cobaloxime complexes with the 2-ce group and the secondary amines and the reaction rates of the photoisomerization from the 2-ce group to the 1-ce group in the cobaloxime complexes were significantly varied due to the complex formation. However, as the crystal structure of the acid–base complex may become quite different if the host amine is exchanged with others, it is very difficult to tune the reaction rate. The design of the crystal structure is a difficult subject because the modification of the host amine causes a different environment around the reactive group.

This problem can be overcome by forming isostructural crystals. The acid–base complexes are effective for making the isostructural crystals, since it is quite common that a small change in the structure of the host amine gives only a slight change in the crystal structure of the acid–base complex. Since the positions of the atoms are almost the same, the effect of replacing the hosts on the reaction rates can be estimated quantitatively in the isostructural acid–base complexes.

In order to make isostructural crystals, the crystals of the acid–base complexes between the cobaloxime complex with isonicotinic acid as an axial base ligand and

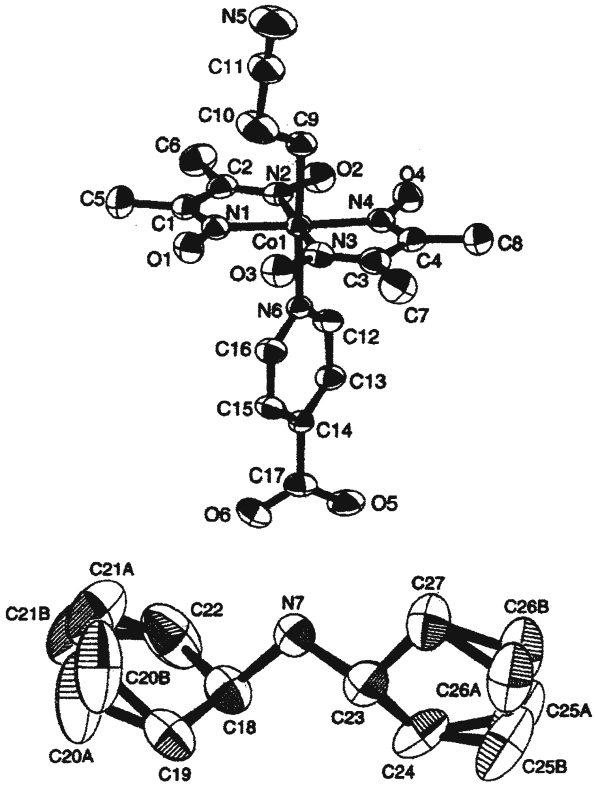

Fig. 6.3 Molecular structure of **II**. The thermal ellipsoids are drawn with 50 % probability. The cyclohexyl rings are disordered

dicyclohexylamine, **IV**, cycloheptylcyclohexylamine, **V**, and cyclohexylcyclooctylamine, **VI**, shown in Scheme 6.1 were prepared. The crystal structure analyses revealed that the three crystals, **IV**, **V**, and **VI**, are isostructural to each other.

The crystal belongs to the monoclinic system and the space group is $P2_1/n$. There are two crystallographically independent complexes, A and B, and two amine molecules, C and D, in the asymmetric unit. The proton of the carboxyl group of the axial isonicotinic acid is transferred to the imino group of the host amine in each crystal, as observed in the previous section. The molecules are connected by the hydrogen bonds between the anions and cations. There are no significantly short contacts of the 2-ce group with the neighboring molecules.

The molecular structures of A and B and of C and D are shown in Fig. 6.4. Both of the disordered 2-ce groups of A take parallel conformations around the C(9A)–C(10A) and C(9A)–C(10E) bonds. On the other hand, the 2-ce group of B has an ordered structure and takes a perpendicular conformation around the C(9B)–C(10B) bond. Both of the cyclohexyl rings have chair conformations. The crystal structures, hydrogen bonding schemes, and molecular structures of **V** and **VI** are almost the same as the corresponding ones of **IV**. All the cyclohexyl rings of C and D in **V** and **VI** take chair conformations, too.

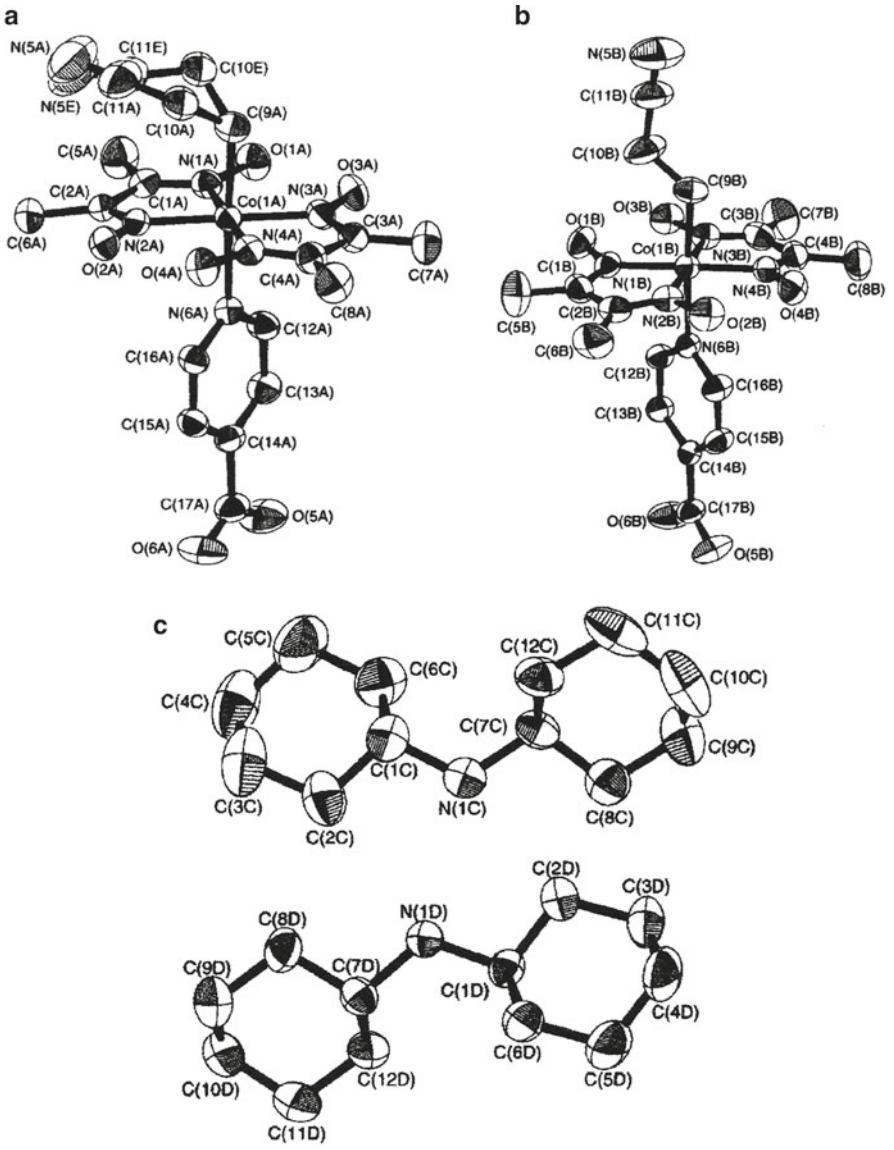

Fig. 6.4 Molecular structures of (**a**) A, the 2-ce group of which is disordered, (**b**) B and (**c**) dicyclohexylamines, C and D

The infrared spectra of the KBr discs including the powdered sample of **IV**, **V**, and **VI** were measured at a constant interval of 5 min. Two peaks appeared at 2,240 and 2,230 cm^{-1}, which are assigned to ν_{CN} of the parallel and perpendicular conformations of the 2-ce groups, respectively. The decrease of these absorption bands within 60 min was explained by first-order kinetics. The rate constant was obtained

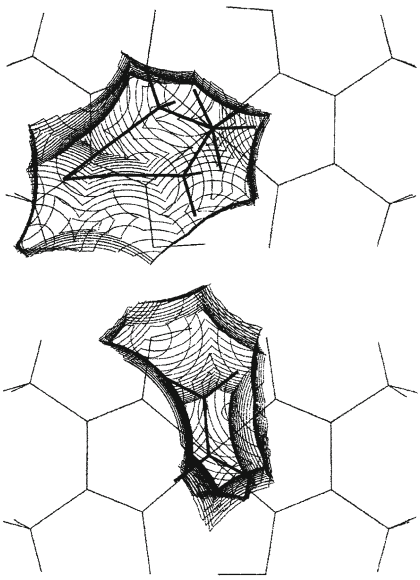

Fig. 6.5 Reaction cavities for the 2-ce groups of A and B molecules before the irradiation

independently from these two bands by least-squares fitting. The reaction rate constants were 2.0, 2.9, and 2.7×10^{-4} s^{-1} for A of **IV**, **V**, and **VI**, respectively, and 1.3, 1.8, and 1.8×10^{-4} s^{-1} for B of **IV**, **V**, and **VI**, respectively.

In order to examine the relation between the above reaction rates and the volumes of the reaction cavities for the 2-ce groups, the reaction cavities for the 2-ce groups of A and B molecules in the three crystals were drawn and the volumes are calculated. Since the conformations of the 2-ce groups are different between the A and B molecules, the shapes of the cavities are different from each other as shown in Fig. 6.5. The volumes of the reaction cavities for the 2-ce groups of A are 15.5, 16.7, and 17.2 $Å^3$ for **IV**, **V**, and **VI**, whereas the cavity volumes of B are 19.2, 19.7, and 17.7 $Å^3$ for **IV**, **V,** and **VI**, respectively.

The reaction rates of A are greater than those of B in the three crystals, although the volumes of the cavities of A are smaller than those of B. Such differences are caused by differences in conformations of the 2-ce groups between A and B molecules, since A molecules have parallel conformations, whereas B molecules have perpendicular conformations. Although the different reaction rates of the two conformers were already observed in the polymorphic crystals of the (2-ce)(pyridine) cobaloxime complex, the reactions in the polymorphic crystals cannot proceed under exactly the same conditions, because different crystals are used. Since the two conformers in the present photoreaction have exactly the same conditions, it was made clear that the 2-ce group with the parallel conformation is isomerized to the 1-ce group faster than that with the perpendicular conformation. The difference in reactivity between the two conformers in the solid state can be made clear in the same way as that in a solution if the two conformers were included in a crystal.

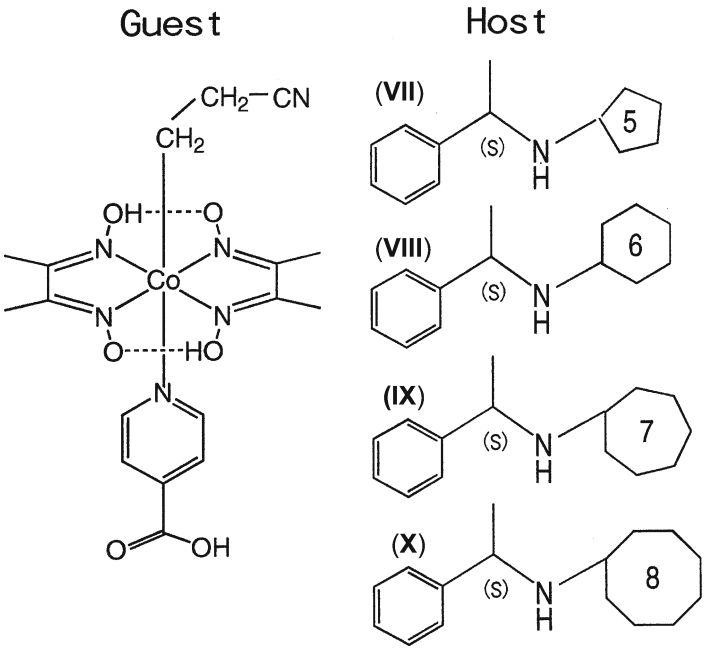

Scheme 6.2 Acid–base complex formation between (2-ce)(isonicotinic acid)cobaloxime isonicotinic acid and the size-tunable secondary amines with cyclopentyl, hexyl, heptyl, and octyl rings

When the reaction rates are compared among the same conformers, there is a good correlation between the reaction rate and the cavity size for the crystals of **IV** and **V**, although there is no correlation in the values of **V** and **VI**. These ambiguities may result from the disordered structure of the host amine of **VI**. This may indicate that if we want to design and control the solid-state reactions exactly, the host amine should have rigid groups to avoid the disordered structure.

6.1.3 Asymmetric Induction

In order to examine the possibility to introduce the asymmetry into the product in the process of the photoisomerization from the 2-ce to 1-ce group using the technique of acid–base complex formation, the cyclohexyl group of the host amine was replaced with (*S*)-1-phenylethyl group and another cycloalkyl group, cyclopentyl, cyclohexyl, cycloheptyl, or cyclooctyl group, was introduced, as shown in Scheme 6.2 [15]. The acid–base complex crystals were formed between the (2-ce)(isonicotinic acid)cobaloxime complex and the (*S*-1-phenylethyl)amines with cyclopentyl, cyclohexyl, cycloheptyl, and cyclooctyl groups, which are called **VII**, **VIII**, **IX**, and **X**, respectively.

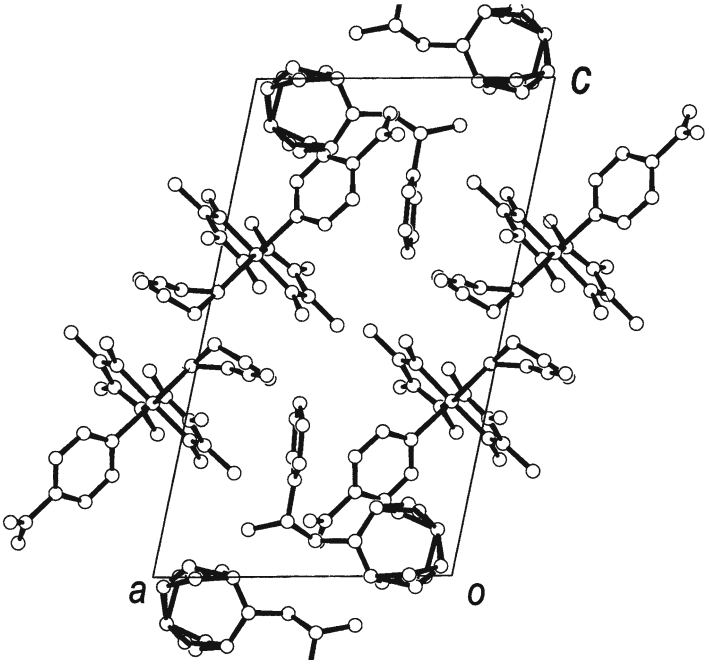

Fig. 6.6 Crystal structure of **IX** viewed along the *b* axis. The cyclohexyl ring is disordered

The crystal of **VII** has two crystallographically independent molecules, A and B, in the P1 cell. Both of the 2-ce groups of A and B take the perpendicular conformation and are contacts with each other around a pseudo inversion center. The crystal was irradiated with a xenon lamp for a week until the crystal was decomposed. The crystal analyzed by X-rays showed no change. This is because the conformation of the 2-ce group is perpendicular to the cobaloxime plane and the cavity volumes, 12.1 and 14.0 $Å^3$ for A and B, are too small. The crystal of **VIII** suitable for X-ray work was not obtained.

The crystal structure of **IX** viewed along the *b* axis is shown in Fig. 6.6. There is one molecule in an asymmetric unit of the $P2_1$ cell. The 2-ce group takes disordered structure with parallel conformations to the cobaloxime plane and is aligned along the 2_1 screw axis. The host amine with the disordered cycloheptyl group is also aligned along the other 2_1 screw axis. The crystal structure of **X** is isostructural to that of **IX**.

The crystal of **IX** was irradiated with a xenon lamp for 2 weeks. The structure analyzed by X-rays indicated that the 2-ce group was isomerized to the 1-ce group with *R* and *S* configurations with retention of the single crystal form. The original 2-ce group was not observed in the electron density map after the irradiation. The occupancy factors of *R* and *S* enantiomers were 34.3 and 65.7 %.

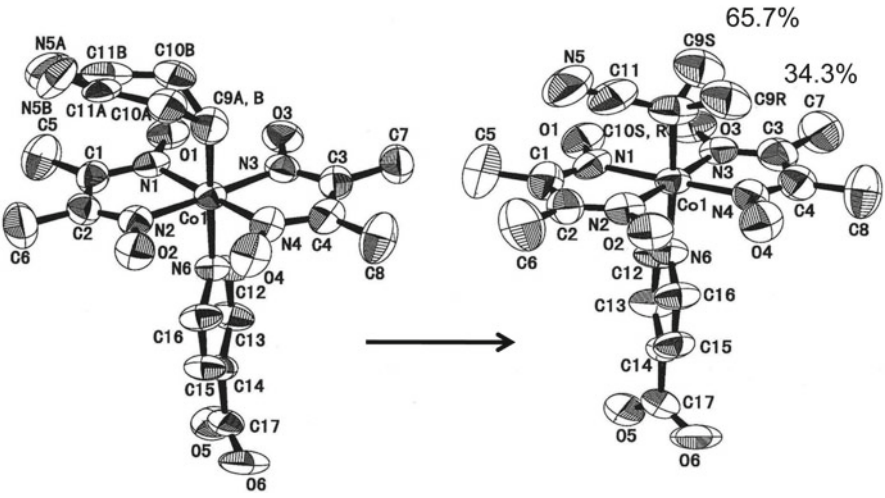

Fig. 6.7 Structural change of the 2-ce group during photo-irradiation

The photoproducts in the crystal after the irradiation were also analyzed by HPLC. The original cobaloxime complex with the 2-ce group remained only by 3.6 %. The other 96.4 % of cobaloxime complex was transformed to the 1-ce complex with the *R* and *S* configurations of 34.7 and 65.3 %, respectively. These values are in good agreement with those analyzed by X-rays. For the crystal of **X**, the similar results were obtained, although the occupancy factors of the *R* and *S* enantiomers were 54.7 and 45.3 %.

In order to make clear the reason why the uneven *R:S* ratio was obtained for the crystal of **IX** after the irradiation, the structures of the 2-ce and 1-ce groups before and after the photo-irradiation are given in Fig. 6.7. The change of the reaction cavities before and after the reaction is shown in Fig. 6.8. If the 2-ce groups of A and B are assumed to slide along the arrows as shown in Fig. 6.9, the *S*-1-ce and *R*-1-ce groups will be made from the 2-ce groups of A and B. The ratio of A to B, 32.9:67.1, is in good agreement with that of *S* to *R* configuration, 34.3:65.7, in the crystal of **IX**. In the crystal of **X**, the ratio of A to B, 58.1:41.9, is in good agreement with that of the *S* to *R* configuration, 54.7:45.3.

Although the optical yields in the photoreactions of **IX** and **X** are not so good because the 2-ce group takes a disordered structure, the mechanism of the 2-ce to 1-ce isomerization was clearly made. In order to control the reaction more precisely, the host amines should occupy the position surrounding the 2-ce group in the crystal structure. If the crystal with an ordered 2-ce group may be made, the photoisomerization would proceed with about 100 % reaction and optical yields in the crystalline state.

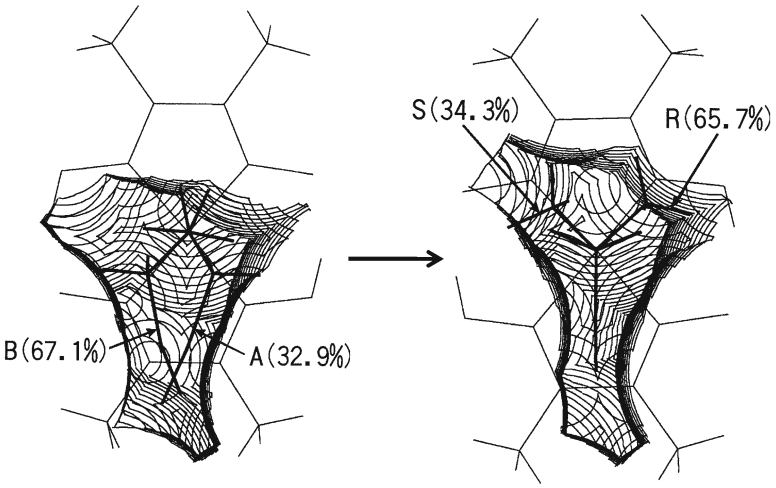

Fig. 6.8 Reaction cavities and the structural change of the 2-ce group. The occupancy factors of the produced 1-ce groups with *R* and *S* configurations are nearly the same as those of the disordered conformations of the original 2-ce group

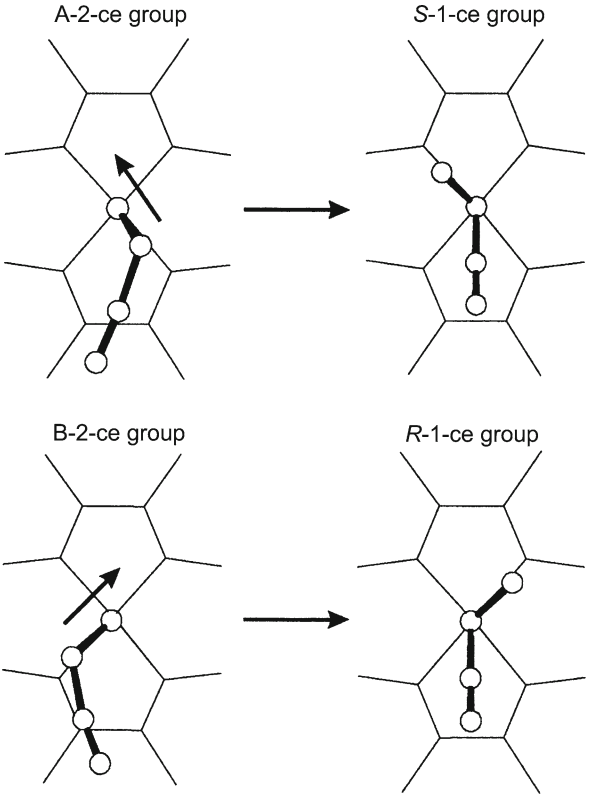

Fig. 6.9 Reaction pathway from the 2-ce to 1-ce group

6.2 Insertion of Bulky Substituent to Control the Reactivity

6.2.1 Insertion of Diphenylboron Group to the Cobaloxime Moiety

In the previous section, a series of the acid–base complexes were formed to control the size of the reaction cavity for the reactive group, changing the substituents of the host amines systematically. Another method to control the size of the reaction cavity is the insertion of the bulky substituents in the vicinity of the reactive group. Among cobaloxime complexes with modified oxime bridges [16–19], a complex with diphenylboron bridging appeared to be very attractive since one of the phenyl groups may have parallel conformation with the axial photo-reactive group as shown in Scheme 6.3 and may have great influence on the motion of the photo-reactive group bonded to the cobalt atom.

More than 40 cobaloxime complexes with diphenylboron bridging were prepared changing the axial base ligand. Only for the two complexes with 3-methylpyridine (3mpy), and *S*-nicotine (*S*-nic), as axial base ligands, the crystals gradually changed the cell dimensions with retention of the single crystal form [20]. The crystals with 3mpy and *S*-nic as axial base ligands are called **I** and **II**. Figure 6.10a, b shows the molecular structures of **I** and **II** before the photo-irradiation, respectively. There are two crystallographically independent molecules, A and B, in an asymmetric unit of **II,** which are related by a pseudo inversion center. The 2-ce groups in both of the crystals take perpendicular conformation to the cobaloxime plane. For the conformation around the Co–C bond, the plane composed of C–C–C–N atoms of the 2-ce group is approximately perpendicular to the axial phenyl ring of the diphenylboron group in the molecule of **I**, while it is almost parallel to the axial phenyl ring in that of **II**.

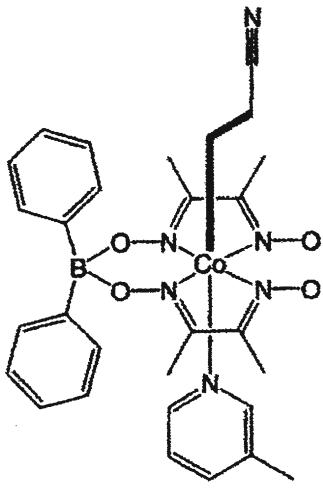

Scheme 6.3 Cobaloxime complex with the diphenylboron bridging

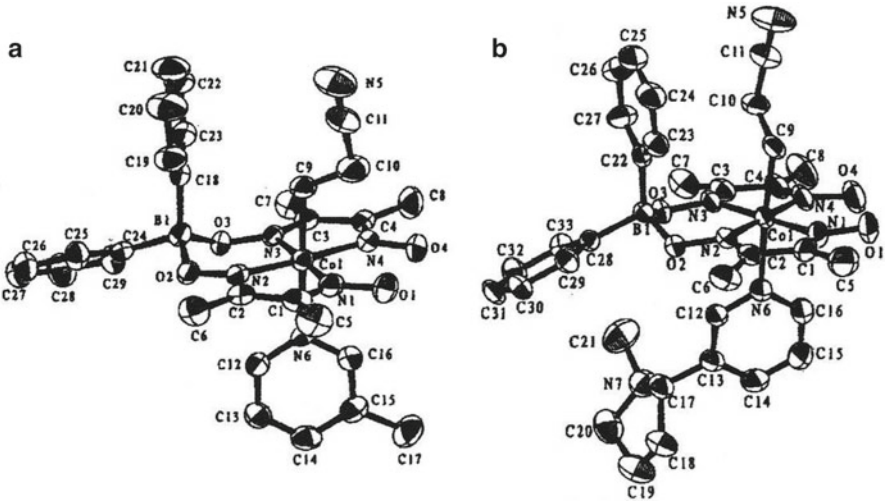

Fig. 6.10 Molecular structures of (**a**) **I** and (**b**) **II**

To examine whether the conformations are stable ones or not, the minimum energies were calculated rotating the 2-ce group around the Co–C bond, using the program Cerius[2]. There are three local minima, the rotation angle around the Co–C bond being 130°, 220°, and 310°. The angles correspond to the parallel, perpendicular, and parallel conformations observed in the molecules of **I** and **II**. This suggests that the conformations observed in the crystal structures may be preserved in solution.

Each crystal was exposed to a xenon lamp. The wavelengths longer than 630 nm were selected using a long-pass filter. The change of the cell dimensions became insignificantly small after 72 and 48 h exposures for **I** and **II**, respectively. The structures after photo-irradiation were analyzed. There appeared extra peaks around the 2-ce group, which were assigned to the atoms of the photo-produced 1-ce group. This is probably because the axial phenyl group strictly keeps the space for the isomerization.

In the molecular structure of **I** after the photo-irradiation, the produced 1-ce group does not take a disordered structure with *R* and *S* configurations. Since the crystal has a center of symmetry, the molecule at the inverted site has the opposite configuration. The molecular structure of A in **II** after the photo-irradiation showed nearly the same structure although the occupancy factor of the photo-produced 1-ce group became 0.30. The molecular structure of B has the inverted structure to A after the photo-irradiation.

The structural changes of the 2-ce groups in **I** and **II**A during the photo-irradiation are shown in Fig. 6.11a, b, in which the molecules are viewed normal to the cobaloxime plane. The molecule **II**B is the mirror image reflected by a plane perpendicular to the cobaloxime plane, passing through the cobalt and boron atoms. In order to explain the reason why one enantiomer of 1-ce group is made at a site, the reaction cavities for

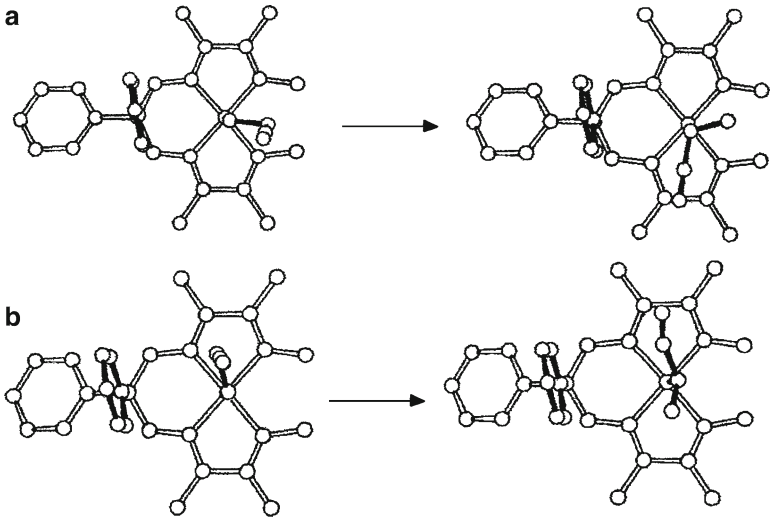

Fig. 6.11 Structural change of the 2-ce groups in (**a**) **I** and (**b**) **II**A during the photoreaction

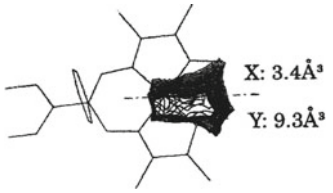

Fig. 6.12 Reaction cavity for the 2-ce group in **I**. The *dot* and *dashed line* is the plane composed of C–C–C–N bonds

the 2-ce groups before the photo-irradiation were drawn and the partial volumes were calculated. The cavity for the 2-ce group of **I** was divided into two by the plane composed of the C–C–C–N atoms. As shown in Fig. 6.12, the upper and down parts of the cavity have 3.4 and 9.3 $Å^3$, respectively. It seems reasonable to assume that the cyano and methyl groups of the produced 1-ce group occupy the larger and smaller parts, respectively. The reaction process in Fig. 6.11 is easily explained. The reaction process for the 2-ce group in **II**A is also explained by the shape of the reaction cavity.

The 3-cyanopropyl (3-cp) group bonded to the cobalt atom in the cobaloxime with diphenylboron group was found to be isomerized to the 1-cyanopropyl (1-cp) group with retention of the single crystal form [21]. When the axial base ligands were 3,4-lutidine, which is shown in Scheme 6.4, the photoisomerization from the 3-cp group to the 1-cp group proceeded with retention of the single crystal form, although the cobaloxime complex without diphenylboron group showed no reaction. Moreover, about 100 % of the 3-cp group was changed to 1-cp group. The molecular structures before and after the photoreaction are shown in Fig. 6.13. The disordered 3-cp group before photoreaction is changed to the ordered 1-cp group after the reaction. The size and shape of the reaction cavity for the 3-cp group clearly indicate the reaction pathway.

Scheme 6.4 The (3-cp)(3,4-lutidine)cobaloxime with the diphenylboron bridging

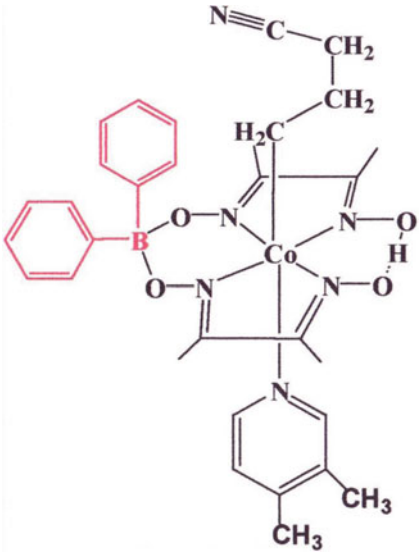

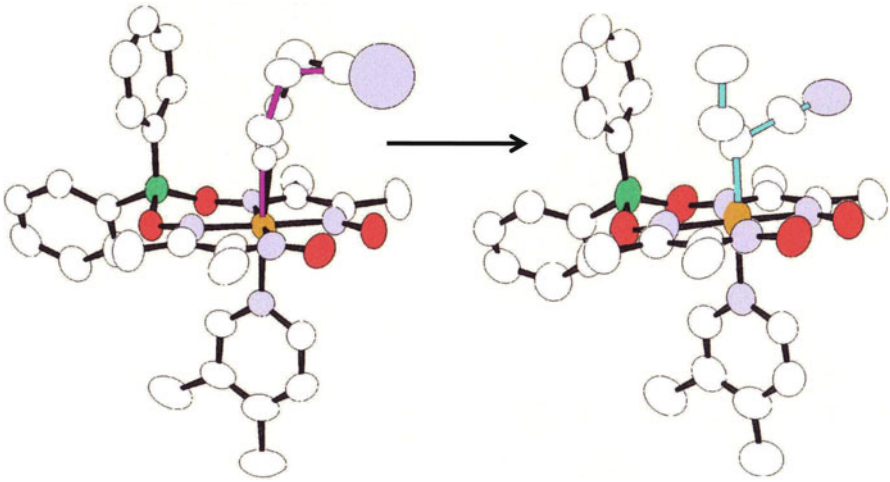

Fig. 6.13 Structural change of the 3-cp group before and after the photoreaction

6.2.2 Direct Observation from 4-Cyanobutyl to 1-Cyanobutyl Group

It was found that the cobaloxime complex with the 4-cyanobutyl (4-cb) group was isomerized only to the 3-cyanobutyl (3-cb) group with retention of the single crystal form. The NMR data indicated that about 6 % of 4-cb group was transformed to the

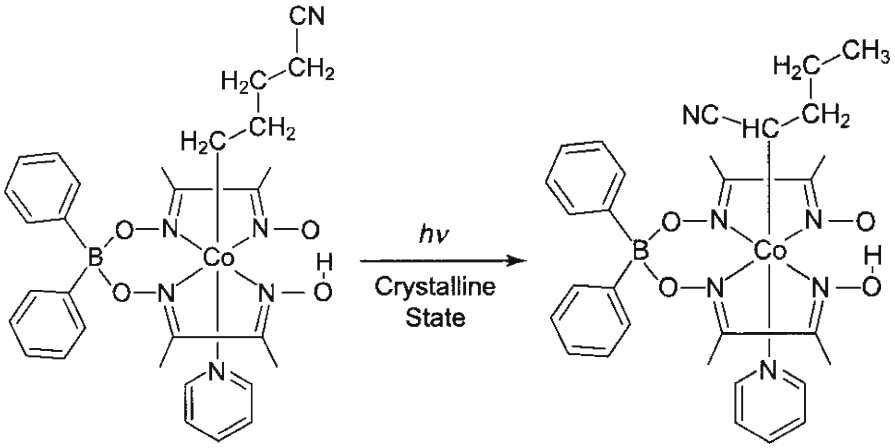

Scheme 6.5 Crystalline-state photoisomerization from the 4-cb to 1-cb group in the (py)cobaloxime complex

2-cyanobutyl (2-cb) group [22]. Since many trials to observe the photoisomerization from the 4-cb group to the 1-cb group in the crystalline state were unsuccessful, we considered to expand and control the reaction cavity for the 4-cb group.

Then the diphenylboron group was introduced to the equatorial ligands to observe the photoisomerization from the 4-cb to the 1-cb group as shown in Scheme 6.5. Among more than 10 complexes with different axial base ligands, the complexes with pyridine (py), 4-ethylpyridine (4epy), and 3,4-lutidine (lut) showed the photoisomerization with retention of the single crystal form. The crystals with py, 4epy, and lut before photo-irradiation are called **I**, **II**, and **III**, respectively [23].

The molecular structure of **I** is shown in Fig. 6.14. One phenyl group of the diphenylboron group is almost perpendicular to the cobaloxime plane, whereas another one is almost parallel to the cobaloxime plane. The conformation of the 4-cb group is all *trans* and is approximately parallel to the perpendicular phenyl group. The 4-cb groups and perpendicular phenyl groups of the two molecules make a pair around an inversion center of the $P2_1/c$ unit cell. When a crystal of **I** was exposed to a halogen lamp for 24 h, the cell volumes increased by 69.6 $Å^3$. The molecular structure after the irradiation is shown in Fig. 6.15. The red-colored 3-cb group was produced. The occupancy factor of the 3-cb group is 0.24(1). Only one enantiomer of the chiral carbon atom was obtained at one site around an inversion center. Since the crystallinity was retained after 24 h exposure, the photo-irradiation was continued for further 48 h. The cell volume decreased by 54.8 $Å^3$ after a total of 72 h exposure. The molecular structure after 72 h exposure is shown in Fig. 6.16. It is clear that the blue 1-cb group was produced after 72 h exposure in addition to the 3-cb groups. Only one enantiomer of the chiral carbon atom was observed at one site of an inversion center. The occupancy factors of 4-, 3-, and 1-cb groups became 0.69(1), 0.15(1), and 0.16(1), respectively. Although the change from 4-cb to 3-cb is small, about a half of 3-cb was transformed to 1-cb. The

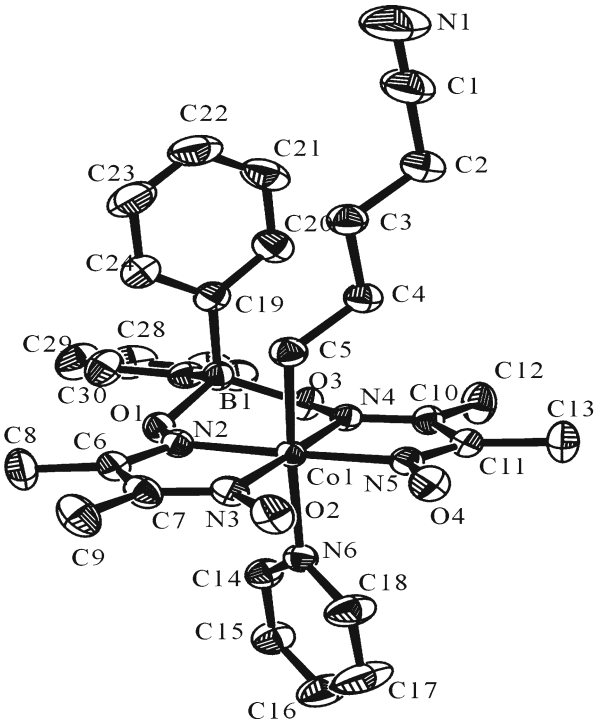

Fig. 6.14 Molecular structure of **I** before photo-irradiation

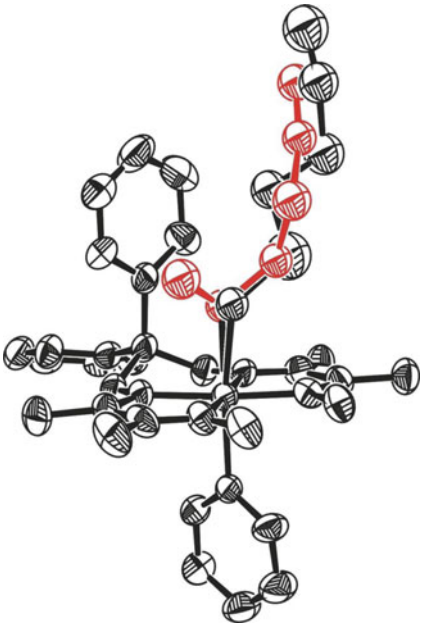

Fig. 6.15 Molecular structure of **I** after photo-irradiation for 24 h. The *red* one is the photo-produced 3-cb group

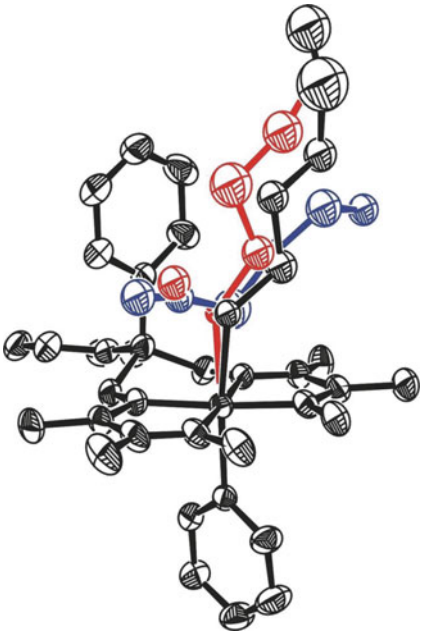

Fig. 6.16 Molecular structure of **I** after photo-irradiation for 72 h. The *blue* one is newly produced 1-cb group

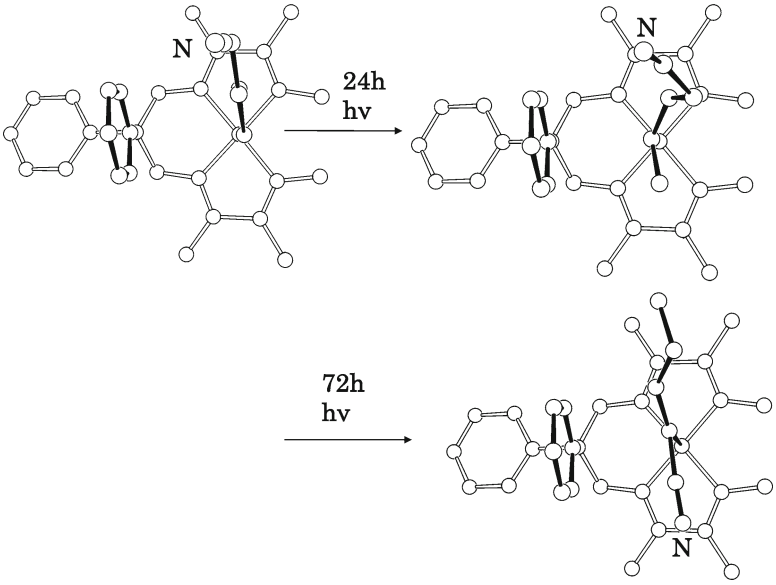

Fig. 6.17 Conformations and configurations of the photo-produced 3-cb and 1-cb groups

decrease of the cell volume is caused by the transformation from 3-cb to 1-cb. In order to examine the conformational change of the cyanobutyl group in the photoisomerization, the structures of the original and photo-produced cyanobutyl groups viewed along the normal to the cobaloxime plane are shown in Fig. 6.17.

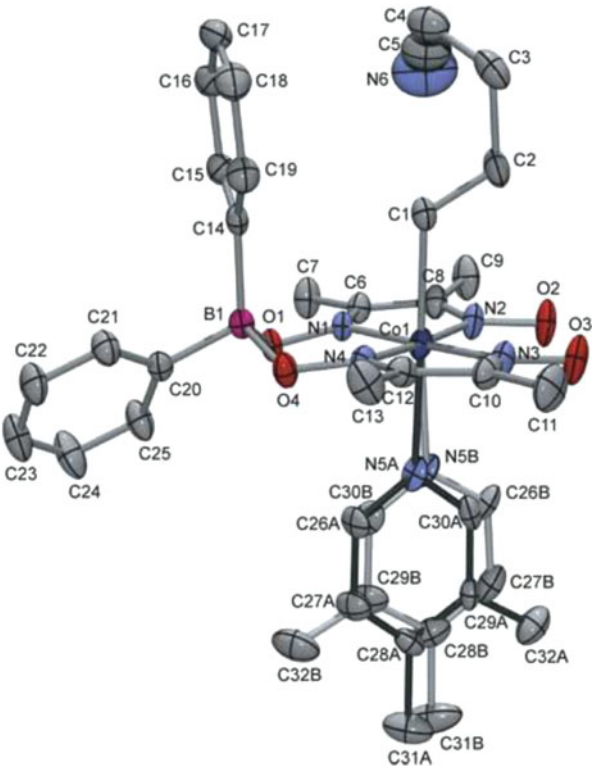

Fig. 6.18 Molecular structure of **III** before photo-irradiation. The conformation of the 4-cb group is different from those of **I** and **II**. The axial base ligand of lutidine is disordered

Considerably large movement of the terminal CN group is necessary to occupy the opposite side to the cobalt atom at the final stage.

The crystal of **II** was exposed the halogen lamp for 24 h. Only the 3-cb group appeared. Although the occupancy factor of the 3-cb group became 0.71(1), there was no indication of the 2-cyanobutyl (2-cb) or 1-cb group. The cell volume decreased by 95 $Å^3$ in the photoreaction. Further exposure was impossible due to the degradation of the crystallinity.

The molecular structure of **III** is shown in Fig. 6.18. The conformation of the diphenylboron group is almost the same as those of **I** and **II**. Such a conformation has been found in the related complex crystals [19, 24]. The conformation of 4-cb group is *trans*, *gauche*, and *gauche* around the C1–C2, C2–C3, and C3–C4, respectively. The axial base ligand of 3,4-lutidine is disordered.

When the crystal was exposed to the halogen lamp, the cell dimensions gradually changed and the change was insignificantly small after 24 h exposure. The molecular structure after 24 h exposure is shown in Fig. 6.19. The occupancy factor of the photo-produced 1-cb group is 0.472(6), which means that about half of 4-cb was isomerized to 1-cb. Although the CN group moves to a great extent, the methylene chain of C1–C2–C3–C4 takes nearly the same position during the photoisomerization.

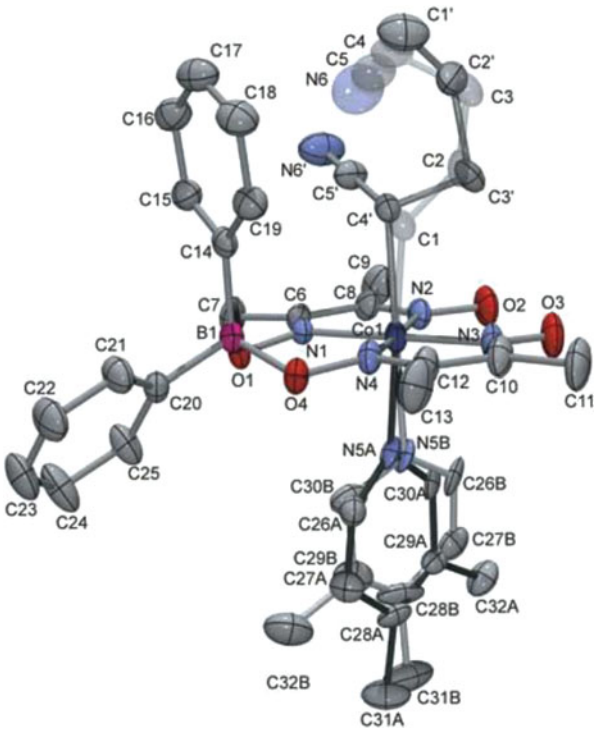

Fig. 6.19 Molecular structure of **III** after the irradiation for 24 h. The occupancy factors of the original 4-cb and photo-produced 1-cb are 0.528(6) and 0.472(6), respectively

The reaction cavities for the 4-cb group were drawn and the volumes were calculated for the crystals of **I**, **II**, and **III** before photo-irradiation. Several KBr pellets for each crystal were irradiated with light and successive FT-IR measurements of the pellets were carried out one by one. The isomerization rate constant at early stages (within 40 min) was estimated from the intensity change of the stretching vibration mode of the C–N triple bond of the 4-cb group. Assuming first-order kinetics, the reaction rate constants for **I**, **II**, and **III** are 6.2, 9.5, and 19.0×10^{-3} s^{-1}, respectively. The reaction cavity volumes of **I**, **II**, and **III** are 38.1, 49.2, and 32.7 $Å^3$, respectively. Since the reaction cavity of **I** is smaller than that of **II**, the rate constant of **I** is smaller than that of **II**. This indicates that the reaction mechanism of **I** from 4-cb to 3-cb at early stages should be the same as that of **II**. However, in spite of the smallest reaction cavity, the rate constant of **III** is the largest and the 4-cb group is isomerized to 1-cb group. This clearly suggests that the reaction mechanism of **III** is different from those of **I** and **II**.

In order to make clear the reason why the 4-cb group of **I** is finally isomerized to 1-cb group, the reaction cavities for 4-cb group before the irradiation are drawn in Fig. 6.20. There are void spaces A and B in the neighborhood of the chiral carbon atom bonded to the cobalt atom. When the 4-cb group is changed to the 1-cb group through the 3-cb group, the cyano and propyl group are accommodated in the space A and B, respectively. This also indicates that the space A is too small for the ethyl

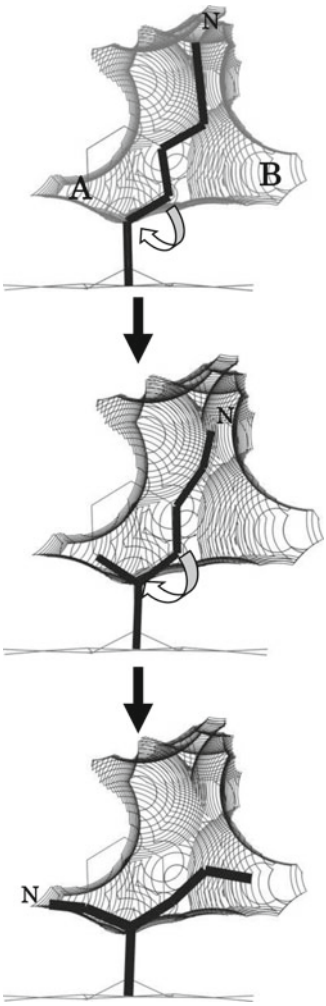

Fig. 6.20 Reaction pathway of the crystal **I** from the 4-cb to 1-cb group in the reaction cavity for the 4-cb group

group when the 2-cb group is produced. It seems adequate to consider that the 2-cb group was not observed in the intermediate stages because it is very unstable due to heavy steric repulsion.

6.2.3 Isomerization Pathway Confirmed by Neutron Diffraction

Although it was clarified that the 4-cb group of **I** is isomerized to 1-cb through 3-cb and 2-cb, the 4-cb group of **III** was directly isomerized to the 1-cb group and the intermediate structures with 3-cb and 2-cb were not observed. In order to elucidate the reaction mechanism, deuterium atoms were introduced in the 4-cb group and

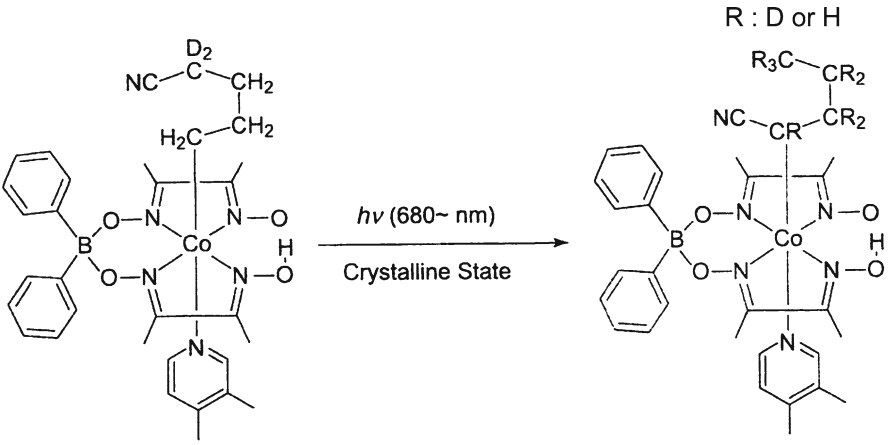

Scheme 6.6 Crystalline-state photoisomerization of the deuterated (4-cb)(3,4-lutidine) cobaloxime complex observed by the neutron diffraction

the structure after photo-irradiation was analyzed by neutron diffraction as shown in Scheme 6.6. Since the neutron diffraction can discriminate between deuterium and hydrogen atoms, it may be clarified which hydrogen atoms are replaced with deuterium atoms.

The longer wavelengths around 700 nm were selected and the crystal size was $4.5 \times 1.5 \times 1.4$ (ca. 9.5) mm^3 was used. The crystal of **III** was exposed to a xenon lamp for 2 days at 273 K [25]. A small part was cut from the crystal and the structure was analyzed by X-rays. The occupancy factor of the disordered 4-cb and 1-cb groups was obtained as 0.528(6):0.472(6).

Figure 6.21 shows the structure of the photo-produced molecule with 1-cb group analyzed by neutron diffraction. It is clear that one of the deuterium atoms is bonded to the chiral carbon, C4′, and that another is distributed as disordered ones in the three terminal methyl hydrogen atoms with the occupancy factor of 1/3. The methylene carbon atoms of C2′ and C3′ have no deuterium atoms.

Three reaction processes from the 4-cb to 1-cb group may be possible as shown in Scheme 6.7. The first one, (a), is called "alkyl slide" isomerization. The successive isomerization from 4-cb to 1-cb through 3-cb and 2-cb was observed in the crystal of **I**. If the reaction proceeds in this route, the two deuterium atoms in the 1-cb group should be located at the C^1 and C^2 atoms, which are different from the structure obtained by neutron diffraction. The second one, (b), is called "cyano rearrangement" isomerization. This is a direct rearrangement of a cyano group from C^4 to C^1 via a 5-membered ring, which is observed in organic reactions [26]. The photo-produced 4-cb radical changes to a five-membered ring to form a new C–C bond between C^1 and the carbon of CN group. Then the C^4 radical abstracts a hydrogen atom from C^1. Finally, a bond is formed between the cobalt and C^1 atoms. The 4–1 isomerization involves no intermediates with 3- and 2-cb groups. If the reaction proceeds in (b), the two deuterium atoms remain in the terminal methyl group as a

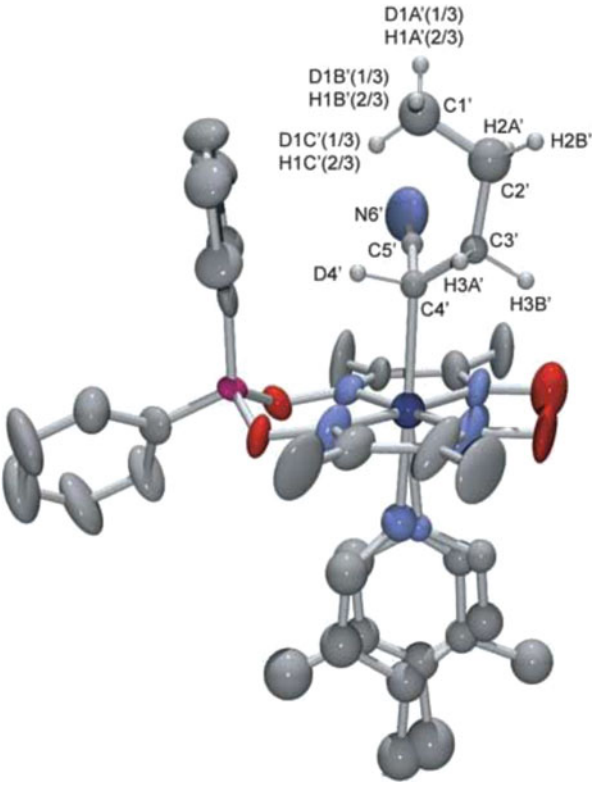

Fig. 6.21 Molecular structure of **III** after the photoreaction. One of the D atoms D4′ is bonded to the chiral carbon, C4′, and another one is distributed in the methyl hydrogen atoms with the occupancy of 1/3

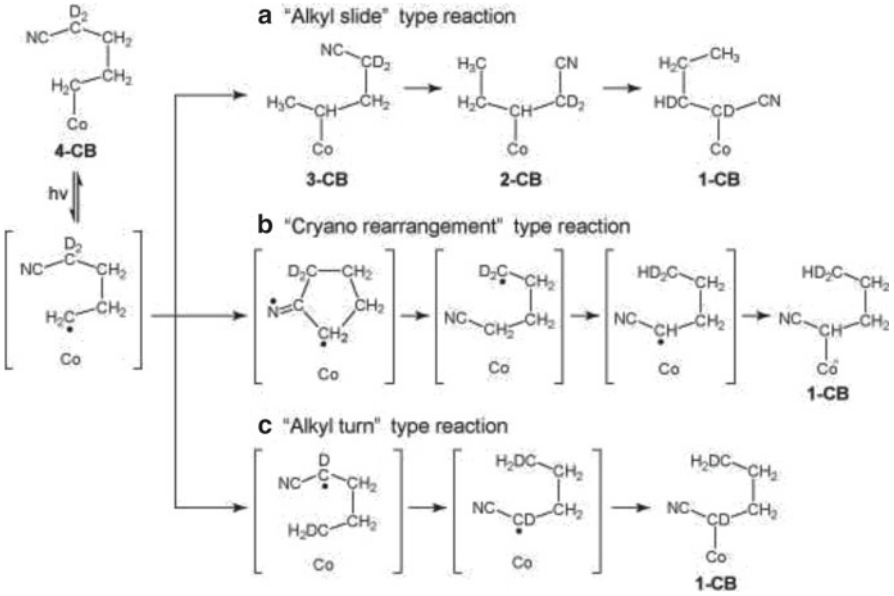

Scheme 6.7 Possible three reaction processes in the photoisomerization from the 4-cb to 1-cb group

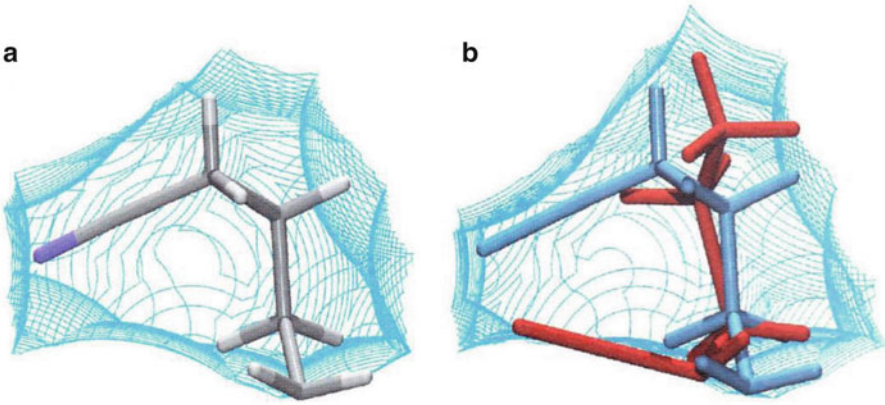

Fig. 6.22 Reaction cavities for the 4-cb group, in which (**a**) the 4-cb group before the irradiation and (**b**) the initial 4-cb and final 1-cb groups are drawn

disordered structure with the occupancy of 2/3, which is different from the structure obtained by neutron diffraction.

The third one, (c), is called "alkyl turn" isomerization. This process also involves no intermediates with 3-cb and 2-cb groups. The C^1 atom of the photo-produced 4-cb radical abstracts one of the deuterium atoms bound to C^4, then the 4-cb radical is turned upside down. Finally, the bond between the cobalt and C^1 atom is formed. The distance between the C^1 and the deuterium atoms is 2.66 Å, which is shorter than the sum of the van der Waals radii. This means that the two deuterium atoms in the structure of 1-cb group should be located at the C^1 and C^4 atoms, which is in good agreement with the observed neutron structure. Since the deuterium atom bonded to the C^1 atom shows 100 % occupancy factor, the process of the alkyl turn should be irreversible. These results clearly indicate that the reaction proceeds in "alkyl turn" pathway.

The "alkyl turn" isomerization is very favorable in the crystalline-state reaction. To explain the movement of the 4-cb group, the reaction cavity for 4-cb in the crystal structure before irradiation is shown in Fig. 6.22a. The reaction cavity after irradiation, which includes both of 4-cb and 1-cb, is shown in Fig. 6.22b. Since the two cavities are very similar, it is reasonable to assume that the reaction cavity does not change to a great extent during the photoisomerization.

The movement of the produced radical is estimated as shown in Fig. 6.23. Since the cavity is large in the lateral direction, the long $–CH_2CN$ part of the photo-produced radical can use this space so as to rotate around the $C^4–C^3$ bond like the pedal motion of a bicycle. Therefore, this reaction can proceed without destruction of the single crystal form. For the other two processes, the intermediate radicals suffer from strong steric repulsion in the cavity. This is the reason why the "alkyl turn" isomerization proceeds in the crystal of **III**. It is clear that the different pathways from 4-cb to 1-cb in the crystals of **I** and **III** are caused by the different reaction cavities for 4-cb groups in the two crystal structures.

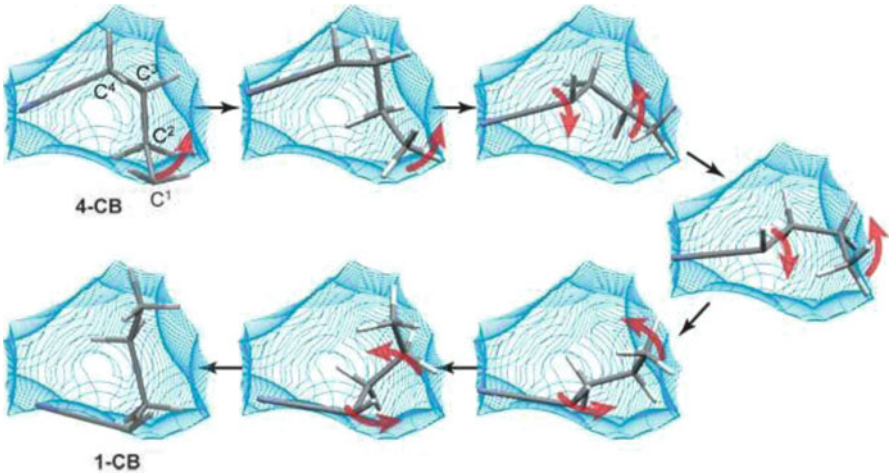

Fig. 6.23 Movement of the photo-produced radical in the cavity for the initial 4-cb group

References

1. Fu TY, Liu Z, Scheffer JR, Trotter J (1993) J Am Chem Soc 115:12202
2. Gudmundsdottir AD, Scheffer JR, Trotter J (1994) Tetrahedron Lett 35:1397
3. Jones R, Liu Z, Scheffer R, Trotter J (1995) Acta Crystallogr B51:888
4. Kinbara K, Kai A, Maekawa Y, Hashimoto Y, Naruse S, Hasegawa M, Saigo K (1996) J Chem Soc Perkin Trans 2:247
5. Ito Y, Borecka B, Olovsson G, Trotter J, Scheffer JR (1995) Tetrahedron Lett 36:6087
6. Ito Y, Borecka B, Trotter J, Scheffer JR (1995) Tetrahedron Lett 36:8083
7. Aoyama H, Miyazaki K, Sakamoto M, Omote Y (1983) J Chem Soc Chem Commun 333
8. Jones R, Scheffer JR, Trotter J, Yang J (1994) Acta Crystallogr B50:601
9. Toda F (1988) Top Curr Chem 149:211
10. Toda F (1995) Acc Chem Res 28:480
11. Gamlin JN, Jones R, Leibovitch M, Patrick B, Scheffer JR, Trotter J (1996) Acc Chem Res 29:203
12. Ohashi Y, Hashizume D (1998) Mol Cryst Liquid Cryst 313:95
13. Hashizume D, Ohashi Y (1998) J Chem Soc Perkin Trans 2:1931
14. Hashizume D, Ohashi Y (1999) J Chem Soc Perkin Trans 2:1689
15. Sugimoto N (1999) Master Thesis, Tokyo Institute of Technology
16. Randaccio L, Bresciani-Pahor N, Zangrando E, Marzelli LG (1989) Chem Soc Rev 18:225
17. Schrauzer GN, Windgassen RJ (1966) J Am Chem Soc 88:3738
18. Gerli A, Sabat M, Mestroni LG, de Savorgnani E (1969) Inorg Chim Acta 3:323
19. Dreos R, Tauzher G, Vuano S, Asaro F, Pellizer G, Nardin G, Randaccio L, Geremis S (1995) J Organomet Chem 505:135
20. Ohashi Y, Iketani G, Uekusa H (2001) Mol Cryst Liquid Cryst 356:53
21. Arai H (2001) Master Thesis, Tokyo Institute of Technology
22. Vithana C, Uekusa H, Sekine A, Ohashi Y (2001) Bull Chem Soc Jpn 74:287
23. Hirano A, Sekine A, Uekusa H, Ohashi Y (2011) Bull Chem Soc Jpn 84:496
24. Asaro F, Dreos R, Geremia S, Nardin G, Pellizer G, Randaccio L, Tauzher G, Vuano S (1997) J Organomet Chem 548:211
25. Hosoya T, Uekusa H, Ohashi Y, Ohhara T, Kuroki R (2006) Bull Chem Soc Jpn 79:692
26. Bury A, Bougeard P, Corker SJ, Johnson MD, Perlmann M (1982) J Chem Soc Perkin Trans 2:1367

Chapter 7
Metastable or Unstable Intermediates in Reversible Processes

Abstract The metastable reaction intermediates were observed in the racemization of the bulky *R*-1,2-bis(methoxycarbonyl)ethyl group and the isomerization from the 4-cyanobutyl to1-cyanobutyl group as shown in the previous chapters. Such examples brought about an idea that the structures of the metastable or unstable reaction intermediates should be observed if the usual organic reactions proceed in the crystalline state. If the occupancy factor of the metastable or unstable intermediate produced in the original crystal exceeds the threshold value, ca. 5 %, it is surely possible to observe the structure of the intermediate with sufficient precision. In this chapter, several examples of the reversible reactions are described. Unstable structures of the lophyl radicals, red species of photochromic salicylideneaniline derivatives, and blue species of photochromic pyridine derivatives were analyzed by X-rays. The unstable structures returned to the original one when the crystals were kept at room temperature in the dark or was irradiated with longer wavelengths. Although the molecular excitation due to photo-irradiation is not exactly a reversible reaction, the unstable excited structure can be observed during the photo-irradiation. If the occupancy factor of the excited molecule exceeds the threshold value, the excited molecule can be observed in the mixed structures at the ground and excited states produced during the photo-irradiation.

Keywords Pyridine derivatives • Salicylideneaniline derivatives • Structure of excited molecule • Structure of lophyl radical • Unstable species of photochromism

7.1 Reversible Radical Formation

Radical species play an important role as reaction intermediates in chemical and biological systems. While a number of radicals have been extensively investigated in the solid state by spectroscopic methods, a crystallographic approach is relatively less common for unstable radicals and has been applied to stable radicals, e.g., radical ion pairs,

Y. Ohashi, *Crystalline State Photoreactions: Direct Observation of Reaction Processes and Metastable Intermediates*, DOI 10.1007/978-4-431-54373-2_7, © Springer Japan 2014

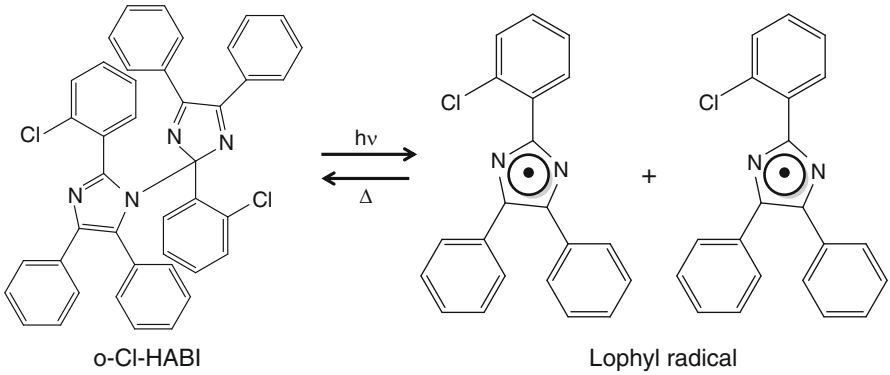

Scheme 7.1 Formation of a pair of lophyl (triarylimidazoyl) radicals from *o*-Cl-HABI

stabilized radicals, and so on [1]. An unprecedented example is the in situ observation of a light-induced radical pair produced in a crystal of 2,2′-di (*o-chlorophenyl*)-4,4′,5,5′-tetraphenyl-biimidazole (*o*-Cl-HABI) by X-ray diffraction, as shown in Scheme 7.1 [2]. HABI derivatives are well known as the photo- and thermochromic compounds, the polymerization photo-initiators in imaging materials, and holographic photopolymers since it was prepared in 1960 [3–5]. It has been proposed that the photolysis of the HABI derivatives in benzene solution instantaneously produces a pair of lophyl (triarylimidazoyl) radicals. The lophyl radical has been proposed to be an initiator for the radical polymerization. Despite the intriguing properties of HABI derivatives, there is very few report [6].

The crystal of *o*-Cl-HABI has two crystallographically independent molecules, A and B. The molecular structure of A is shown in Fig. 7.1. The B molecule has essentially the same structure as A. On exposure to the high-pressure Hg lamp for 20 min at 103(2) K, the crystal turned from pale yellow to reddish brown. Although the space group was retained after the irradiation, the unit-cell volume decreased by 64.9(3) Å^3. The C–N bond connecting the two triarylimidazoyl groups of the B molecule, C4B–N2B, was cloven to yield two planar lophyl radicals closely located in a crystal cage as a radical pair, which is shown in Fig. 7.2. The occupancy factor of the produced radical pair is 0.105(1). The molecule A retained unchanged. The produced lophyl radical pair clearly indicates that an unpaired electron is delocalized over each imidazoyl ring. Only the produced lophyl radicals are shown in Fig. 7.3. The C4B···N2B distance changed from 1.479 to 3.1 Å.

In order to make clear the reason why only B was changed to the radical pair whereas A retained unchanged, the reaction cavities for the two molecules A and B and for the produced radical pair were calculated. The volumes of the cavities are 355, 381, and 383 Å^3 for A, B, and the radical pair, respectively. These values indicate that molecule A is too closely packed in a crystalline lattice to form its radical pair.

When the crystal was warmed up to room temperature, the color returned to the original one and the ESR signal showing the triplet state disappeared. However, the crystal structure analysis was very difficult because of its poor crystallinity, although

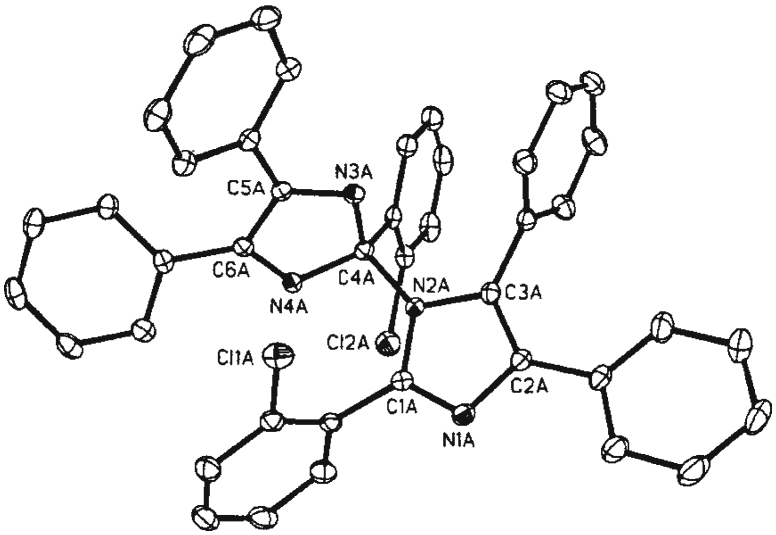

Fig. 7.1 Molecular structure of A in the crystal of *o*-Cl-HABI before the irradiation

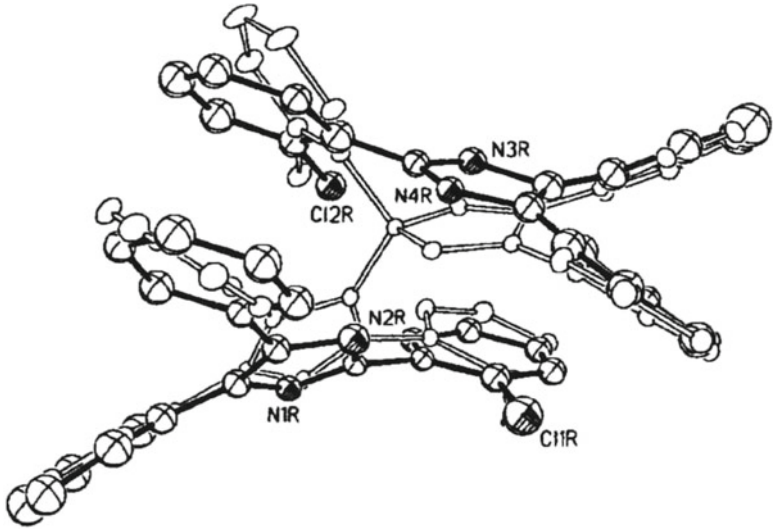

Fig. 7.2 Molecular structures *o*-Cl-HABI after photo-irradiation. The molecules with *white bonds* and *black bonds* are the original and the photo-produced ones, respectively

the crystal should have the same structure as that before the photo-irradiation considering from its cell dimensions.

Using the structure of the light-induced radical pair, the ESR spectra, and the DFT calculation, the intermolecular exchange coupling has successively determined for the first time [7]. Since the ESR measurement revealed that the drastic

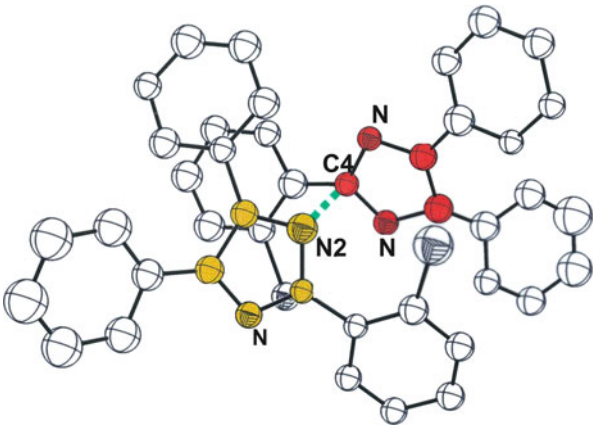

Fig. 7.3 A pair of the produced lophyl radicals viewed along the normal to the radical plane. The *dotted line* between C4 and N2 indicates the bond before the irradiation

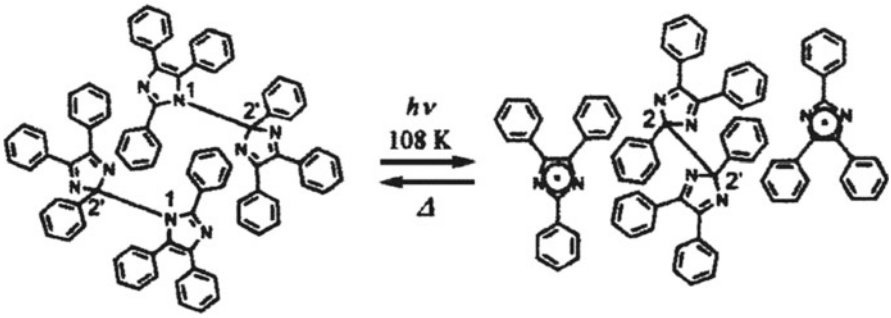

Scheme 7.2 Formation of a piezodimer and a pair of lophyl radicals from two HABI molecules

spin-multiplicity change occurred during 2–40 K, the structures of the light-induced radical pair from *o*-Cl-HABI were analyzed at 23, 30, 40, and 70 K using the synchrotron radiation at SPring-8 [8]. The combined results of the structures with the theoretical calculation, IR, UV–vis spectroscopy suggested that a slight conformational change of the radical pair causes the drastic spin-multiplicity change.

The direct observation of the radical pair formation was performed for the crystal of the HABI mother compound, 2,2′-diphenyl-4,4′,5,5′-tetraphenyl-biimidazole as shown in Scheme 7.2 [9]. Since the molecule is composed of two monomer molecules bonded between N1 and C2′, this is called 1,2′-dimer. The molecular structure before photo-irradiation is similar to that of *o*-Cl-HABI. A pale yellow crystal of HABI was irradiated with a high-pressure Hg lamp for 30 min at low temperatures under 108 K. The disordered molecular structures of 1,2′-dimers and the photo-produced ones around an inversion center are shown in Fig. 7.4. The original 1,2′-dimer is drawn with white bonds. The new molecules with black bonds appeared, which have the occupancy factor of 0.139(2). There are two lophyl radicals in both sides and

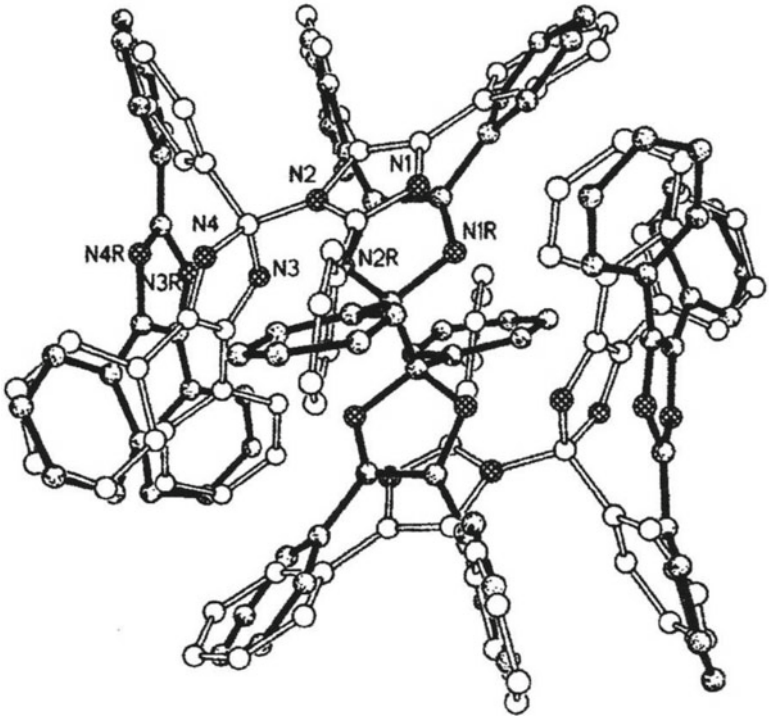

Fig. 7.4 Molecular structures of HABI after photo-irradiation at 108 K. The original two HABI molecules, 1,2′-dimer, are drawn with *white bonds*. The photo-produced 2,2′-dimer and two lophyl radicals are drawn with *black bonds*. On warming to 298 K, the photo-produced molecules returns to the original two 1,2′-dimers

one dimer molecule which has a C2–C2′ bond connecting the monomer molecule. The new dimer, 2,2′-dimer, is called piezodimer [10]. The photoreaction is shown in Scheme 7.2, in which two 1,2′-dimers around an inversion center are changed to 2,2′-dimer with inversion symmetry and two lophyl radicals. On warming to 298 K, the black crystal returned to the initial pale yellow HABI crystal. The black crystal was considerably stable at room temperature in contrast with the irradiated crystal of *o*-Cl-HABI containing lophyl radical pairs only.

The IR spectra after irradiation were assigned to the original 1,2′-dimer, produced 2,2′-dimer and lophyl radical. Moreover, the spectra also indicate that this photochemical process is reversible. The existence of the 2,2′-dimer has been assumed from the spectroscopy but the structure analysis has not been successful, because the 2,2′-dimer is easily transformed to the 1,2′-dimer. The 2,2′-dimer with 4π–4π electron system is less stable than the 1,2′-dimer with 4π–6π system. The theoretical calculation indicated that the 1,2′-dimer is stabler by 5.9 kcal mol^{-1} than the 2,2′-dimer. The in situ X-ray crystallography shown here is a very powerful method to capture the light-induced metastable intermediates such as a 2,2′-dimer.

7.2 Photochromism of Salicylideneanilines

7.2.1 Direct Observation of Structural Change in Photochromism

Light-induced reversible color change of substances is known as photochromism and organic photochromic compounds have attracted much attention over the past decades for their applications in optic data storage, electronic display systems, optical switching devices, ophthalmic glasses, and so on [11–13]. *N*-Salicylideneanilines, which are the condensation products of salicylaldehydes and anilines, exhibit photochromism both in solution and in the solid state [14, 15]. Photochromic salicylideneanilines are usually pale yellow and exist in the enol form in crystals. It was proposed from spectroscopic data that the hydrogen atom of the hydroxyl group is translocated to the imine nitrogen atom on irradiation with ultraviolet light. A subsequent geometrical rearrangement in the excited state is assumed to form a red photoproduct. The deep red color can be erased by irradiation with visible light or by thermal fading in the dark. Although many studies have been carried out over three decades, there remains a controversy about the structure of the colored species [16–26]. Salicylideneanilines exhibit also thermochromism both in the solution and in the solid state. The structural changes in the thermochromism were already reported [27].

The first example was selected to be *N*-3,5-di-*tert*-butylsalicylidene-3-nitroaniline, **1** [28], as shown in Scheme 7.3, because the photoproduct of **1** was reported to have the longest lifetime among a number of salicylideneanilines [29]. When the crystal **1** was irradiated with UV light, the pale yellow crystals turned dark red. However, there is a very difficult problem to obtain the structure of the colored species. In order to produce enough amounts of the colored species to be detected by X-ray diffraction analysis, the light for excitation should meet the following two conditions: (1) the absorbance of the crystal at the wavelength must be very small and (2) the light should not be strongly absorbed only by the colored species. An inherent property of the photo-reversible systems, however, makes it very difficult to meet both conditions at the same time. Figure 7.5 shows the absorption spectra of compound **1** and its photoproduct (red species). Irradiation of **1** with 365 nm UV light yielded a colored species which has an absorption band with a maximum at 480 nm. When the photoreaction is carried out by irradiation with strongly absorbed light (~365 nm), the light intensity drops off drastically in the bulk of the crystal, and

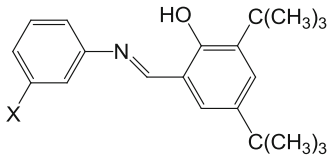

X = NO_2 : (**1**)
= COOH : (**2**)

Scheme 7.3 Two salicylideneanilines, **1** and **2**, with the nitro and carboxyl groups, respectively

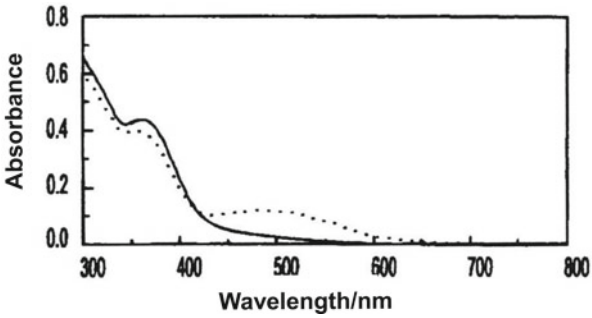

Fig. 7.5 Absorption spectra of *N*-3,5-di-*tert-butylsalicylidene*-3-aniline, **1**, before (*solid line*) and after (*dotted*) photo-irradiation

the photoreaction takes place only near the surface of the crystal. Light with much longer wavelength than that of the absorption maximum readily penetrates into the crystals and meets with the first condition [30, 31]. Light with such wavelengths, however, lies within the newly developed absorption band of the colored species and erases the color. This conflicts the second condition. Therefore, there is practically no suitable wavelength for an effective photoreaction in the bulk of the crystal. For this reason, the structure of the metastable red species has been undetermined by X-ray diffraction for a long time.

The difficulty was solved by using two-photon excitation. Two-photon excitation by 730 nm radiation gives molecules with the same energy as one-photon excitation at 365 nm. Because the probability of two-photon excitation is much smaller than that of one-photon excitation, the light intensity hardly decreases in the bulk of the crystal. Thus the two-photon excitation makes it possible to excite the bulk of the crystal and to form enough photoproduct for X-ray analysis. The two-photon excitation mentioned here is a concerted absorption of two photons by individual molecules and does not mean two sequential one-photon absorption events [32]. The IR spectra revealed that the powdered sample of photoproduct obtained by two-photon excitation was identical with that obtained by one-photon excitation.

The crystal structure before photo-irradiation was analyzed by X-rays at 90 K. The molecular structure is shown in Fig. 7.6a. The bond distances of C2–O1, C1–C7, and C7–N1 are 1.361(1), 1.454(1), and 1.295(1) Å, respectively, and the hydrogen atom is bonded to O1. It is clear that the molecule **1** exists in an enol form before photo-irradiation. The photoreaction was performed by irradiation with output pulse of an optical parametric oscillator with wavelength of 730 nm at room temperature. Because compound **1** has no absorption band at 730 nm, the reaction was induced by two-photon excitation. Among the laser-irradiated dark-red crystals, a crystal whose quality did not deteriorate was selected and the intensity data were collected. The unit-cell volume was increased by 7.89(9) $Å^3$, which is less than 1 % of the total volume. The difference electron density map showed additional peaks around the original salicylideneaniline molecule. The peaks were assigned and successfully refined as another molecule (with black bonds) which coexists with the original enol form (with white bonds) in the crystal as shown in Fig. 7.6b. The occupancy factor of the newly produced molecule is 0.104(2).

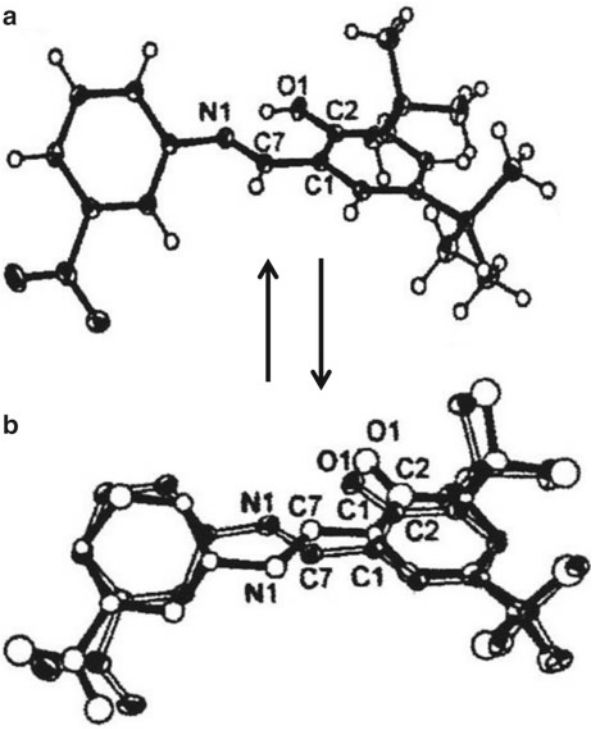

Fig. 7.6 Molecular structures of **1** (**a**) before and (**b**) after photo-irradiation

In the produced molecule, the oxygen atom O1 and the nitrogen atom N1 are in a *trans* position with regard to the C1–C7 bond, although they were *cis* before the photo-irradiation. The observed bond lengths of C2–O1, C1–C7, and C7–N1 were 1.30(2), 1.42(1), and 1.35(2) Å, respectively. Although the small occupancy factor of the produced molecule prevents the accurate determination of the structure, these C2–O1, C1–C7, and C7–N1 bonds are significantly shorter, shorter, and longer, respectively, than the corresponding ones of the enol form before the photo-irradiation. It is clear that the newly produced red species is a trans-keto form of **1.** When the same crystal was irradiated with a xenon lamp with a filter ($\lambda > 530$ nm) at room temperature, the dark-red color returned to the original pale yellow. The crystal structure analyzed under the same conditions is essentially the same as that of the enol form before photo-irradiation. These results clearly indicate that the photo-reversible color change in the crystal is caused by an interconversion between the *cis-enol* and *trans-keto* forms as shown in Scheme 7.4.

Although the transformation demonstrated here involves large structural change and seems difficult to take place in a crystal, it can easily occur through the motion of a pair of benzene rings analogous to the pedal motion of a bicycle, which is extensively studied in the thermochromism of azobenzenes containing similar molecular skeletons to those of salicylideneanilines [33].

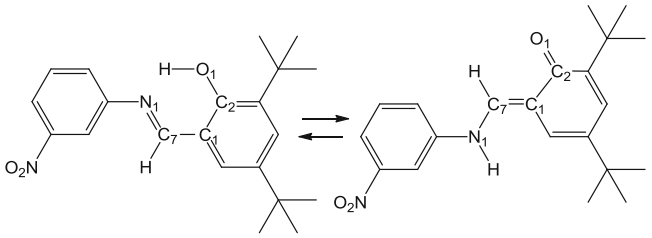

Scheme 7.4 Structural change from *cis-enol* form of compound **1** to its *trans-keto* form

7.2.2 *Different Photochromic Properties in Polymorphic Crystals*

The results observed in the previous section clearly show why photochromism occurs in the crystal of salicylideneaniline. However, it remained unclear why the metastable colored species of different crystals have different lifetime in photochromism. Recently three polymorphic crystals, **α**(colorless needle), **β**(pale yellow parallelepiped), and **γ**(orange block), were found in the crystallization of *N*-3,5-di-*tert*-butylsalicylidene-3-carboxyaniline, **2**, shown in Scheme 7.3. Each crystal form was irradiated with a high-pressure Hg lamp through a glass filter which transmits with wavelengths around 360 nm more than 10 h at room temperature [34]. The crystals of **2α** and **2β** turned red whereas **2γ** was unchanged, as shown in Fig. 7.7a, b. When the three crystals were kept in the dark at room temperature for 30, 60, 80 min, and 72 h, the color change of each crystal is shown in Fig. 7.7c, d, e, and f, respectively. The color of **2α** faded very quickly whereas the crystal of **2β** showed red color for a long time and the color finally faded after 72 h. However, the color of **2γ** was unchanged.

In order to examine the lifetime of the colored species of **2α**, **2β**, and **1** more quantitatively, KBr pellets (0.5 wt %) of the three crystals were prepared and were irradiated with UV light at room temperature. A new absorption band appeared around 3,400 cm^{-1}, which was assigned to the N–H stretching vibration mode of the produced *trans-keto* form. From the intensity change of the band, the rate constant κ and lifetime τ were calculated for the three crystals. The observed lifetime τ values for **2α**, **2β**, and **1** are 17, 780, and 1,200 min, respectively. Although it was reported that **1** has a lifetime of 40 d from the change of the UV reflectance spectra [29], the lifetime from the IR spectra is only 20 h. Probably the lifetime seems to depend strongly on the measurement methods.

The UV–vis spectra of **2α**, **2β**, and **2γ** before and after 40 min irradiation are shown in Fig. 7.8a, b, and c, respectively. The crystal of **2α** shows no absorption at wavelengths more than 450 nm before UV irradiation but a new band appears between 420 and 600 nm. This causes the color change from colorless to red. The absorption band of **2β** before irradiation has a tail from 450 to 530 nm. This causes the pale yellow color of **2β** before irradiation. After irradiation, a similar band to that of **2α** appears between 420 and 600 nm. This causes the color change from the pale

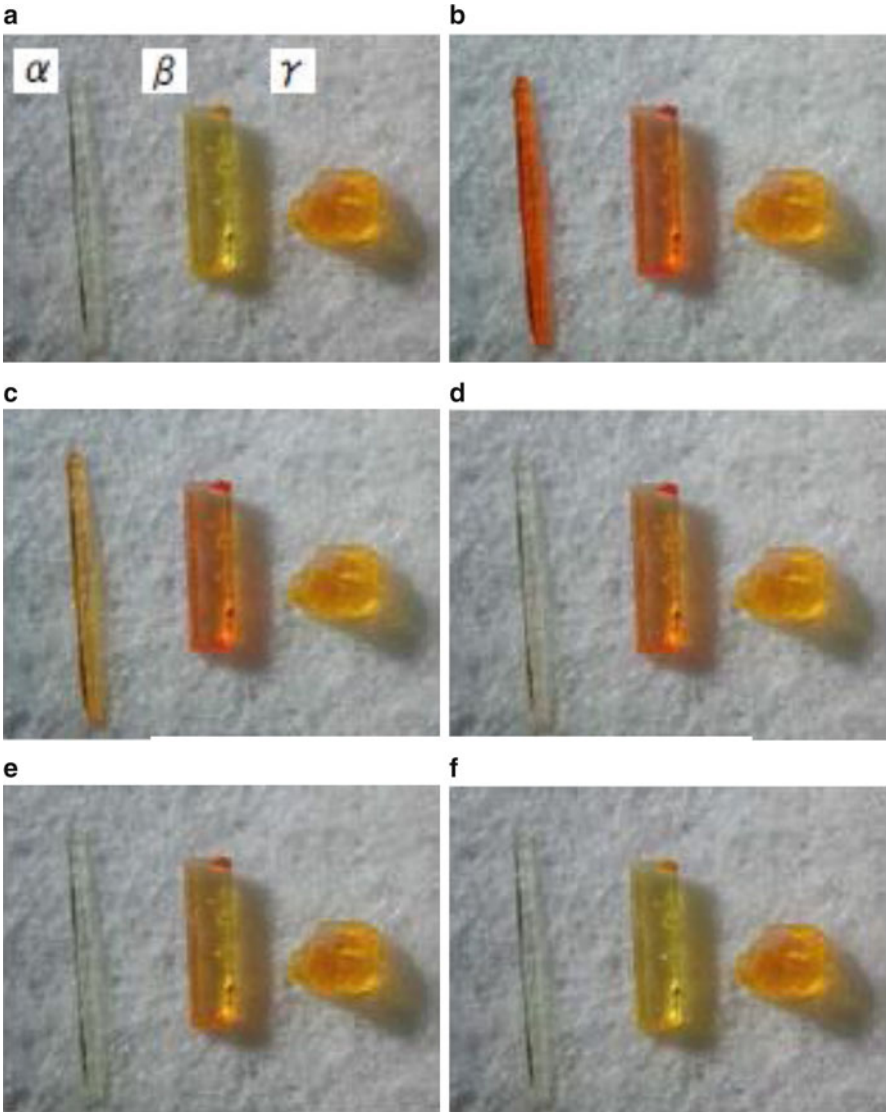

Fig. 7.7 Color change of three polymorphic crystals, **2α**, **2β**, and **2γ**, (**a**) before photo-irradiation and (**b**) just after photo-irradiation, and then (**c**) after 30 min, (**d**) after 60 min, (**e**) after 80 min, and (**f**) after 72 h, kept in the dark at room temperature

yellow to red. On the other hand, **2γ** before irradiation has a tail from 450 to 570 nm. This causes the orange color of **2γ**. Moreover, **2γ** shows no new absorption after irradiation, so that color change was not observed. The absorption tails observed in **2β** and **2γ** before irradiation may indicate that not only the major portion of the enol form but also the minor portion of the *cis-keto* form coexists in the crystal before photo-irradiation as suggested by Fujiwara et al. [35].

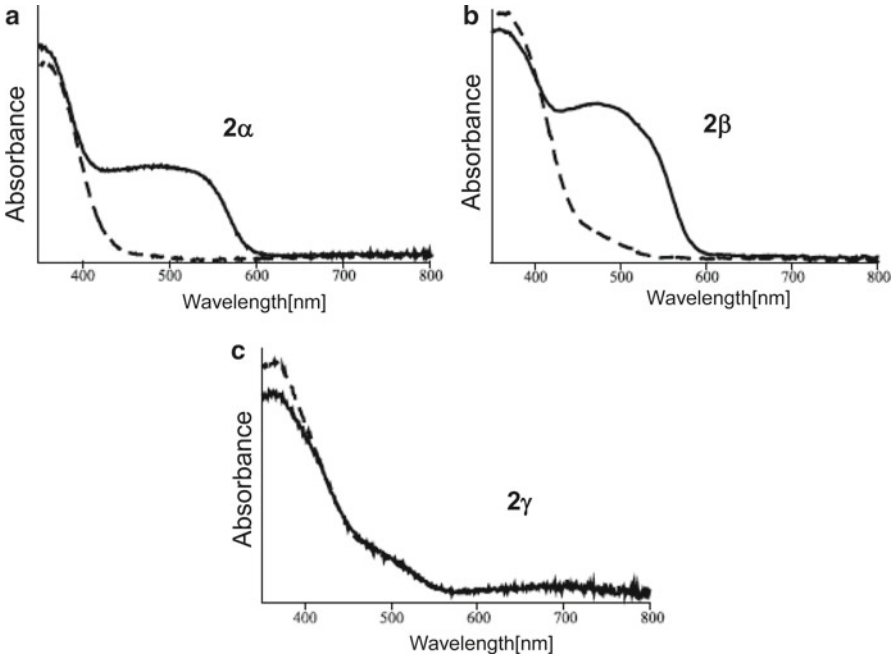

Fig. 7.8 UV-vis spectra of (**a**) **2α**, (**b**) **2β**, and (**c**) **2γ** before (*dotted lines*) and after (*solid lines*) 40 min irradiation

In order to examine the relation between the lifetime and the crystal structure, the crystal structures of the three forms before the photo-irradiation were analyzed. In each crystal, the carboxyl group makes two hydrogen bonds with the carboxyl group of a neighboring molecule to form a dimer structure. The molecular structures are very similar to each other as shown in Fig. 7.9, except the torsion angle of aniline ring in **2α** is different from the other two.

It was proposed that the dihedral angle between two phenyl rings of the salicylideneaniline molecule plays an important role in showing photochromic properties [36]. The salicylideneaniline crystal with larger dihedral angle shows the photochromic properties. To check this proposal, 24 kinds of salicylideneaniline crystals with different substituents in two phenyl groups were prepared and the crystal structures were analyzed. Crystals with the dihedral angles less than 20° were non-photochromic, whereas those with the dihedral angles more than 30° were photochromic. Crystals with the dihedral angle between 20° and 30° were either photochromic or non-photochromic [37]. The dihedral angles for **2α**, **2β,** and **2γ** are 60.95, 37.34, and 28.90°, respectively. This indicates that **2α** and **2β** would show photochromic property but that **2γ** may probably be non-photochromic. This well explains the photochromic properties for the three polymorphic crystals. It was recently reported that crystals with dihedral angles more than 80° are non-photochromic [38]. However, it was found that these molecules have two bulky substituents at the ortho positions in the aniline ring to prevent the pedal motion [33].

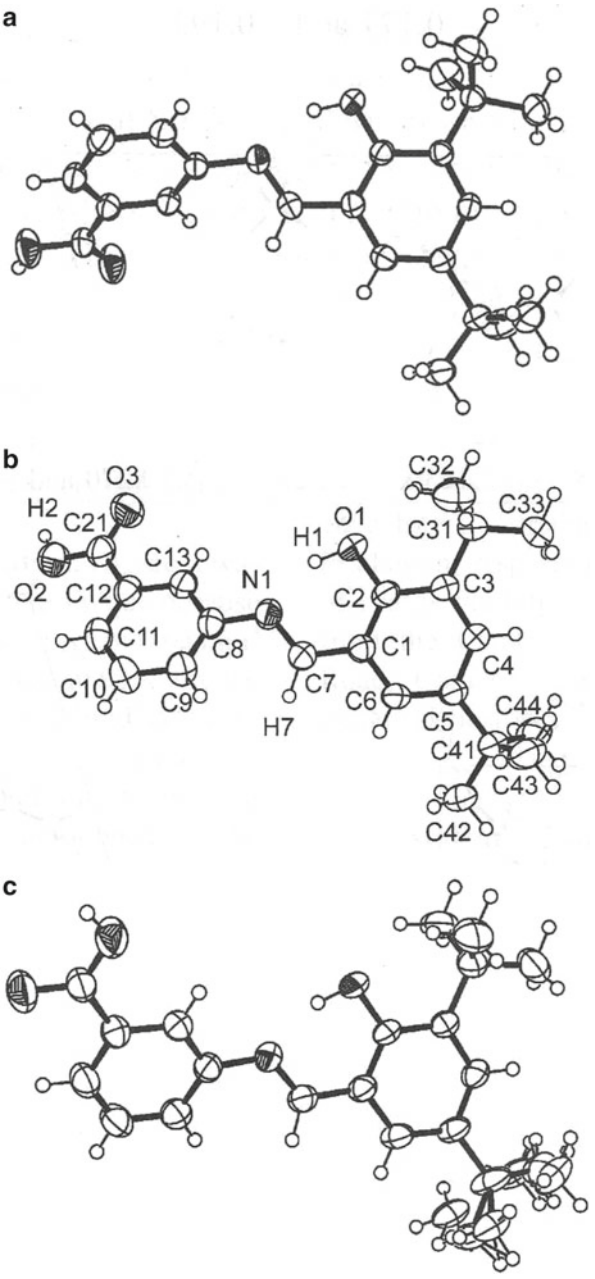

Fig. 7.9 Molecular structures of (**a**) **2α**, (**b**) **2β**, and (**c**) **2γ** before photo-irradiation

Since a very thin crystal of **2α** (0.03 mm) was obtained, the crystal was irradiated with UV light (365 nm) using the high-pressure Hg lamp through the glass filter at 267 K for 40 min. Then the intensity data were collected at 93 K. On the difference electron density map, there appeared new peaks which were assigned to the atoms

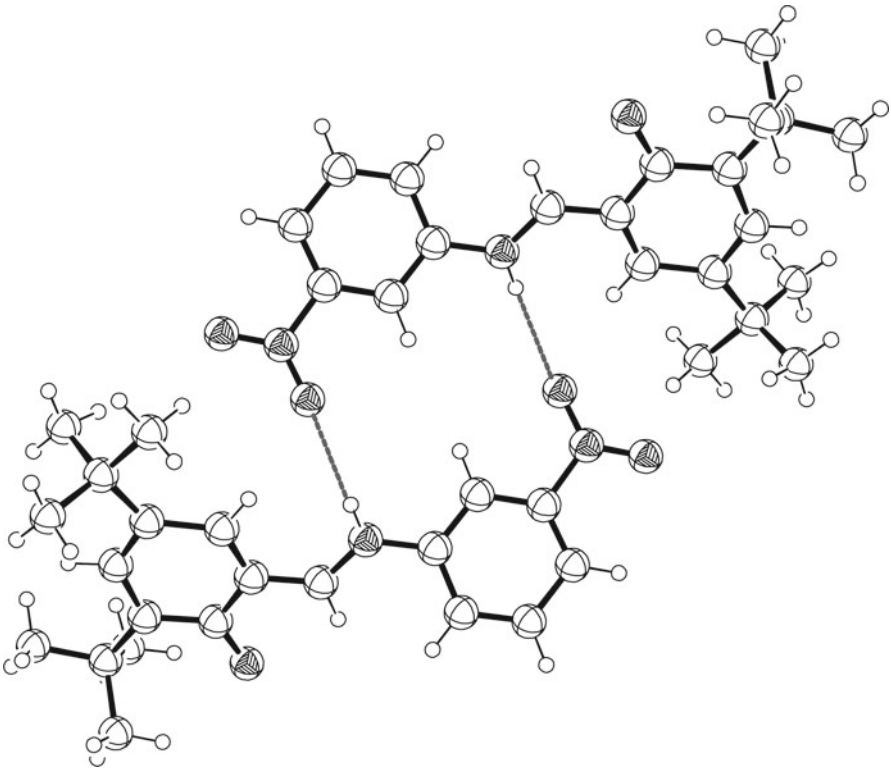

Fig. 7.10 The *trans-keto* form of the photo-produced **1** makes two hydrogen bonds with the neighboring photo-produced one

of *trans-keto* form, which is very similar to the corresponding one of the crystal **1** shown in Fig. 7.6. The occupancy factor of the produced *keto form* is 0.117(2).

In the structure of the photo-colored crystal of **1**, the two intermolecular hydrogen bonds were made between the N–H group of the *trans-keto* imine group and the oxygen atom of the nitro group around an inversion center as shown in Fig. 7.10. It was theoretically proposed that the intermolecular hydrogen bonds are responsible for the stabilization of the *trans-keto* form and that the longest lifetime of the photo-colored species comes from the stabilization energy due to the hydrogen bond formation, −39.36 kJ mol^{-1} [39].

In order to compare the structure of the photo-colored species of **2α** with that of **1**, the two photoproducts around an inversion center are shown in Fig. 7.11. The N–H group of the imino group is surrounded by the methyl groups of the *tert*-butyl group of the neighboring molecule. No hydrogen bond is formed in the two structures. This is why the photo-colored species of **2α** has shorter lifetime (17 min) than that of **1** (1,200 min). When the crystal was irradiated with a xenon lamp, the crystal color changed from red to colorless. The intensity data were collected at 110 K. The analyzed structure is essentially the same as that before the photo-irradiation with UV light.

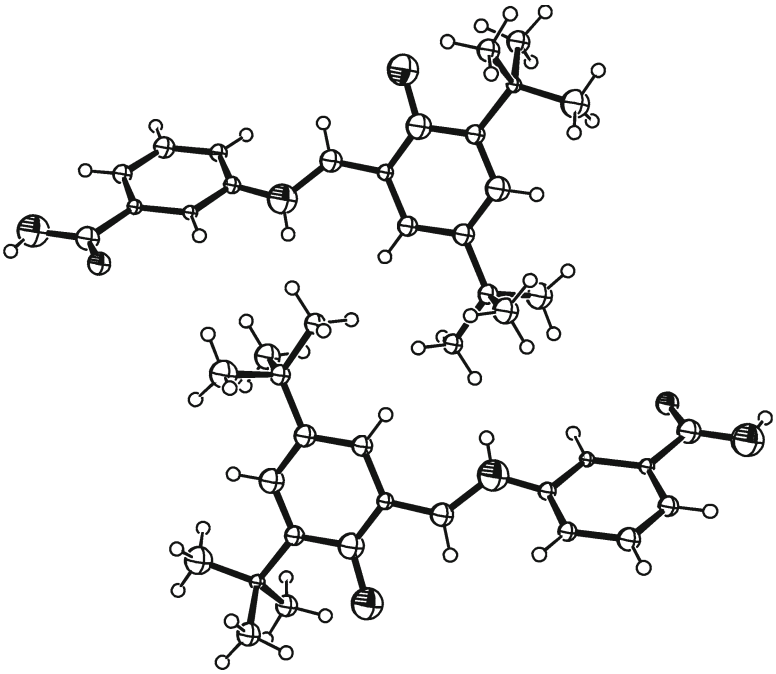

Fig. 7.11 Molecular structure of **2α** after photo-irradiation. No possibility to make an intermolecular hydrogen bond between the *trans-keto* form of the photo-produced **2α**

For the crystal of **2β** the same experiments were performed. Although it was impossible to obtain the additional peaks in the difference electron density map because the crystal of **2β** was not so thin as that of **2α** and the amount of photoproduct may be too small, it seems adequate to assume that the *trans-keto* form has the essentially the same structure as those of **2α** and **1**, which are produced using the pedal motion. The molecule with the *trans-keto* form of **2β** was situated instead of the enol form in the crystal of **2β** before photo-irradiation. As shown in Fig. 7.12, the N–H group of the trans-keto form of **2β** makes a hydrogen bond with the oxygen atom of the carboxyl group of the neighboring molecule. This may be a reason why **2β** has a longer lifetime than **2α**. Although the hydrogen bond makes a ribbon if all the molecules of **2β** take the *trans-keto* form, such a ribbon formation may be difficult, since the occupancy factor may be less than 0.1. On the other hand, the dimer of **1** with the *trans-keto* form may easily be formed even if the total occupancy factor of the *trans-keto* form is not so large. This is why the lifetime of **2β** (780 min) is significantly shorter than that of **1** (1,200 min).

The final problem remains why the crystal of **2α** showed the color change faster than that of **2β**. In the transformation from the *enol* to *trans-keto* form, the central –N=CH– plane becomes upside down in the pedal motion, keeping the two phenyl rings in both sides almost unchanged. This means that the rate of the transformation should be affected by the size of reaction cavity for the central –N=CH– group.

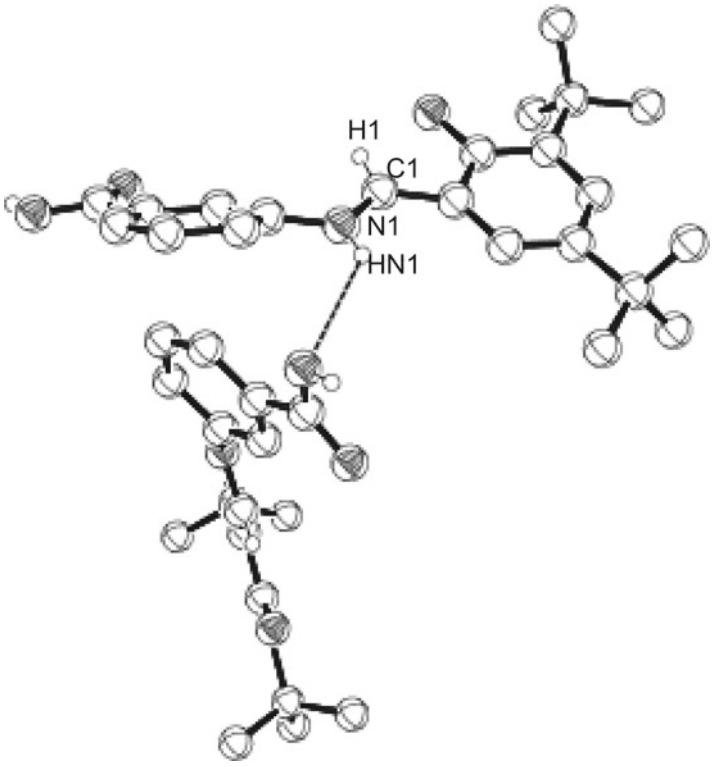

Fig. 7.12 Calculated structure of **2β** after photo-irradiation. An intermolecular hydrogen bond can be made between the two photo-produced molecules of **2β**

The volumes were calculated to be 3.5 and 1.6 Å^3 for **2α** and **2β**, respectively. These values are in good agreement with the rate of the color change as observed in Fig. 7.7.

7.2.3 Photochromism in the Acid–Base Complex Crystals

More interesting results were obtained when the complex crystals between the salicylideneanilines with carboxyl group and the dibenzyl- or dicyclohexylamine were examined [40, 41]. The compound of *N*-salicylidene-3-carboxyaniline, **3**, makes acid–base complexes with dibenzylamine, **3-a**, and dicyclohexylamine, **3-b**, whereas *N*-salicylidene-4-carboxyaniline, **4**, forms an acid–base complex with dibenzylamine, **4-a**, which are shown in Scheme 7.5. The crystals of **3** and **4** have orange color and show no photochromism, whereas the colorless, orange, and colorless crystals of **3-a**, **3-b**, and **4-a**, respectively, turned red when they were irradiated with UV light. The UV–vis spectra before and after photo-irradiation for **3**, **3-a**, and **3-b** are shown in Fig. 7.13, which are very similar to those of **2γ**, **2α**, and **2β**, respectively. The spectra of **4** and **4-a** are similar to those of **3** and **3-b**.

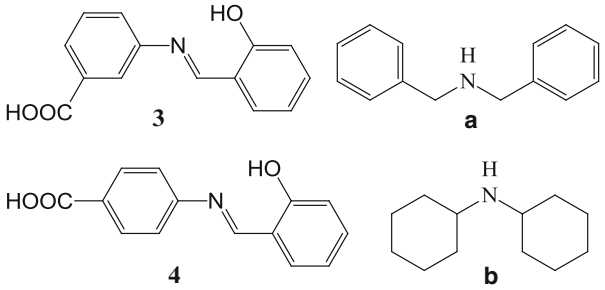

Scheme 7.5 Formation of an acid–base complex between **3** and **4** as acids and **a** and **b** as bases

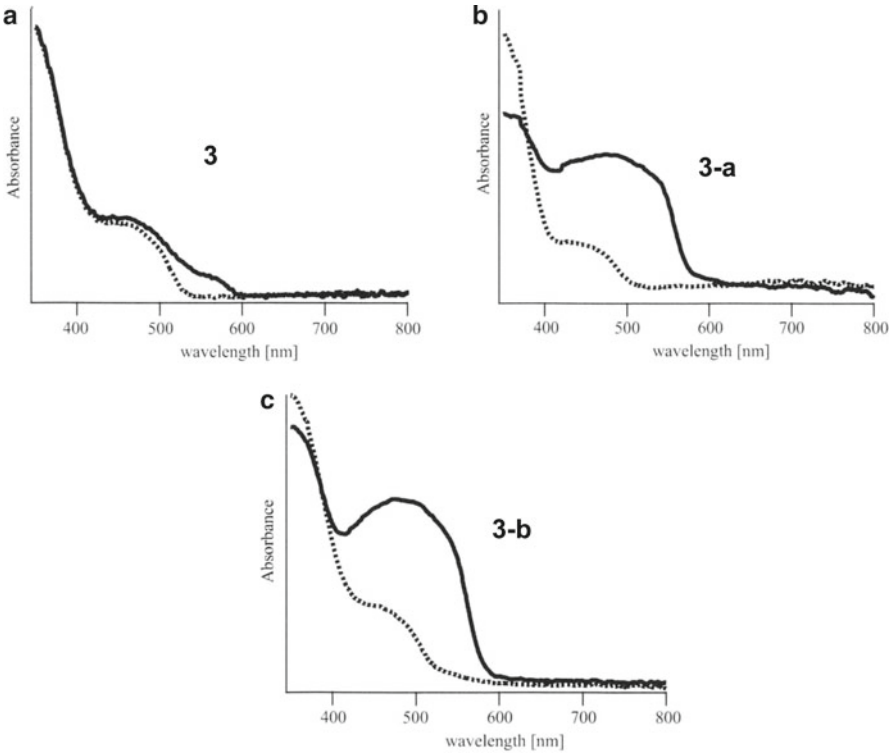

Fig. 7.13 UV-vis spectra of **3**, **3-a**, and **3-b** before (*dotted*) and after (*solid*) photo-irradiation

The color fading processes after UV irradiation for **3-a** and **3-b** are shown in Fig. 7.14. Although the red color of **3-a** disappeared after 30 s, that of **3-b** returned to the original color after 10 min at room temperature.

The crystal structures of **3**, **3-a**, and **3-b** before irradiation were determined by X-rays. The two salicylideneaniline molecules, **3**, make a dimer using the 3-carboxyl group around an inversion center. The dihedral angle of the two phenyl rings is 26.72(6)°. The two hydrogen bonds are formed between O3 and O2 of **3** and N2 of

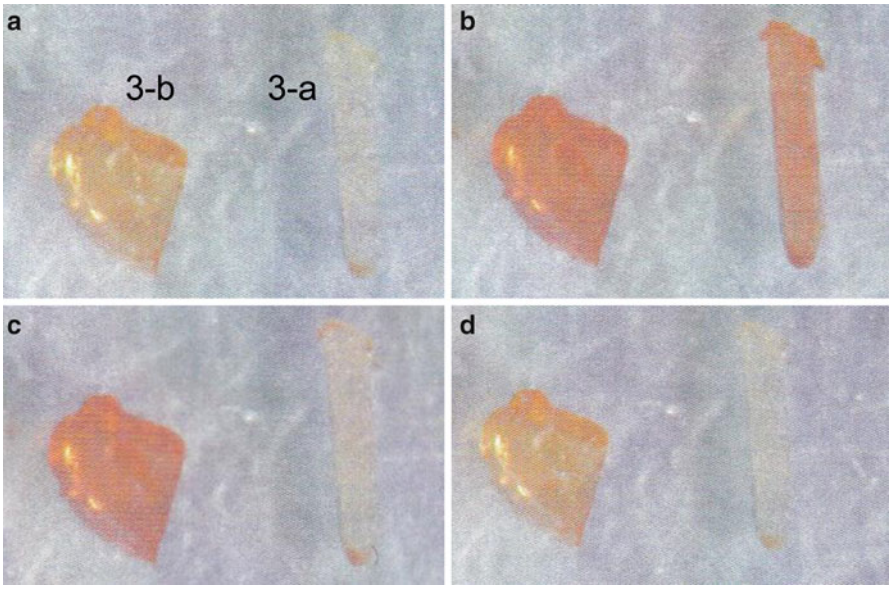

Fig. 7.14 Color fading processes of **3-a** and **3-b**; (**a**) before photo-irradiation, (**b**) just after photo-irradiation, (**c**) after 30 s, and (**d**) after 10 min, kept at room temperature in the *dark*

a in the crystal of **3-a**. These hydrogen bonds make the dihedral angle of **3** to be 49.47(6)°. The crystal of **3-b** has two crystallographically independent molecules, A and B. The dihedral angles of A and B of **3** in **3-b** become 47.7(1)° and 40.5(1)°, respectively, because of the intermolecular hydrogen bonds between **3** and **b** molecules. Considering from the photochromic nature of the salicylideneaniline derivatives, the dihedral angles of 26.72(6)°, 49.47(6)°, and 47.7(1)° and 40.5(1)° observed for the crystals of **3**, **3-a,** and A and B of **3-b**, respectively, well explain the photochromic properties of the crystals.

Although the crystal structures of **3-a** and **3-b** after the photo-irradiation have not been determined yet, the structures of *trans-keto* forms were calculated from the *cis-enol* form before UV irradiation. The calculated structures with the *trans-keto* form for **3-a** and **3-b** are shown in Fig. 7.15. It is clear that any hydrogen bond cannot be formed between the metastable structures with the *trans-keto* form in **3-a,** whereas N1B–H1B···O2A hydrogen bond stabilizes the metastable *trans-keto* form in **3-b**. The difference in lifetime of photochromism between the two crystals is well explained by the calculated structures.

7.3 Photochromism of Pyridine Derivatives

Another intriguing photochemical reaction known for over 70 years is the photo-induced and thermally activated proton transfer between the colorless CH and blue NH forms of 2-(2′,4′-dinitrobenzyl)pyridine (DNBP). The reaction process was

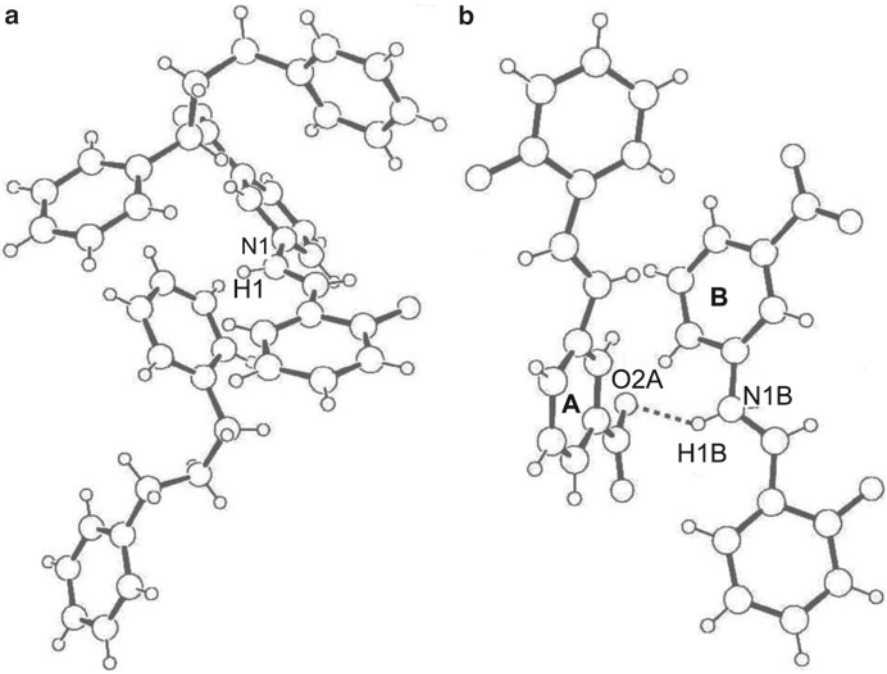

Fig. 7.15 Calculated *trans-keto* forms for (**a**) **3-a** and (**b**) for **3-b** after photo-irradiation. An intermolecular hydrogen bond can be made for **3-b**

assumed as shown in Scheme 7.6 [42]. Spectroscopic observations suggested that the photoexcited CH form was isomerized to the NH form in either process from the CH to NH forms directly or through an intermediate aci-nitro structure of the OH form [43]. Theoretical results supported that the CH to NH reaction in a crystal proceeded through an OH-like intermediate [44]. Since the direct crystallographic evidence for the NH and OH species was lacking, these structures were analyzed by X-rays employing the two-photon excitation technique [45].

The UV–vis spectra of the colorless CH and photo-induced blue NH forms are shown in Fig. 7.16. When the crystal was irradiated with UV light of the wavelength of 254 nm, which is the maximum absorption band of the CH form, only the surface of the crystal was colored. Then the crystal was irradiated with the laser light of 502 nm, since the wavelength of 502 nm is approximately twice of 254 nm and is apart from the maximum absorption band of the NH form (~600 nm).

The molecular structure of the CH form in the blue crystal after photo-irradiation resembles that before the irradiation. When the atomic positions of the CH form was refined, additional peaks of the photoproduct and the transferred proton, except for the o-nitro nitrogen atom, were observed in the difference electron density map. Both of the closely overlapped CH and NH molecules were refined with the isotropic model. The occupancy factor of the photo-produced NH form became 32.8 %. The conversion to the NH form up to 36.4 % was confirmed from the UV–vis spectrum. Under these conditions, the OH form had accumulated to less than 0.5 %.

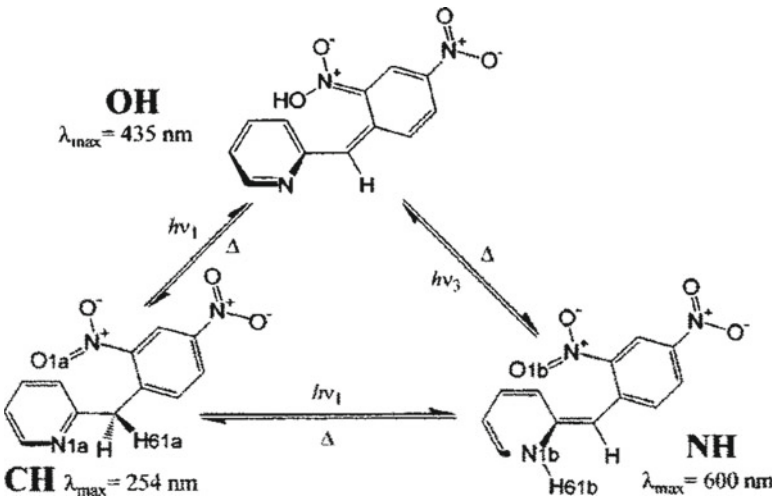

Scheme 7.6 Structural changes of 2-(2′,4′-dinitrobenzyl)pyridine (DNBP) during the photoreactions

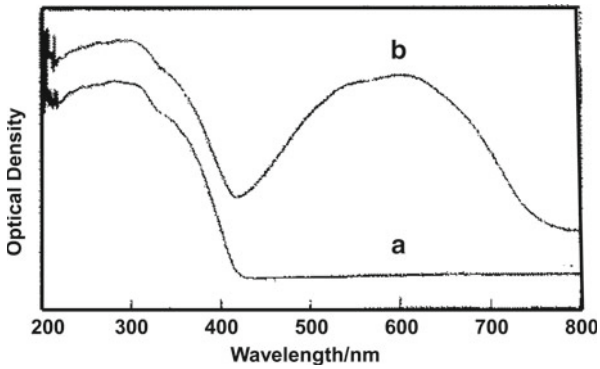

Fig. 7.16 UV-vis spectra of (**a**) original colorless CH and (**b**) photo-induced blue NH forms

The NH form in the disordered blue crystal evidences only minor structural rearrangement as shown in Fig. 7.17, in which the atomic names with the labels a and b belong to the CH and NH forms, respectively. The dynamic proton is transferred over a distance of nearly 3.16 Å from H61a to H61b. The active oxygen O1a is 2.28 Å far from the proton H61a in the CH form. After the proton transfer and the structural relaxation, O1b changed from O1a is placed 2.88(1) Å away from the transferred proton H61b and 3.19(1) Å from the aryl proton H62b. The final separation between the heavy centers O1b and N1b amounts to 3.13(1) Å.

The structural change between the CH and NH forms clearly suggests the following reaction mechanism: (1) The blue coloration of 2-(2′,4′-dinitrobenzyl) pyridine exposed to light can be ascribed to the NH tautomer. (2) The proton transfer

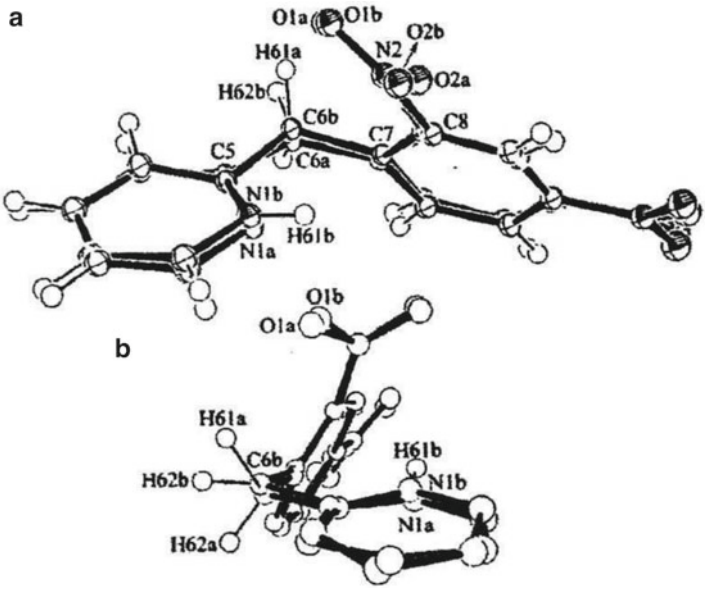

Fig. 7.17 (**a**) Molecular structures of the CH and photo-produced NH forms and (**b**) the side view

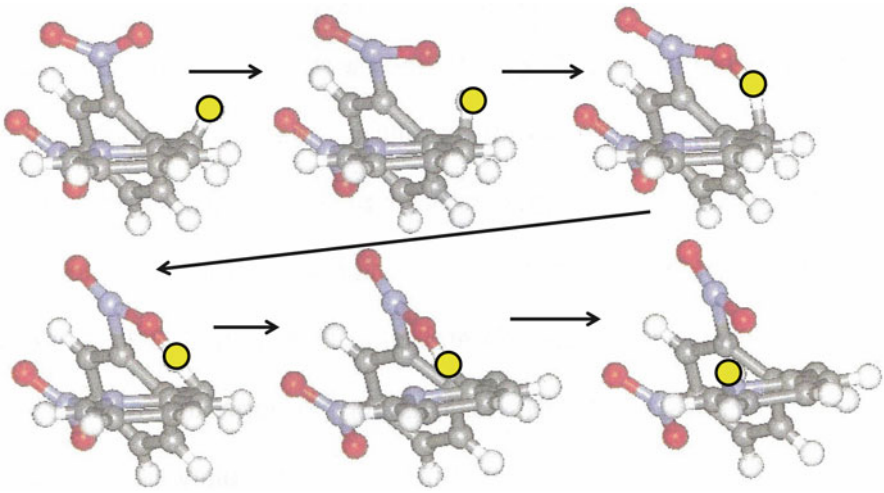

Fig. 7.18 Motion of the nitro group during the reaction, bringing a H61a hydrogen atom to H61b bonded to N1b

occurs in an intramolecular process, since there is no significant intermolecular interaction. (3) The OH form should be an intermediate between the CH and NH forms, since the proton transfer proceeds despite of the unfavorable structure in the reactant CH form (C6a–H61a···N1a = 40.2° as shown in Fig. 7.17). (4) The *o*-nitro group of the OH form may rotate around the C8–N2 bond to bring the H61a proton to H61b bonded to N1b, as shown in Fig. 7.18. More precise mechanism was reported [46–48].

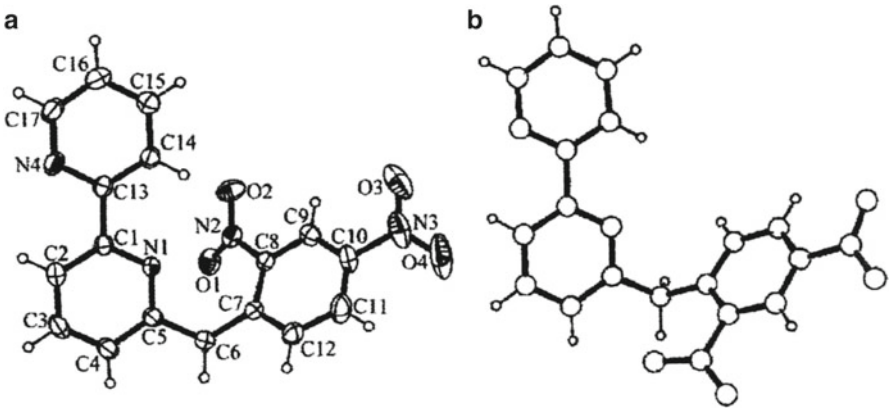

Fig. 7.19 Molecular structure of DNBBP in the crystals of (**a**) γ-form, which is very similar to α-form and (**b**) β-form

In order to examine the above reaction process more quantitatively, the pyridine moiety was replaced with 2,2′-bipyridine and the resulting molecule, 6-(2′,4′-dinitrobenzyl)-2,2′-bipyridine (DNBBP), was chosen as a target compound [49]. It was already reported that DNBBP crystallized in a photochromic orthorhombic form (α-form) from an ether-hexane solution while it crystallized in a non-photochromic monoclinic form from an ethanol solution (β-form) [50, 51]. By recrystallization from an acetone–methanol solution, a new crystal form, γ-form, was obtained. The γ-form showed photochromic [49].

The crystal structures of the α- and γ-forms before photo-irradiation were analyzed at 78 K. The two crystal structures are similar to each other, although there are two crystallographically independent molecules in the α-form whereas there is an independent molecule in the γ-form. The β-form has an independent molecule, which is completely different structure from those of the α- and γ-forms. The molecular structure of the γ-form is shown in Fig. 7.19a, which is very similar to that of the α-form. However, it is different from that of the β-form, which is shown in Fig. 7.19b. The *ortho*-nitro group and biphenyl nitrogen N1 are positioned on the opposite side of the methylene bridge plane (C5–C6–C7). The distance between N1and O1 atoms and the interplanar angle between the phenyl and pyridyl rings are larger than the corresponding ones of the α- and γ-forms; the interplanar angles are 57.6(2)°, 65.1°, and 51.1(1)° on average, and the N1···O1 distances are 3.194(5), 4.004(6), and 3.056(2) Å on average for α-, β-, and γ-forms, respectively. Since the α-form has two crystallographically independent molecules, the interplanar angles and the distances are averaged.

The above discussion suggests that the ability of the nitro group to abstract a proton from the proton donor (the benzylic carbon C6) and to bring it to the proton accepter (the pyridyl nitrogen N1), that is, rotational freedom of the nitro group in the crystal, is one of the decisive factors for the photochromic activity. The steric requirements for the rotation of the nitro group were investigated by means of the reaction cavity concept. The reaction cavity for the fragment [N1–C5–C6(H2)–C7–C8–N_2–O_1] was calculated in each molecule, since both of the rotational freedom and the ability of the nitro group to transfer the proton to the

nitrogen acceptor are crucial factors for the creation of the blue NH, and thus for photochromic activity.

The volumes of the reaction cavities for the fragment are as follows: 20.40 Å^3 for α-form (averaged), 17.34 Å^3 for β-form, and 21.31 Å^3 for γ-form. The cavity volume for the same fragment in the 2-(2′,4′-dinitrobenzyl)pyridine is 21.60 Å^3. In the related pyridine crystals showing photochromic properties, the cavities for the same fragment have the volume greater than 20 Å^3. It was made clear that the rotational freedom of the *ortho*-nitro group is the most important factor for the photochromism. This fact is the additional support for the proposed nitro-assisted proton transfer mechanism.

7.4 Photoexcitation

7.4.1 Photoexcited Structure of a Diplatinum Complex

The Pt complex anion of diplatinum complex, $[Pt_2(H_2P_2O_5)_4]^{4-}$, as shown in Fig. 7.20, has a strong singlet absorption band, $^1A_{2u} \leftarrow {}^1A_{1g}$, which can populate a strong emissive long-lived triplet state, $^3A_{2u}$, that can undergo many different chemical reactions. A number of studies have been carried out to elucidate the spectroscopy, photophysics, and photochemistry associated with the excited electronic states of the diplatinum complex in the 300–500 nm regions. It was proposed from the vibronically resolved absorption and emission spectra that the Pt–Pt bond distance at the $^3A_{2u}$ state becomes shorter by about 0.21 Å than that at the $^1A_{1g}$ ground state. The similarity of the bandwidths and the excited-state vibrational wavenumbers at the $^1A_{2u}$ and $^3A_{2u}$ states suggest that they have almost the same structure [52, 53]. From the combination of the EXAFS method with rapid-flow laser spectroscopy in an aqueous solution with glycerol, it was estimated that

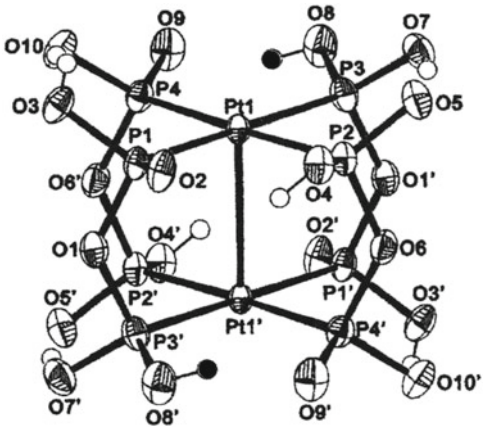

Fig. 7.20 Molecular structure of the $[Pt_2(H_2P_2O_5)_4]^{4-}$ complex anion. If two protons (*black circles*) are bonded to the O8 and O8′ atoms, the Pt complex is represented as $[Pt_2(H_2P_2O_5)_2(H_3P_2O_5)_2]^{2-}$

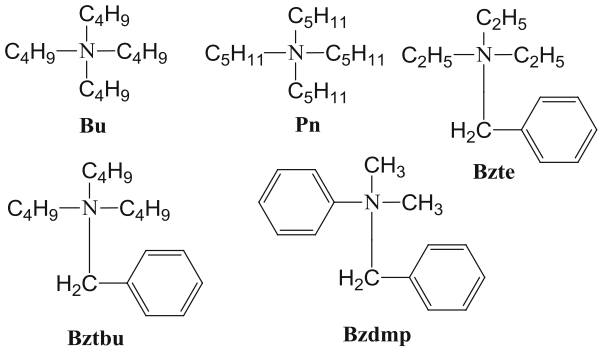

Scheme 7.7 Five alkylammonium cations for the formation of the acid–base complexes with the Pt complex anion

the $^3A_{2u}$ state with a lifetime of about 4 μs undergoes a contraction in the Pt–Pt distance of 0.52 ± 0.13 Å and in the Pt–P distance of 0.047 ± 0.011 Å relative to the $^1A_{1g}$ [54]. From a resonance Raman intensity analysis of the $^1A_{2u} \leftarrow {}^1A_{1g}$ transition, it was reported that the Pt–Pt bond distance contraction was about 0.225 Å in the initially excited $^1A_{2u}$ state relative to the $^1A_{1g}$ ground state [55]. The density function theory predicted a Pt–Pt shortening of 0.18–0.51 Å and a Pt–P lengthening of 0.01–0.05 Å [56].

The powder X-ray diffraction peaks of the diplatinum complex with the tetrabutylammonium cation showed shifts to their higher diffraction angles when the powdered sample was irradiated with a xenon lamp at room temperature and returned to the original angles when the irradiation was stopped [57]. The reversible shift of the powder pattern indicated that the structure of the diplatinum complex at the excited state was significantly changed and the concentration of the excited diplatinum complex was enough to analyze the structural change due to the photoexcitation by X-rays.

We intended to analyze the photoexcited structure of the diplatinum complex by X-rays using a single crystal in collaboration with three research groups. The first group prepared various diplatinum complexes changing the alkylammonium cations. The diplatinum complex crystals with five different alkylammonium cations suitable for X-ray work were obtained, tetrabutylammonium (Bu), tetrapentylammonium (Pn), benzyltriethylammonium (Bzte), benzyltributylammonium (Bztbu), a nd benzyldimethylphenylammonium (Bzdmp), which are shown in Scheme 7.7. The preliminary structure analyses revealed that two protons are attached to the four $(H_2P_2O_5)^{2-}$ anions in the Bu, Pn, Bzte, and Bztbu crystals. Therefore, there are only two ammonium cations per one diplatinum complex. This indicated that the diplatinum complexes in the four crystals should be represented as $[Pt_2(H_2P_2O_5)_2(H_3P_2O_5)_2]^{2-}$. The diplatinum complex in the Bzdmp crystal has four cations. The complex should be represented as $[Pt_2(H_2P_2O_5)_4]^{4-}$.

The second group developed a new detector which can collect a whole intensity data of a crystal within a second. They succeeded that a whole intensity data of a standard sample were collected within 2 s and the structure was successfully analyzed, using the new gas detector developed, MSGC, and a rotating anode X-ray generator [58]. A crystal of the Pn complex was mounted on the diffractometer with

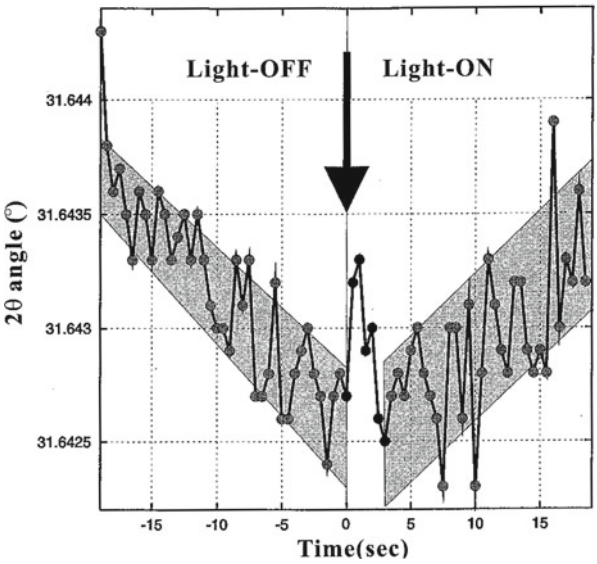

Fig. 7.21 Gradual change in the angle of an intense diffraction spot recorded at 500 ms time intervals at 80 K. The unexplained abrupt change was observed at $t=0$

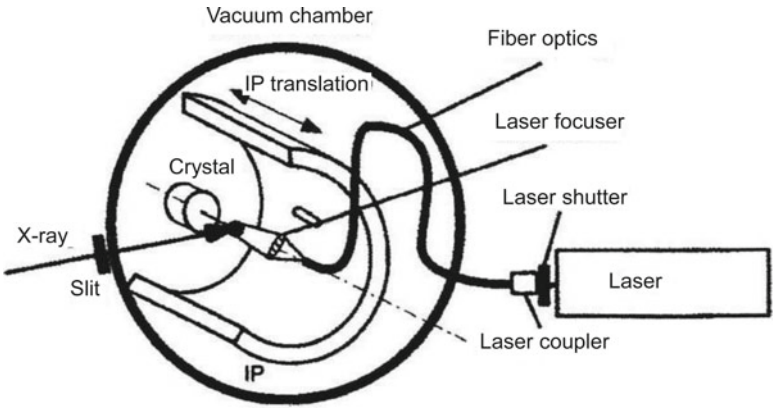

Fig. 7.22 Schematic drawing of the new diffractometer set up at SPring-8

the MSGC detector and was irradiated with a xenon lamp at the beamline of BL46XU at SPring-8. The change of the angle of an intense diffraction spot was recorded at 500 ms time intervals at 80 K. The diffraction angle gradually increased after the light was put on and it gradually decreased after the light off. The change did not reach the equilibrium state within 20 s, as shown in Fig. 7.21 [59, 60]. The unexplained abrupt change was observed around $t=0$.

The third group made a new Weissenberg-type diffractometer (LTV) using an imaging plate (IP) as shown in Fig. 7.22 [61]. The diffractometer was set at the BL02B1 beamline at SPring-8. The intensity data were recorded on the IP which was set in a vacuum chamber. A crystal of $(Bu)_2[Pt_2(H_2P_2O_5)_2(H_3P_2O_5)_2]$ was set at the center of the vacuum chamber and was irradiated with CW He-Cd blue laser

(442 nm, 100 mW). Although the Bu complex has the same chemical formula as that used in the first group, two crystals are polymorphic to each other. After the data at the light-off stage were taken, the IP frame was shifted in parallel with the cylindrical axis by 1–2 mm to record the diffraction data at the light-on stage on the same IP under the same conditions. The diffraction data at the two stages were collected at 54 K. The lattice constants, however, slightly increased and the unit-cell volume expanded by 3.2(3) $Å^3$ at the light-on stage. The heating effect by the laser irradiation caused a small temperature rise, although the crystal was kept in the vacuum camera at 54 K. However, the difference map using ($|F_{on}| - |F_{off}|$) indicated a displacement of the Pt atom in the direction toward the other Pt atom in the anion. This gave the Pt–Pt bond shrinkage, which was proposed spectroscopically. The subsequent quantitative analysis of the changes is based on least-squares refinement of the response ratios, $\eta = (I_{on} - I_{off})/I_{off}$. The Pt–Pt bond of the excited-state molecule becomes 2.70(4) Å, which is 0.23(4) Å shorter than that of the ground-state molecule, 2.9289(2) Å. The occupancy factor of the excited-state Pt atoms converged at 0.014(2).

During the above experiments an excited structure of a diplatinum complex, $[N(C_2H_5)_4]_3[Pt_2(H_2P_2O_5)_3(H_3P_2O_5)]^{3-}$, was first reported using the stroboscopic method [62]. The method means that the diffraction data were taken at 17 K just after the crystal was irradiated with the pulsed laser light (Nd/YAG, $\lambda = 355$ nm). The diffraction data without the irradiation were collected under the same conditions as those at the light-on stage. The increased temperature by the laser irradiation was corrected using the Wilson plots. The difference map using ($|F_{on}| - |F_{off}|$) indicated the Pt–Pt bond shrinkage and the subsequent quantitative analysis of the changes was performed based on the refinement of the response ratios, which is the same as that used in the third group. The Pt–Pt bond of the excited-state molecule became 2.63(9) Å, which is 0.28(9) Å shorter than that of the ground-state molecule. The occupancy factor of the excited-state Pt atom was 0.02. The value of the shortening of the Pt–Pt bond at the excited state is in good agreement with the values assumed from the spectroscopic methods and the theoretical calculation.

Although the stroboscopic method is very attractive, there are several questions should be solved before the method is applied to the structure analysis of the excited molecule. The first question is that although it is indispensable to irradiate the crystal with the wavelength of the absorption maximum to excite the molecules effectively in a short time, such a light can excite only the surface molecules [30, 31]. The light with longer wavelengths is essential for the excitation of the molecules inside the crystal. The second question is how to confirm the equilibrium state of the crystal at the time of 1 ns or 1 ps after the crystal is irradiated with the pulsed laser. If the crystal is not in the equilibrium state, which is essential for the crystal to have a periodic structure, it is impossible to transform the diffraction data in the reciprocal space to the electron density map in the real space using the Fourier transform technique. Although the structural change of the diplatinum complex was reported, there was no description about the change of the unit-cell dimensions at the light-on stages. If there was no change in the unit-cell dimensions, it is impossible to consider that enough amounts of excited molecules with definite orientation were generated in the crystalline lattice. The third question is why the stroboscopic method

should be applied to the structural change in a reversible process, such as the excited-state structure. If there are only two structures at the ground and excited states in the crystal at the light-on stage, the diffraction should be caused by the periodic structure composed of the equilibrium structure between the ground and excited states. If the concentration of the excited molecules may exceed the threshold value in the equilibrium structure, the structure of the excited molecule can be analyzed using the conventional diffraction data collection and structure analysis at the light-on stage, no matter how quickly the molecule may be excited up and dropped down to the ground state. The reversible change of the powder pattern upon photo-irradiation clearly indicated that enough amounts of the excited molecules are generated in the photo-irradiated crystal.

The first group applied the conventional structure analyses using five crystals and the visible light from a xenon lamp. At first, a Pn crystal was irradiated with a xenon lamp through a cutoff filter (>400 nm) [63]. The crystal color changed from colorless to bright green as shown in Fig. 7.23. The cell dimensions at light-off and light-on stages were determined at temperatures of 223, 173, and 123 K. The unit-cell volumes of the light-on stage at 223, 173, and 123 K decreased by 2.30(8), 11.1(2), and 8.5(3) $Å^3$, respectively, compared with the corresponding ones of the light-off stage. This indicated that the numbers of the ground- and excited-state molecules reached an equilibrium state at the light-on stage and that the number of the excited-state molecules became a maximum at ca.173 K. This suggested that the experimental temperature is an important factor to observe the excited-state structure in a crystal. Then, the wavelengths of light were selected to be $\lambda = 470 \pm 80$ nm using a xenon lamp with two filters, which corresponds the excitation of the triplet state. The absorption spectra of the Pn complex in an aqueous solution are shown in Fig. 7.24.

The differences in the unit-cell dimensions between the light-on and light-off stages were measured for the five crystals [64]. The temperatures were fixed at 173 K for the Bu, Pn and Bzdmp crystals and at 103 K for the Bzte and Bztbu crystals. The space group, number of molecules in a unit cell, crystal density, unit-cell volume change, $\Delta|V_{off} - V_{on}|$, and the ratio of $\Delta|V_{off} - V_{on}|/V_{off}$, for the five crystals are shown in Table 7.1. The ratios of the volume changes, $\Delta|V_{on} - V_{off}|/V_{off}$, are more than 0.6 % for the Bu, Pn, and Bzte complexes, whereas those of the Bztbu and Bzdmp complexes were less than 0.2.

The powder diffraction patterns of the Pn complex at the light-off and light-on stages are shown in Fig. 7.25a. The diffraction peaks of the light-on pattern shift to the higher angles than those at the light-off stage. Since the diffraction peaks at the light-on stage are sharp, it means that the excited- and ground-state molecules reached the equilibrium state and the new crystalline lattice corresponding to the equilibrium state was produced. The plots of the diffraction pattern calculated from the cell dimensions of the single crystal at the light-off and light-on stages are shown in Fig. 7.25b. The two patters are essentially identical to each other. This may suggest that the equilibrium structure is independent of the irradiation conditions such as the size of the crystal and the intensity of the irradiation light if a sufficient number of photons are exposed to the sample.

The structures of each crystal at light-off and light-on stages showed no significant differences in the alkylammonium cations. On the other hand, the bond

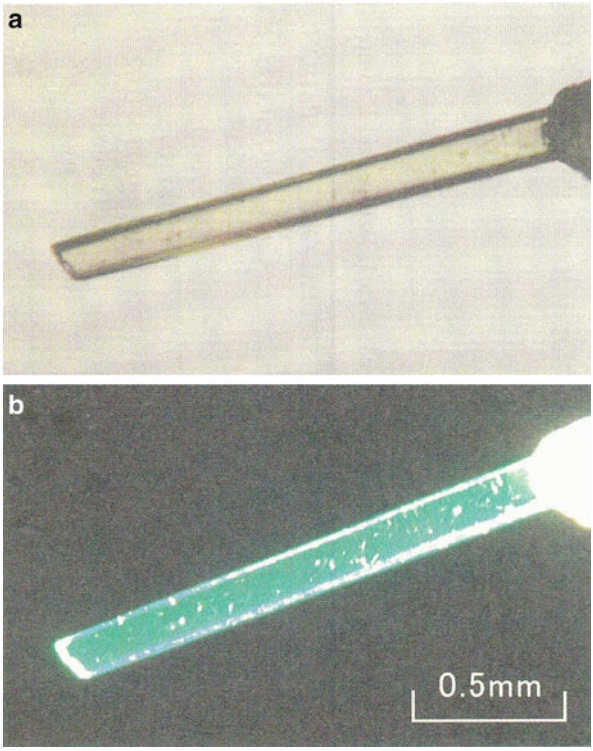

Fig. 7.23 Color change at the (**a**) light-off and (**b**) light-on stages

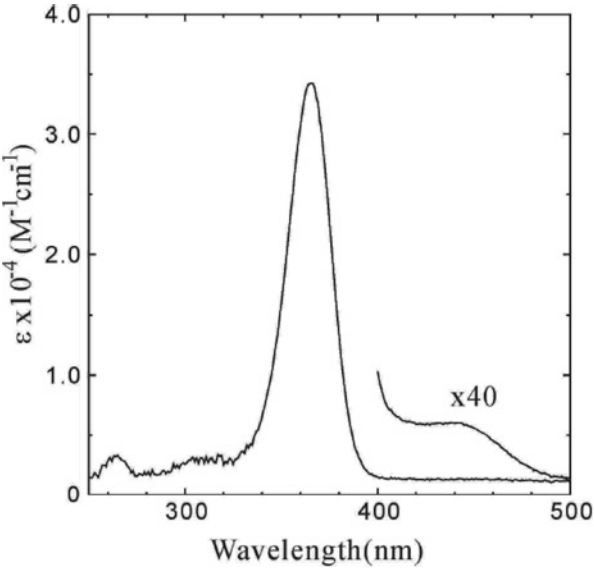

Fig. 7.24 Absorption spectra of the Pn complex

Table 7.1 Space group, number of molecules in a unit cell (Z), calculated crystal density (D_{calcd}), the unit-cell volumes at light-off (V_{off}) and light-on (V_{on}) stages, and the values of $\Delta(V_{on} - V_{off})$ and $\Delta|V_{on} - V_{off}|/V_{off}$ for the five crystals

Crystal data	Bu	Pn	Bzte	Bztbu	Bzdmp
Space group	P1-	P1-	P1-	P1-	$P2_1/n$
Z	1	2	2	2	4
D_{calcd} (Mg m^{-3})	1.828	1.706	2.130	1.873	1.727
V_{off} (Å^3)	1,320.18(3)	3,046.45(7)	2,108.78(12)	2,696.42(16)	3,613.30(6)
V_{on} (Å^3)	1,312.16(5)	3,026.12(17)	2,094.92(11)	2,691.27(12)	3,607.44(6)
$\Delta(V_{on} - V_{off})$ (Å^3)	−8.02(5)	−20.3(1)	−13.9(1)	−5.1(1)	−5.86(6)
$\Delta\|V_{on} - V_{off}\|/V_{off}$ (%)	0.61	0.67	0.66	0.19	0.16

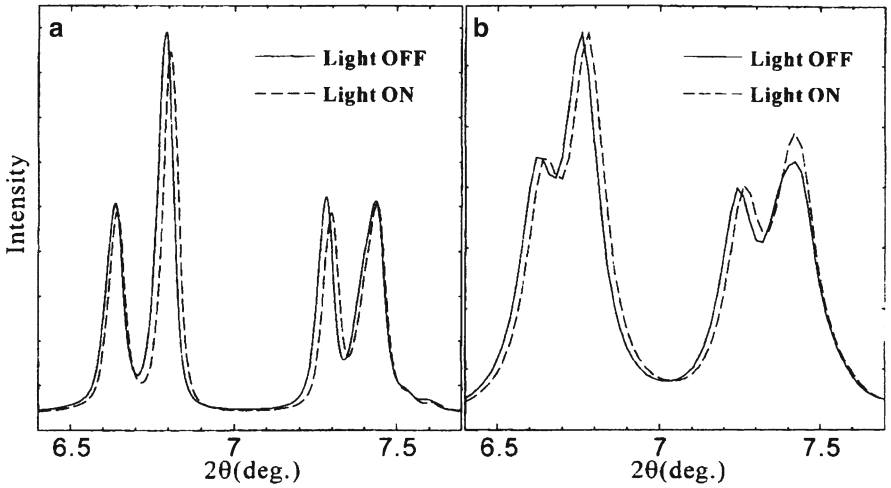

Fig. 7.25 (**a**) Change of the powder diffraction pattern of the Pn complex at the light-off and light-on stages and (**b**) the corresponding pattern calculated from the lattice constants of the single crystal at the light-off and light-on stages

distances in the diplatinum complex anions at light-on stage are significantly changed from the corresponding ones at light-off stage. However, it was very difficult to separate the excited-state molecule from the ground-state one in the difference electron density map. The refinement method used in the stroboscopic method was not applied because the refinement should not depend on the initial model. Only the same parameters as those of the structure before the photo-irradiation were refined in the conventional least-squares calculation.

This means that the refined structure is the weighted average of the ground-state and the excited-state molecules. Assuming the D_{4h} (4/m) symmetry, the endocyclic Pt–P and P–O bonds and the exocyclic P=O and P–O bonds were averaged in each diplatinum complex. The Pt–Pt and Pt–P bond distances in the five crystals are significantly shorter at light-on stage than those at light-off stage. The changes of the other bonds are within the experimental error. The averaged bond distances of Pt–Pt and Pt–P for the five crystals are listed in Table 7.2.

Table 7.2 Differences (ΔD) in bond distances between those at the light-off (D_{off}) and light-on (D_{on}) stages in the five crystals

Bond	ΔD(Bu) (Å)	ΔD(Pn) (Å)	ΔD(Bzte) (Å)	ΔD(Bztbu) (Å)	ΔD(Bzdmp) (Å)
Pt–Pt	−0.0038(3)	−0.0081(3)	−0.0127(6)	−0.0031(3)	−0.0019(2)
Pt–P	−0.0069(11)	−0.0053(11)	−0.0085(14)	−0.0019(12)	−0.0033(8)
P–O(−P)	−0.003(3)	−0.003(4)	−0.011(5)	−0.002(4)	−0.002(3)
P=O	−0.005(3)	−0.004(3)	−0.006(5)	−0.006(4)	−0.001(3)
P–O(−H)	−0.002(3)	−0.004(4)	−0.005(5)	0.001(4)	−0.003(3)

There are two ways to explain the structural change at the equilibrium state between the ground and excited states. One is the concentration ratios of the excited-state molecules to the ground-state molecule are different among the five crystals. If the structure of the excited-state molecule is assumed to be constant among the different crystals, the difference in the structural changes depends on the different amounts of the excited molecules. Another explanation is that the different structures at the light-on stage are attributable to the different structures of the excited molecules affected by the different crystal environment. The theoretical calculation is performed without any intermolecular interactions, whereas the molecules in a crystal are closely packed with the surrounding molecules. This means that the structure cannot alter at the excited state as if the molecule exists in vacuum. The structure at the excited state depends on the environment in the crystalline lattice. Probably two factors, the amount of the excited molecules and the crystal environment, play main roles in the structural change at the equilibrium state.

It is noticeable that the shortenings of the Pt–Pt and Pt–P distances, $|\Delta$(Pt–Pt)$|$ and $|\Delta$(Pt–P)$|$, of the Pn and Bzte crystals are 0.0081(3) and 0.005(1) Å, and 0.0127(5) and 0.008(1) Å, respectively, which are the largest two among the five crystals. The ratios of $|\Delta$(Pt–Pt)$|/|\Delta$(Pt–P)$|$ are 1.62 and 1.59 for the Pn and Bzte crystals, respectively, which are very close to each other. This suggests that the excited diplatinum complex anion may have the same structure in the two crystals, and the concentrations of the excited molecules may be different between the two crystals. On the other hand, the excited structures in the Bu, Bztbu and Bzdmp crystals may be different due to the different crystal environment. The change at the excited state is schematically drawn in Fig. 7.26. Not only the Pt–Pt distance but also Pt–P distance is shortened at the excited state of the diplatinum complex anion, which is in good agreement with the experimental results observed from the combination of the EXAFS method with rapid-flow laser spectroscopy [54].

7.4.2 Photoexcited Structures of the Vanadium and Gold Complexes

The bond elongation at the excited state was observed in a vanadium complex, as shown in Scheme 7.8a [65]. The complex crystal of bis(acetylacetonato)oxovanadium (IV), $VO(acac)_2$, has the space group of P1- and two molecules in the unit cell.

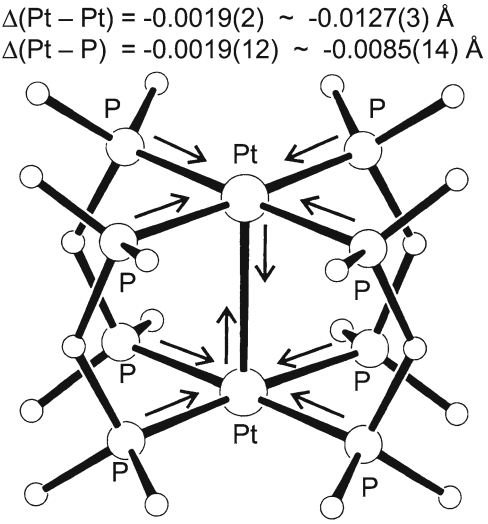

Fig. 7.26 Structural change of the four Pt complexes at the excited state

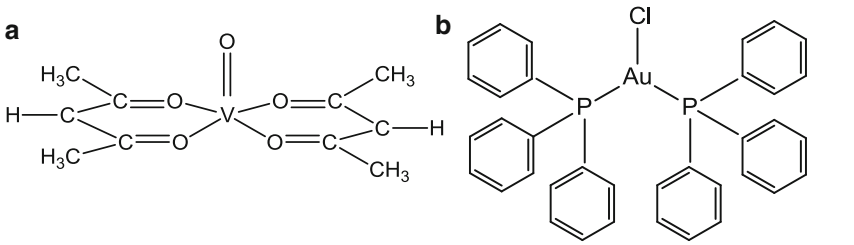

Scheme 7.8 (a) Structures of bis(acetylacetonato)oxovanadium(IV), $VO(acac)_2$, and (b) bis(triphenylphosphine) goldchloride, $[AuCl(PPh_3)_2]$

The cell dimensions and the intensity data were measured at four temperatures (168, 160, 150, and 140 K) in the dark (light off) and under photo-irradiation (λ = 400–450 nm, light-on). At every temperature, the unit-cell volume significantly expanded at light-on stage. The changes of the cell dimensions are different between the photo-irradiation and the warming, comparing from the differences of the cell dimensions between the light-off and light-on stages at 140 K (photo-change), and the differences between the cell dimensions at the light-off stages at 140 and 168 K (thermal change). The expansion of the unit cell due to the photo-irradiation is more anisotropic than that of the thermal expansion. This suggests that the crystal reached the equilibrium state between the ground and excited states.

The differences in bond distances between light-off and light-on stages at four temperatures are shown in Table 7.3. The V–O, O–C, and C–C distances in the chelate rings are averaged assuming C_{2v} symmetry. It is clear that essentially the same change of the bond distances can be observed at every temperature. As the temperature decreased, the amount of the change increased within the temperature range, 168–140 K. This is probably due to the increased amount of the excited

Table 7.3 Change of each bond distance by photo-irradiation

Bond length/Å	168 K	160 K	150 K	140 K
V=O	+0.0012(9)	+0.0018(9)	+0.0027(8)	+0.0025(8)
V–O	+0.0019(8)	+0.0032(8)	+0.0035(8)	+0.0049(8)
O–C	+0.0003(14)	+0.0019(13)	+0.0020(13)	+0.0033(13)
C–C	+0.0008(17)	+0.0020(16)	+0.0025(15)	+0.0031(15)

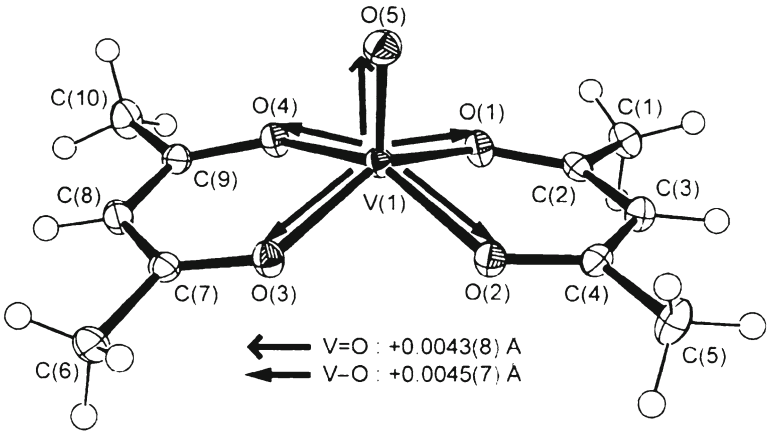

Fig. 7.27 Structural change of the vanadium complex. The bond elongation indicated by *arrows* is observed at the light-on stage

molecules at low temperatures. Although the elongation of the O–C and C–C bonds is within the experimental errors, the V=O and V–O bond distances significantly increase at the light-on stage at 150 and 140 K. The changes of the bond angles and the torsion angles are also within the experimental errors. The changes are schematically drawn in Fig. 7.27. Such bond elongations suggest that the electrons in the bonding orbital of the V–O bonds are transferred to the anti-bonding orbital of the V=O bond in the "d–d" transition. This result clearly indicates that even if the lifetime is very short, the excited structure can be observed in the structure at the equilibrium state between the ground and excited states.

The excited structure of the gold complex was also observed at the equilibrium state using the same technique [66]. When the crystal of $[AuCl(PPh_3)_2]CHCl_3$, as shown in Scheme 7.8b, was irradiated with the high-pressure Hg lamp, the green emission was observed. The crystal and intensity data were measured in the light-off and light-on stages at 175, 156, 136 and 84 K. The cell volume decreased at the light-on stage. The amount of the decrease in unit-cell volume at light-on stages at 84 K was 10.23(6) $Å^3$, which was the largest among those at four temperatures. The shortening of the bond distances between the light-off and light-on stages at 84 K are 0.0055(4), 0.0057(4), 0.0043(18), and 0.003(3) Å for Au–P, Au–Cl, P–C, and C–C, respectively, which is schematically drawn in Fig. 7.28. The shortenings of the Au–P and Au–Cl bonds are significant, but the changes of the other bond

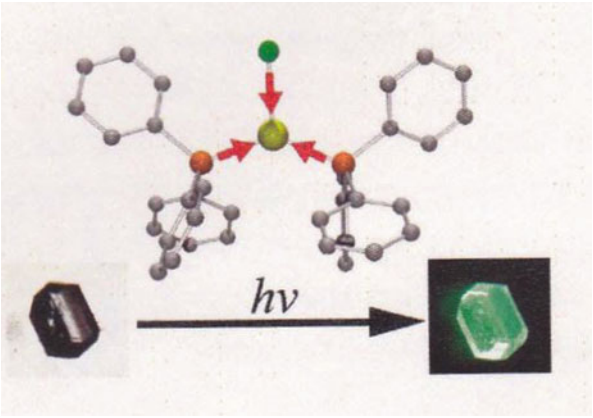

Fig. 7.28 Structural change of the Au complex. The bond shrinkage indicated by *arrows* is observed at the light-on stage. The crystal color change from *black* at the light-off stage to *bright green* at the light-on stage

distances are within the experimental error. These shortenings correspond to the excitation of $^3E'' \leftarrow {}^1A_1'$ derived from the electronic transition from d_{xy}, d_{x2-y2} (antibonding) orbital to p_z (bonding) orbitals [67–69]. From the theoretical calculation involving $[Au(PH_3)]^{3+}$, the Au–P bonds are shortened in the excited state if the excited-state structure is constrained to D_{3h} symmetry, and the shortening in a free molecule was estimated to be 0.05 Å. The experimental results well explain the orbital theory, although the amount of the shortening, of course, is smaller than that predicted by the theoretical calculation.

7.4.3 Excited Structure Analyzed by Equilibrium Method

In the platinum, vanadium and gold complexes, each crystal was irradiated with the xenon or high-pressure Hg lamp, the wavelength of which was selected to be longer than its absorption maximum with the combinations of filters at low temperatures (84–173 K). The molecules in each crystal should cycle between the excited and ground states and the ratio of the molecules at the two states should become a constant value, which is called equilibrium state. The unit-cell volume decreases or increases depending on the shrinkage or expansion of the molecular structure at the excited state. The reversible change of the powder pattern of the Pt complex at light-off (ground state) and light-on (equilibrium state) stages clearly indicates that the excited-state molecules exist in the equilibrium state as a disordered structure with the ground-state molecules. It requires a delay time to reach the equilibrium, depending on the temperature, crystal packing and lifetime of the excited state. It may be possible to discriminate the structure of the excited-state molecule from the ground-state molecule introducing the heavy constraints in the least-squares refinement.

However, the extent of the bond elongation or shrinkage is somewhat smaller than the predicted one by the theoretical calculation. Since the molecules in a crystal are closely packed with the neighboring molecules, it is naturally expected that

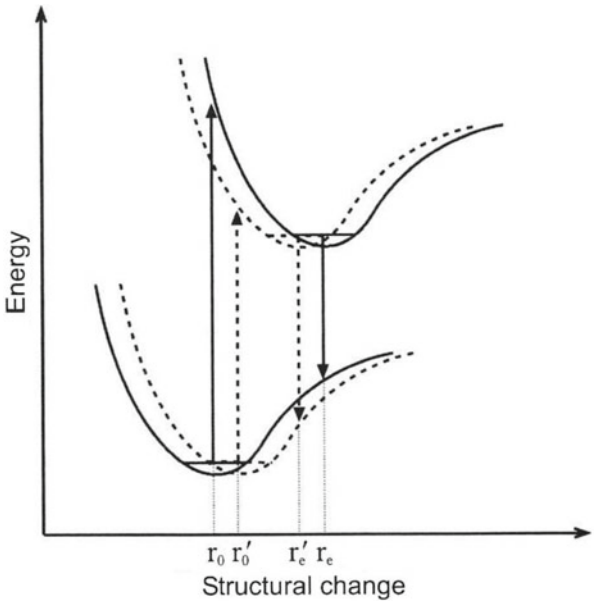

Fig. 7.29 The energy diagram with the reaction coordinate at the ground and excited states

the change of the bond length in a crystal is much smaller than the corresponding one calculated for a free molecule. Moreover, the structure at the equilibrium state should be somewhat different from that at the excited state of a free molecule. As shown in Fig. 7.29, the solid curves show the energy diagram of the ground and excited states of a free molecule. The ground-state molecule with the minimum energy is excited and then reaches the structure with the minimum energy in the excited curve. The excited molecule drops down to the ground state and returns to the structure with the minimum energy. However, this diagram is applicable to the molecule only in vacuum. Owing to the crystal packing, the structural change should be smaller than that in vacuum, as indicated by a dotted curve of the excited state. When the molecule shuttles between the ground state and the excited state, the ground-state energy curve should be shifted to the excited-state curve, as shown by a dotted curve. This indicates that the structural change at the equilibrium state, $\Delta|r_e' - r_0'|$, is much smaller than that in vacuum, $\Delta|r_e - r_0|$. We must reconsider what is the excited state and what is the excited structure. We cannot obtain the value of $\Delta|r_e - r_0|$ but that of $\Delta|r_e' - r_0'|$ in the crystalline state and the latter depends on the experimental conditions. However, the direction of the change, elongation or shrinkage of a bond, is absolutely true, although the amount of the change is variable.

If any change occurs in a crystal, the diffraction data may be changed. It is possible to detect the time-resolved diffraction data by the stroboscopic method. However, any structural change cannot be obtained from the diffraction data using Fourier transform technique before the change extends to all the unit cells and the periodic lattice structure is reconstructed. There is an essential difference between

the time-resolved diffraction data measurement and time-resolved structure analysis. It is essential that the reconstruction of periodic lattice structure should occur just after the photo-irradiation. How to reduce the reconstruction time is the key point to success in the time-resolved structure analysis. There is a dilemma, however, that although the loose crystal packing may reduce the reconstruction time, the observed structure may be obscure because of the large thermal vibration or disordered position of each atom. Recently new detectors were developed for rapid data collection and the three-dimensional intensity data were collected within 1 s [58, 70]. It may be possible to observe the structural change less than 1 s in near future. The time-resolved structure analysis will be applicable to the multi-step and irreversible reactions which proceed less than 1 s.

References

1. McBride JM (1983) Acc Chem Res 16:304
2. Kawano M, Sano T, Abe J, Ohashi Y (1999) J Am Chem Soc 121:8106
3. Hayashi T, Maeda K (1960) Bull Chem Soc Jpn 33:565
4. Maeda K (1995) In: Krongauz VV, Trifunac AD (eds) Photoreactive polymers. Chapman & Hall, New York, p 90
5. Monroe BM, Weed GC (1993) Chem Rev 93:435
6. Okada K, Imamura K, Oda M, Koizumi M, Morimoto Y, Ishino K, Tashiro K (1998) Chem Lett 891
7. Abe J, Sano T, Kawano M, Ohashi Y, Matsushita MM, Iyoda T (2001) Angew Chem Int Ed 40:580
8. Kawano M, Ozawa Y, Matsubara K, Imabayashi H, Mitsumi M, Toriumi K, Ohashi Y (2002) Chem Lett 1130
9. Kawano K, Sano T, Abe J, Ohashi Y (2000) Chem Lett 1372
10. White DM, Sonnenberg J (1966) J Am Chem Soc 88:3825
11. Duerr H, Bouas-Laurent H (eds) (1990) Photochromism, molecules and systems in organic chemistry, vol 40. Elsevier, Amsterdam
12. Crano JC, Guglielmetti RJ (eds) (1999) Organic photochromic and thermochromic compounds, vol 1 and 2. Plenum, New York
13. Irie M (2000) Photochromism, memories and switches. Chem Rev 100(5):1683
14. Senier A, Shepheard FG (1909) J Chem Soc Trans 95:1943
15. Senier A, Shepheard FG, Clarke R (1912) J Chem Soc Trans 101:1950
16. Cohen MD, Schmidt GMJ (1962) J Chem Phys 66:2442
17. Cohen MD, Schmidt GMJ, Flavian S (1964) J Chem Soc 2041
18. Cohen MD, Hirshberg Y, Schmidt GMJ (1964) J Chem Soc 2051
19. Bregman J, Leiserowitz L, Schemidt GMJ (1964) J Chem Soc 2068
20. Cohen MD (1968) J Chem Soc Sec B 373
21. Hadjoudis E (1995) Mol Eng 5:301
22. Nakagaki R, Kobayashi T, Nakamura J, Nagakura S (1977) Bull Chem Soc Jpn 50:1909
23. Rosenfeld T, Ottolenghi M, Meyer AY (1973) Mol Photochem 5:39
24. Lewis JW, Sandorfy C (1982) Can J Chem 60:1738
25. Turbeville W, Dutta PK (1990) J Phys Chem 94:4060
26. Yuzawa T, Takahashi H, Hamaguchi H (1993) Chem Phys Lett 202:221
27. Ogawa K, Kasahara Y, Ohtani Y, Harada J (1998) J Am Chem Soc 120:7107
28. Harada J, Uekusa H, Ohashi Y (1999) J Am Chem Soc 121:5809

29. Kawato T, Koyama H, Isshiki M (1985) J Photochem 28:103
30. Enkelmann V, Wegner G, Novak K, Wegener KB (1993) J Am Chem Soc 115:10390
31. Novak K, Enkelmann V, Wegner G, Wagener KB (1993) Angew Chem Int Ed Engl 32:1614
32. Goeppert-Meyer M (1931) Ann Phys 9:273
33. Harada J, Ogawa K, Tomoda S (1997) Acta Crystallogr B53:662
34. Johmoto K, Sekine A, Uekusa H, Ohashi Y (2009) Bull Chem Soc Jpn 82:50
35. Fujiwara T, Harada K, Ogawa K (2004) J Phys Chem B 108:4035
36. Bregman J, Leiserowitz L, Osaki K (1964) J Chem Soc 2086
37. Johmoto K, Ishida T, Sekine A, Uekusa H, Ohashi Y (2012) Acta Crystallogr B68:297
38. Fukuda H, Amimoto K, Koyama H, Kawato T (2003) Org Biomol Chem 1:1578
39. Mikami M, Nakamura S (2004) Phys Rev B 69:134205
40. Johmoto K (2005) M.Sc Thesis, Tokyo Institute of Technology
41. Johmoto K, Sekine A, Uekusa H (2012) Cryst Growth Des 12:4779
42. Chichibabin AE, Kunidzhi BM, Benewolenshaja SW (1925) Ber Dtsch Chem 28:1580
43. Casalegon R, Corval A, Kuldova K, Eichen Y, Pikramenau Z, Lehn JM, Trommsdorff HP (1997) J Lumin 72–74:78
44. Khatib S, Tal S, Godsi O, Peskin U, Eichen Y (2000) Tetrahedron 56:6753
45. Naumov P, Sekine A, Uekusa H, Ohashi Y (2002) J Am Chem Soc 124:8540
46. Naumov P, Ohashi Y (2004) J Phys Org Chem 17:1
47. Naumov P, Sakurai K, Ohashi Y, Ng SW (2005) Chem Mater 17:5394
48. Naumov P, Sakurai K, Ishikawa T, Takahashi J, Koshihara J, Ohashi Y (2005) J Phys Chem A 109:7264
49. Naumov P, Ohashi Y (2004) Acta Crystallogr B60:343
50. Eichen Y, Lehn J-M, Schert M, Haarer D, Fischer J, DeCian A, Corval A, Trommsdorff HP (1995) Angew Chem Int Ed Engl 34:2530
51. Scherl M, Haarer D, Fischer J, DeCian A, Lehn J-M, Eichen Y (1996) J Phys Chem 100:16175
52. Rice SF, Gray HB (1983) J Am Chem Soc 105:4571
53. Stiegman AE, Rice SF, Gray HB, Miskowski VM (1987) Inorg Chem 26:1112
54. Thiel DJ, Livins P, Stern EA, Lewis A (1993) Nature 362:40
55. Leung KH, Phillips DL, Che C-M, Miskowski VM (1999) J Raman Spectrosc 30:987
56. Novozhilova IV, Volkov AV, Coppens P (2003) J Am Chem Soc 125:1079
57. Ikagawa T, Okumura T, Otsuka T, Kaizu Y (1997) Chem Lett:829
58. Ochi A, Uekusa H, Tanimori T, Ohashi Y (2001) Nucl Inst Meth Phys Res A467–468:1148
59. Yasuda N (2002) Dsc Thesis, Tokyo Institute of Technology
60. Ohashi YJ (2004) Cryst Soc Jpn 46:59–64
61. Ozawa Y, Terashima M, Mitsumi M, Toriumi K, Yasuda Y, Uekusa H, Ohashi Y (2003) Chem Lett 32:62
62. Kim CD, Pillet S, Wu G, Fullagar K, Coppens P (2002) Acta Crystallogr A58:133–137
63. Yasuda N, Kanazawa M, Uekusa H, Ohashi Y (2000) Chem Lett 132
64. Yasuda N, Uekusa H, Ohashi Y (2004) Bull Chem Soc Jpn 77:933
65. Hoshino M, Sekine A, Uekusa H, Ohashi Y (2005) Chem Lett 34:1228
66. Hoshino M, Uekusa H, Ohashi Y (2006) Bull Chem Soc Jpn 79:1362
67. King C, Khan MNI, Staple RJ, Fackler JP Jr (1992) Inorg Chem 31:3236
68. McClesky TM, Gray HB (1992) Inorg Chem 31:1733
69. Barakat KA, Cundari TR, Omary MA (2003) J Am Chem Soc 125:14228
70. Takeda A, Uekusa H, Kubo H, Miuchi K, Nagayoshi T, Ohashi Y, Okada Y, Orito R, Takada A, Tanimori T (2005) J Synchrotron Rad 12:820

Chapter 8
Metastable or Unstable Intermediates in Reversible Processes

Abstract In the examples of the irreversible reactions, the original molecule is broken down on exposure to UV light and releases a part of the molecule to become a new product. The reverse reaction cannot occur. The triplet carbenes are formed from the bis(2,4,6-triphenyl)diazomethane derivatives and the arylnitrenes are produced from the arylazide derivatives on exposure to UV light. The unstable carbenes and nitrenes were observed after the crystal was irradiated with UV light at 80 K. Moreover, the further reaction processes were observed from the intermediate nitrenes to the final products, azobenzene derivatives or five-membered ring derivatives. The acid–base complex formation between arylazides and amine derivatives is very effective to observe the reaction processes of nitrenes.

Keywords Azobenzene formation • Structure of nitrene • Structure of triplet carbene

8.1 Carbene Formation

A carbene is an unstable species and has a very reactive carbon center that has two nonbonded electrons. Carbenes have unique reactivity and physical properties attributable to the two electrons, which may occupy either the different orbitals separately (triplet state) or one orbital with opposite spins (singlet state). The pioneering work of Staudinger during the 1910s on the decomposition of diazo compounds contributed much to the recognition of carbenes as a new reactive species [1]. Since then, a variety of spectroscopic and computational researches have been extensively developed and many attempts have been made to isolate the transient species by chemical modification [2–8]. These carbenes are stabilized by heteroatom substituents connected to the carbenic atom and thus each has a singlet ground state. These structures with singlet carbenes were analyzed by X-rays at room temperature [9, 10].

Y. Ohashi, *Crystalline State Photoreactions: Direct Observation of Reaction Processes and Metastable Intermediates*, DOI 10.1007/978-4-431-54373-2_8, © Springer Japan 2014

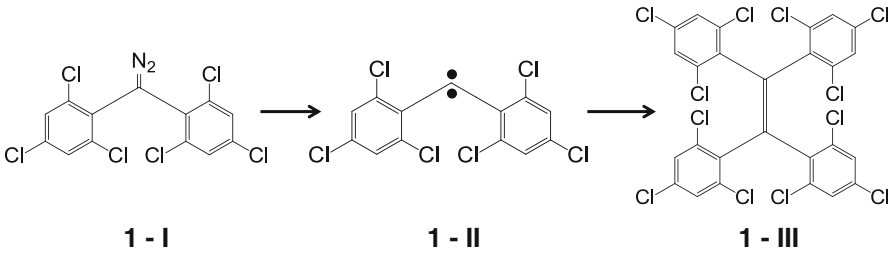

Scheme 8.1 Formation of a carbene from bis(2,4,6-trichlorophenyl)-diazomethane

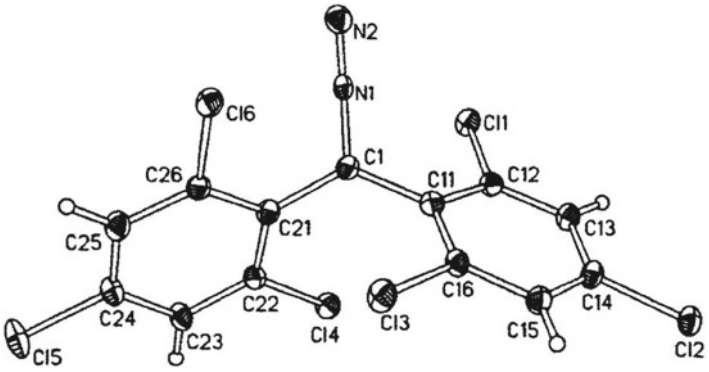

Fig. 8.1 Molecular structure of **1** before photo-irradiation at 80 K

On the other hand, triplet carbenes stable enough for X-ray analysis have not been realized for a long time. This is partly because a triplet state is less readily stabilized thermodynamically than its singlet counterpart. Many attempts have been made to stabilize triplet carbenes kinetically by protecting the carbene center with a bulky group, but the voracious appetite for electrons has made it extremely difficult to realize a triplet carbene stable enough for isolation and X-ray analysis, although fairly stable triplet carbenes have been available [11, 12].

The compound of bis(2,4,6-trichlorophenyl)diazomethane, **1-I**, is well known as one of the representative precursors for persistent triplet carbenes [13, 14]. In benzene solution, photolysis of **1-I** with ultraviolet light generates a dinitrogen molecule to leave a triplet carbene, bis(2,4,6-trichloro-phenyl)carbene, **1-II**. This carbene subsequently undergoes dimerization to yield the tetra(2,4,6-trichlorophenyl)ethylene, **1-III**, as shown in Scheme 8.1.

A crystal of **1-I** was mounted on an X-ray diffractometer and cooled below 80 K using the cold-nitrogen gas-flow method [15]. The intensity data were collected and the structure was analyzed. The molecular structure of **1-I** is shown in Fig. 8.1. Then the crystal was irradiated with 365 nm light using a high-pressure Hg lamp in combination with a band-path filter at 80 K for 2 h. The intensity data were collected under the same conditions as those before the photo-irradiation.

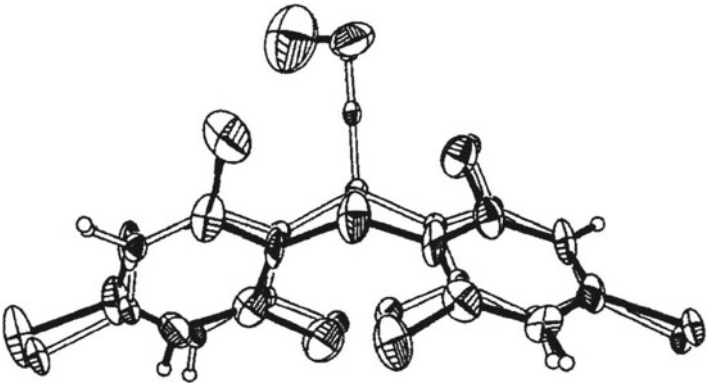

Fig. 8.2 Molecular structure of **1** after 2 h photo-irradiation at 80 K. The molecule with *white bonds* is the original one and those with *black bonds* are the photo-produced ones. The occupancy factors of the original and photo-produced ones are 0.803(5) and 0.197(5), respectively

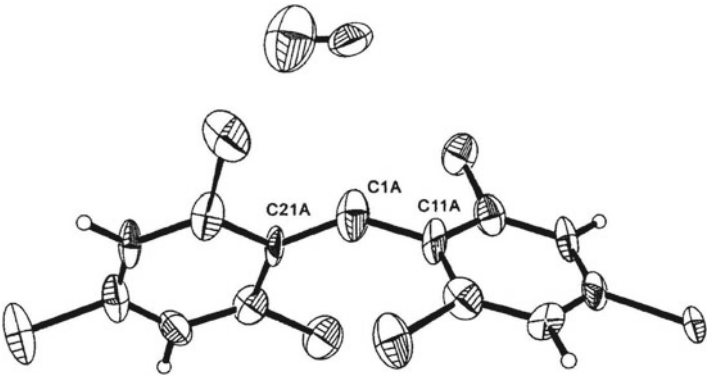

Fig. 8.3 Molecular structures of the photo-produced carbene and dinitrogen

There appeared several new peaks around the diazo group, which were refined as a photo-produced nitrogen molecule and a carbene molecule as shown in Fig. 8.2. The occupancy factors of the original **1-I** and the produced **1-II** are 0.803(5) and 0.197(5), respectively. The photo-produced carbene is shown in Fig. 8.3. The carbenic angle of C11A–C1A–C21A became 142(2)°, which is wider by 15(2)° than the original diazomethane, 127.1(1)°. The carbenic bond distances of C1A–C11A and C1A–C21A became 1.44(2) and 1.42(2) Å, respectively, which are significantly shorter than the original bond distances, 1.477(1) and 1.480(1) Å of **1-I**, respectively.

The IR spectra confirmed that the photolysis of **1-I** at 365 nm in a KBr matrix generate only a product of **1-II** in ca. 100 % yield. The ESR spectra at 77 K showed no clear signal ascribed to the triplet carbene probably because of a strong exchange coupling of the triplet states and/or antiferromagnetic interaction. The theoretical calculations indicated that the observed carbenic angle of 142(2)° is between the calculated energy-minimum angle of the singlet state, 131°, and that of the triplet

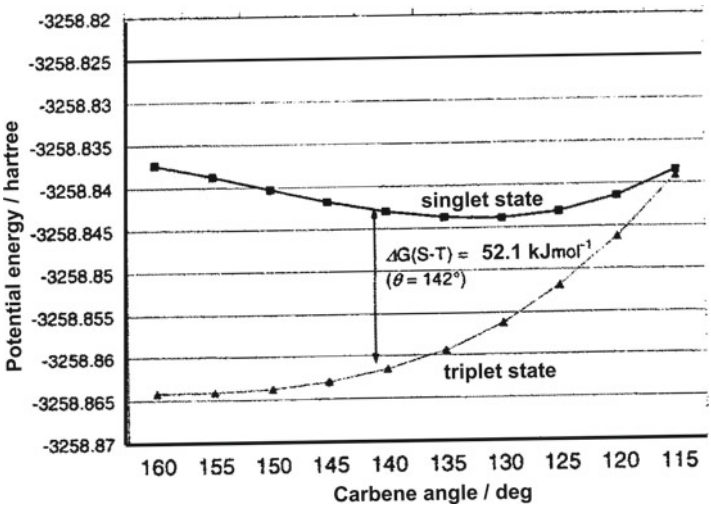

Fig. 8.4 Energy diagram of the singlet and triplet states of the carbene with the carbene angle

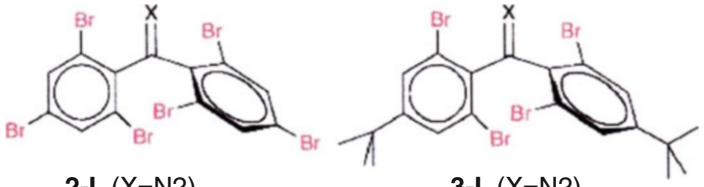

2-I (X=N2) **3-I** (X=N2)
2-II (X= :) **3-II** (X= :)

Scheme 8.2 Structures of bis(2,4,6-tribromophenyl)diazomethane, **2-I**, and the photo-produced carbene, **2-II**, and bis(2,6-dibromo-4-methylphenyl)-diazomethane, **3-I**, and the photo-produced carbene, **3-II**

state, 160°. The potential energy surface calculated as a function of carbenic angle θ in the range of 115–160° for both states indicated that the triplet state is more stable in energy than the singlet state at every angle, as shown in Fig. 8.4. At the angle of 142°, the triplet is more stable by 52.1 kJ mol^{-1} than the singlet state. This indicates that the produced carbene should be in the triplet state.

In order to determine the carbene structure more precisely, four related bis(substituted phenyl)diazomethane compounds were prepared, in which bis(2,4,6-tribromophenyl) diazomethane, **2-I**, and bis(2,6-dibromo-4-*tert*-butyl-phenyl)diazomethane, **3-I**, as shown in Scheme 8.2, revealed the photo-reactive characters [16]. The bond distances and angles of **2-I** and **3-I** are essentially the same as the corresponding ones of **1-I**. The carbenic angle, dihedral angle between the two phenyl rings, and carbenic bond distances in **1-II**, **2-II**, and **3-II** with the estimated standard deviation in parentheses are listed in Table 8.1. The corresponding values estimated from the CASSCF(6,8)/6-31G*

Table 8.1 Selected bond lengths and angles for 1, 2, and 3 after photo-irradiation. The lower value in each box is the theoretical one

Carbene	Carbene bond angle (°)	Dihedral angle of phenyl rings (°)	Carbene bond length (Å)
1-II	127.1(1)	87.09(2)	1.480(1), 1.477(1)
	126.3	88.93	1.480
2-II	127.6(1)	86.45(4)	1.470(2), 1.479(2)
	126.3	85.55	1.480
3-II	127.0(1)	87.74(2)	1.480(1), 1.479(1)
	126.2	84.69	1.481

theoretical calculation are also listed in Table 8.1. Since the crystal structure of **2-I** is isostructural to that of **1-I**, the produced structure of **2-II** is very similar to that of **1-II**. The crystal structure of **3-I** is completely different from **1-I** and **2-I**, and the carbene structure of **3-II** is slightly different from the corresponding ones of **1-II** and **2-II**.

It must be emphasized that the metastable species such as carbene has nearly the same energy in the wide range of the structural parameter such as the carbenic angle. This means that the structure observed in the crystalline state may be heavily affected by the packing energy or intermolecular interaction and may be somewhat different from the structure in free space. However, the easiness of the structural change of metastable species can be estimated from the analyzed structures of related ones. This character should be very important, since we want to know the structure of the metastable species not in free space but in the condensed matter, when we consider the reaction mechanism.

8.2 Nitrene Formation

8.2.1 Nitrene Formation from Arylazide

A reaction intermediate consisting of a phenyl group and an electrically neutral nitreno group, phenylnitrene, was proposed by Bertho when phenylazide was dimerized thermally as shown in Scheme 8.3 [17]. The existence of the triplet phenylnitrene was confirmed as a reaction intermediate by ESR measurement [18]. The electronic spectra of phenylnitrene after photo-irradiation of phenylazide were reported in an organic matrix at 77 K [19, 20]. Since then, phenylnitrene and its derivatives, arylnitrenes, have created considerable interest owing to their potential applications to organic synthesis [21, 22], photoaffinity labeling [23], and materials science [24].

Arylnitrenes are unstable substances and are difficult to trap because the nitreno group does not obey the octet rule. Several attempts have been made by organic and physical chemists to analyze reaction pathways involving an arylnitrene [25–29]. Scheme 8.4 shows the proposed reaction pathways through arylnitrene. The singlet arylnitrene is produced upon photolysis or thermolysis of arylazide [30–32]. The benzene ring of the singlet arylnitrene expands to an unstable seven-membered ring, azacycloheptatetraene [33], and further reaction proceeds to form the 3H-azepine in

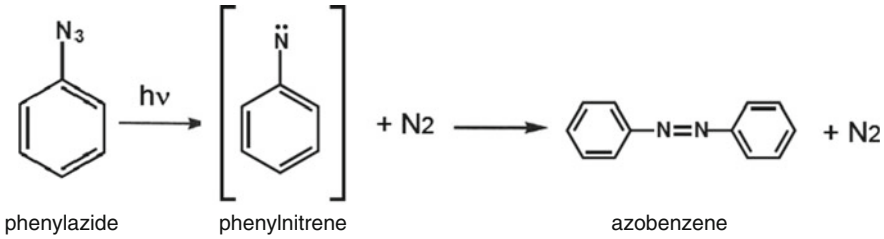

Scheme 8.3 Formation of phenylnitrene, as proposed by Bertho (1928)

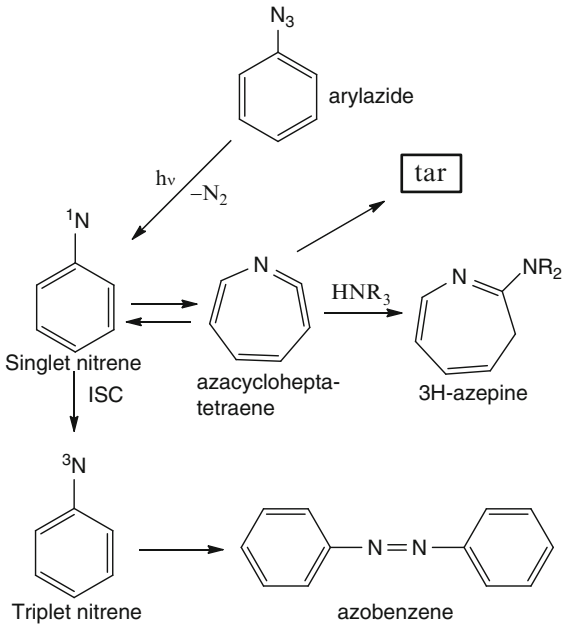

Scheme 8.4 Various reaction pathways, as proposed based on spectroscopic and synthetic studies

amine solvents [34] or to polymerize with itself to give tar [35]. In gas phase the singlet arylnitrene gave cyanocyclopentadiene [36]. Since the lifetime of the singlet arylnitrene is very short [37], its intermolecular reactions have been reported few. The singlet arylnitrene converts to the triplet state via intersystem crossing (ISC). The triplet arylnitrene is more stable energetically than the singlet one and has strong biradical properties. It has been reported that the triplet arylnitrenes dimerize to azobenzene [17] or abstract hydrogen atoms to afford primary amines or anilines as final products [38]. Such different reaction pathways may be affected by many factors, for example, temperatures [39], solvents and/or matrices [40], substituents [41, 42], and so on.

Arylnitrenes revealed the characteristic behaviors in the crystalline state different from those in solution, grass-matrices, or gas state. The half-lifetimes of arylnitrene derivatives in crystalline state were ~10 d at room temperature [43] and that the ratio of final products produced from arylnitrene was controlled by the time and temperature of

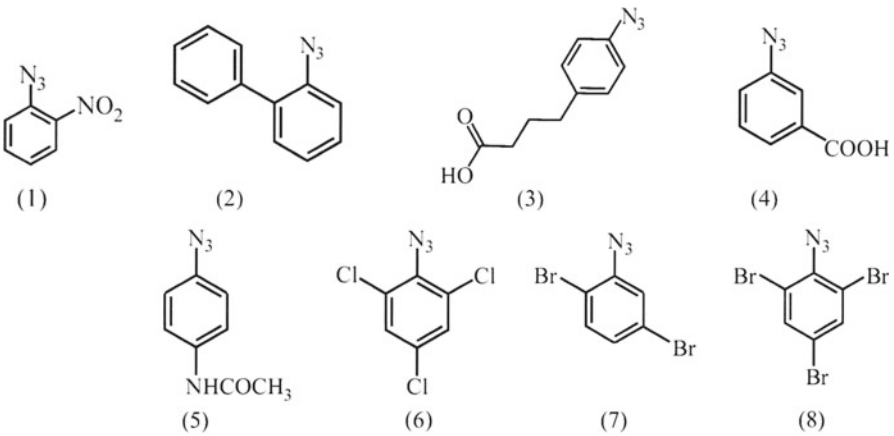

Scheme 8.5 Various arylazide derivatives produced for the nitrene formation

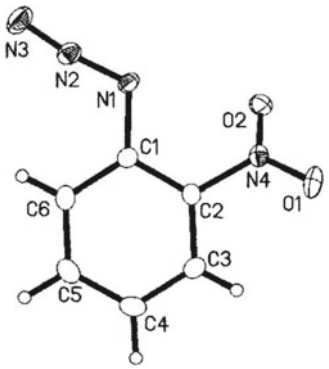

Fig. 8.5 Molecular structure of 1-azido-2-nitrobenzene, **1**, at 80 K

photo-irradiation [44, 45]. However, the structure of arylnitrene was impossible to be analyzed by X-rays, since the amount of the produced arylnitrene was very few.

In order to observe the structure of arylnitrene directly, several kinds of arylazide derivatives were prepared and the crystal structures before and after photo-irradiation were analyzed [46, 47]. Crystals of the prepared arylazide derivatives, however, were nonreactive or easily broken on exposure to the UV lamp, except 1-azido-2-nitrobenzene, **1**, and 2-azido-biphenyl, **2,** as shown in Scheme 8.5.

The intensity data of the crystal **1** was collected at 80 K and the structure was analyzed by X-rays [46]. The molecular structure of **1** is shown in Fig. 8.5. The intramolecular distance of N1···O2 is 2.710(1) Å, which is significantly shorter than the sum of van der Waals radii (3.07 Å), although the nitro group does not take a coplanar structure with the phenyl ring, the dihedral angle of the nitro group being 37.6(1)°, to avoid the steric repulsion between N1 and O2. Then the crystal was irradiated with light of 436 nm wavelength using a combination of a high-pressure Hg lamp and a band-path filter at 80 K for 30 min. The difference electron density

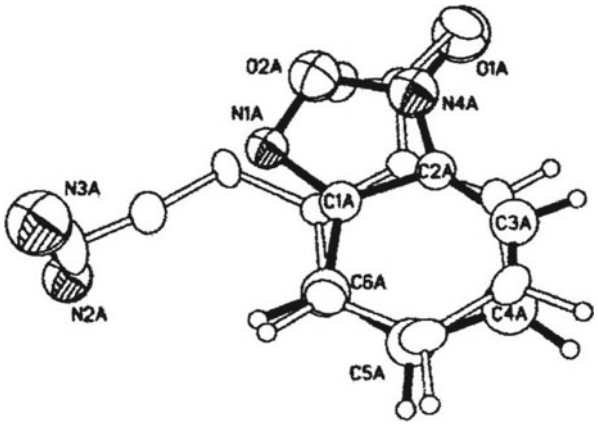

Fig. 8.6 Molecular structure of **1** after photo-irradiation. The molecule with *white bonds* and *black bonds* are before and after the photo-irradiation, respectively

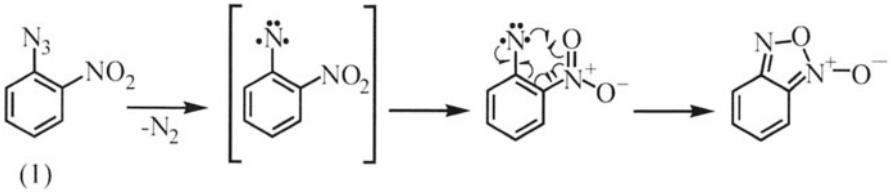

Scheme 8.6 Formation of benzofuroxan from compound **1**

map revealed the formation of a five-membered ring lying in the molecular plane. The other peaks appeared upper and lower the N3 atom, which are ascribable to a dinitrogen molecule produced from the azido group. The refined structure revealed that the photoproducts are benzofuroxan and dinitrogen molecules as shown in Fig. 8.6. The population of the benzofuroxan is 0.103(3). The dinitrogen molecule fits well into the reaction cavity for the N2 and N3 groups. Such a fitting is one of the essential conditions to prevent deterioration of the crystallinity upon photolysis.

The ESR measurement indicated that the triplet nitrene produced at 5.4 K disappeared at 80 K. The IR spectra were observed under photo-irradiation at temperatures of 7–300 K. In addition to the produced benzofuroxan, the peaks ascribed to 1,2-dinitrosobenzene appeared at 7 K and they disappeared at 80 K. The 1,2-dinitrosobenzene is formed if the nitrene extracts one of the oxygen atoms from the nitro group. The above results suggest that heterocyclic ring formation of benzofuroxan from **1** is generally believed to occur via an intermediate showing triplet nitrene character, probably because the distance between the reaction centers, N1 and O2 (2.710(1) Å), is very short so that the cyclization can smoothly proceed via singlet nitrene (small activation energy). The reaction scheme is shown in Scheme 8.6. Since benzofuroxan is easily produced, it may be impossible to trap triplet nitrenes as a main product at low temperatures.

The crystal structure of **2** before photo-irradiation was analyzed by X-rays at 83 K [47]. The crystal structure is shown in Figure 8.7. Two azido groups are aligned

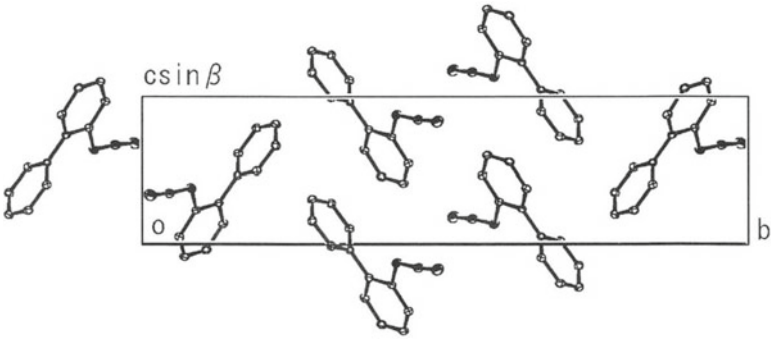

Fig. 8.7 Crystal structure of 2-azido-biphenyl, **2**, at 83 K viewed along the *a* axis

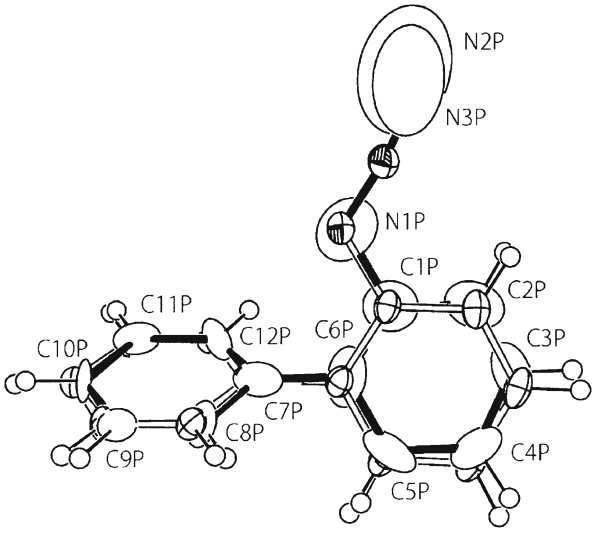

Fig. 8.8 Molecular structure of **2** after photo-irradiation at 83 K. The molecules with *white* and *black bonds* are before and after photo-irradiation, respectively. The thermal parameters of dinitrogen are very large. The nitreno atom, N1P, is overlapped on the N1 of the original azido group

across an inversion center. The azido group is almost coplanar with the attached benzene ring, the torsion angle of N2–N1–C1–C2 being –4.9(1)°. The two benzene rings of the biphenyl group are not coplanar and have an angle of 61.2(1)° between them. This is because of the short contact between N1 and C12, 3.091(1) Å. Then the crystal was irradiated with a high-pressure Hg lamp and UV cut-filter which removes the wavelengths shorter than 420 nm. After 5 h exposure, the crystallinity was kept. The cell dimensions were significantly expanded. The intensity data were collected under the same conditions as before the irradiation. In the difference electron density map, new peaks and troughs appeared in the vicinity of the azido group. This indicates that the 2-azido-biphenyl molecule is partly transformed to dinitrogen and 2-biphenylnitrene molecules as shown in Fig. 8.8. The disordered model

composed of the produced and original molecules was refined with the severe constraints. Although it is clear that 2-biphenylnitrene was observed, it is difficult to discuss its precise structure since the heavy constraints were applied to separate the photoproducts from the overlapped azide molecule. The by-product, dinitrogen molecule, shows its unique behavior in the crystal lattice. The dinitrogen molecule is captured in the cavity around the N2 and N3.

8.2.2 Nitrene from Acid–Base Complexes of Arylazides

In the previous section, it was found that most of the arylazide crystals are nonreactive or decomposed after photo-irradiation, because the structural changes were too large to keep the single crystal form. Only the 2-azido-biphenyl was still crystalline after photo-irradiation; the structure of its product, 2-biphenylnitrene, was successfully analyzed by X-rays. However, it was very difficult to observe the precise nitrene structure, because the produced nitrene and the reactant 2-azidebiphenyl are superimposed in the crystal structure after photo-irradiation.

The above results suggest that if the acid–base complex crystals between the arylazides and dibenzylamines could be prepared, the photoreaction should proceed with retention of the single crystal form. This idea has already been applied in the crystalline-state photoreactions of cobaloxime complexes, as described in Sect. 6.1, introducing the carboxyl group to the axial base of the cobaloxime complexes and the dibenzylamine or dicyclohexylamine as a base compound. A variety of the acid–base complexes were formed between them. The three merits for the acid–base complex formation are considered as follows: (1) the crystallinity should be kept during the reaction, because the cavity around the reactive group may be expanded compared with that of the crystal of the reactant molecule only, (2) the light can penetrate into the complex crystal deeper than the crystal of the reactant molecule only, because the base amine may play a role of reaction matrix, and (3) the crystals suitable for X-ray works may be easily obtained, because the phenyl or cyclohexyl group of the amines may improve the crystallinity.

A variety of acid–base complex crystals were prepared, using 2-azidobenzoic acid (**2a**), 3-azidobenzoic acid (**3a**), and 4-azidobenzoic acid (**4a**) as acids and dibenzylamine (**db**), *N*-benzyl-2-phenylethylamine (**bp**), and dicyclohexylamine (**dc**) as bases, which are shown in Scheme 8.7 [48]. Among nine combinations of acid–base complexes, suitable crystals for X-ray work were obtained for the six complexes of **2a**-**db**, **3a-db**, **3a-dc**, **4a-bp**, **4a-db**, and **4a-dc**. For the other three complexes of **2a-dc**, **2a-bp**, and **3a-bp**, suitable crystals were not obtained. For the complexes of **3a-db** and **4a-db**, two crystal forms, **I** and **II**, were obtained. The crystal structures for the eight kinds of crystals before the photo-irradiation were analyzed by X-rays. Then each crystal was irradiated with a high-pressure Hg lamp with a filter to select the wavelength longer than 420 nm or 390 nm at ca. 80 K for 2–32 h. The intensity data were collected at ca. 80 K and the structures were analyzed. For the three crystals, **4a-db-I**, **4a-db-II**, and **4a-dc**, it was impossible to analyze the structures after photo-irradiation, because of poor intensity data.

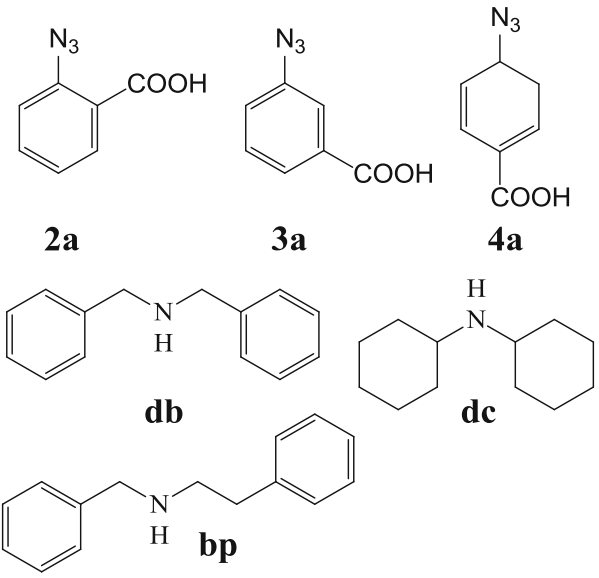

Scheme 8.7 Formation of an acid–base complex between compounds **2a**, **3a,** and **4a** as acids and **db**, **dc**, and **bp** as bases

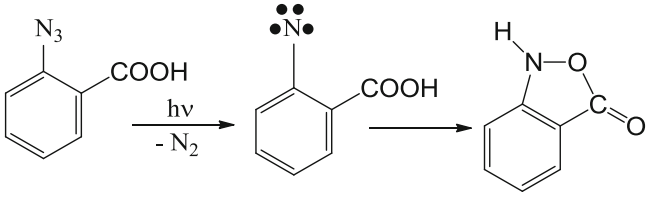

Scheme 8.8 Formation of 2,1-benzisooxazolone from acid–base complex **2a-db**

For the complex crystal of **2a-db**, the difference electron density map after photo-irradiation showed the formation of the five-membered ring. This means that the produced nitrene forms a bond with one of the oxygen atoms of carboxylate anion and 2,1-benzisooxazolone was formed, as shown in Scheme 8.8. No significant change was observed in the structure of dibenzylamine. The disordered structure after photo-irradiation is shown in Fig. 8.9. The atoms with and without P correspond to the photo-produced and original atoms, respectively. The occupancy factors of dinitrogen and 2,1-benzisoxazolone molecules are 0.131(8) and 0.105(5), respectively. The difference of 0.026 may indicate the existence of the intermediate 2-carboxyphenylnitrene, whose existence is assumed from the ESR measurement. Recently it was reported from UV and IR spectra of 2-azidobenzoic acid crystalline samples that the heterocyclic ring of 2,1-benzisoxazolone was produced via singlet arylnitrene and the dimer, 2,2′-dicarboxyazobenzene, was produced via triplet arylnitrene [49]. Since the produced nitreno group was too far from the neighboring nitreno in the crystal structure, it was not dimerized to 2,2′-dicarboxyazobenzene, keeping the single crystal form after ISC from singlet to triplet.

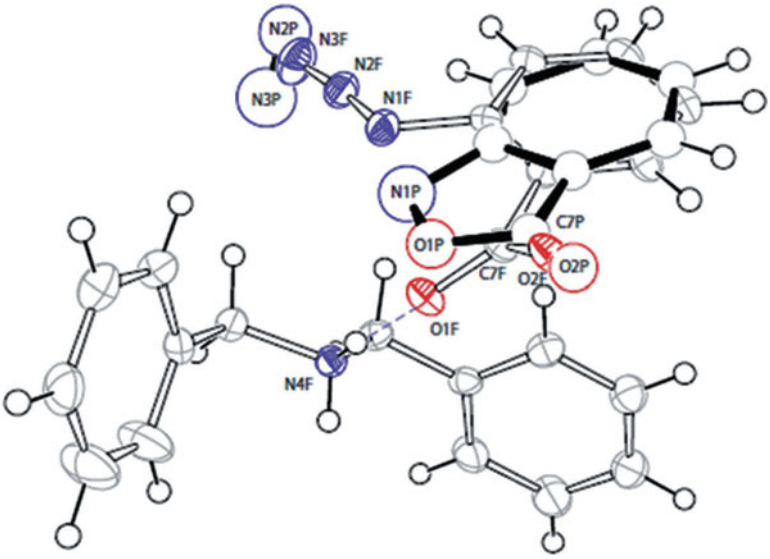

Fig. 8.9 Molecular structure of **2a-db** after photo-irradiation. The photo-produced atoms are the numbers with *P* and the bonds are *black*

For the complex crystal of **3a-db-I**, the difference electron density map after photo-irradiation revealed a disordered structure as shown in Fig. 8.10. The nitrogen molecule, N2P–N3P, is produced from the azido group. The occupancy factor of the dinitrogen molecule converged to 0.25(2). Since the original 3-azidobenzoic acid and produced 3-carboxyphenylnitrene almost overlap each other, it was impossible to separate the two molecules. Then the intensity data collected at the BL02B1 station of SPring-8 at 25 K. The analyzed structure after photo-irradiation is essentially the same as that at 80 K described above, although the occupancy factor of the dinitrogen molecule was 0.075 at 25 K [50]. The intermolecular hydrogen bonds of N4···O1 and N4′···O2 fix the carboxyl group of the benzoic acid tightly to the dibenzylamines at 25 K; the produced 3-carboxyphenylnitrene was slightly shifted from the original position of the 3-azidobenzoic acid due to the steric repulsion with the produced dinitrogen molecule, as shown in Fig. 8.11. The C1–N1(nitrene) bond was successfully analyzed to be 1.34(4) Å. The closest arylazides are related by twofold screw axis so that the azido group is surrounded with inert phenyl rings of adjacent molecules. The intermolecular distance between the closest N1 atoms is 5.782(2) Å in the structure before photo-irradiation. There is no possibility for the produced 3-carboxyphenylnitrene to make a dimer with the neighboring one. This is the reason why the unstable nitrene can be observed in the crystal after photo-irradiation.

For the crystal of **3a-db-II**, the difference electron density map is shown in Fig. 8.12. New residual peaks appeared in the vicinity of the azido group, which were assigned to a dinitrogen molecule from the azido group. Moreover, new peaks appeared between 3-azidobenzoic acid molecules related by an inversion. This indicates that two photo-produced 3-carboxyphenylnitrenes came close to each other and a dimer, 3,3′-dicarboxy-*trans*-azobenzene, was formed. The

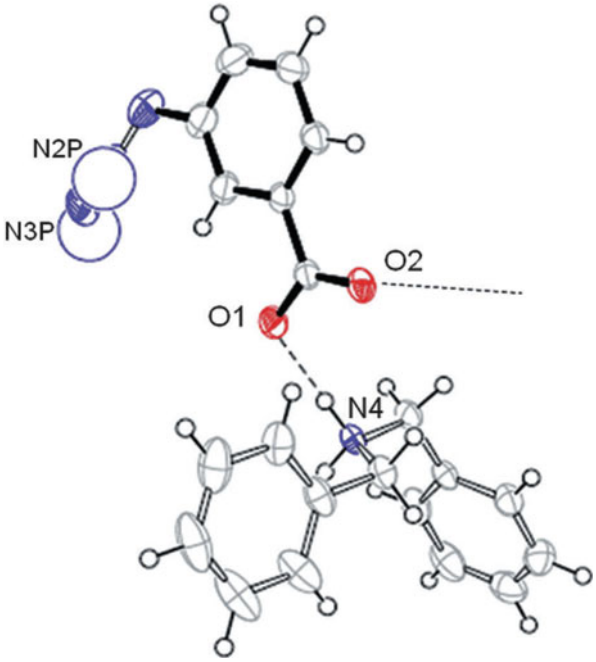

Fig. 8.10 Molecular structure of **3a-db-I** after photo-irradiation at 80 K. Although the dinitrogen molecules are clearly assigned, the nitrene is completely overlapped on the original 3-azidobenzoic acid

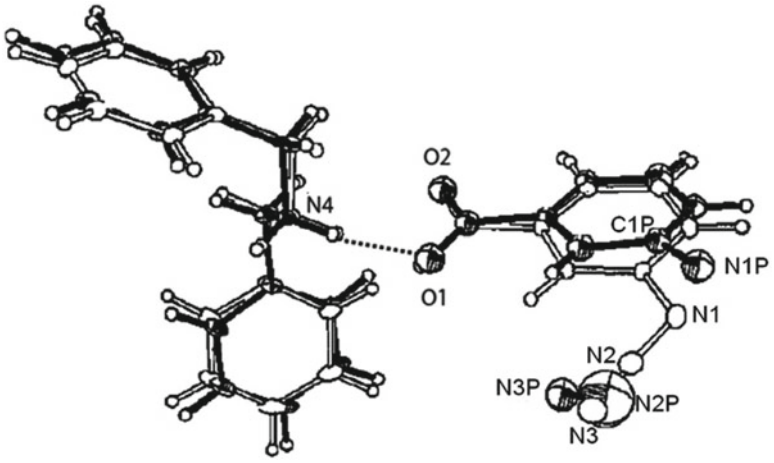

Fig. 8.11 Molecular structure of **3a-db-I** after photo-irradiation at 25 K. The photo-produced nitrene is slightly shifted from the original position

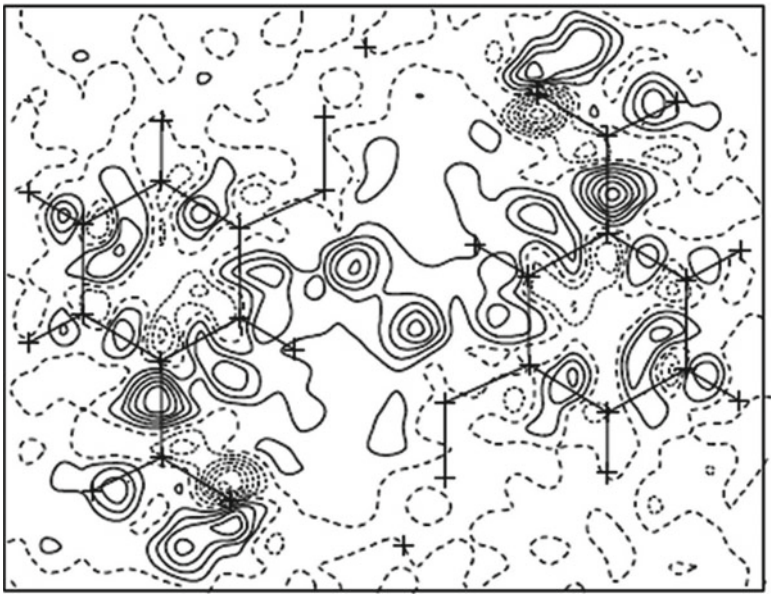

Fig. 8.12 Difference electron density map of **3a-db-II** after photo-irradiation at 80 K. The central two residual peaks correspond the N=N moiety of the dimerized azobenzene

disordered structure after photo-irradiation is shown in Fig. 8.13. The intermolecular distance between the N1 atoms related by an inversion center (4.067(2) Å) before photo-irradiation is shorter than **3a-db-I**. After photo-irradiation, the N1P–N1P′ distance became 1.29(7) Å, which is the N=N double bond. The hydrogen bonds of N4···O1 and N4···O2 before irradiation, 2.723(1) and 2.710(1) became 2.66(3) and 2.45(3) Å, respectively. It is clear that the crystal packing around the produced arylnitrene plays an important role in the reaction pathway. The occupancy factors are 0.177(4) for the dinitrogen molecule and 0.074(4) for 3,3′-dicarboxy-*trans*-azobenzene. The ESR spectra indicated the existence of the triplet arylnitrene. This means that the triplet 3-carboxyphenylnitrene with the occupancy factor of 0.103 is overlapped with the original 3-azidobenzoic acid molecule or may have random orientation. Although the IR spectra also indicated the existence of azacycloheptatetraene, it was impossible to assign the azacycloheptatetraene molecule in the difference electron density map since it may be completely buried in the disordered structure of arylazide, arylnitrene, and azobenzene, if it may be produced in the crystal.

For the complex crystal of **3a-dc**, the difference electron density map showed the photoproducts, dinitrogen and 3-carboxyphenylnitrene, as shown in Fig. 8.14, in which the nitrene is completely overlapped with the benzoic acid. The occupancy factor of the dinitrogen molecule is 0.183(4). The distance of the closest nitreno groups related by the inversion center is too long, 5.890(1) Å, to make a dimer. The intermolecular hydrogen bonds of N4···O1 and N4···O2 before irradiation, 2.7888(8) and 2.7194(8) Å, are nearly the same as those after photo-irradiation, 2.783(1) and 2.727(1) Å, respectively.

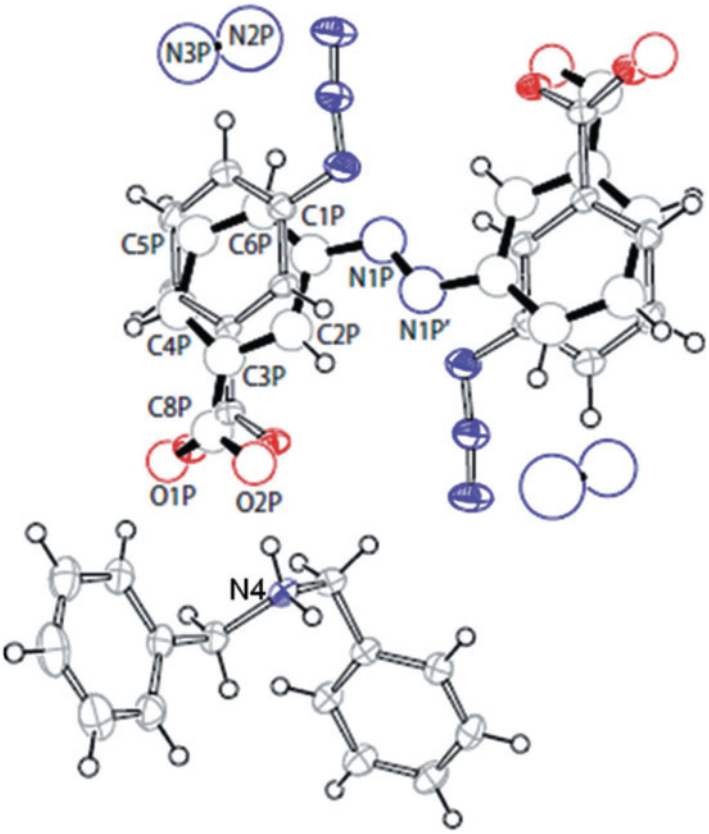

Fig. 8.13 Molecular structure of **3a-db-II** after photo-irradiation

For the complex crystal of **4a-bp**, the difference electron density map in the vicinity of the two azido groups related by an inversion revealed 4,4′-dicarboxy-*trans*-azobenzene and two dinitrogen molecules as shown in Fig. 8.15. The center of the N=N bond of 4,4′-dicarboxy-*trans*-azobenzene is situated on the crystallographic inversion center. Two 4-azidobenzoic acids contact each other around an inversion center, which is the closest one. The intermolecular distance between the closest N1 atoms by the inversion center, 3.411(2) Å, before photo-irradiation is shorter than that of **3a-db-II**. After photo-irradiation, the N1P–N1P′ bond became 1.33(4) Å, which is N=N double bond. The intermolecular hydrogen bonds of N4···O1 and N4···O2 before photo-irradiation are 2.669(1) and 2.691(2), which are somewhat different from the distances after photo-irradiation, 2.52(2) and 2.71(2) Å, respectively. Such differences may be caused by an N=N bond formation in the opposite site of the benzene rings. The occupancy factor for 4,4′-dicarboxy-t*rans*-azobenzene became 0.149(4), but the factor for dinitrogen was 0.088(5). The latter factor may be too small, probably due to the severe overlap with the azido group. The IR spectra showed no peaks due to the formation of azacycloheptatetraene.

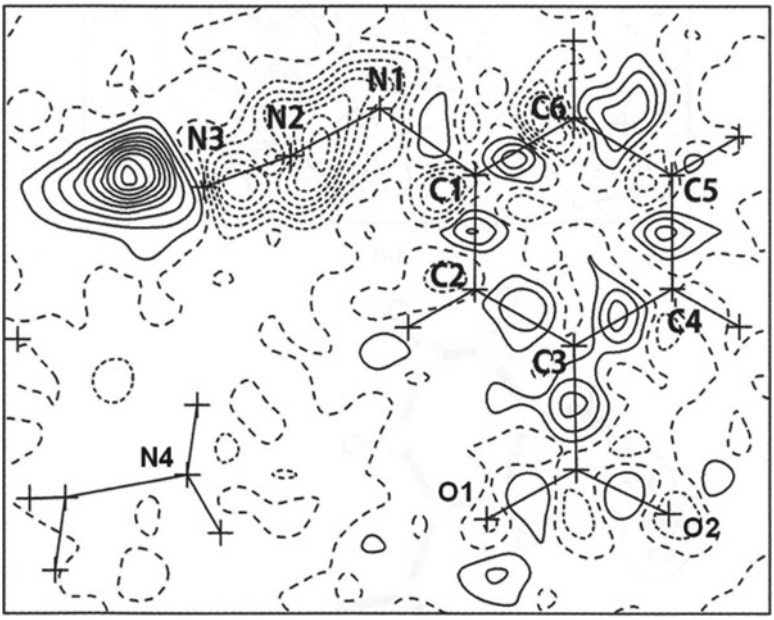

Fig. 8.14 Difference electron density map of **3a-dc** after photo-irradiation

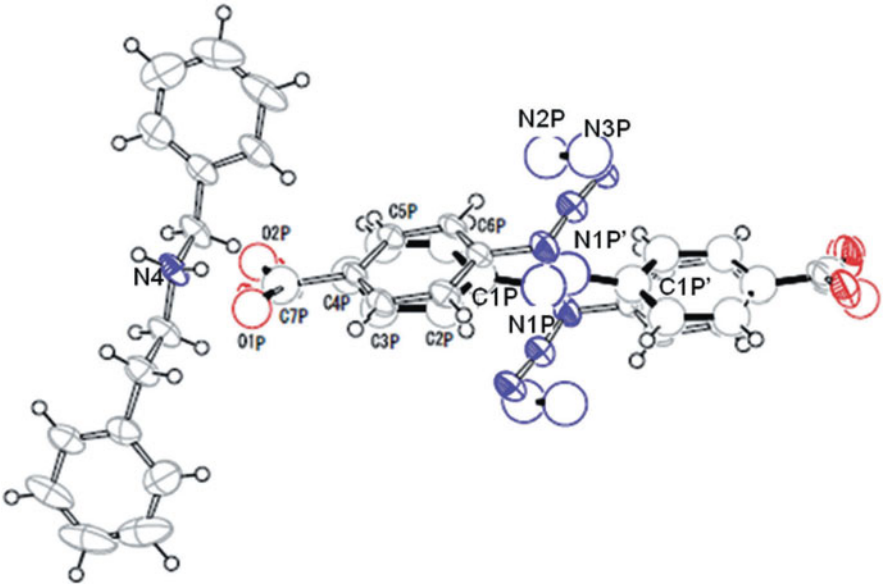

Fig. 8.15 Molecular structure of **4a-bp** after photo-irradiation. The dimer molecule, 4,4′-dicarboxy-*trans*-azobenzene, is produced. *Blue* and *red atoms* are nitrogen and oxygen, respectively

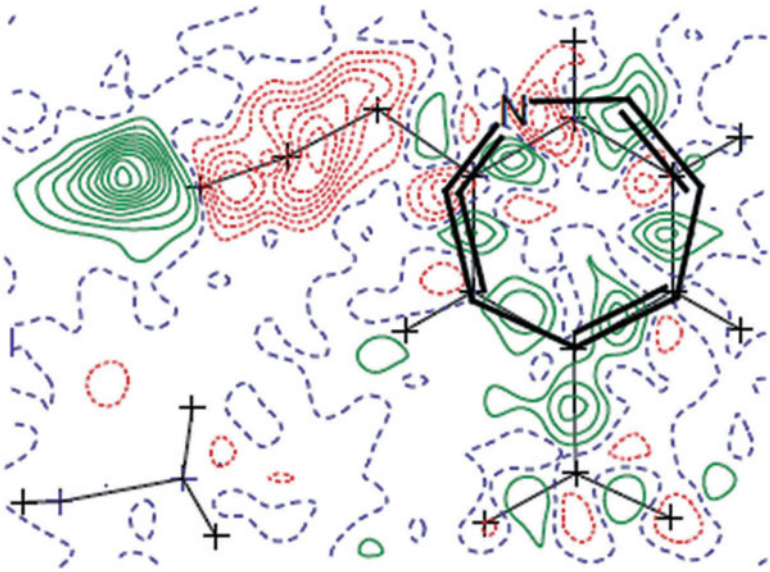

Fig. 8.16 Difference electron density map of **3a-dc** after photo-irradiation. The photo-produced azacycloheptatriene molecule may be assigned in the map

For the crystals of **3a-db-I** and **3a-dc**, only arylnitrene and dinitrogen appeared after photo-irradiation. The final difference electron density map of **3a-dc** showed a peak beside C15–C16 bond. Since the IR spectra suggested the formation of azacycloheptatetraene, the peak should be assigned to one of the carbon atoms consisting azacycloheptatetraene, as shown in Fig. 8.16. However, the low occupancy factor (<0.02) and severe overlapping with the original 3-azidobenzoic acid and produced 3-carboxyphenylnitrene make it impossible to divide the whole azacycloheptatetraene molecule from the residual density map. For **3a-db-I**, there is a peak beside the C5–C6 bond too. This peak also indicates the existence of the seven-membered ring as indicated in the IR spectra.

Using the acid–base complexes, four different pathways of arylnitrenes can be observed, as shown in Scheme 8.9. If the produced nitreno group is close to the nitrogen or oxygen atom of the neighboring group (less than the sum of van der Waals contact), the new N–N or N–O bond is formed and the new molecule with five-membered ring is produced as observed in the crystal of 1-azido-2-nitrobenzene or the complex crystal of **2a-db**. If the produced nitreno groups of the neighboring molecules are close to each other (less than ca. 4.5 Å), the two nitreno groups make a N=N bond to form a dimer, *trans*-azobenzene, molecule as observed in the complex crystals of **3a-db-II** and **4a-dp**. This is the direct evidence that the azobenzene derivatives are produced from arylazides through arylnitrenes, which was first proposed about 85 years ago by Bertho [17].

If the produced nitreno group is apart from those of the neighboring molecules (greater than ca. 5.5 Å), the arylnitrene is kept intact in the crystalline lattice at

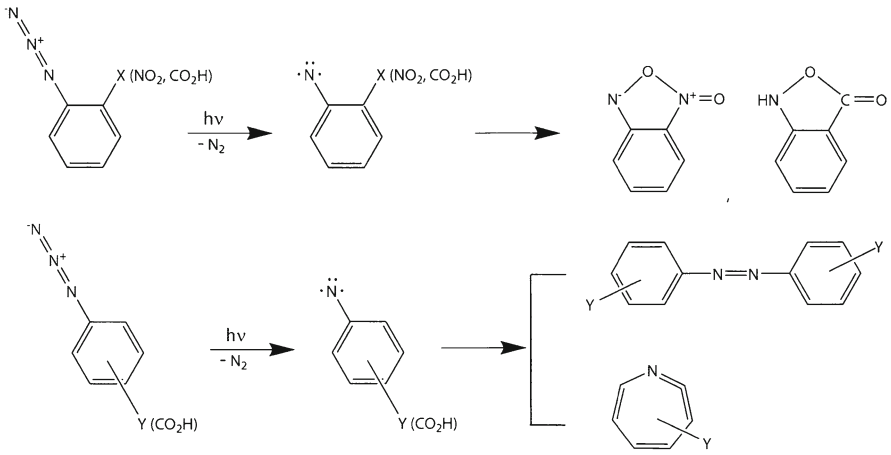

Scheme 8.9 Different pathways in various photoreactions of arylnitrenes

low temperatures as shown in **3a-db-I** and **3a-dc**. Moreover, a small portion of azacycloheptatetraene with a seven-membered ring coexists in the crystalline lattice, which may be produced from the singlet nitrene, as observed in **3a-db-I** and **3a-dc**.

Although a variety of arylazide crystals were prepared and were irradiated with the Hg lamp to observe the structure of arylnitrene, all the crystals except the 2-azido-biphenyl were decomposed or nonreactive after photo-irradiation. The acid–base complex crystals were made, introducing the carboxyl group to the arylazide molecule as a substituent. The metastable structures were observed directly by X-ray analysis. This is because the complex crystal has three merits to observe the metastable species described above. It will be an indispensable technique to make an acid–base complex if the reactivity of molecule will be examined in the crystalline state to observe the metastable intermediates by X-ray analysis.

References

1. Staudinger H, Kupfer O (1912) Ber Dtsch Chem Ges 45:501
2. Kirmse W (1961/1971) Carbene chemistry, 2nd edn. Academic, New York
3. Moss RA, Jones M Jr (eds) (1973/1975) Carbenes, vol I and II. Wiley, New York
4. Brinker UH (ed) (1994, 1998 and 2000) Advances in carbene chemistry, vols 1 and 2. JAI Press, Greenwich
5. Arduengo AJ III (1999) Acc Chem Rev 32:913
6. Bourissou D, Guernet O, Gabbai FP, Betrand G (2000) Chem Rev 100:39
7. Sekiguch A, Lee VY (2003) Chem Rev 103:1429
8. Moss AM, Platz MS, Jones M Jr (eds) (2004) Reactive intermediate chemistry. Wiley, New York
9. Arduengo AJ III, Goerlich JR, Marshell WJ (1995) J Am Chem Soc 117:11027
10. Alder RW, Allen PR, Murray M, Orpen AG (1996) Angew Chem Int Ed Engl 35:1121

11. Tomioka H (1997) Acc Chem Rev 30:315
12. Tomioka H (1998 and 2000). In: Brinker UH (ed) Advances in carbene chemistry, vols 2 and 8. JAI Press Inc, Greenwich
13. Zimmerman HE, Paskovich DH (1964) J Am Chem Soc 86:2149
14. Tomioka H, Hirai K, Fujii C (1992) Acta Chim Scand 46:680
15. Kawano M, Hirai K, Tomioka H, Ohashi Y (2001) J Am Chem Soc 123:6904
16. Kawano M, Hirai K, Tomioka H, Ohashi Y (2007) J Am Chem Soc 129:2383
17. Bertho A (1924) Chem Ber 57:1138
18. Smolinski G, Wasserman E, Yager WA (1962) J Am Chem Soc 84:3220
19. Reiser A, Frazer V (1965) Nature 208:682
20. Reiser A, Bowers G, Horne R (1966) J Trans Faraday Soc 62:3162
21. Iddon B, Meth-Cohn O, Scriven EFV, Suschitzky H, Gallagher PT (1979) Angew Chem Int Ed 18:900
22. Wentrup C (1981) Adv Heterocycl Chem 28:231
23. Kotzyba-Hibert F, Kapfer I, Goeldner M (1995) Angew Chem Int Ed 34:1296
24. Meijer EW, Nijhuis S, Vroonhoven FCBMV (1988) J Am Chem Soc 110:7209
25. Scriven EFV (1984) Azide and nitrene reactivity and utility. Acadimic, New York
26. Platz MS (1995) Acc Chem Res 28:487
27. Borden WT, Gritsan NP, Hadad CM, Karney WL, Kemnitz CR, Platz MS (2000) Acc Chem Res 33:765
28. Karney WL, Borden WT (2001) Adv Carbene Chem 3:205
29. Gritsan NP, Platz MS (2001) Adv Phys Org Chem 36:255
30. Marcinek A, Leyva E, Whitt D, Platz MS (1993) J Am Chem Soc 115:8609
31. Gritsan NP, Yuzawa T, Platz MS (1997) J Am Chem Soc 119:5059
32. Born R, Burda C, Senn P, Wirz J (1997) J Am Chem Soc 119:5061
33. Chapman OL, Roux J-PL (1978) J Am Chem Soc 100:282
34. Doering WE, Odum RA (1966) Tetrahedron 22:81
35. Horner L, Christmann A, Gross A (1963) Chem Ber 96:399
36. Crow WD, Wentrup C (1967) Tetrahedron Lett 44:4379
37. Gritsan NP, Zhu Z, Harad CM, Platz MS (1999) J Am Chem Soc 121:1202
38. Hall JH, Hill JW, Fargher JM (1968) J Am Chem Soc 90:5313
39. Leyva E, Platz MS (1985) Tetrahedron Lett 26:2147
40. Dunkin IR, Lynch MA, AcAlpine F, Sweeny D (1997) J Photochem Photobiol Chem 102:207
41. Leyva E, Platz MS, Persy G, Wirz J (1986) J Am Chem Soc 108:3783
42. Li Y-Z, Kirby JP, George MW, Poliakoff M, Schuster GB (1988) J Am Chem Soc 110:8092
43. Mahé L, Izuoka A, Sugawara T (1992) J Am Chem Soc 114:7904
44. Sasaki A, Izuoka A, Sugawara T (1996) Mol Cryst Liquid Cryst 277:17
45. Sasaki A, Mahe L, Izuoka A, Sugawara T (1998) Bull Chem Soc Jpn 71:1259
46. Takayama T, Kawano M, Uekusa H, Ohashi Y, Sugawara T (2003) Helv Chim Acta 86:1352
47. Takayama T, Mitsumori T, Kawano M, Sekine A, Uekusa H, Ohashi Y, Sugawara T (2010) Acta Crystallogr B66:639
48. Mitsumori T, Sekine A, Uekusam H, Ohashi Y (2010) Acta Crystallogr B66:647
49. Budruev AV, Karyakina LN, Oleinik AV (2003) High Energy Chem 37:29
50. Kawano M, Takayama T, Uekusa H, Ohashi Y, Ozawa Y, Matsubara K, Imabayashi H, Mistumi M, Toriumi K (2003) Chem Lett 32:922

Chapter 9
Conclusion

Since a racemization reaction of a chiral alkyl group bonded to a cobalt atom in a cobaloxime crystal on exposure to visible light was found in 1977, a variety of photoreactions of the cobaloxime complexes were observed with keeping the single crystal form. We call them "crystalline-state reactions" discriminating the usual solid-state reactions. The most important merit of the crystalline-state reactions is that we can directly "observe" the structural change occurring in a crystal by X-ray crystal structure analysis. By virtue of crystalline-state reactions, the mechanisms of racemic-to-chiral transformation of the 1-cyanoethyl group only by photo-irradiation, and the chirality inversion process of the 1-(ethoxycarbonyl)ethyl group, an unstable intermediate structure of the bulky *R*-1,2-bis(methoxycarbonyl)ethyl group can be made clear in the observation of the structural changes. Of course, the metastable structures of carbenes, nitrenes, *trans-keto* forms of salicylideneanilines, lophyl radicals, and the unstable excited structures can be observed in the crystalline-state reactions.

Furthermore, if the hydrogen atoms at the active site are replaced with the deuterium atoms and the structure change caused by photo-irradiation can be analyzed by neutron diffraction, the movement of the proton during the reaction can be directly observed. The different pathways from the 4-cyanobutyl group to 1-cyanobutyl group were elucidated from the direct "observation" by neutron diffraction.

The reaction cavity can be easily defined in the crystalline-state reaction, since the reaction proceeds with retention of the single crystal form. The relation between the reaction rate and the cavity size holds well in almost all the crystalline-state reactions. Moreover, the shape of the reaction cavity well explains the asymmetric induction during the reactions. The asymmetric induction in the photoisomerization from 2-cyanoethyl to 1-cyanoethyl groups are well explained by the shape of the reaction cavity. Moreover, the marvelous *R:S* ratio of 70:30 after the racemic-to-chiral transformation and the singular *R:S* ratio of 18:82 after the chirality inversion are caused by the asymmetric shape of the reaction cavity before photoreaction.

Furthermore, it was made clear that the concept of reaction cavity is applicable to the usual solid-state reactions. In almost all the solid-state photoisomerization from the 2-cyanoethyl group to 1-cyanoethyl group, the reaction cavity is a good

Y. Ohashi, *Crystalline State Photoreactions: Direct Observation of Reaction Processes and Metastable Intermediates*, DOI 10.1007/978-4-431-54373-2_9, © Springer Japan 2014

guide to explain the reaction mechanism. It may be better to explain the reaction mechanism with the reaction cavity in the usual solid-state reaction instead of an abstract word of "topochemical."

One challenging problem is keeping the single crystal form during photoreaction. One of the important requirements is that the radiation with the wavelengths longer than absorption maximum should be used because not only the surface molecules but also the inner molecules can absorb the radiation. The acid–base complex formation is a very effective and convenient method. The photoisomerization from the 2-cyanoethyl group to 1-cyanoethyl group in the cobaloxime complexes was successfully performed in the acid–base complex crystals. This method is applied to the photoreactions of nitrene formation, salicylideneaniline photochromism, and photoexcitation of Pt complexes. A wide variety of crystal environment may be made around the active site of the reactant molecule in the complex crystals.

Another problem is how fast we can observe the structural change. Although the diffraction data from a crystal can be obtained less than several picoseconds after the photo-irradiation, it may be necessary more than a second before the crystal will have a new lattice structure again. For the structure analysis using the diffraction data, that is, the observation of electron density, it is indispensable to check whether or not the crystal is in the equilibrium state and a lattice structure is made in the whole crystal. Although we have not had a good technique to check the crystallinity yet, I hope the technique will be solved in the near future. Furthermore, new facilities for neutron diffraction experiments have been constructed. J-PARC/MLF in Tokai, Japan, is one of them. We will obtain a whole neutron diffraction data for the organic and protein crystals of 0.01 and 1 mm^3 within 1 day and 1 week, respectively [1]. With all these developments, new discoveries will be made in the future.

Reference

1. Tanaka I, Kusaka K, Hosoya T, Niimura N, Ohhara T, Kurihara K, Yamada T, Ohnishi Y, Tomoyori K, Yokoyama T (2010) Acta Crystallogr D66:1194